PERFORMANCE ANALYSIS OF HYBRID SATELLITE-TERRESTRIAL NETWORKS OVER GENERALIZED FADING CHANNELS

Ph.D. Thesis

by

VINAY BANKEY

DISCIPLINE OF ELECTRICAL ENGINEERING
INDIAN INSTITUTE OF TECHNOLOGY INDORE

JANUARY 2020

PERFORMANCE ANALYSIS OF HYBRID SATELLITE-TERRESTRIAL NETWORKS OVER GENERALIZED FADING CHANNELS

A THESIS

Submitted in partial fulfillment of the

requirements for the award of the degree

of

DOCTOR OF PHILOSOPHY

by

VINAY BANKEY

DISCIPLINE OF ELECTRICAL ENGINEERING

INDIAN INSTITUTE OF TECHNOLOGY INDORE

JANUARY 2020

INDIAN INSTITUTE OF TECHNOLOGY INDORE

CANDIDATE'S DECLARATION

I hereby certify that the work which is being presented in the thesis entitled **"PERFORMANCE ANALYSIS OF HYBRIDSATELLITE-TERRESTRIALNETWORKS OVER GENERALIZED FADING CHANNELS"**in thepartial fulfillment of the requirements for the award of the degree of DOCTOR OF PHILOSOPHY and submitted in the DISCIPLINE OF ELECTRICAL ENGINEERING, Indian Institute of Technology Indore, is an authentic record of my own work carried out during the time period from December 2015to December 2019under the supervision of Dr. Prabhat Kumar Upadhyay, Associate Professor, Indian Institute of Technology Indore, India.

The matter presented in this thesis has not been submitted by me for the award of any other degree of this or any other institute.

Vinay Bankey
20/01/2020

Signature of the student with date

(VINAY BANKEY)

This is to certify that the above statement made by the candidate is correct to the best of my knowledge.

20/01/2020

Signature of Thesis Supervisor with date

(Dr. PRABHAT KUMAR UPADHYAY)

Vinay Bankeyhas successfully given his/her Ph.D. Oral Examination held on27/05/2020.

27/5/2020

Signature of Chairperson (OEB)
Date:27/05/2020

Signature of External Examiner
Date: 27/05/2020

27/5/2020

Signature of Thesis Supervisor
Date: 27/05/2020

Signature of PSPC Member #1
Date:27/05/2020

Signature of PSPC Member #2
Date: 27/05/2020

27/5/2020

Signature of Convener, DPGC
Date: 27/05/2020

27/05/2020

Signature of Head of Discipline
Date: 27/05/2020

ACKNOWLEDGEMENTS

I take this opportunity to acknowledge my heartfelt gratitude to all those who have directly or indirectly supported me throughout my PhD. First and foremost, I praise God, the Almighty for giving me the ability, strength, knowledge, and opportunity to undertake this research study and to complete it successfully. Then, I would like to express my deep gratitude to my supervisor and mentor, Dr Prabhat K. Upadhyay, for his invaluable guidance, continuous encouragement, and kind support towards my thesis work. He has given me all the freedom to pursue my research, and provided helpful career advice and suggestions. He will be my source of inspiration all my life.

Next, I would like to sincerely thank the members of my comprehensive evaluation of research progress committee, Dr Mukesh Kumar and Dr Surya Prakash, for their fruitful discussions and excellent advises towards my research. I am thankful to all the faculty members and the staffs at IIT Indore for their cooperation throughout my PhD.

I express my appreciation to all the members of Wireless Communications Research Group for creating a friendly and conducive environment. It was my privilege to share the office with Vibhum Singh, Chandan K. Singh, and Alok K. Shukla. I am immensely grateful to my seniors Dr Pankaj K. Sharma, Dr Devendra S. Gurjar, and Dr Sourabh Solanki for providing their help and valuable suggestions both technically and non-technically during my work. I am extremely thankful to Dr Praveen K. Singya for his unforgettable stimulus for this research study. My appreciation also goes to Shishir Maheshwari, Vijay Anand, and Ajinkya Sonawane for making a wonderful company and for sharing all the casual and valued moments during this study. Special thanks go to my great friends Pawan Kumar, Dr Anveshkumar Nella, and Chetan Waghmare for all the cheerful talks and encouragement.

I would like to thank Ministry of Electronics & Information Technology (MeitY), Government of India and IIT Indore for providing financial assistance. I would also like to thank Department of Science and Technology (DST), Science & Engineering Research Board (SERB), Government of India for providing me with the international travel support for attending the overseas conference. I will also thank the finance, administration, academic, and R&D sections of IIT Indore for all the necessary support.

Above all, I am indebted to my parents, Manisha Bankey and Ramjiwan Bankey, for always encouraging and supporting me. My heart felt regard goes to my grandmother, Kesar Bankey, for her love and moral support. Also I express my thanks to my brother, Vijay, and sister-in-law, Pooja, for their support and valuable prayers. Big thanks to my sweet sister, Radhika, for her selfless love, care, and endless support. I owe thanks to my beloved wife, Preeti, for his continued and unfailing love, support, and understanding during my pursuit of PhD that made the completion of thesis possible. I appreciate my beautiful little girl, Dhruvika, for abiding my ignorance during my thesis writing, I am so blessed to have you as my daughter. I salute you all for the selfless love, care, pain, and sacrifice you did to shape my life.

Lastly, I want to thank everyone who were part of this journey and has, in one way or another, helped me to successfully complete this research work.

Vinay Bankey

Dedicated to
my family

ABSTRACT

In the past few decades, wireless communication technologies have witnessed the rapid development of mobile devices and their involvement in various aspects of our day-to-day life. This evolution eventually demands the high-speed transmission and seamless connectivity anytime at anyplace. In this context, satellite-based communication systems have become popular by rendering a terrestrial experience with broadband access to mobile users. Indeed, the integration of satellite and terrestrial networks has been envisioned to realize the desirable traits. Recently, hybrid satellite-terrestrial networks (HSTNs) have received tremendous research attention owing to their advantage of providing high-speed connectivity to portable and mobile devices. The performance of HSTNs can be further improved by exploiting cooperative communication technology which may extend the satellite coverage, especially in remote areas. Hence, it is viable to incorporate cooperative techniques into HSTNs to improve the overall system performance and reliability. To meet this, terrestrial cooperative techniques have been unified with the HSTNs, thereby, formed relay-assisted HSTNs, referred to as hybrid satellite-terrestrial relay networks (HSTRNs). Despite the various advantages, HSTNs are associated with different practical issues such as outdated channel state information (CSI), co-channel interference (CCI), security attacks, etc. In this thesis, we aim to comprehensively analyze the performance of HSTNs over generalized fading channels to address the design objectives of the future wireless networks.

Firstly, we discuss statistical characterization of the land mobile satellite (LMS) channel model and analyze the performance of LMS systems using the physical layer security (PLS) technique. We investigate the performance of an interference-limited single-user LMS system in the presence of an eavesdropper. For the performance assessment, we derive an accurate expression of secrecy outage probability (SOP) by considering multiple CCI signals over Nakagami-m fading at the user destination node. We also conduct asymptotic secrecy outage analysis to reveal more insights and extract diversity order of the considered LMS system. We further investigate the performance of a single-user LMS system with an eavesdropper by employing an unmanned aerial vehicle-based friendly jammer. Here, we derive analytical and asymptotic SOP expressions and depict the impact of jammer along with various key parameters on performance of the considered LMS system.

Then, we consider an amplify-and-forward (AF) relay assisted multi-user HSTRN by employing a multi-antenna satellite. In this system design, we investigate the impact of outdated CSI and CCI under uncorrelated and correlated shadowed-Rician fading channels of satellite links. Herein, we employ opportunistic user scheduling of multiple users with outdated CSI over Nakagami-m fading channels of pertinent links and consider CCI at the relay. For the performance assessment of this system, we first derive novel and accurate analytical expressions of outage probability. We also perform asymptotic analysis to investigate the diversity order of the considered system. We further derive ergodic capacity expressions by making use of the moment generating function transform. Thereafter, we derive tight closed-form analytical and asymptotic expressions of the average symbol error probability for the considered system. The derived analytical expressions provide efficient tools to characterize the impact of CCI, outdated CSI, and antenna correlation on the system performance of HSTRNs. Our analysis for this system leads to various interesting insights into achievable performance gains. We illustrate that the considered systems can achieve full diversity as long as the interference power level remains low, otherwise the performance remarkably deteriorates. In addition, we depict that the advantage of multi-user diversity cannot be realized when the CSI is outdated. Moreover, we highlight the advantages of a multi-antenna satellite and reveal that the achievable diversity gain of the considered HSTRN is not affected by correlation in satellite antennas.

Next, we turn our focus on the secrecy performance analysis of HSTRNs. By adopting shadowed-Rician fading for satellite links and Nakagami-m fading for terrestrial links, we investigate the PLS performance of different HSTRN configurations with single eavesdropper and multiple eavesdroppers scenarios. With a single-eavesdropper scenario, we explore the configurations of multi-user HSTRNs and multi-relay HSTRNs. We examine the performance of multi-user HSTRNs in the presence of a single eavesdropper. Herein, by employing opportunistic scheduling of terrestrial users, we derive the analytical SOP expression. For the multi-relay HSTRNs, we propose optimal and partial relay selection schemes and derive novel closed-form SOP expressions. Based on our results, we herein manifest that the optimal relay selection scheme outperforms partial relay selection scheme. Further, we investigate the PLS performance in HSTRNs with multiple eavesdroppers scenario.

Specifically, we consider an AF relay based single-relay single-user HSTRN with independent and non-identically distributed multiple colluding eavesdroppers. For the secrecy performance assessment of this system, we derive the SOP and ergodic secrecy capacity (ESC) expressions. We next analyze a more generalized multi-user multi-relay HSTRN configuration with multiple eavesdroppers. For this overall setup, we conduct a comprehensive PLS analysis for two different wiretapping scenarios, i.e., non-colluding and colluding eavesdroppers under AF and decode-and-forward relaying protocols. Herein, we present opportunistic user-relay selection criteria and then derive accurate analytical and asymptotic expressions of the SOP to reveal useful insights. We also obtain the ESC expressions under AF relaying protocol for both the wiretapping scenarios. Our results enlighten that the achievable diversity order remains unaffected by the number of eavesdroppers and scenarios of wiretapping.

Above all, the theoretical findings in thesis address various technical design aspects of HSTNs and eventually provide useful guidelines for their possible applications in the future wireless networks.

CONTENTS

LIST OF FIGURES

List of Symbols

- Basic arithmetic and calculus notations have standard definitions.

Elementary & Special Functions

Notation	Definition
$\Gamma(x)$	Gamma function
$\Upsilon(x,y)$	lower incomplete Gamma function
$\Gamma(x,y)$	upper incomplete Gamma function
$\mathcal{K}_{\upsilon}(x)$	modified Bessel function of the second kind of order υ
$G_{p,q}^{m,n}\left[\cdot\middle\vert^{\cdot}_{\cdot}\right]$	Meijer's G-function
$\mathcal{W}_{u,v}(\cdot)$	Whittaker function
${}_1F_1(\cdot;\cdot;\cdot)$	Confluent hypergeometric function of the first kind
$\log_i(\cdot)$	logarithm to base i

Probability & Statistics

Let X be a random variable, and $\mathcal{A}$ be an arbitrary event.

Notation	Definition
$\mathbb{E}(\cdot)$	expectation
$f_X(\cdot)$	probability density function (PDF) of X
$F_X(\cdot)$	cumulative distribution function (CDF) of X
$\Pr[\mathcal{A}]$	probability of $\mathcal{A}$
$X \sim \mathcal{CN}(\mu, \sigma^2)$	X is complex normal distributed with mean μ and variance σ^2

Miscellaneous

Notation	Definition
$\lvert\cdot\rvert$	absolute value
$\triangleq$	equality by definition
$n!$	factorial of n
$\mathcal{C}_r^n = \binom{n}{r} = \frac{n!}{r!(n-r)!}$	binomial coefficient
$\arg\max\limits_i b_i$	index i corresponding to the largest b_i
$\min(b_1, b_2)$	minimum of scalars b_1 and b_2
$\max(b_1, b_2)$	maximum of scalars b_1 and b_2

List of Abbreviations

3D	Three-Dimensional
3GPP	Third-Generation Partnership Project
5G	Fifth-Generation
AF	Amplify-and-Forward
AS	Average Shadowing
AWGN	Additive White Gaussian Noise
B5G	Beyond 5G
BPSK	Binary Phase-Shift Keying
CCI	Co-Channel Interference
CDF	Cumulative Distribution Function
COL	Colluding
CSI	Channel State Information
DVB	Digital Video Broadcasting
DVB-SH	Digital Video Broadcasting-Satellite Handheld
DF	Decode-and-Forward
EC	Ergodic Capacity
EH	Energy Harvesting
ESC	Ergodic Secrecy Capacity
HS	Heavy Shadowing
HSTN	Hybrid Satellite-Terrestrial Network
HSTRN	Hybrid Satellite-Terrestrial Relay Network
i.i.d	Independent and Identically Distributed
i.ni.d	Independent and Non-Identically Distributed
LOS	Line-of-Sight
LMS	Land Mobile Satellite
MGF	Moment Generating Function
MIMO	Multiple-Input Multiple-Output
MRC	Maximal-Ratio Combining
MRT	Maximal-Ratio Transmission
N-COL	Non-Colluding
NLOS	Non Line-of-Sight

NOMA	Non-Orthogonal Multiple Access
NTN	Non-Terrestrial Network
OP	Outage Probability
PDF	Probability Density Function
PLS	Physical Layer Security
QoS	Quality-of-Service
RV	Random Variable
SEP	Symbol Error Probability
SINR	Signal-to-Interference-Plus-Noise Ratio
SNR	Signal-to-Noise Ratio
SOP	Secrecy Outage Probability
UAV	Unmanned Aerial Vehicle
UAV-J	Unmanned Aerial Vehicle Based Jammer

CHAPTER 1

INTRODUCTION

Wireless communications have experienced tremendous growth in the number of mobile users and applications in the past few years. The wide popularization of mobile users makes wireless communication to become an important part of our daily life. The future wireless communication networks are expected to provide service coverage to a large number of mobile users. However, currently, there are still a lot of users who exist without mobile service coverage, especially in less developed remote areas. With rapidly increasing number of mobile applications, we have been witnessing the revolutionary growth in mobile data traffic, which is presumed to enhance 1000-fold in the next 20 years. Such continually rising data traffic eventually puts more and more pressure to the wireless networks. Thereby, in addition to the issue of coverage, next-generation communication systems also require to guarantee the service continuity. It has become clear that extensive signal coverage and high-speed connectivity are turning out to be desirable traits for wireless systems in the forthcoming years. Nonetheless, existing wireless networks may not always achieve these service requisition due to their limited potentials. In order to cope with this deficiency, wireless networks must evolve either within themselves or through the deployment of completely modern networks suited to the required service provisions. To this end, satellite communication systems have earned significant consideration due to its advantage of providing wide radio coverage. As such, one satellite may cover an area of thousands of kilometers in radius and efficiently provide signal coverage with lower cost. Whereas, the terrestrial networks can provide high-speed data service at low cost. Therefore, satellite and terrestrial communication networks can be integrated to harness the advantages of both the systems. Such hybrid networks have been identified as an efficient solution to compete with the high-data rate and wide coverage requirements. There is increasing interest and involvement in third-generation partnership project (3GPP) working group, from the satellite communication industry, for an integrated satellite and terrestrial network infrastructure in the context of fifth-generation (5G). In essence, the newest 3GPP Releases under 5G development provide a promising opportunity to integrate space components with terrestrial networks. Thereby, the coexistence and cooperation between satellite and terrestrial communication networks would be a great deal for the 5G and beyond 5G (B5G) wireless communications.

1.1 Integration of Satellite and Terrestrial Networks

The growing demand of high-fidelity services anytime at any-place can only be satisfied by integration of networks, specifically integration of satellite and terrestrial networks. To accomplish this, satellite systems have been well integrated with the terrestrial networks, thus, form a new architecture named as hybrid satellite-terrestrial network (HSTN). A HSTN has been incorporated in Digital Video Broadcasting (DVB) system which provides Satellite services to Handheld devices (SH) by making use of a geostationary satellite operating at S (2/4 GHz) band, leading to a high performance new generation standard, known as DVB-SH [1]. However, the operational frequency band may vary, depending upon the different service requirements and various application scenarios (like personal mobile communication, navigation, military emergency, etc). Recently, the 3GPP group is now standardizing use of non-terrestrial networks (NTN)[1], i.e. satellite and others, including unmanned aerial vehicles, such that multiple access networks can be used to support 5G networks [2]. In this regard, the adoption of HSTNs arises as a necessary step in the evolution of 5G systems. Moreover, the land mobile satellite (LMS) system, an elementary HSTN, has earned many consideration owing to its capability of providing unicast and multicast services over a wide range of coverage area [3]. In LMS systems, satellite broadcasts signals to serve terrestrial mobile users over a wide area and the quality-of-service (QoS) provided by such systems firmly depends on the line-of-sight (LOS) links between the satellite and terrestrial users [4]. However, it is not always possible for mobile users, in satellite communication, to receive signals from satellite directly. This may happen due to long distance communication and

[1]Beyond satellites, NTN refer to networks, or segments of networks, using an airborne or space-borne vehicle to embark a transmission equipment relay node or base station.

masking effect caused by intense shadowing and various obstacles. This limitation may become more severe when the user terminal is in motion. In order to implement a reliable communication, an intermediate node is needed to assist the transmission of signals. Thereby, researchers have envisaged a relay-assisted HSTN, which basically implants terrestrial relay cooperation into satellite mobile communications [5], [6]. This new architecture is termed as hybrid satellite-terrestrial relay network (HSTRN) [7]. Such HSTRNs have potential to provide broadcast/multicast services and seamless connectivity to portable and mobile users. They can enhance indoor coverage and retain service reliability, especially in the areas where users do not have LOS communication like shopping malls, tunnels, etc.

1.2 Basics of Cooperative Relaying

The time varying nature of wireless channels poses many technical challenges in the design of wireless systems. A wireless medium is a complex mix of physical phenomena including channel impairments, multipath propagation, path loss, shadowing, noise, etc. These all above-said impairments are collectively counted on as fading. Radio signal propagation in a wireless channel typically suffers from fading resulting degradation in the quality of radio signal. Thereby, fading is the foremost problem encountered in wireless communication design process.

The exploitation of cooperative diversity [8] has been regarded as an effective solution to mitigate the effect of fading in wireless systems. This can be accomplished by spatially located devices, known as relays, which allow the signals to reach at the receiver via multiple paths. Since the signal propagation over each path experiences independent statistical changes, the possibility to go all the paths into deep fade decreases drastically.

In cooperative communication, independent paths between transmitter and receiver are generated via introducing a relay channel which was initially studied in [9] from an information theoretic perspective. Afterward, based on the processing of the signal received, various cooperative relaying protocols have been proposed [10], [11]. These relaying protocols are broadly classified into two categories, viz., amplify-and-forward (AF) and decode-and-forward (DF) relaying protocols.

AF Relaying: Relay, operating in AF mode, simply receives signal from the source and transmits an amplified version of it to the receiver destination. Here, amplification of the received signal is done basically to combat the fading. The amplification factor is defined based on the channel gain between source and relay. On the basis of this amplification factor, AF protocol is further divided into two categories, i.e., fixed-gain AF and variable-gain AF.

In fixed-gain AF, relay fixes the amplification factor over a given time period to a certain value. This amplification factor is typically an inverse function of the average channel gain between source and relay which depends on long-term statistics of the channel or network.

Besides, variable-gain AF relaying protocol differs from the case of fixed gain amplification. Under variable-gain AF, the amplification factor is adjusted to instantaneous changes in the channel and network. The amplification factor, herein, is an inverse function of the instantaneous channel gain between source and relay unlike to fixed-gain AF.

DF Relaying: In DF mode, relay decodes the received signal, re-encodes it and transmit this to the destination. Thereby, this relaying is also known as regenerative relaying. While doing this, noise at the relay could be surpassed unlike to AF relaying. However, in DF, there is a possibility of false decoding at relay which results in an error propagation. In such case, decoding at the relay becomes meaningless.

Both the aforementioned relaying protocols have been widely adopted in various cooperative systems to improve the signal coverage and reliability of communication. In addition to cooperative strategy, the performance of a cooperative system is often influenced by network configuration. A multi-relay configuration has been greatly emphasized to improve the performance of cooperative networks, where the best relay is selected to forward information toward the destination.

Opportunistic Relay Selection in Multi-Relay Networks: Opportunistic relay selection was introduced by Bletsas et al. in [104], [112] for both AF and DF protocols, in which the best relay node is selected to forward the information. Various studies demonstrated that cooperative diversity benefits may be exploited even when a single opportunistic relay assists the transmission between source and destination.

1.3 Issues and Challenges in Hybrid Satellite-Terrestrial Networks

HSTNs are involved with several issues and challenges due to their heterogeneous nature of communication. The terrestrial nodes, in the HSTNs, inevitably encounter with a co-channel interference (CCI) environment due to the highly aggressive frequency reuse. It may stem from other licensed users of the same spectrum or from other frequency channels injecting energy into the channel of interest [12]. The CCI significantly deteriorates the system performance. In fact, it causes a more severe performance degradation than thermal noise [13].

Moreover, multi-user HSTNs have become promising architecture for future wireless systems. In such networks, an inherent multi-user diversity can be harnessed with opportunistic user selection to realize performance gains. In fact, the channel state information (CSI) plays an important role to attain the achievable performance gain in multi-user networks. The CSI should be acquired perfectly to facilitate the multi-user selection process. However, in practice, the CSI may get outdated due to various reasons such as user mobility, high feedback latency associated with satellite communication, etc.

In addition, the channel and propagation characteristics of satellite links are different from the terrestrial links, thereby, potential exploitation of multiple antennas at the satellite is of primary concern. The main difference lies in the LOS characterization of satellite channels and the lack of scatterers around the satellite. This may result into a strong LOS and a high channel correlation due to insufficient antenna separation and sparse scattering environment at the transmitting satellite. Therefore, the achievable multi-antenna gains may not always be attained.

Apart from above discussed practical issues in HSTNs, there is an another major challenge i.e., security problems that require an equal attention. Interception of information is a critical problem in HSTNs. It is worth-noting that the inherent broadcasting nature of wireless communication always keeps an open invitation for intercepting, and thereby, HSTNs are more exposed to the attacks of adversaries. Security problems in such networks have been rapidly increasing over the years and posing a challenge of attaining a secure communication.

Therefore, with such issues and challenges, the performance investigations of HSTNs are in prime need to reveal their true potentials.

1.4 Wireless Channel Characteristics

This section presents some technical background required for this thesis. Specifically, we discuss the generalized fading models to characterize the satellite and terrestrial channels. We also elucidate the fundamental measures to analyze the performance of wireless systems over pertinent fading channels.

1.4.1 Fading Distributions for Satellite and Terrestrial Channels

Radio signal propagation through wireless channel experiences various fading effects such as path-loss with distance, multi-path propagation, shadowing from obstacles, etc. The precise mathematical description of these fading effects is quite intricate in practice. However, considerable efforts have been devoted to characterize these fading effects and thus, a range of statistical models have been evolved in the literature [14], [15]. These statistical models depend on the particular propagation scenario and the underlying channel environment. In the following, we discuss the statistical models to characterize the terrestrial and satellite channels.

Rayleigh Fading: The Rayleigh fading distribution is generally used to model multipath fading with no LOS path. The probability density function (PDF) $f(a)$ for Rayleigh distributed signal envelope is given by

$$f(a) = \frac{2a}{\Omega}\exp\left(-\frac{a^2}{\Omega}\right) \qquad \text{for } \ a \geq 0, \tag{1.1}$$

where Ω is the average power.

Nakagami-m Fading: Nakagami-m fading distribution is often used to model propagation paths consisting of one strong direct LOS component and many random scattered components. The Nakagami-m distribution is a more generalized fading distribution which characterizes a variety of fading scenarios and comprises the Rayleigh distribution as a special case. Thereby, the Nakagami-m fading is well-suited for the modeling of terrestrial channels. It is also appropriate to model interference from multiple sources. The PDF of the received signal envelope for Nakagami-m fading is given by

$$f(a) = \frac{2}{\Gamma(m)}\left(\frac{m}{\Omega}\right)^m a^{2m-1}\exp\left(-\frac{ma^2}{\Omega}\right) \qquad \text{for } \ a \geq 0, \tag{1.2}$$

where m is the fading severity parameter. Interestingly, with $m = 1$, (1.2) reduces to Rayleigh fading. Note that when $m = \infty$, there is no fading since as m increases the severity of fading decreases.

Shadowed-Rician Fading: Under this model, the amplitudes of the LOS and scattered components respectively follow Nakagami-m and Rayleigh distributions. The shadowed-Rician channel model accurately describes the satellite communication channel and also agrees quite well with mobile-satellite environments [16]. The PDF of the fading amplitude is given by

$$f(a) = \frac{1}{2b}\left(\frac{2bm}{2bm+\Omega}\right)^m \exp\left(-\frac{a}{2b}\right) {}_1F_1\left(m; 1; \frac{a\,\Omega}{2b(2bm+\Omega)}\right) \qquad \text{for } \; a \geq 0, \tag{1.3}$$

where Ω and $2b$ represent the average power of LOS and multipath components, respectively, and m is a parameter that describes the severity of shadowing. Herein, ${}_1F_1(\cdot;\cdot;\cdot)$ is the confluent hypergeometric function of the first kind [59, eq. 9.210.1].

Throughout this thesis, we have adopted shadowed-Rician fading model for satellite channels and Nakagami-m fading distribution for the terrestrial channels.

1.4.2 System Performance Measures

Here, we briefly introduce the key performance measures of wireless systems that we have explored in this thesis.

Instantaneous Signal-to-Noise Ratio

The most basic and well understood performance metric in communication system is signal-to-noise ratio (SNR). The instantaneous SNR, denoted by Λ, is defined as

$$\Lambda = \frac{\text{Power of signal component at receiver}}{\text{Power of noise component at receiver}}. \tag{1.4}$$

However, when a communication system subjects to fading impairments, average SNR turns to be an appropriate metric for the performance investigation, which can be obtained by averaging the instantaneous SNR.

Outage Probability

Outage probability (OP) is an important performance criterion which is defined as the probability of the event when output SNR falls below a certain predefined threshold γ_{th}. In simple mathematical terms, if $f_\Lambda(x)$ denotes the PDF of SNR Λ, then OP is given by

$$\mathcal{P}_{\text{out}} = \Pr[\Lambda < \gamma_{\text{th}}] = \int_0^{\gamma_{\text{th}}} f_\Lambda(x)dx, \tag{1.5}$$

which, eventually, is the cumulative distribution function (CDF) of SNR Λ.

Ergodic Capacity

Ergodic capacity (EC) is another standard performance metric which is basically an average of instantaneous capacity of a communication system operating over fading channels. Mathematically, it is given by

$$\overline{C}_{\text{EC}} = \int_0^{\infty} B \log_2(1+\Lambda) f_\Lambda(x)dx, \tag{1.6}$$

where B is the received signal bandwidth.

Average Symbol Error Probability

An another performance criterion is average symbol error probability (SEP) which is the average of the conditional SEP over the fading statistics. The evaluation of average SEP is, undoubtedly, considered as the most difficult one among all other metrics. The reason behind this lies in the fact that the conditional SEP is, in general, a nonlinear function of the instantaneous SNR and thus entails modulation/detection scheme to be employed by the system.

In this sequence, the key measures to evaluate the secrecy performance of a wireless system are defined as secrecy rate, ergodic secrecy capacity, and secrecy outage probability, which will be introduced briefly in the Section 2.2 of Chapter 2.

1.5 Motivation and Objectives

In this section, we present the motivation and objectives behind the research work in this thesis.

1.5.1 Motivation

Extensive signal coverage and high-speed connectivity are the important design objectives for the 5G and B5G wireless communication systems [17]. Recently, HSTNs have earned great applause while achieving these objectives to a certain extent. However, in satellite communication systems, masking effect becomes a major problem which eventually limits their communication reliability. As a consequence, enhancing the performance of such systems becomes critical and challenging, especially in dense and remote areas. Many efforts have been devoted in the existing literature towards the performance improvements of HSTNs. Among others, integration of cooperative relaying techniques has been shown to dramatically improve the performance of HSTNs [5]. A relay assisted HSTN, known as HSTRN, has emerged as a promising candidate to provide broad signal coverage and seamless connectivity to portable and mobile users, especially in the remote regions where LOS communication is not feasible [6]. Such HSTRNs have been extensively studied in the literature [18]-[26].

Despite of various contributions, the current literature on HSTRN still lacking on several fronts. Majority of existing works have concentrated on a single-user HSTRN scenario. In contrast, a multi-user relay network is a promising architecture for future mobile communications, wherein a relay can assist the communication between a source and multiple destinations/users [27]. The multi-user architecture has been incorporated in a number of standards like IEEE 802.11s and IEEE 802.16j [28]. Few works [29], [30] have considered the multi-user configuration in HSTRN assuming perfect CSI to facilitate the user selection process. However, in practice, the CSI acquired at the time of user selection may differ from the CSI at time of transmission. This may occur due to various reasons such as feedback delay, user mobility, etc. In fact, this outdated CSI significantly affect the diversity performance of HSTRNs which has been ignored in the literature. In addition, HSTRN is more likely to suffer from CCI due to the dense frequency reuse. This may derive from the other licensed users operating at the same spectrum or from other frequency channels injecting energy into the channel of interest [12]. The CCI can severely hinder the performance of a multi-user HSTRN which has also been overlooked in the literature. It would be highly interesting to study the impact of outdated CSI and CCI over multi-user HSTRN architecture for the practical design in future communication.

Moreover, a multi-antenna satellite is greatly emphasized to improve the performance of satellite-terrestrial systems. However, the radio signal propagation in satellite links differs from terrestrial links due to the LOS characterization of satellite channels and lack of scatterers around the satellite. Indeed, a strong LOS and sparse scattering environment at the satellite may result into a high channel correlation which limits the achievable antenna gains and deteriorates the system performance. Although, authors in [31] have explored the correlated satellite channels, nevertheless, it is important to analyze the impact of correlated satellite antennas on the performance of multi-user HSTRNs under various realistic scenarios.

On the other front, security issues have attracted much more attention compared to other issues in the past. Resulting from the openness of wireless medium, wireless systems are more susceptible to security threats for a variety of devices connected everywhere with different capabilities. The information signal propagating in the wireless medium is not only received by the authorized user but also available to the adjacent illegal user. Therefore, security and privacy concerns in wireless communication networks have been the focus of continuous attention. Typically, there are two types of techniques to ensure the security of wireless networks i.e., upper-layer encryption (also known as cryptographic) technique and physical layer security (PLS) technique. In the upper-layer encryption technique, information signal is encrypted via encryption algorithms and a secret key such that the original signal can not be deciphered at eavesdroppers. However, the computational cost for either encryption or decryption is usually very high and rely upon the hardness of their underlying mathematical problems. Moreover, secret key generation depends on a trusted key management center, which may not be always feasible in wireless networks. Thereby, cryptographic schemes through upper-layer are not necessarily reliable. As a complementary solution, the concept of PLS is to harness the randomness and time-varying feature of wireless channels to defend against eavesdroppers in wireless transmissions. The PLS technique does also not require the secret key generation and complex cryptographic calculations. These undeniable advantages pave the way to PLS applicability in the development of wireless communication networks. Hence, research on transmission security would undoubtedly be of theoretical and practical interest, especially relevant to the aforementioned key technique for 5G communications.

Meanwhile, security problems are critical concern in HSTNs which is considered as a challenging design objective for future communication systems. Note that due to the broadcasting nature of wireless channels, HSTNs are more vulnerable to the security attacks. Security problems in such networks have been rapidly increasing over the years and posing a challenge of attaining a secure communication. Thereby, the HSTN security has been drawn more and more attention. Recently, information-theoretic approach based physical layer security (PLS) emerges as a promising technique to ensure overall security in wireless communications. Unlike conventional cryptographic method, PLS technique basically exploits the physical characteristics of wireless fading channels and provides confidentiality for radio transmissions. Traditionally, security in satellite communication systems has been ensured by cryptography techniques at upper layers [32], [33]. Some works in the literature have studied the PLS of satellite-based communication systems [43]-[49] and [98]-[101]. However, the PLS performance analysis in hybrid satellite-terrestrial systems is still infancy and becomes an open area for research, especially in regard to rich network functionality in the 5G era.

1.5.2 Objectives

The above mentioned research gaps have motivated this thesis to achieve the following objectives:

- To characterize the performance of the LMS systems with CCI and friendly jammer.
- To analyze the performance of multi-user HSTRNs with outdated CSI, CCI, and antenna correlation.
- To study the secrecy performance in HSTRNs with a single-eavesdropper scenario.
- To investigate the secrecy performance in HSTRNs with multiple eavesdroppers scenario.

With aforementioned objectives, this thesis presents the comprehensive performance analysis of HSTNs over generalized fading channels. We address various technical aspects of HSTNs through exhaustive mathematical analysis and highlight important guidelines towards the design of future wireless networks.

1.6 Thesis Outline and Contributions

In this thesis, we comprehensively analyze the performance of HSTNs by adopting shadowed-Rician fading for the satellite channels and Nakagami-m fading for the terrestrial channels. The shadowed-Rician channel model accurately characterizes the LMS channel and has proved as an efficient tool for the performance analysis

[16]. Moreover, Nakagami-m fading distribution is versatile through its parameter m, it can model signal fading conditions that range from severe to moderate, to light fading or no fading. Thereby, the Nakagami-m fading is considered to be appropriate for the modeling of terrestrial channels. Throughout this thesis, we adopt these aforementioned fading models for the performance analysis. Besides the current chapter, which gives a general introduction about the background of the work, discusses various technical aspects involved in this thesis work, research objectives and their motivation, the contributions from other chapters are summarized as follows:

- In Chapter 2[2], we discuss the LMS systems and describe the statistical properties of the shadowed-Rician fading model for satellite channels. Herein, we explore the performance of LMS systems under different shadowing scenarios of satellite links. We first investigate the secrecy performance of a LMS system, where a satellite transmits information signal to an interference-limited legitimate user in the presence of an eavesdropper. For the performance assessment, we derive an accurate expression of secrecy OP (SOP) by considering multiple CCI signals over Nakagami-m fading at the user destination node. To gain more insights, we examine asymptotic behavior of the SOP expression at high SNR regime and illustrate that system can attain a unity diversity order even under the influence of multiple interferers. Then, we investigate the secrecy performance of a LMS system with a legitimate user and an eavesdropper by employing an unmanned aerial vehicle (UAV)-based friendly jammer. For the considered system, we derive analytical and asymptotic expressions of the SOP under pertinent heterogeneous channels for the satellite links and the air-to-ground jamming links. We validate the theoretical results through Monte-Carlo simulations. Our results demonstrate that while the satellite channel conditions have severe impact on the LMS system performance, the

[2]The contributions of this chapter are presented in the following papers:

1. V. Bankey, P. K. Upadhyay, and D. B. da Costa, "Physical layer security of interference-limited land mobile satellite communication systems," in Proc. *International Conference on Advanced Communication Technologies and Networking (CommNet)*, Morocco, Apr. 2018.

2. V. Bankey and P. K. Upadhyay, "Improving secrecy performance of land mobile satellite systems via a UAV friendly jammer," in Proc. *IEEE Consumer Communications and Networking Workshop (CCNC Workshop): Unmanned Aerial Vehicle (UAV'20) Communications and Networks*, Las Vegas, United States, Jan. 2020.

UAV jammer can notably improve the secrecy performance.

- In Chapter 3[3], we investigate the performance of a multi-user HSTRN by employing opportunistic user scheduling with outdated CSI and CCI. The overall transmission in the considered HSTRN takes place using an AF relaying protocol in two phases. Herein, we derive novel expressions for OP, EC, and average SEP of the proposed HSTRN. We further examine achievable diversity order for this system. Importantly, we conduct performance analysis of the considered system by taking both uncorrelated and correlated shadowed-Rician fading channels into account. We obtain the EC expressions for fixed-gain AF and variable-gain AF relaying. Our derived analytical expressions provide efficient tools to characterize the impact of CCI, outdated CSI, and antenna correlation on the system performance of HSTRNs. Our results illustrate that the antenna correlation at the satellite does not affect the overall system diversity order. We also depict the impact of outdated CSI and CCI on the performance of HSTRNs. Finally, we validate our theoretical developments using Monte-Carlo simulations.

- In Chapter 4[4], we investigate the secrecy performance of a multi-user HSTRN in the presence of a single eavesdropper. For this system, by employing opportunistic scheduling of terrestrial users, we derive analytical expression of the SOP. We further obtain the asymptotic SOP expression at high SNR regime. Based on the asymptotic secrecy outage behavior, we illustrate practical insights on the achievable diversity order of the system. Numerical and simula-

[3] The contributions of this chapter are presented in the following papers:

1. V. Bankey and P. K. Upadhyay, "Ergodic capacity of multiuser hybrid satellite-terrestrial fixed-gain AF relay networks with CCI and outdated CSI," *IEEE Transactions on Vehicular Technology*, vol. 67, no. 5, pp. 4666-4671, Jan. 2018.
2. V. Bankey, P. K. Upadhyay, D. B. da Costa, P. S. Bithas, A. G. Kanatas, and U. S. Dias, "Performance analysis of multi-antenna multiuser hybrid satellite-terrestrial relay systems for mobile services delivery," *IEEE Access*, vol. 6, no. 1, pp. 24729-24745, Apr. 2018.
3. V. Bankey and P. K. Upadhyay, "Average symbol error probability of interference-limited multiuser hybrid satellite-terrestrial relay networks with outdated channel state information," in Proc. *IEEE Region 10 International Conference (TENCON)*, Kochi, Kerala, India, Oct. 2019.

[4] The contributions of this chapter are presented in the following papers:

1. V. Bankey and P. K. Upadhyay, "Physical layer secrecy performance analysis of multi-user hybrid satellite-terrestrial relay networks," *CSI Transactions on ICT*, vol. 6, no. 2, pp. 187-193, Jun. 2018.

tion results are provided to vindicate our analysis and to show the impact of various key channel/system parameters on system secrecy performance. We also demonstrate that how an eavesdropper can severely degrade the system secrecy performance.

- In Chapter 5[5], we examine the secrecy performance of a multi-relay HSTRN with a single eavesdropper, where a satellite communicates with a terrestrial destination via multiple relays in the presence an eavesdropper. Particularly, we present AF based optimal and partial relay selection schemes, and derive the SOP expressions by considering pertinent fading channels for the satellite and terrestrial links. We further perform the asymptotic secrecy outage analysis at high SNR regime to highlight the achievable diversity gain under both optimal and partial relay selection schemes. We show that the optimal relay selection scheme outperforms the partial relay selection scheme. In addition, our results reveal that an increase in the number of terrestrial relays plays an important role in improving the secrecy performance of the considered HSTRN.

- In Chapter 6[6], we investigate the performance a single-user single-relay HSTRN in the presence of multiple eavesdroppers. We conduct secrecy performance analysis by considering independent and non-identically distributed (i.ni.d.) colluding eavesdroppers over Nakagami-m fading. For the performance assessment of this network, we derive the SOP and ergodic secrecy capacity (ESC) expressions by considering multiple antennas at the satellite. We further perform the asymptotic analysis of SOP at high SNR regime and reveal the system achievable diversity order. We illustrate that the system becomes less secure when a large number of eavesdroppers succeed in attacking. Moreover, we depict that system secrecy performance can be notably improved by deploying

[5]The contributions of this chapter are presented in the following papers:

1. V. Bankey and P. K. Upadhyay, "Secrecy outage analysis of hybrid satellite-terrestrial relay networks with opportunistic relaying schemes," in Proc. *IEEE 85th Vehicular Technology Conference (VTC)*, Sydney, Australia, Jun. 2017.

[6]The contributions of this chapter are presented in the following papers:

1. V. Bankey and P. K. Upadhyay, "Physical layer security of hybrid satellite-terrestrial relay networks with multiple colluding eavesdroppers over non-identically distributed Nakagami-m fading channels," *IET Communications*, vol. 13, no. 14, pp. 2115-2123, Aug. 2019.

multiple antennas at the satellite.

- In Chapter 7[7], we examine the secrecy performance of a multi-user multi-relay HSTRN in the presence of independent and identically distributed (i.i.d.) multiple eavesdroppers. For multiple eavesdroppers, we consider two specific scenarios of eavesdropping, i.e., colluding and non-colluding. We conduct a comprehensive secrecy performance analysis for both eavesdropping scenarios under AF and DF relaying protocols. We present opportunistic user-relay selection criteria and derive accurate expressions of the SOP by adopting pertinent fading channels for the satellite and terrestrial links. We also obtain asymptotic SOP expressions to determine the main channel/system parameters that regulate the secrecy performance at high SNR regime. In addition, we study the ESC performance of the considered system with a single AF relay. Our results elucidate that system diversity gain remains unaffected by the method of relaying protocol and type of eavesdropping.

Finally, in Chapter 8, we draw the conclusions from the work in this thesis and provide the possible future directions.

[7]The contributions of this chapter are presented in the following papers:

1. V. Bankey and P. K. Upadhyay, "Physical layer security of multiuser multirelay hybrid satellite-terrestrial relay networks," *IEEE Transactions on Vehicular Technology*, vol. 68, no. 3, pp. 2488-2501, Mar. 2019.
2. V. Bankey and P. K. Upadhyay, "Ergodic secrecy capacity analysis of multiuser hybrid satellite-terrestrial relay networks with multiple eavesdroppers," in Proc. *IEEE International Conference on Communications Workshops (ICC Workshops): Wireless Physical Layer Security*, Shanghai, China, May 2019.

CHAPTER 2

LAND MOBILE SATELLITE SYSTEMS WITH CO-CHANNEL INTERFERENCE AND JAMMING

The aim of next generation wireless communication systems comprises a large number of connected devices, data transfer speed with the range of Gigabits per second, lower latencies, increased reliability, and improved coverage. Mobile satellite systems have drawn extensive interest in modern technology, since they offer mobile communication services to many users in different environments over a wide area. In this regard, land mobile satellite (LMS) systems have acquired significant research interest over past few years owing to their exclusive competences such as broad coverage, navigation, high-speed data transmission and inherent multicasting/broadcasting capabilities [16]. The LMS system is basically a satellite-based communication system that assists terrestrial mobile users. In such system, satellite broadcasts signals to serve terrestrial mobile users over a wide area with low cost. Consequently, LMS systems can offer more advantages to remote lands, ocean, and aeronautical services. In addition, LMS systems can efficiently provide various telecommunication and multimedia services to mobile devices in remote terrains that are not well served by existing terrestrial networks. Thereby, LMS systems have become vitally crucial in the present generation of wireless communications. In the recent years, substantial efforts have been made towards the performance analysis of LMS systems [34]-[40]. However, the implementation of such systems still encounters some limitations regarding connectivity, stability, and security, resulting into unreliable communication. The QoS provided by such LMS systems firmly depends on the broadcasting channel between the satellite and the mobile user. In fact, due to inherent broadcasting nature of satellite channel, LMS systems are more vulnerable to suffer from eavesdropper's attacks, such as wiretapping. Therefore, security in LMS systems are becoming a more critical issue [41]. Surprisingly, very limited attention has been paid towards the security concern in such systems. Traditionally, security in satellite communication systems has been ensured by cryptography at upper layers [33]. However, cryptographic techniques, implemented at the upper-layers of the protocol stack, require high storage and computational capabilities for the encryption and decryption of the secret codes [32]. To combat and complement cryptographic schemes, physical layer security (PLS) technique raises out as a popular and promising scheme to improve the secrecy performance by leveraging the physical properties of radio channels at the waveform level. The idea of PLS has initially been proposed by Wyner [42], which exploits the characteristics of fading channels to improve the security performance. Basically, PLS depends on an information-theoretic metric defined as secrecy rate or secrecy capacity. Under this context, few recent works have analyzed the PLS of satellite networks [43]-[46], and these are briefly discussed next.

In [43], authors have introduced PLS technique in satellite communication, where individual secrecy rate constraint was used as key metric to ensure the security. Later in [44], the secrecy performance of satellite communication networks has been analyzed for different cases of shadowed-Rician fading channel. Furthermore, PLS of satellite communication systems has been investigated in [45] and [46] under rain fading channel model. Specifically, the authors in [45] have examined the secrecy performance for satellite networks under rain attenuated environment conditions. While in [46], it was demonstrated that the security could be achieved in multi-beam satellite systems through transmit beamforming optimization under rain fading channel. Although the above-mentioned literature laid a significant research for secrecy of satellite networks, very few works have investigated the secrecy performance of LMS systems [47]-[49]. To be specific, in [47], the probability of secrecy outage and positive secrecy capacity have been obtained for LMS communication systems. Likewise in [48], authors have investigated the average secrecy capacity of LMS systems by considering multi-antenna terrestrial nodes. The work of [48] was then further extended by employing spot beam transmission at satellite in [49]. However, the impact of multiple terrestrial interferers on secrecy performance of LMS systems has not been investigated in the literature so far. In fact, a terrestrial user may exist in the intensive environment which causes CCI and thus affect communication system's performance adversely [50]. The terrestrial destination may get affected by CCI from other sets of users and/or earth stations existing nearby. Hence, it is important to analyze the impact of co-channel interferers on LMS systems for their potential deployment in 5G or B5G wireless networks.

Moreover, secrecy performance can be further improved by employing cooperative jamming techniques where jammer is utilized to disturb the eavesdropper by emitting the artificial noise and to prevent it from wiretapping the information of legitimate node [51]. The authors in [52]-[54] have analyzed the secrecy performance using friendly jammer. In [52], authors have employed friendly jammer to improve the secrecy performance of a multi-user wireless network. A cooperative jamming relay has been introduced to degrade the reception at eavesdropper in [53]. Further, the authors in [54] have optimized the secrecy rate in a wireless network using full-duplex jamming receivers. Although the above-said works have analyzed the PLS performance incorporating friendly jamming, however, they are only limited to the terrestrial communication scenarios. The PLS performance analysis of LMS systems with cooperative jamming has not been studied so far. Note that the jammer, by sending an artificial noise signal, can confuse the eavesdropper and thereby enhance the secrecy performance.

Motivated by the above, in this chapter, we explore the PLS performance in LMS systems. We first study the secrecy performance of an interference-limited LMS system in the presence of a single eavesdropper, where the terrestrial user is inflicted by CCI. In the sequel, we investigate the impact of jamming on the secrecy performance of LMS systems. For the performance assessment, we derive analytical and asymptotic SOP expressions and highlight the important insights. We identify the key channel/system parameters influencing the secrecy performance of LMS systems through numerical and simulation results. Prior to continuing further, we present the statistical characteristics of the shadowed-Rician model that we have utilized, in this thesis, to model the LMS channels.

2.1 Shadowed-Rician Model for LMS Channels

The fluctuations of the radio signal envelope in a narrow-band LMS channel are generally associate with two types of fading, i.e., LOS shadowed fading and multipath fading [55]. The shadowed-Rician model (also known as shadowed Rice model) originally proposed by Loo [56] where he assumed that the amplitude of the LOS component is a log-normal random variable and multipath component is a Rice random variable. However, the application of the log-normal distribution results into complex expressions for the key channel statistics [57]. Moreover, the analytic manipulation of such expressions becomes quite difficult since they cannot be resolved in terms of known mathematical functions. Therefore, the average bit-error rate performance evaluation or interference calculation become more intricate even for a single-channel.

Besides, it is found that the gamma distribution, as an alternative to the log-normal distribution, can lead in simpler statistical models with the same performance under various practical scenarios [57]. Thereby, Loo's model was further modified by Abdi [16] who has proposed a new simple shadowed-Rician model in which the power of the LOS component is assumed to be a Gamma random variable. This new shadowed-Rician channel model, defined by Abdi [16], describes accurately the LMS communication channel, where a random LOS component follows Nakagami-m distribution with $0 \leq m \leq \infty$, while the multipath component follows the Rician fading. It is widely adopted in literature [18], [58] for the performance analysis of hybrid satellite-terrestrial systems since it offers less computational burden as compared to other models like Loo's model.

Let h_{sr} be the fading amplitude of a shadowed-Rician channel between the satellite s and the terrestrial node r. Then, the pdf of $f_{|h_{sr}|^2}$ can be derived as [16]

$$f_{|h_{sr}|^2}(x) = \alpha\, \mathrm{e}^{-\beta x}\, {}_1F_1\left(m_s; 1; \delta x\right), \ x \geq 0, \tag{2.1}$$

where $\alpha = \frac{(2bm_s/(2bm_s+\Omega_s))^{m_s}}{2b}$, $\beta = \frac{1}{2b}$, and $\delta = \dfrac{\Omega_s}{(2b(2bm_s+\Omega_s))}$ with Ω_s and $2b$ be the average power of LOS and multipath components, respectively, m_s is the fading severity parameter. For analytical tractability, we consider only the integer values of the fading severity parameter of the satellite link [58]. Thus, the hypergeometric function can be represented via Kummer's transform [60] as

$${}_1F_1(a; b; x) = \mathrm{e}^{x} \sum_{n=0}^{a-b} \frac{(a-b)!x^n}{(a-b-n)!n!(b)_n}, \tag{2.2}$$

where $(\cdot)_n$ is the Pochhammer symbol [59, p. xliii]. Thereby, for integer m_s, we can simplify ${}_1F_1\left(m_s; 1; \delta x\right)$ in (2.1) using (2.2) to represent the PDF $f_{|h_{sr}|^2}(x)$ as

$$f_{|h_{sr}|^2}(x) = \alpha \sum_{\kappa=0}^{m_s-1} \zeta(\kappa) x^{\kappa} \mathrm{e}^{-(\beta-\delta)x}, \tag{2.3}$$

where $\zeta(\kappa) = (-1)^{\kappa}(1-m_s)_{\kappa}\delta^{\kappa}/(\kappa!)^2$.

The PDF $f_{|h_{sr}|^2}(x)$ will be used for the performance analysis in this thesis. Now, before delving into the secrecy performance analysis of the considered LMS systems, we briefly discuss the fundamentals of the PLS and key measures to estimate the level of the secrecy.

2.2 Basics of Physical Layer Security

To ensure the security is wireless communication systems, a new approach has recently attracted increasing attention known as PLS technique. The PLS has come out as a key technique to guarantee reliability and trustworthiness for future generation wireless communication systems. The fundamental conception of PLS is to exploit inherent physical characteristics of the wireless channel, such as fading, interference, and noise, to realize key-less secure transmission [61].

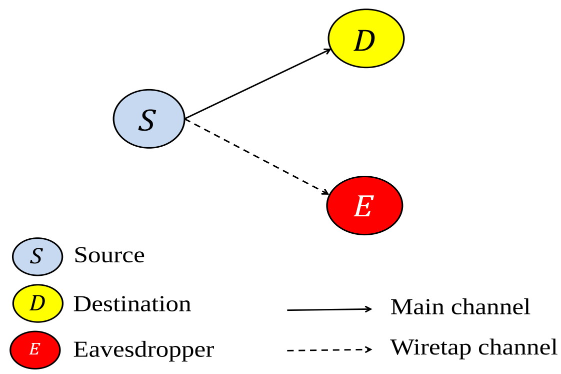

Figure 2.1: Basic three-node wiretap model.

In PLS framework, the three-node system is considered as a basic network, as shown in Fig. 2.1, which comprises a transmitting source, a legitimate destination, and an eavesdropper where the source wishes to transmit secret information to legitimate destination without being intercepted by eavesdropper. The idea of the information-theoretic based security in such system was first suggested by Shannon [62], who demonstrated that the perfect information-theoretic secrecy can only be achieved when eavesdropper does not attain any information about the transmitted message from the received signal. This line of work was further explored by Wyner [42], who introduced wiretap channel and established the possibility of creating highly secure communication links. Wyner showed that when the wiretap channel begins to be degraded than the main channel, it becomes easily possible for source and destination to exchange perfectly secure messages, while the eavesdropper can get nothing about this from its perceptions. Later, Csiszàr and Körner [63] generalized Wyner's approach to the transmission of secret information over broadcast channels. To estimate the level of the secrecy in any wireless system using the PLS technique, there are three major secrecy metrics which are discussed as follows:

Secrecy Rate/Capacity

Secrecy rate is a core measure in PLS to evaluate the level of secrecy against eavesdropping attacks. A rate at which perfectly secure transmission can be accomplished from the source to desired destination is known as secrecy rate, and the maximal achievable secrecy rate is named as the secrecy capacity. Secrecy capacity is the maximum achievable level of secrecy rate below which a reliable and secure transmission can be guaranteed. In terms of the mathematical definition, the secrecy capacity is defined as the non-negative difference between the channel capacity of main channel and that of wiretap channel [51]. It is generally expected that the main channel has a larger SNR than the wiretap channel, thereby, the secrecy capacity would be considered as a positive value. Let, C_D and C_E denote the channel capacity of main and wiretap channels, respectively, then, the secrecy capacity can be expressed as

$$C_{\text{sec}} = [C_D - C_E]^+, \tag{2.4}$$

where $[x]^+ \triangleq \max(x, 0)$.

Ergodic Secrecy Capacity (ESC)

The secrecy capacity is determined for the fixed channel, neglecting the fading nature of wireless channel. In fact, the wireless channels are time-varying in nature. Thus, to examine the time-varying feature of these channels, one of the key measures to quantify the capability of average secure transmission is the ESC [64]. It evaluates the average secrecy rate over a sufficiently large number of varying states of wireless fading channels under different delay-tolerant applications [65].

Secrecy Outage Probability (SOP)

In PLS analysis, SOP is an another important metric. The SOP is defined as the probability of an event when the achievable secrecy rate is less than a required threshold secrecy rate [61]. The SOP can be derived using the statistical characteristics of the fading channels of pertinent wireless system.

2.3 Secrecy Performance Analysis of a LMS System with CCI

In this section, we investigate the secrecy performance of a LMS system, where a satellite transmits signal to a legitimate user in the presence of an eavesdropper at the ground. Herein, we consider that CCI signals are present at the user destination node. By leveraging the statistics of underlying shadowed-Rician fading channels for satellite links and Nakagami-m fading for interfering terrestrial links, we derive an accurate expression for SOP of the considered LMS system. To gain more insights, we derive an asymptotic expression for SOP at high SNR regime. We manifest analytically that the CCI significantly affects the performance gain of the system. Moreover, we provide numerical and simulation results to validate our analytical hypothesis.

2.3.1 System and Channel Model Descriptions

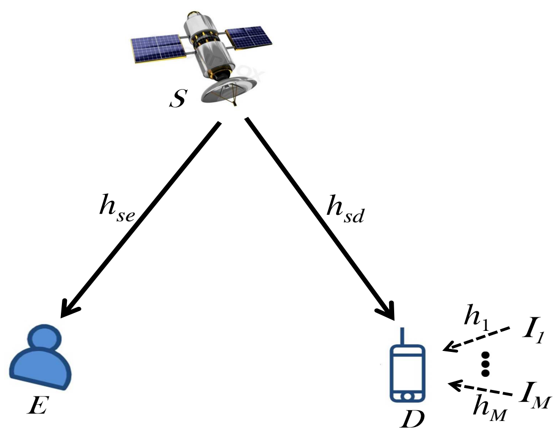

Figure 2.2: System model of an interference-limited LMS system.

We consider a downlink LMS system consisting of a satellite source S, a destination D, and an eavesdropper E as shown in Fig. 2.2. All nodes are equipped with a single-antenna. The destination node is inflicted by M interferers $\{I_i\}_{i=1}^{M}$. The $S \to D$ link and $S \to E$ link are referred to as main link and the wiretap link, respectively. Herein, we consider that both links experience the independent but non-identically distributed (i.ni.d.) shadowed-Rician fading and they are inflicted by additive white Gaussian noise (AWGN) with zero mean and variance σ_j^2, for $j \in \{d, e\}$. Throughout this chapter, we use subscript s for source node S, and subscripts d and e for receiving nodes D and E, respectively.

Satellite S transmits its signal x_s, satisfying $\mathbb{E}[|x_s|^2]=1$, to destination D, where $\mathbb{E}[\cdot]$ represents the expectation operator. The received signal at D can be thus given by

$$y_d = \sqrt{P_s} h_{sd} x_s + \sum_{i=1}^{M} \sqrt{P_i} h_i x_i + n_d, \tag{2.5}$$

where P_s is the transmit power at source S, h_{sd} is the channel coefficient for $S \to D$ link, and n_d represents AWGN at destination D. Herein, P_i is the power of the interferer I_i, h_i is the channel coefficient between ith interferer and D, and x_i is the transmitted signal (with unit energy) from ith interferer.

Meanwhile, eavesdropper E tries to overhear the transmitted signal from S. Thus, the received signal at E can be written as

$$y_e = \sqrt{P_s} h_{se} x_s + n_e, \tag{2.6}$$

where h_{se} is the channel coefficient between S and E, and n_e is the AWGN variable at E.

From (2.5) and (2.6), the instantaneous signal-to-interference-plus-noise ratio (SINR) at destination D and SNR at eavesdropper E can be given, respectively, as

$$\gamma_D = \frac{\gamma_{sd}}{\gamma_I + 1} \tag{2.7}$$

$$\text{and} \qquad \gamma_E = \rho_e |h_{se}|^2 \triangleq \gamma_{se}, \tag{2.8}$$

where $\gamma_{sd} = \rho_d |h_{sd}|^2$, $\gamma_I = \sum_{i=1}^{M} \eta_i |h_i|^2$, with $\rho_d = \frac{P_s}{\sigma_d^2}$, $\rho_e = \frac{P_s}{\sigma_e^2}$, and $\eta_i = \frac{P_i}{\sigma_d^2}$. As such, we can define instantaneous capacity of the main channel (for destination) and of the wiretap channel (for eavesdropper) by $C_D = \log_2(1+\gamma_D)$ and $C_E = \log_2(1+\gamma_E)$, respectively. As the CSI of eavesdropper's channel is available with satellite [48], it can transmit confidential signals at a rate of C_{sec} to ensure perfect secrecy of the considered LMS system.

As the satellite links follow independent shadowed-Rician fading distribution, the PDF of the squared amplitude of the channel coefficient h_{sj} between satellite S and corresponding terrestrial node (i.e., destination D and eavesdropper E), for $j \in \{d, e\}$, can be given by following (2.3) as

$$f_{|h_{sj}|^2}(x) = \alpha_j \sum_{\kappa=0}^{m_j-1} \zeta_j(\kappa) x^{\kappa} \mathrm{e}^{-(\beta_j - \delta_j)x}, \tag{2.9}$$

where $\alpha_j = (2b_j m_j/(2b_j m_j+\Omega_j))^{m_j}/2b_j$, $\beta_j = 1/2b_j$, and $\delta_j = \Omega_j/(2b_j(2b_j m_j+\Omega_j))$, and $\zeta_j(\kappa) = (-1)^\kappa(1-m_j)_\kappa \delta_j^\kappa/(\kappa!)^2$. The PDF of $\gamma_{sd} = \rho_d|h_{sd}|^2$ can be thus derived, by simply applying the transformation of variable, as

$$f_{\gamma_{sd}}(x) = \alpha_d \sum_{\kappa=0}^{m_d-1} \frac{\zeta_d(\kappa)}{(\rho_d)^{\kappa+1}} x^\kappa \mathrm{e}^{-\beta_{\delta_d} x}, \tag{2.10}$$

where $\beta_{\delta_d} = \frac{\beta_d-\delta_d}{\rho_d}$. Similarly, the PDF of γ_{se} can be given as

$$f_{\gamma_{se}}(x) = \alpha_e \sum_{r=0}^{m_e-1} \frac{\zeta_e(r)}{(\rho_e)^{r+1}} x^r \mathrm{e}^{-\beta_{\delta_e} x}, \tag{2.11}$$

where $\beta_{\delta_e} = \frac{\beta_e-\delta_e}{\rho_e}$. By integrating the PDF in (2.10) with the aid of [59, eq. 3.351.2], we can obtain the CDF of γ_{sd} as

$$F_{\gamma_{sd}}(x) = 1 - \alpha_d \sum_{\kappa=0}^{m_d-1} \frac{\zeta_d(\kappa)}{(\rho_d)^{\kappa+1}} \sum_{p=0}^{\kappa} \frac{\kappa!}{p!} \beta_{\delta_d}^{-(\kappa+1-p)} x^p \mathrm{e}^{-\beta_{\delta_d} x}. \tag{2.12}$$

Now, we present the statistical characterization of terrestrial CCI links. As mentioned earlier, the interferer-destination links are assumed to undergo Nakagami-m fading. The derivation of exact PDF of γ_I is very complicated since it involves the sum of i.ni.d. Gamma random variables. Therefore, we use a highly accurate approximation method as proposed in [66] and [67], by which the PDF of γ_I can be given effectively to that of a single Gamma random variable as

$$f_{\gamma_I}(y) \approx \left(\frac{m_I}{\Omega_I}\right)^{m_I} \frac{y^{m_I-1}}{\Gamma(m_I)} \mathrm{e}^{-\frac{m_I}{\Omega_I} y}, \tag{2.13}$$

where the parameters m_I and Ω_I are calculated from moment-based estimators. Hereby, we define $\Phi = \sum_{i=1}^{M} |h_i|^2$. We assume no power control is used i.e., $P_i = P_I$ or $\eta_i = \eta_I$, for $i = 1, ..., M$. Then, we have $\Omega_I = \eta_I \mathbb{E}[\Phi]$ with $\mathbb{E}[\Phi] = \sum_{i=1}^{M} \Omega_i$ and $m_I = \frac{(\mathbb{E}[\Phi])^2}{\mathbb{E}[\Phi^2]-(\mathbb{E}[\Phi])^2}$. For this, the exact moments of Φ can be obtained in terms of the individual moments of the summands as

$$\begin{aligned} \mathbb{E}[\Phi^n] = & \sum_{n_1=0}^{n} \sum_{n_2=0}^{n_1} \cdots \sum_{n_{M-1}=0}^{n_{M-2}} \mathcal{C}_{n_1}^{n} \mathcal{C}_{n_2}^{n_1} \cdots \mathcal{C}_{n_{M-1}}^{n_{M-2}} \\ & \times \mathbb{E}\left[|h_1|^{2(n-n_1)}\right] \mathbb{E}\left[|h_2|^{2(n_1-n_2)}\right] \cdots \mathbb{E}\left[|h_M|^{2(n_{M-1})}\right], \end{aligned} \tag{2.14}$$

where

$$\mathbb{E}\left[|h_i|^n\right] = \frac{\Gamma\left(m_i + \frac{n}{2}\right)}{\Gamma(m_i)} \left(\frac{\Omega_i}{m_i}\right)^{\frac{n}{2}}. \tag{2.15}$$

2.3.2 Secrecy Outage Performance Analysis

In this section, we first derive the SOP expression of the considered LMS system and then examine the achievable diversity order through asymptotic behavior of the SOP expression.

SOP Analysis

The secrecy outage event is said to occur when the secrecy capacity falls below a predefined secrecy rate $\mathcal{R}_{\mathrm{s}}$. Thus, the SOP of the considered LMS system can be formulated as

$$\mathcal{P}_{\mathrm{sec}} = \Pr\left[C_{\mathrm{sec}} < \mathcal{R}_{\mathrm{s}}\right]. \tag{2.16}$$

On inserting C_{sec} from (2.4) into (2.16), $\mathcal{P}_{\mathrm{sec}}$ can be further represented as

$$\mathcal{P}_{\mathrm{sec}} = \Pr\left[\frac{1+\gamma_D}{1+\gamma_E} < \gamma_{\mathrm{s}}\right], \tag{2.17}$$

where $\gamma_{\mathrm{s}} = 2^{\mathcal{R}_{\mathrm{s}}}$. Thus, we can write SOP as

$$\mathcal{P}_{\mathrm{sec}} = \int_0^\infty F_{\gamma_D}(x\gamma_{\mathrm{s}} + \gamma_{\mathrm{s}} - 1) f_{\gamma_E}(x)dx. \tag{2.18}$$

To solve the integral in (2.18), we first require CDF of γ_D. Under the interference-limited scenario, γ_D can be simplified to $\gamma_D \simeq \frac{\gamma_{sd}}{\gamma_{Id}}$, and hence, $F_{\gamma_D}(x)$ can be given as

$$F_{\gamma_D}(x) = \int_0^\infty F_{\gamma_{sd}}(xy) f_{\gamma_I}(y)dy. \tag{2.19}$$

On invoking (2.12) and (2.13) into (2.19), we can calculate $F_{\gamma_D}(x)$ with the help of [59, eq. 3.351.3], which is given as

$$\begin{aligned} F_{\gamma_D}(x) = 1 - \alpha_d \sum_{\kappa=0}^{m_d-1} \frac{\zeta_d(\kappa)}{(\rho_d)^{\kappa+1}} \sum_{p=0}^{\kappa} \frac{\kappa!}{p!} \beta_{\delta_d}^{-(\kappa+1-p)} \\ \times x^p \left(\frac{m_I}{\Omega_I}\right)^{m_I} \frac{\Gamma(p+m_I)}{\Gamma(m_I)} \left(\beta_{\delta_d} x + \frac{m_I}{\Omega_I}\right)^{-(p+m_I)}. \end{aligned} \tag{2.20}$$

Finally, by substituting (2.20) and (2.11) into (2.18), performing the simplification using the identity of Meijer's G-function [59, eq. 9.3] as

$$(1+ax)^{-k} = \frac{1}{\Gamma(k)} G_{1,1}^{1,1}\left[ax \middle| \begin{matrix} 1-k \\ 0 \end{matrix}\right], \tag{2.21}$$

and then solving the integration with the aid of [59, eq. 7.813.1], we obtain SOP as given as

$$\mathcal{P}_{\rm sec} = 1 - \alpha_d \sum_{\kappa=0}^{m_d-1} \frac{\zeta_d(\kappa)}{(\rho_d)^{\kappa+1}} \sum_{p=0}^{\kappa} \frac{\kappa!}{p!} \beta_{\delta_d}^{-(\kappa+1-p)} \sum_{q=0}^{p} \mathcal{C}_q^p \left(\frac{m_I}{\Omega_I}\right)^{m_I} \frac{\gamma_{\rm s}^q (\gamma_{\rm s}-1)^{p-q}}{\Gamma(m_I)}$$
$$\times \left(\beta_{\delta_d}(\gamma_{\rm s}-1) + \frac{m_I}{\Omega_I}\right)^{-(p+m_I)} \alpha_e \sum_{r=0}^{m_e-1} \frac{\zeta_e(r)}{(\rho_e)^{r+1}} \beta_{\delta_e}^{-(q+r+1)}$$
$$\times G_{2,1}^{1,2}\left[\frac{\beta_{\delta_d}\gamma_{\rm s}}{\beta_{\delta_e}\left(\beta_{\delta_d}(\gamma_{\rm s}-1) + \frac{m_I}{\Omega_I}\right)} \middle| \begin{matrix} -(q+r), 1-(p+m_I) \\ 0 \end{matrix}\right]. \tag{2.22}$$

Asymptotic Analysis

To examine the diversity order of system, we perform an asymptotic analysis of SOP at high SNR regime (i.e., assuming $\rho_d \to \infty$). Thus, to evaluate (2.18), we require the asymptotic expression of $F_{\gamma_D}(x)$. For this, first we apply Maclaurin series expansion as $\mathrm{e}^{-z} \underset{z\to 0}{\simeq} 1 - z$ in (2.10) and use only initial term since higher order terms tend to zero. Consequently, the PDF in (2.10) at high SNR follows

$$f_{\gamma_{sd}}(x) \simeq \frac{\alpha_d}{\rho_d} + o(x), \tag{2.23}$$

and the corresponding CDF can be obtained by integrating (2.23) as

$$F_{\gamma_{sd}}(x) \simeq \frac{\alpha_d}{\rho_d} x. \tag{2.24}$$

Further, invoking (2.24) and (2.13) into (2.19), $F_{\gamma_D}(x)$ can be evaluated as

$$F_{\gamma_D}(x) \simeq \frac{\alpha_d x}{\rho_d} \left(\frac{\Omega_I}{m_I}\right) \frac{\Gamma(m_I+1)}{\Gamma(m_I)}. \tag{2.25}$$

Now, inserting (2.25) and (2.11) into (2.18), and using [96, eq. (24)], the asymptotic expression for SOP can be obtained as

$$\mathcal{P}_{\rm sec}^{\infty} \simeq \frac{\alpha_d}{\rho_d} \Omega_I \left[(\gamma_{\rm s}-1) + \gamma_{\rm s}\alpha_e \sum_{r=0}^{m_e-1} \frac{\zeta_e(r)}{(\rho_e)^{r+1}} (r+1)! \beta_{\delta_e}^{-(r+2)} \right]. \tag{2.26}$$

Remarks: Our asymptotic analysis of SOP reveals that the system attains a diversity order of unity. Importantly, the diversity order is not influenced by the fading severity parameters of satellite links and the co-channel interferers.

2.3.3 Numerical and Simulation Results

In this section, we perform numerical investigations to highlight the secrecy performance of the considered LMS system. For this, we assume that the $S \to D$ and

Table 2.1: Estimated Parameters for Interfering Signals involved in (2.13)

No. of interferers	2	3	4	5
m_I	2.9697	5.4340	8.4317	11.9136
Ω_I	3.5	6	9.2	12.7

$S \to E$ links follow shadowed-Rician fading and may experience heavy shadowing (HS) with parameters $(m_j, b_j, \Omega_j) = (1, 0.063, 0.0007)$ and average shadowing (AS) with parameters $(m_j, b_j, \Omega_j) = (5, 0.251, 0.279)$ [58].

Moreover, the channel parameters of interference links are assigned as $\{m_i\}_{i=1}^5 = \{1, 2, 2.5, 3, 3.5\}$ and $\{\Omega_i\}_{i=1}^5 = \{1, 2.5, 2.5, 3.2, 3.5\}$. For each set of multiple interfering signals, the required parameters in (2.13) are computed and illustrated in Table 2.1. To show the impact of interferers on the secrecy performance, we consider M number of interferers at destination node. We fix the interference power $\eta_I = 1$ dB throughout our analysis. Monte-Carlo simulation results are also provided to validate our theoretical analysis.

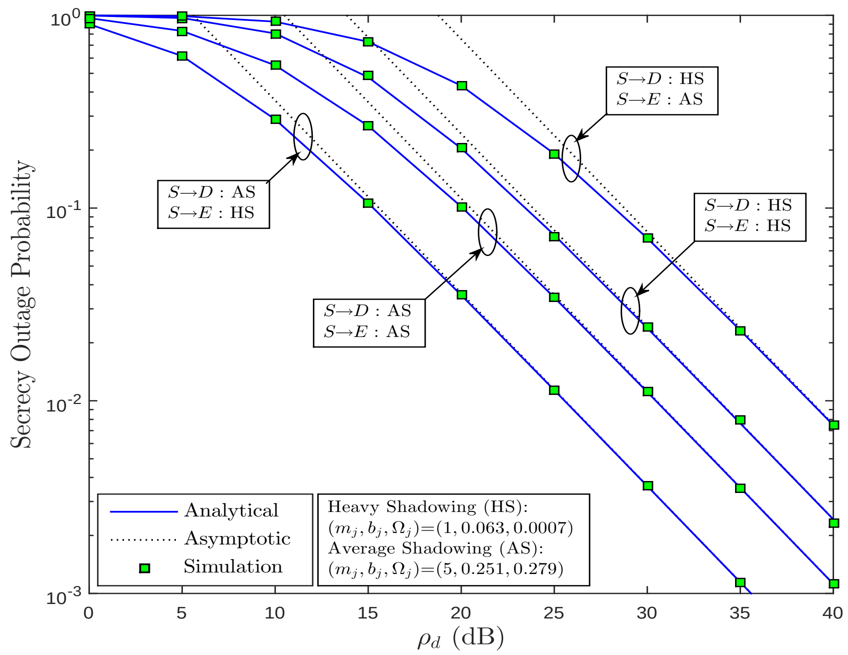

Figure 2.3: SOP performance versus ρ_d for different shadowing scenarios.

Fig. 2.3 shows the SOP curves of considered system for different shadowing scenarios of main (i.e., $S \to D$) and wiretap (i.e., $S \to E$) links. Analytical and asymptotic curves are plotted using (2.22) and (2.26), respectively, and they are found to be well aligned at high SNR. Herein, we plot the SOP curves for four possible different cases with two shadowing scenarios (i.e., AS and HS). For this, we set secrecy rate $\mathcal{R}_s = 0.5$, $\rho_e = 2$ dB, and number of interferers $M = 2$. Specifically, we can observe that system gives better performance for the case when $S \rightarrow D$ link experiences AS and $S \rightarrow E$ link experiences HS. On the other hand, system SOP performance goes worsen when $S \rightarrow D$ and $S \rightarrow E$ links undergo HS and AS, respectively. Moreover, it is apparent from slopes of the curves that system attains diversity order of one. More importantly, it is found that the diversity order remains unaffected from fading severity parameters of the satellite channels.

Fig. 2.4 illustrates the impact of multiple interferers on system's SOP performance. Herein, we set $\mathcal{R}_s = 0.5$, $\rho_e = 2$ dB, and we also consider that both the links (i.e., $S \rightarrow D$ and $S \rightarrow E$) undergo HS. One can observe that the SOP performance of the considered LMS system improves with decreasing number of interferers at destination. For example, better secrecy performance can be realized with less number of interferers at destination as clear from the curves for $M = 1$ as compared to $M = 5$. However, the system diversity order remains unaffected from the number of co-channel interferers.

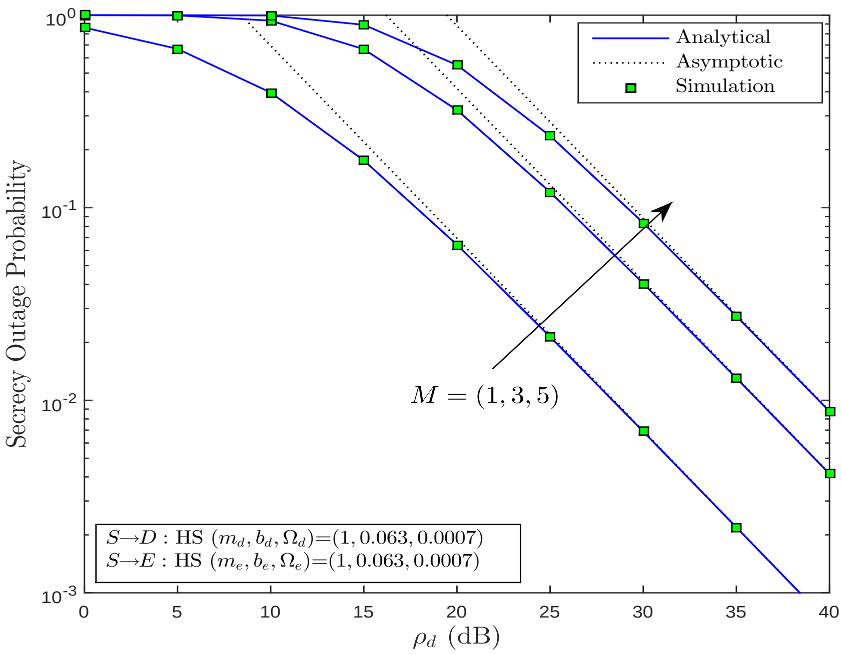

Figure 2.4: Impact of different number of interferers on SOP performance.

2.4 Secrecy Performance Analysis of a LMS System with a UAV-based Friendly Jammer

LMS systems and unmanned aerial vehicles (UAVs) are the key enablers for broadband wireless networks to serve terrestrial mobile users over a broad area with low cost. As such UAVs are gaining a lot of research attraction due to their low cost, high-speed, wireless coverage, and flexible deployment above the ground [68]. UAV has also been deployed as a mobile relay to provide cooperative communication in satellite networks [69]. The integration of the UAV with satellite communications can lead to promising solutions for broadcasting, surveillance, rescue, and navigation [70].

In this section, we investigate the secrecy performance of a LMS system by employing a UAV-based friendly jammer in the presence of an eavesdropper. Herein, we derive the SOP of the considered LMS system under the pertinent heterogeneous channels for the satellite links and the air-to-ground jammer. We further derive an asymptotic SOP expression to gain more insights into the system performance. We reveal the impact of UAV position and other key parameters on the secrecy performance of LMS systems.

2.4.1 System and Channel Model Descriptions

As shown in Fig. 2.5, we consider a downlink LMS system where a satellite source S communicates with a legitimate terrestrial destination D, while an eavesdropper E on the ground attempts to overhear the communication between them. To improve the security performance, we assume that a UAV-based jammer (UAV-J) is employed above the ground, which sends a jamming signal to prevent the eavesdropper from intercepting the confidential information. Note that, hereafter in this chapter, we use subscript u to represent UAV-J. We have adopted shadowed-Rician fading model for the satellite links as discussed in Section 2.1. Further, we assume a three-dimensional (3D) Cartesian coordinate system to represent air-to-ground environment where the horizontal coordinates of the terrestrial node j for $j \in \{d, e\}$ are (x_j, y_j), in meter, and UAV-J is located at $(R\cos\varphi, R\sin\varphi, H)$, with R being the horizontal distance from origin to UAV-J and φ representing the angle of the circle of UAV location with respect to x axis. Herein, it is assumed that both terrestrial nodes are fixed and

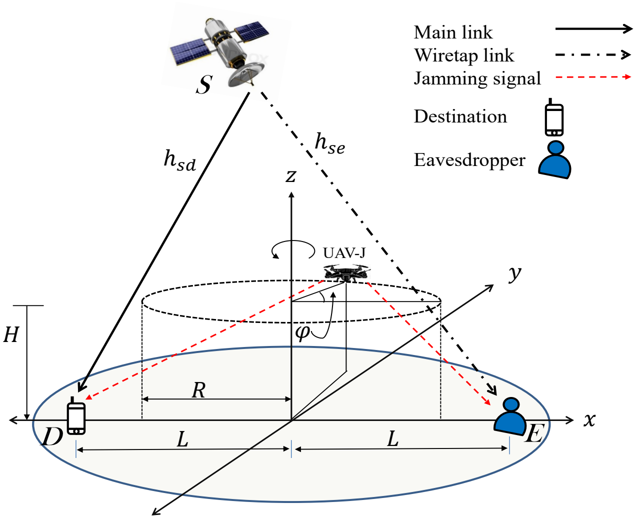

Figure 2.5: System model of a LMS system with a UAV-based friendly jammer.

their locations are known[1] to the UAV-J. Moreover, it is assumed that the UAV-J will hover horizontally at a fixed[2] altitude H, in meter, above the ground. Note that we consider air-to-ground channel model as proposed in [73], whereby the path loss between the UAV-J and ground user j is defined, for LOS and non-LOS (NLOS) links, as

$$\mathcal{L}_j(x,y) = \begin{cases} |d_{uj}|^{a_j}\varsigma_{\text{LOS}}, & \text{for LOS link} \\ |d_{uj}|^{a_j}\varsigma_{\text{NLOS}}, & \text{for NLOS link,} \end{cases} \tag{2.27}$$

where a_j is the path loss exponent over the UAV-J to ground node j link, $|d_{uj}|$ is the distance between the UAV-J and ground node j, and ς_{LOS} and ς_{NLOS} are the attenuation coefficients for the LOS and NLOS links, respectively. In this sequence, the probability of LOS connection mainly depends on the environment such as height and density of buildings, the location of the UAV-J and the users, and the elevation angle between them. Assuming ψ and ϖ being the environmental dependent constants and θ_j as the elevation angle between ground node j and UAV-J, the probability of LOS connection is given as [73]

$$\mathcal{P}_j^{\text{LOS}} = \frac{1}{1+\psi \mathrm{e}^{-\varpi(\theta_j-\psi)}}, \tag{2.28}$$

[1]It is noteworthy that UAV can trace the location of any terrestrial ground node, specifically, of eavesdropper, with the aid of the optical camera and synthetic aperture radar mounted on the UAV [71].

[2]In practice, the value of H can be assigned as a minimum required altitude to avoid building or terrain for safely flying. In addition, the fixed altitude also reduces the required energy consumption in aircraft vertical adjustment [72].

where $\theta_j = \frac{180}{\pi}\sin^{-1}(\frac{H}{d_{uj}})$. Thus, based on (2.28), the probability of NLOS connection is written as $\mathcal{P}_j^{\mathrm{NLOS}} = 1 - \mathcal{P}_j^{\mathrm{LOS}}$.

Now, based on (2.27) and (2.28), the average path loss can be defined as

$$\overline{\mathcal{L}}_j(x,y) = \mathcal{P}_j^{\mathrm{LOS}}|d_{uj}|^{a_j}\varsigma_{\mathrm{LOS}} + \mathcal{P}_j^{\mathrm{NLOS}}|d_{uj}|^{a_j}\varsigma_{\mathrm{NLOS}}. \tag{2.29}$$

Thereby, the average interference from UAV-J to ground node j can be expressed as

$$I_{uj} = \frac{P_J}{\overline{\mathcal{L}}_j(x,y)}, \tag{2.30}$$

where P_J is the transmit power at UAV-J.

Let h_{sd} and h_{se} represent the channel coefficients of the satellite to destination and satellite to eavesdropper channels, and σ_d^2 and σ_e^2 be the AWGN powers at D and E, respectively. During the communication, the satellite S transmits its unit energy signal x_s to destination D with transmit power P_s, meanwhile eavesdropper E tries to wiretap the same signal. Thus, the instantaneous SINRs at destination D and eavesdropper E can be given, respectively, as

$$\Gamma_D = \frac{\gamma_{sd}}{1+\gamma_{ud}} \tag{2.31}$$

and

$$\Gamma_E = \frac{\gamma_{se}}{1+\gamma_{ue}}, \tag{2.32}$$

where $\gamma_{sd} = \rho_d|h_{sd}|^2$, $\gamma_{se} = \rho_e|h_{se}|^2$ with $\rho_d = \frac{P_s}{\sigma_d^2}$ and $\rho_e = \frac{P_s}{\sigma_e^2}$ are transmit SNRs. Herein, $\gamma_{uj} = \frac{I_{uj}}{\sigma_j^2}$ represents the interference-to-noise ratio for ground node j, for $j \in \{d, e\}$. The aforementioned formulation of the SINRs will help in understanding the subsequent discussion.

2.4.2 Secrecy Outage Performance Analysis

In this section, we investigate the secrecy performance of the considered LMS system in terms of the SOP. To delve into SOP analysis, we first write the instantaneous capacity of the main and wiretap channels, respectively, as

$$C_D = \log_2(1+\Gamma_D) \tag{2.33}$$

and

$$C_E = \log_2(1+\Gamma_E). \tag{2.34}$$

Using (2.33) and (2.34) into (2.4), one can obtain the secrecy capacity $\mathcal{C}_{\text{sec}}$ of the considered LMS system. Now, using (2.4) the SOP of the considered LMS system can be expressed as

$$\mathcal{P}_{\text{sec}} = \Pr\left[\frac{1+\Gamma_D}{1+\Gamma_E} < \gamma_{\text{s}}\right]. \tag{2.35}$$

We can hence write $\mathcal{P}_{\text{sec}}$ as

$$\mathcal{P}_{\text{sec}} = \int_0^\infty F_{\Gamma_D}(x\gamma_{\text{s}} + \gamma_{\text{s}} - 1) f_{\Gamma_E}(x) dx. \tag{2.36}$$

Now, to solve the integral in (2.36), we require CDF $F_{\Gamma_D}(\cdot)$ and PDF $f_{\Gamma_E}(\cdot)$. Using (2.31), $F_{\Gamma_D}(x)$ can be given as

$$F_{\Gamma_D}(x) = \int_0^x f_{\gamma_{sd}}(\varrho x) dx. \tag{2.37}$$

where $\varrho = 1 + \gamma_{ud}$. Further, invoking (2.10) into (2.37) and solving the involved integral using [59, eq. 3.351.1], we obtain $F_{\Gamma_D}(x)$ as

$$F_{\Gamma_D}(x) = 1 - \alpha_d \sum_{\kappa=0}^{m_d-1} \frac{\zeta_d(\kappa)}{(\rho_d)^{\kappa+1}} \sum_{p=0}^{\kappa} \frac{\kappa!}{p!} \varrho^p \beta_{\delta_d}^{-(\kappa+1-p)} x^p \mathrm{e}^{-\varrho\beta_{\delta_d} x}. \tag{2.38}$$

Then, the $f_{\Gamma_E}(x)$ can be calculated using (2.11) as $f_{\Gamma_E}(x) = \vartheta f_{\gamma_{se}}(\vartheta x)$ where $\vartheta = 1 + \gamma_{ue}$, and given as

$$f_{\Gamma_E}(x) = \vartheta\alpha_e \sum_{r=0}^{m_e-1} \frac{\zeta_e(r)}{\vartheta^{-r}(\rho_e)^{r+1}} x^r \mathrm{e}^{-(\vartheta\beta_{\delta_e})x}. \tag{2.39}$$

Finally, on invoking (2.38) and (2.39) into (2.36), and performing the solution with the aid of [59, eq. 3.351.3], we get the SOP $\mathcal{P}_{\text{sec}}$ as

$$\begin{aligned}\mathcal{P}_{\text{sec}} = 1 - \alpha_d \sum_{\kappa=0}^{m_d-1} \frac{\zeta_d(\kappa)}{(\rho_d)^{\kappa+1}} \sum_{p=0}^{\kappa} \frac{\kappa!}{p!} \varrho^p \beta_{\delta_d}^{-(\kappa+1-p)} \sum_{q=0}^{p} \mathcal{C}_q^p \gamma_{\text{s}}^q (\gamma_{\text{s}} - 1)^{p-q} \\ \times \sum_{r=0}^{m_e-1} \frac{\zeta_e(r)\alpha_e}{(\rho_e)^{r+1}} (q+r)! \mathrm{e}^{-\varrho\beta_{\delta_d}(\gamma_{\text{s}}-1)} \vartheta^{r+1} \left(\beta_{\delta_d}\varrho\gamma_{\text{s}} + \vartheta\beta_{\delta_e}\right)^{-(q+r+1)}. \end{aligned} \tag{2.40}$$

To obtain further insights, we analyse the asymptotic behaviour of the SOP expression at high SNR regime (i.e., assuming $\rho_d \to \infty$). Thus, we first calculate the asymptotic expression of $F_{\Gamma_D}(x)$ at high SNR, after inserting (2.23) into (2.37), as

$$F_{\gamma_D}(x) \simeq \varrho \frac{\alpha_d}{\rho_d} x. \tag{2.41}$$

Now, on invoking (2.41) and (2.11) into (2.36), and solving the integration with the help of [59, eq. 3.351.3], the asymptotic expression for SOP can be evaluated as

$$\mathcal{P}_{\mathrm{sec}}^{\infty} \simeq \varrho \frac{\alpha_d}{\rho_d} \sum_{r=0}^{m_e-1} \frac{\zeta_e(r)\alpha_e}{(\rho_e)^{r+1}} (q+r)! \vartheta^{r+1} \left(\vartheta \beta_{\delta_e}\right)^{-(r+1)} \\ \times \left(\gamma_{\mathrm{s}}(r+1)! \left(\vartheta \beta_{\delta_e}\right)^{-1} - (\gamma_{\mathrm{s}}-1) r!\right). \tag{2.42}$$

From (2.42), it can be observed that the considered system achieves a diversity order of unity. It is worth noting that the achievable diversity order is independent of fading severity parameter of the satellite link.

2.4.3 Numerical and Simulation Results

We perform the numerical investigations to examine the impact of different UAV-J's locations and shadowing scenarios of the satellite links on SOP performance of the considered system. For this, we consider two scenarios of shadowing, namely, average shadowing (AS) and heavy shadowing (HS) for the main and wiretap links, whose channel parameters are kept same as given in Section 2.3.3. Without loss of generality, we consider suburban environment with $\psi = 4.88$, $\varpi = 0.43$, $\varsigma_{\mathrm{LOS}} = 0.1$ dB, and $\varsigma_{\mathrm{NLOS}} = 21$ dB, and fix the altitude of the UAV-J $H = 100$ meters and path loss exponent $a_j = 2$ for $j \in \{d, e\}$. In addition, we consider the horizontal coordinates of D and E are fixed as $(-L, 0)$ and $(L, 0)$, respectively, with $L = 100$ in meters. Monte-Carlo simulation results are also provided to justify our theoretical analysis.

In Fig. 2.6, we plot the SOP curves versus ρ_d for different values of φ. Here, we consider both main and wiretap links undergo HS of shadowed-Rician fading. We set $R = 100$ meters, $\rho_e = 10$ dB, $P_J = 40$ dB, and $\mathcal{R}_s = 0.1$. Recall that the φ and R collectively define the location of the UAV-J. Accordingly, when $\varphi = 0^0$, UAV-J is located near to the eavesdropper. Besides, for $\varphi = 180^0$, UAV-J flies near to the destination. From Fig. 2.6, it can be found that the system achieves better SOP performance for $\varphi = 0^0$ (i.e., when UAV-J is near to eavesdropper E) as compared to for $\varphi = 180^0$ (i.e., when UAV-J is near to destination D). This is owing to the fact that when UAV-J is located near to eavesdropper, it can more effectively seize the eavesdropper from intercepting the satellite information. These observation indicates that the secrecy level of a LMS system can be enhanced by deploying UAV-J near to eavesdropper location.

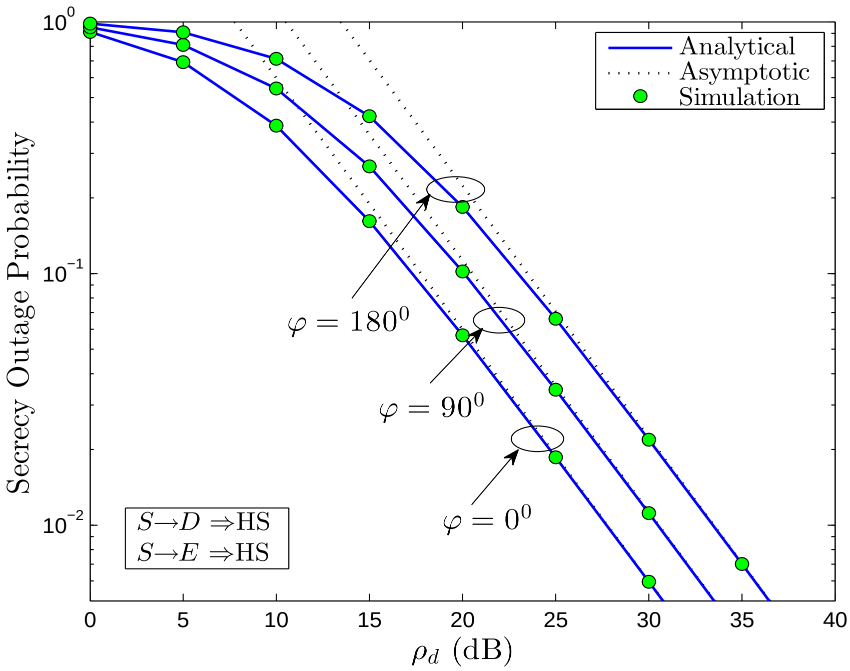

Figure 2.6: SOP of the considered system for different values of φ.

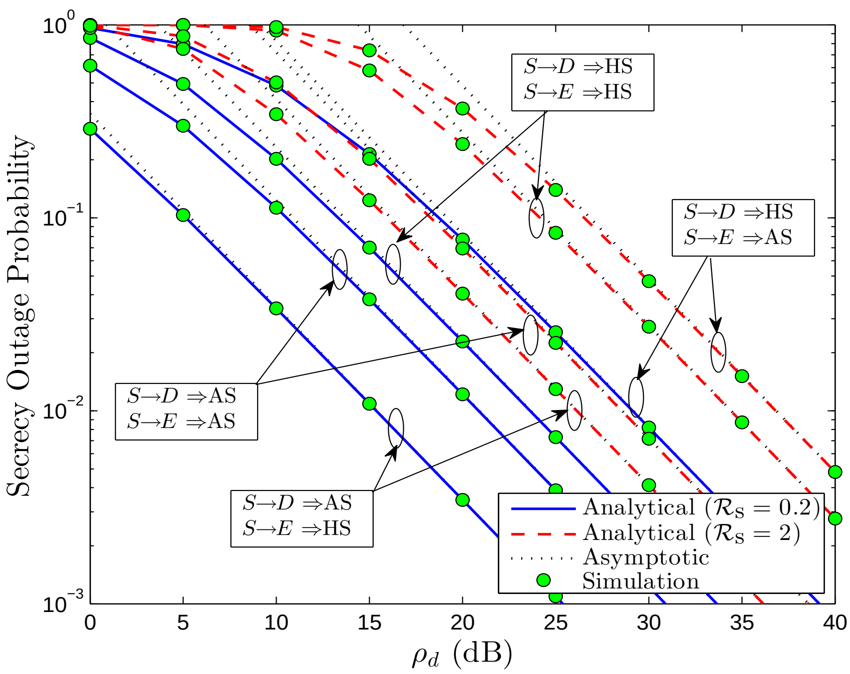

Figure 2.7: SOP for different shadowing scenarios.

Fig. 2.7 depicts the SOP performance of the considered system with different shadowing scenarios of the satellite links for $\mathcal{R}_s \in \{0.2, 2\}$. Herein, we keep $\varphi = 45^0$, $\rho_e = 0$ dB, $P_J = 40$ dB, and $R = 100$ meters. We can see from the SOP curves that system achieves best performance when $S \rightarrow D$ link experiences AS and $S \rightarrow E$ link experiences HS, whereas, for vice-versa case i.e., $S \rightarrow D$ and $S \rightarrow E$ links undergo

HS and AS, respectively, system SOP performance goes worsen. We also observe, from Fig. 2.7, that the SOP increases with an increasing $\mathcal{R}_s$, which indicates that the system can attain improved secrecy performance with small target secrecy rate.

2.5 Summary

In this chapter, we investigated the secrecy performance of LMS systems with a single terrestrial eavesdropper. First, we evaluated the secrecy performance of a LMS system in the presence of CCI at terrestrial user. We derived accurate and asymptotic SOP expressions for the considered system. We characterized the system diversity order and deduced that it remains unaffected by the fading severity parameters of satellite links and the number of co-channel interferers. Further, we investigated the secrecy performance of a LMS system using a UAV-based friendly jammer in the presence of an eavesdropper on the ground. For this configuration, we derived the exact and asymptotic SOP expressions over pertinent channels of the satellite-ground and the UAV-ground links. Our results demonstrated that while the satellite channel conditions and interference have severe impact on the LMS systems performance, the UAV jammer can notably improve the secrecy performance. Finally, we provided numerical results to vindicate the analytical derivations and to enlightened the impact of various key parameters on secrecy performance of the considered LMS systems.

CHAPTER 3

MULTI-USER HYBRID SATELLITE-TERRESTRIAL RELAY NETWORKS WITH OUTDATED CHANNEL STATE INFORMATION AND CO-CHANNEL INTERFERENCE

In the previous chapter, we analyzed the LMS systems where the satellite directly communicates with the terrestrial users. However, the LOS links between satellite and terrestrial users are blocked due to severe shadowing and heavy obstacles [6]. This unavailability of LOS link is known as the masking effect. The end-to-end communication requires a consistent network that can overcome the problem of masking effect and can provide uninterrupted connectivity in remote areas while minimizing the deployment cost. To meet this challenge, researchers have envisioned the terrestrial cooperation with satellite communication systems. To realize this, the satellite networks have integrated well with existing terrestrial networks, introducing a new architecture defined as HSTRN [3], [7]. Recently, HSTRNs have received considerable attention due to its several advantages in variety of applications such as navigation, disaster relief, military, and defense [5].

While many works have analyzed the performance of HSTRN using AF [18]-[23] and DF relaying [24]-[26], they have focussed on a single-user scenario. It is worthwhile to notice that the future generation of communication requires to handle and serve a vast number of ground users, thus, studying a multi-user scenario is critically important. Multi-user relay network is a more challenging configuration, mainly due to the involved heterogenous channels' complexity and increased dynamics. In a multi-user relay network, the relay assists the communication between a source and multiple destinations/users [27]. The HSTRN has also been extended to a multi-user scenario [29], [30] since the futuristic 5G mobile systems need to provide high throughput services to a large number of terrestrial users. Specifically, in [29], a multi-user HSTRN has been studied with opportunistic user scheduling to exploit multi-user diversity. In [30], a multi-user multi-relay architecture for HSTRN has been explored. However, these works have assumed the knowledge of perfect channel state information (CSI) to facilitate the user selection process. In practice, the CSI for user selection may be outdated due to various reasons such as feedback delay, mobility, etc. In addition, with dense frequency reuse in wireless networks, the HSTRN is susceptible to CCI, which is inevitable in practical scenarios. Although few works [21]-[23], [26] have considered the impact of CCI on the performance of HSTRN, they are limited to the single-user scenarios.

On another front, significant research attention has been directed towards deploying multiple-input multiple-output (MIMO) technology with satellite communication systems to achieve performance gains with multiple antennas [74]-[76]. Indeed, the channel and propagation characteristics of satellite links are different from the terrestrial links and thereby potential MIMO exploitation in satellite communication is of primary concern. Basically, sparse scattering environment and insufficient antenna separation at the transmitting satellite leads to a strong LOS and high channel correlation. As such, the multipath fading effects over the spatial dimension may get subsided and the potential benefits of MIMO could not be fully exploited in such scenario. With this view point, few recent works have considered correlated fading channels over satellite links, and exploited beamforming [77], [31] and space-time coding [38], respectively, in dual-hop and single-hop LMS systems. Besides these, majority of the works on MIMO satellite communications (e.g., see [78]-[80] and references therein) have adopted i.i.d. assumptions for the pertaining multiple channels. In fact, the theoretical studies on such topics have recently begun with a main focus on determining the system performance limits. Moreover, in the most recent literature [81]-[83], it has been emphasized that the satellite communication system must be integrated with the terrestrial network to fulfil the requirements of 5G wireless network. Thereby, it is important to evaluate the performance of multi-user HSTRNs with MIMO configuration in realistic operating conditions.

Motivated by the above, in this chapter, we study a more generalized HSTRN architecture[1] by configuring with multiple terrestrial users, multiple co-channel interferers at the AF relay, and multiple antennas at the satellite and users/destinations.

[1] This corresponds to a downlink multi-user HSTRN, where a source satellite communicates with multiple users with the assistance of a single-antenna relay at the ground.

Specifically, we employ maximal-ratio transmission (MRT) and maximal-ratio combining (MRC) based transmit and receive beamforming at the satellite and land mobile users respectively. Considering mobility of land users, we employ user scheduling with outdated CSI over Nakagami-m fading channels of pertinent links. Moreover, by adopting both i.i.d. and correlated shadowed-Rician fading channels for satellite links[2], we conduct a comprehensive performance analysis of the proposed HSTRN in terms of OP, EC and average SEP. Such investigation is important to understand the achievable performance of HSTRN for its potential deployment in futuristic wireless systems. The major contributions of this chapter can be summarized as follows:

- We study a multi-user HSTRN employing AF relaying in the presence of CCI and opportunistic scheduling of terrestrial users in the presence of outdated CSI, under shadowed-Rician faded satellite links and Nakagami-m faded terrestrial links.

- By considering both i.i.d. and correlated shadowed-Rician fading scenarios at satellite, we derive accurate expressions of OP and EC for the proposed HSTRN over generalized hybrid channels. Moreover, we derive average SEP expressions under i.i.d. shadowed-Rician fading scenarios.

- We further deduce asymptotic OP and average SEP expressions in the high SNR regime to evaluate the diversity performance of the considered HSTRN and illustrate that the achievable diversity order would not get affected with antenna correlation at the satellite. Our numerical and simulation results highlight the impact of various key parameters on the system performance of HSTRNs.

The rest of this chapter is organized as follows. In Section 3.1, we describe system and channel model for a multi-antenna multi-user HSTRN. We carry out the performance analysis of proposed HSTRN in Section 3.2. Section 3.3 presents the numerical and simulation results, and finally, the summary of the chapter is presented in Section 3.4.

[2]Herein, we assume perfect CSI acquisition with negligible Doppler spread over the satellite-relay links by considering a satellite and a fixed location of the terrestrial relay. In fact, the CSI acquisition would be difficult for the satellite links due to high latency and fast variation. Although such problems of channel estimation and associated imperfection have been studied in [19] for a basic HSTRN, the research in this domain is in still infancy and is a topic for future investigation. Nevertheless, our presented results in this chapter will serve as a benchmark of system performance for the multi-antenna multiuser HSTRN.

3.1 System and Channel Model Descriptions

As shown in Fig. 3.1, we consider a multi-antenna multi-user HSTRN wherein a satellite source S communicates with N terrestrial destinations $\{D_n\}_{n=1}^{N}$ via a terrestrial AF relay R. The satellite S and all destinations D_n are equipped with N_s and N_d antennas, respectively, while the relay R is equipped with a single-antenna. Further, we consider that the relay node is inflicted by M co-channel interferers $\{I_i\}_{i=1}^{M}$ and each user is inflicted by the AWGN. This is a commonly adopted scenario with respect to frequency division relaying systems [24], [26], [84] wherein the relay and user nodes experience different interference patterns[3]. Due to shadowing effects, the direct links between the satellite and the terrestrial users are not available. These direct links could be masked in certain scenarios such as heavy shadowing, obstacles in the environment, users moving to tunnels, indoor users, etc. We denote $\mathbf{h}_{sr}$ as the $N_s \times 1$ shadowed-Rician channel vector between N_s antennas

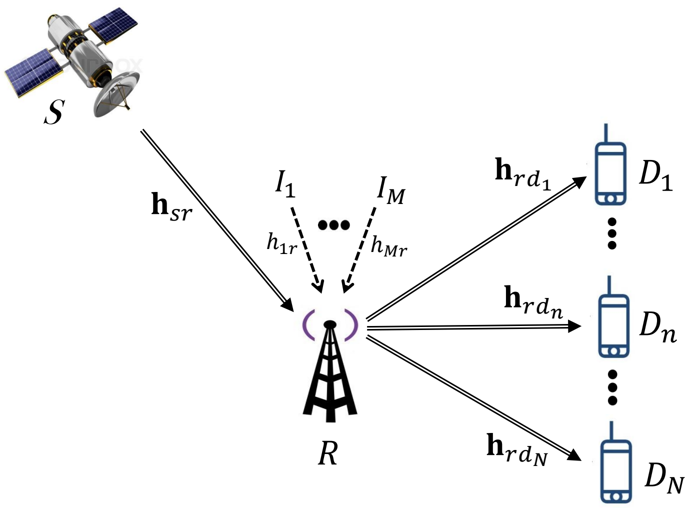

Figure 3.1: HSTRN model with MIMO configuration.

at S and the single antenna at R. Likewise, $\mathbf{h}_{rd_n}$ represents the $N_d \times 1$ Nakagami-m channel vector between the single antenna at R and the N_d antennas at nth destination D_n. Whereas, h_{ir} denotes the channel coefficient of the link between ith interferer and relay. We assume that the fading coefficients $\{h_{ir}\}_{i=1}^{M}$ are independent and non-identically distributed (i.ni.d.) Nakagami-m random variables (RVs) with corresponding severity parameters $\{m_{ci}\}_{i=1}^{M}$ and average powers $\{\Omega_{ci}\}_{i=1}^{M}$.

[3]This could be possible when the AF relay lies close to other earth stations and/or other relays and/or clusters of non-targeted land users, while it cannot support advanced interference management techniques. As such, the relay in our proposed system model may encounter with a CCI environment.

The overall communication takes place in two temporal phases by employing opportunistic scheduling of terrestrial users. In the first phase, satellite S beamforms its unit energy signal x_s to the relay R. The received signal at R can be expressed as

$$y_r = \sqrt{P_s}\mathbf{h}_{sr}^{\dagger}\mathbf{w}_{sr}x_s + \sum_{i=1}^{M}\sqrt{P_{ci}}h_{ir}x_i + n_r, \tag{3.1}$$

where P_s is the transmit power at S, $\mathbf{w}_{sr}$ is the $N_s \times 1$ transmit weight vector, P_{ci} is the transmit power of the ith interferer, x_i is the unit energy signal of the ith interferer, and $n_r \sim \mathcal{CN}(0, \sigma^2)$ is AWGN at relay R. The transmit beamforming vector $\mathbf{w}_{sr} \in \mathbb{C}^{N_s \times 1}$ is chosen according to the principle of MRT [85] as $\mathbf{w}_{sr} = \frac{\mathbf{h}_{sr}}{||\mathbf{h}_{sr}||_F}$. Note that this requires CSI for the satellite-relay links only and hence may offer a low implementation complexity[4].

During the second phase, the relay R first amplifies the received signal y_r by a gain factor $\mathcal{G}$ and then forwards it to the selected destination D_n. Hence, the received signal at D_n after MRC is expressed as

$$y_{d_n} = \mathcal{G}\sqrt{P_r}\mathbf{w}_{rd_n}^{\dagger}\mathbf{h}_{rd_n}y_r + \mathbf{w}_{rd_n}^{\dagger}\mathbf{n}_{d_n}, \tag{3.2}$$

where P_r is the transmit power at R, $\mathbf{w}_{rd_n}$ is the $N_d \times 1$ receive weight vector, and $\mathbf{n}_{d_n} \sim \mathcal{CN}(\mathbf{0}, \sigma^2\mathbf{I})$ is the $N_d \times 1$ AWGN vector. According to the MRC principle [85], the receive beamforming vector is chosen as $\mathbf{w}_{rd_n} = \frac{\mathbf{h}_{rd_n}}{||\mathbf{h}_{rd_n}||_F}$. Thus, based on (3.2), the end-to-end SINR can be obtained as

$$\gamma_{sd_n} = \frac{\gamma_{sr}\gamma_{rd_n}}{\gamma_{rd_n}(\gamma_c + 1) + \frac{1}{\mathcal{G}^2\sigma^2}}, \tag{3.3}$$

where $\gamma_{sr} = \eta_s||\mathbf{h}_{sr}||_F^2$, $\gamma_{rd_n} = \eta_r||\mathbf{h}_{rd_n}||_F^2$, $\gamma_c = \sum_{i=1}^{M}\eta_{ci}|h_{ir}|^2$, with $\eta_s = \frac{P_s}{\sigma^2}$, $\eta_r = \frac{P_r}{\sigma^2}$ and $\eta_{ci} = \frac{P_{ci}}{\sigma^2}$. For variable-gain relaying, the gain $\mathcal{G}$ in (3.3) can be determined as

$$\mathcal{G} = \sqrt{\frac{1}{P_s|\mathbf{h}_{sr}^{\dagger}\mathbf{w}_{sr}|^2 + \sum_{i=1}^{M}P_{ci}|h_{ir}|^2 + \sigma^2}}, \tag{3.4}$$

wherein it is assumed that the amplification process is performed by a simple normalization of the total received power at the relay without applying any interference mitigation technique, as widely adopted in similar studies [23], [27], [80]. Thus, the instantaneous end-to-end SINR, for variable-gain AF relaying, at the nth destination

[4]This is in contrast to other beamforming schemes which may require CSI of overall links to attain a better performance. It would however be very difficult for the satellite to acquire the CSI of interfering links as well as that of multi-antenna multi-user links over the second hop in practice.

is given by

$$\gamma_{sd_n} = \frac{\gamma_{sr}\gamma_{rd_n}}{\gamma_{sr} + (\gamma_{rd_n} + 1)(\gamma_c + 1)}. \tag{3.5}$$

To harness the multi-user diversity inherent in the considered network, an opportunistic scheduling of D_n is employed, wherein the transmissions are scheduled based on the channel quality of multiple destinations with the relay. For this, the relay first selects the destination with the strongest R-D_n link, and then feeds back the index of the selected user to the satellite S. As such, the instantaneous SNR of the relay-user link is formulated by

$$\gamma_{rd} = \max_{n=1,\ldots,N} \gamma_{rd_n}. \tag{3.6}$$

In realistic scenarios, where the channel changes rapidly enough, the CSI obtained by the relay could be outdated [86]. Thereby, a delay exists between the user selection phase and the data transmission phase. Hence, the actual end-to-end SINR associated with the scheduled user can be given by

$$\gamma_{sd} = \frac{\gamma_{sr}\widetilde{\gamma}_{rd}}{\gamma_{sr} + (\widetilde{\gamma}_{rd} + 1)(\gamma_c + 1)}, \tag{3.7}$$

where $\widetilde{\gamma}_{rd}$ is the delayed version of γ_{rd}. Let $\widetilde{\gamma}_{rd_n}$ be the delayed version of γ_{rd_n} and is given by $\widetilde{\gamma}_{rd_n} = \eta_r||\widetilde{\mathbf{h}}_{rd_n}||_F^2$, where $\widetilde{\mathbf{h}}_{rd_n}$ is the delayed version of $\mathbf{h}_{rd_n}$. The correlation coefficient between $\widetilde{\gamma}_{rd_n}$ and γ_{rd_n} can be given by $\rho_{rd} = J_0^2(2\pi f_o \tau)$ [87] with $J_0(\cdot)$ being the zeroth-order Bessel function of the first kind [59, eq. 8.411], f_o is the Doppler frequency, and τ is the time delay.

Now, we discuss the channel model and statistical characteristics of the satellite and terrestrial links. Considering uncorrelated shadowed-Rician fading model, the PDF of the squared amplitude of the channel coefficient $h_{sr}^{(\imath)}$ between satellite's $\imath$th antenna and the relay R is given by [16]

$$f_{|h_{sr}^{(\imath)}|^2}(x) = \alpha\, \mathrm{e}^{-\beta x}\, {}_1F_1(m_s; 1; \delta x), \; x \geq 0. \tag{3.8}$$

Considering $\mathbf{h}_{sr}$ with i.i.d. enteries, we can simplify (3.8) for integer-valued severity parameters, using (2.2), as

$$f_{|h_{sr}^{(\imath)}|^2}(x) = \alpha \sum_{\kappa=0}^{m_s-1} \zeta(\kappa) x^{\kappa} \mathrm{e}^{-(\beta-\delta)x}. \tag{3.9}$$

The PDF of γ_{sr} can be derived, by following the procedure given in [58, App. A] and making a transformation of variates using (3.9), as

$$f_{\gamma_{sr}}(x) = \sum_{i_1=0}^{m_s-1} \cdots \sum_{i_{N_s}=0}^{m_s-1} \frac{\Xi(N_s)}{(\eta_s)^{\Lambda}} x^{\Lambda-1} \mathrm{e}^{-\beta_\delta x}, \tag{3.10}$$

where $\Xi(N_s) = \alpha^{N_s} \prod_{\kappa=1}^{N_s} \zeta(i_\kappa) \prod_{t=1}^{N_s-1} \mathcal{B}(\sum_{\iota=1}^{t} i_\iota + t, i_{t+1}+1)$, $\Lambda = \sum_{\kappa=1}^{N_s} i_\kappa + N_s$, $\beta_\delta = \frac{\beta-\delta}{\eta_s}$, and $\mathcal{B}(.,.)$ is the Beta function [59, eq. 8.384.1]. After integrating (3.10) using the fact [59, eq. 3.351.2], the corresponding CDF can be obtained as

$$F_{\gamma_{sr}}(x) = 1 - \sum_{i_1=0}^{m_s-1} \cdots \sum_{i_{N_s}=0}^{m_s-1} \frac{\Xi(N_s)}{(\eta_s)^{\Lambda}} \sum_{p=0}^{\Lambda-1} \frac{\Gamma(\Lambda)}{p!} \beta_\delta^{-(\Lambda-p)} x^p \mathrm{e}^{-\beta_\delta x}. \tag{3.11}$$

Next, we discuss the statistical characteristics of the satellite channel under correlated shadowed-Rician fading. Let us define $\mathbf{A}_s$ as $N_s \times N_s$ positive definite matrix with constituent elements as correlation coefficients of the LOS components of the shadowed-Rician fading links, we can model the channel vector $\mathbf{h}_{sr} = \mathbf{A}_s^{\frac{1}{2}} \bar{\mathbf{h}}_{sr} + \tilde{\mathbf{h}}_{sr}$, where the LOS component $\bar{\mathbf{h}}_{sr}$ constitutes i.i.d. Nakagami-m RVs and the scattering component $\tilde{\mathbf{h}}_{sr}$ comprises the i.i.d. complex Gaussian RVs [16], [31], and $\mathbf{A}_s^{\frac{1}{2}}$ is the matrix square root of $\mathbf{A}_s$. As such, by following the procedure as given in [60, Th.2], the PDF and CDF of γ_{sr} can be derived, respectively, as

$$f_{\gamma_{sr}}(x) = \zeta \sum_{k=0}^{\infty} \varrho_k \sum_{\ell=0}^{m_s N_s + k - N_s} \varpi_{k,\ell}\, x^{N_s+\ell-1} \mathrm{e}^{-\left(\frac{\varphi}{\eta_s}\right)x} \tag{3.12}$$

and

$$F_{\gamma_{sr}}(x) = 1 - \zeta \sum_{k=0}^{\infty} \varrho_k \sum_{\ell=0}^{m_s N_s + k - N_s} \varpi_{k,\ell} \sum_{p=0}^{N_s+\ell-1} \frac{\Gamma(N_s+\ell)}{p!} \left(\frac{\varphi}{\eta_s}\right)^{-(N_s+\ell-p)} x^p \mathrm{e}^{-\left(\frac{\varphi}{\eta_s}\right)x}, \tag{3.13}$$

where $\zeta = \prod_{i=1}^{N_s} \left(\frac{\lambda}{\lambda_i}\right)^{m_s}$, $\varrho_k = \frac{\epsilon_k}{(2b)^{N_s}} \left(\frac{2b}{2b+\lambda}\right)^{m_s N_s + k}$, $\varpi_{k,\ell} = \frac{(-1)^\ell (N_s - m_s N_s - k)_\ell}{\eta_s^{N_s+\ell}\, \ell!\, \Gamma(N_s+\ell)} \left(\frac{\lambda}{2b(2b+\lambda)}\right)^{\ell}$, $\varphi = \frac{1}{2b} - \frac{\lambda}{2b(2b+\lambda)}$, $\lambda = \min\{\lambda_i, i = 1, ..., N_s\}$, λ_i are the eigenvalues of matrix $\widetilde{\mathbf{R}}_s = \left(\frac{\Omega_s}{m_s}\right) \mathbf{R}_s$, $\epsilon_0 = 1$, and

$$\epsilon_{k+1} = \frac{m_s}{k+1} \sum_{j=1}^{k+1} \left[\sum_{i=1}^{N_s} \left(1 - \frac{\lambda}{\lambda_i}\right)^j \right] \epsilon_{k+1-j}, \quad k = 0, 1, 2, \ldots$$

Considering the terrestrial links with a cluster of $\{D_n\}_{n=1}^{N}$ users, the pertinent channels follow i.i.d. Nakagami-m fading[5] with fading severity m_d and average power

[5] As in various works [27], [80], we follow i.i.d. assumption for terrestrial users to keep the system performance analysis tractable. Such scenario may however be realized in practice when the terrestrial users are clustered relatively close together (location-based clustering).

Ω_d. As such, the PDF and CDF of channel gain γ_{rd_n} are given, respectively, by

$$f_{\gamma_{rd_n}}(x) = \left(\frac{m_d}{\Omega_d \eta_r}\right)^{m_d N_d} \frac{x^{m_d N_d - 1}}{\Gamma(m_d N_d)} \mathrm{e}^{-\frac{m_d x}{\Omega_d \eta_r}} \tag{3.14}$$

and

$$F_{\gamma_{rd_n}}(x) = \frac{1}{\Gamma(m_d N_d)} \Upsilon\left(m_d N_d, \frac{m_d x}{\Omega_d \eta_r}\right), \tag{3.15}$$

where $\Upsilon(\cdot,\cdot)$ and $\Gamma(\cdot)$ represent, respectively, the lower incomplete and the complete gamma functions [59, eq. 8.350].

Lemma 1. *The PDF of $\widetilde{\gamma}_{rd}$ can be given by*

$$f_{\widetilde{\gamma}_{rd}}(x) = N \sum_{j=0}^{N-1} \mathcal{C}_j^{N-1} \frac{(-1)^j}{\Gamma(m_d N_d)} \sum_{l=0}^{j(m_d N_d - 1)} \omega_l^j \sum_{i=0}^{l} \mathcal{C}_i^l \times \left(\frac{m_d}{\Omega_d \eta_r}\right)^{m_d N_d + i} \xi_{i,j,l}\, x^{m_d N_d - 1 + i} e^{-\frac{x}{\chi_j}}, \tag{3.16}$$

where $\xi_{i,j,l} = \frac{\Gamma(m_d N_d + l)\rho_{rd}^i (1-\rho_{rd})^{l-i}}{\Gamma(m_d N_d + i)[j(1-\rho_{rd})+1]^{m_d N_d + l + i}}$, $\chi_j = \frac{[j(1-\rho_{rd})+1]\Omega_d \eta_r}{m_d(j+1)}$ and the coefficients ω_l^j, for $0 \le l \le j(m_d N_d - 1)$, can be calculated recursively (with $\varepsilon_l = \frac{1}{l!}$) as $\omega_0^j = (\varepsilon_0)^j$, $\omega_1^j = j(\varepsilon_1)$, $\omega_{j(m_d N_d - 1)}^j = (\varepsilon_{m_d N_d - 1})^j$, $\omega_l^j = \frac{1}{l\varepsilon_0}\sum_{g=1}^{l}[gj - l + g]\varepsilon_g \omega_{l-g}^j$ for $2 \le l \le m_d N_d - 1$, and $\omega_l^j = \frac{1}{l\varepsilon_0}\sum_{g=1}^{m_d N_d - 1}[gj - l + g]\varepsilon_g \omega_{l-g}^j$ for $m_d N_d \le l < j(m_d N_d - 1)$.

Proof. By applying order statistics, the PDF of γ_{rd} can be represented as

$$f_{\gamma_{rd}}(x) = N[F_{\gamma_{rd_n}}(x)]^{N-1} f_{\gamma_{rd_n}}(x), \ x \ge 0. \tag{3.17}$$

On invoking the CDF $F_{\gamma_{rd_n}}(x)$ with series form of $\Upsilon(\cdot,\cdot)$ [59, eq. 8.352.1] and the respective PDF into (3.17), and then applying binomial and multinomial expansions [59, eq. 0.314], we get

$$f_{\gamma_{rd}}(x) = N \sum_{j=0}^{N-1} \mathcal{C}_j^{N-1} \frac{(-1)^j}{\Gamma(m_d N_d)} \sum_{l=0}^{j(m_d N_d - 1)} \left(\frac{m_d}{\Omega_d \eta_r}\right)^{m_d N_d + l} \omega_l^j\, x^{m_d N_d + l - 1} \mathrm{e}^{-\frac{m_d (j+1) x}{\Omega_d \eta_r}}. \tag{3.18}$$

Since $\widetilde{\gamma}_{rd}$ and γ_{rd} are correlated Gamma-distributed RVs, the PDF of $\widetilde{\gamma}_{rd}$ can be obtained as

$$f_{\widetilde{\gamma}_{rd}}(x) = \int_0^\infty f_{\widetilde{\gamma}_{rd}|\gamma_{rd}}(x|y) f_{\gamma_{rd}}(y) dy, \tag{3.19}$$

where $f_{\widetilde{\gamma}_{rd}|\gamma_{rd}}(x|y)$ is the conditional PDF of $\widetilde{\gamma}_{rd}$, conditioned on γ_{rd}. It can be given by [85]

$$f_{\widetilde{\gamma}_{rd}|\gamma_{rd}}(x|y) = \frac{1}{(1-\rho_{rd})}\left(\frac{m_d}{\Omega_d \eta_r}\right)\left(\frac{x}{\rho_{rd} y}\right)^{\frac{m_d N_d - 1}{2}} \times \mathrm{e}^{-\frac{m_d(\rho_{rd} y + x)}{(1-\rho_{rd})\Omega_d \eta_r}} \mathcal{I}_{m_d N_d - 1}\left(\frac{2 m_d \sqrt{\rho_{rd} x y}}{(1-\rho_{rd})\Omega_d \eta_r}\right), \tag{3.20}$$

where $\mathcal{I}_\nu(\cdot)$ is the νth order modified Bessel function of the first kind [59, eq. 8.406.1]. On substituting (3.20) and (3.18) into (3.19), and simplifying using the approach in [87], we obtain (3.16). ■

Now, differently from $f_{\gamma_{sr}}(x)$ and $f_{\widetilde{\gamma}_{rd}}(x)$, the derivation of exact PDF of γ_c is rather intractable since it involves the sum of i.ni.d. Gamma RVs and hence needs to perform a multifold convolution, becoming cumbersome even for small number of interferers. Therefore, as in [66] and [88], we resort to a highly accurate approximation approach [67] by which the PDF of γ_c can be represented effectively to that of a single Gamma RV as

$$f_{\gamma_c}(x) \approx \left(\frac{m_I}{\Omega_I}\right)^{m_I} \frac{x^{m_I - 1}}{\Gamma(m_I)} \mathrm{e}^{-\frac{m_I}{\Omega_I} x}, \tag{3.21}$$

where the parameters m_I and Ω_I are calculated from moment-based estimators. For this, we define $\Phi = \sum_{i=1}^{M} |h_{ir}|^2$ and, without loss of generality, we assume no power control is used i.e., $P_{ci} = P_c$ or $\eta_{ci} = \eta_c = \frac{P_c}{\sigma^2}$. Then, from [66] and [88], we have $\Omega_I = \eta_c \Omega_c$ with $\Omega_c = \mathbb{E}[\Phi] = \sum_{i=1}^{M} \Omega_{ci}$ and $m_I = \frac{\Omega_c^2}{\mathbb{E}[\Phi^2] - \Omega_c^2}$. Herein, the exact moments of Φ can be obtained in terms of the individual moments of the summands as

$$\mathbb{E}[\Phi^n] = \sum_{n_1=0}^{n} \sum_{n_2=0}^{n_1} \cdots \sum_{n_{M-1}=0}^{n_{M-2}} \mathcal{C}_{n_1}^{n} \mathcal{C}_{n_2}^{n_1} \cdots \mathcal{C}_{n_{M-1}}^{n_{M-2}} \times \mathbb{E}\left[|h_{1r}|^{2(n-n_1)}\right] \mathbb{E}\left[|h_{2r}|^{2(n_1-n_2)}\right] \cdots \mathbb{E}\left[|h_{Mr}|^{2(n_{M-1})}\right], \tag{3.22}$$

where

$$\mathbb{E}\left[|h_{ir}|^n\right] = \frac{\Gamma\left(m_{ci} + \frac{n}{2}\right)}{\Gamma(m_{ci})} \left(\frac{\Omega_{ci}}{m_{ci}}\right)^{\frac{n}{2}}. \tag{3.23}$$

3.2 Performance Analysis

In this section, we conduct the performance analysis of the considered network by deriving expressions of OP and EC under both uncorrelated and correlated shadowed-Rician fading, and average SEP under uncorrelated shadowed-Rician fading.

3.2.1 OP Analysis

The OP is defined as the probability that the instantaneous end-to-end SINR γ_{sd} falls below a certain threshold γ_{th}. It can be mathematically represented as

$$\mathcal{P}_{\mathrm{out}} = \Pr\left[\gamma_{sd} < \gamma_{\mathrm{th}}\right] = F_{\gamma_{sd}}(\gamma_{\mathrm{th}}). \tag{3.24}$$

We now evaluate OP in (3.24) under uncorrelated and correlated shadowed-Rician fading cases. First, we derive OP under uncorrelated shadowed-Rician fading case in the following theorem.

With Uncorrelated Shadowed-Rician Fading

Theorem 1. *The closed-form expression of CDF $F_{\gamma_{sd}}(x)$, under uncorrelated shadowed-Rician fading, can be given as*

$$\begin{aligned}
F_{\gamma_{sd}}(x) &= 1 - N \sum_{i_1=0}^{m_s-1} \cdots \sum_{i_{N_s}=0}^{m_s-1} \frac{\Xi(N_s)}{\eta_s^{\Lambda}} \sum_{p=0}^{\Lambda-1} \frac{\Gamma(\Lambda)}{p!} \sum_{j=0}^{N-1} \mathcal{C}_j^{N-1} \frac{(-1)^j}{\Gamma(m_d N_d)} \sum_{l=0}^{j(m_d N_d-1)} \omega_l^j \sum_{i=0}^{l} \mathcal{C}_i^l \\
&\times \left(\frac{m_d}{\Omega_d \eta_r}\right)^{m_d N_d+i} \xi_{i,j,l}\, e^{-\frac{x}{\chi_j}} \sum_{q=0}^{p} \mathcal{C}_q^p \sum_{\nu=0}^{m_d N_d+i-1} \mathcal{C}_\nu^{m_d N_d+i-1} \beta_\delta^{-\Lambda+p+\frac{\nu-q}{2}} \chi_j^{1+\frac{\nu-q}{2}} (1+x)^{\frac{\nu+q}{2}} \\
&\times x^{m_d N_d+i+p-1-\left(\frac{\nu+q}{2}\right)} \frac{1}{\Gamma(m_I)} \left(\frac{m_I}{\Omega_I}\right)^{m_I} \Gamma\left(1+p+m_I+\nu-q\right) \Gamma\left(p+m_I\right) \vartheta_{x,I}^{-\frac{1}{2}[2(p+m_I)+\nu-q]} \\
&\times e^{\frac{\beta_\delta x(1+x)}{2\vartheta_{x,I}\chi_j}} \mathcal{W}_{-\frac{1}{2}[2(p+m_I)+\nu-q],\frac{1}{2}(\nu-q+1)} \left(\frac{\beta_\delta x(1+x)}{\vartheta_{x,I}\chi_j}\right),
\end{aligned} \tag{3.25}$$

where $\vartheta_{x,I} = \beta_\delta x + \frac{m_I}{\Omega_I}$ and $\mathcal{W}_{u,v}(\cdot)$ is the Whittaker function [59, eq. 9.222].

Proof. See Appendix 3.A. ∎

Now, by substituting (3.25) into (3.24), the OP for HSTRN can be computed directly at $x = \gamma_{\mathrm{th}}$.

Theorem 1 presents an analytical expression for the precise OP evaluation of the considered HSTRN, and it allows for the complicated hybrid channel scenario in the presence of outdated CSI and CCI with arbitrary number of antennas, number of interferers, and number of users over entire SNR regime.

Achievable Diversity Order

Although the analytical OP expression using (3.25) is quite useful and provide several insights from numerical plots, it is too complex to predict diversity order for the proposed HSTRN. Therefore, we need to obtain an equivalent OP expression in asymptotically large SNR regime that helps in identifying the joint impact of outdated CSI, CCI, system configuration, and channel fading parameters on the achievable diversity order. For this, in the high SNR regime, we assume $\eta_s, \eta_r \to \infty$ with the ratio $\frac{\eta_s}{\eta_r}$ held constant. Consequently, we derive the asymptotic CDF of γ_{sd} under two scenarios, namely outdated CSI ($\rho_{rd} < 1$) and perfect CSI ($\rho_{rd} = 1$), under the influence of CCI as

$$F_{\gamma_{sd}}(x) \simeq \frac{\alpha^{N_s} x^{N_s}}{N_s!(\eta_s)^{N_s}} \left(\frac{\Omega_I}{m_I}\right)^{N_s} \frac{\Gamma(N_s+m_I)}{\Gamma(m_I)} + \begin{cases} \Psi_1(x), & \text{if } \rho_{rd} < 1 \\ \Psi_2(x), & \text{if } \rho_{rd} = 1 \end{cases}, \tag{3.26}$$

where $\Psi_1(x)$ and $\Psi_2(x)$ are given, respectively, as

$$\Psi_1(x) = N \sum_{j=0}^{N-1} \mathcal{C}_j^{N-1} \frac{(-1)^j}{\Gamma(m_d N_d)} \frac{\left(\frac{m_d}{\Omega_d}\right)^{m_d N_d} x^{m_d N_d}}{[j(1-\rho_{rd})+1]^{m_d N_d} (\eta_r)^{m_d N_d}} \tag{3.27}$$

and $$\Psi_2(x) = \frac{1}{[\Gamma(m_d N_d + 1)]^N} \left(\frac{m_d x}{\Omega_d \eta_r}\right)^{m_d N_d N}. \tag{3.28}$$

Proof. See Appendix 3.B. ■

Now, plugging (3.26) into (3.24) and evaluating at $x = \gamma_{\text{th}}$, an asymptotic OP expression can be obtained. Thereby, one can examine the achievable diversity order for the considered HSTRN under the following cases.

Case-1: For perfect CSI ($\rho_{rd} = 1$) and low level of CCI ($\eta_c \ll \eta_s$), the achievable diversity order (defined by the smallest negative exponent of η_s or η_r) is $\min(N_s, m_d N_d N)$.

Case-2: For outdated CSI ($\rho_{rd} < 1$) and low level of CCI ($\eta_c \ll \eta_s$), the achievable diversity order is $\min(N_s, m_d N_d)$.

Case-3: For a high level of CCI i.e., when η_c increases in the same level as η_s while maintaining the ratio $\frac{\eta_c}{\eta_s}$ a finite constant, the diversity order reduces to zero regardless of the perfect or outdated CSI cases.

Remarks: The advantage of a multi-antenna satellite is clearly highlighted by the achievable diversity order of the considered HSTRN. Specifically, with a low level of CCI and perfect CSI condition, the system can exploit multi-user diversity when the number of antennas at satellite is sufficiently high, otherwise the system performance is bottlenecked by the satellite-relay link whose fading parameter m_s does not contribute to the diversity order. Hence, the deployment of multiple antennas at the satellite is important to realize the achievable performance gain. In addition, when the CSI is outdated, the advantage of multi-user diversity cannot be realized.

With Correlated Shadowed-Rician Fading

Now, we present the analytical OP expression for the considered HSTRN over correlated shadowed-Rician fading channels by deriving the pertaining CDF of γ_{sd} in the following theorem.

Theorem 2. *The expression of CDF $F_{\gamma_{sd}}(x)$, under correlated shadowed-Rician fading, is given as*

$$F_{\gamma_{sd}}(x) = 1 - \zeta N \sum_{k=0}^{\infty} \varrho_k \sum_{\ell=0}^{m_s N_s + k - N_s} \varpi_{k,\ell} \sum_{p=0}^{N_s+\ell-1} \frac{\Gamma(N_s+\ell)}{p!} \sum_{j=0}^{N-1} \mathcal{C}_j^{N-1} \frac{(-1)^j}{\Gamma(m_d N_d)} \sum_{l=0}^{j(m_d N_d - 1)} \omega_l^j$$
$$\times \sum_{i=0}^{l} \mathcal{C}_i^l \left(\frac{m_d}{\Omega_d \eta_r}\right)^{m_d N_d + i} \xi_{i,j,l}\, e^{-\frac{x}{\chi_j}} \sum_{q=0}^{p} \mathcal{C}_q^p \sum_{\nu=0}^{m_d N_d + i - 1} \mathcal{C}_\nu^{m_d N_d + i - 1} \left(\frac{\varphi}{\eta_s}\right)^{-N_s - \ell + p + \frac{\nu - q}{2}} \chi_j^{1 + \frac{\nu - q}{2}}$$
$$\times (1+x)^{\frac{\nu+q}{2}} x^{m_d N_d + i + p - 1 - \left(\frac{\nu+q}{2}\right)} \frac{1}{\Gamma(m_I)} \left(\frac{m_I}{\Omega_I}\right)^{m_I} \Gamma\left(1 + p + m_I + \nu - q\right) \Gamma\left(p + m_I\right)$$
$$\times \left(\vartheta'_{x,I}\right)^{-\frac{1}{2}[2(p+m_I)+\nu-q]} e^{\frac{\varphi x(1+x)}{2\eta_s \vartheta'_{x,I} \chi_j}} \mathcal{W}_{-\frac{1}{2}[2(p+m_I)+\nu-q], \frac{1}{2}(\nu-q+1)} \left(\frac{\varphi x(1+x)}{\eta_s \vartheta'_{x,I} \chi_j}\right), \tag{3.29}$$

where $\vartheta'_{x,I} = \frac{\varphi}{\eta_s} x + \frac{m_I}{\Omega_I}$ and other parameters are the same as defined previously.

Proof. See Appendix 3.C. ∎

Thus, invoking (3.29) in (3.24) and evaluating at $x = \gamma_{\text{th}}$ yield the desired OP for correlated shadowed-Rician fading case.

Achievable Diversity Order

To examine the diversity order of HSTRN under correlated shadowed-Rician fading channels, we first obtain the CDF $F_{\gamma_{sd}}(x)$ at high SNR as

$$F_{\gamma_{sd}}(x) \simeq \zeta \sum_{k=0}^{\infty} \frac{\epsilon_k x^{N_s} \Gamma(N_s + m_I)}{(2b)^{N_s} (N_s - 1)! (\eta_s)^{N_s}} \left(\frac{2b}{2b+\lambda}\right)^{m_s N_s + k}$$
$$\times \frac{1}{\Gamma(m_I)} \left(\frac{\Omega_I}{m_I}\right)^{N_s} + \begin{cases} \Psi_1(x), & \text{if } \rho_{rd} < 1 \\ \Psi_2(x), & \text{if } \rho_{rd} = 1 \end{cases}, \tag{3.30}$$

where $\Psi_1(x)$ and $\Psi_2(x)$ are same as defined previously.

Proof. See Appendix 3.D. ∎

From (3.30), we can deduce that the achievable diversity order of HSTRN under correlated shadowed-Rician fading is $\min(N_s, m_d N_d N)$ for $\rho_{rd} = 1$ and $\min(N_s, m_d N_d)$

for $\rho_{rd} < 1$. This is same as obtained for the case of uncorrelated shadowed-Rician fading.

Remarks: The system diversity order of proposed HSTRN is not affected by correlation in satellite antennas as clear from (3.30). It is important to note that due to a strong LOS and sparse scattering environment, the channel correlation would exist at the transmitting satellite. However, since the diversity order does not get affected, the deployment of multiple antennas at satellite in HSTRN is greatly motivated for futuristic wireless system design.

3.2.2 Average SEP Analysis

In this subsection, we evaluate the average SEP performance of the considered system. As such the SEP evaluation requires an additional integration which makes it more complex even for a single-channel. For analytical tractability, we herein consider a single-antenna at user destination node (i.e., $N_d = 1$) and derive the analytical and asymptotic average SEP expressions for uncorrelated shadowed-Rician fading case. Since the correlation of satellite antennas would affect average SEP performance similar to OP performance, moreover, the diversity order does not get affected from antenna correlation. Therefore, we have focused only on uncorrelated shadowed-Rician fading case. For typical modulation formats, the average SEP can be expressed as

$$\mathcal{P}_e = aE_{\gamma_{sd}}\left[Q\left(\sqrt{2b\gamma_{sd}}\right)\right], \tag{3.31}$$

where $Q(\cdot)$ represents the Gaussian-Q function, and a and b are the modulation-specific constants, e.g., $a = 1$ and $b = 1$ for binary phase-shift keying (BPSK); $a = 2$ and $b = \sin^2\left(\frac{\pi}{\mathcal{M}}\right)$ for $\mathcal{M}$-ary phase-shift keying (when $\mathcal{M} \geq 4$). Further, we can statistically simplify (3.31) as

$$\mathcal{P}_e = \frac{a}{2}\sqrt{\frac{b}{\pi}}\int_0^\infty \mathrm{e}^{-bx}F_{\gamma_{sd}}(x)dx. \tag{3.32}$$

Theorem 3. *The closed-form expression of average SEP, under uncorrelated shadowed-*

Rician fading, can be obtained as

$$\mathcal{P}_e = \frac{a}{2} - N\frac{a}{2}\sqrt{\frac{b}{\pi}}\sum_{i_1=0}^{m_s-1}\cdots\sum_{i_{N_s}=0}^{m_s-1}\frac{\Xi(N_s)}{\eta_s^{\Lambda}}\sum_{p=0}^{\Lambda-1}\frac{\Gamma(\Lambda)}{p!}{\beta_\delta}^{-(\Lambda-p)}\sum_{q=0}^{p}\mathcal{C}_q^p\left(\frac{m_I}{\Omega_I}\right)^{m_I}\sum_{j=0}^{N-1}\mathcal{C}_j^{N-1}$$
$$\times\frac{(-1)^j}{\Gamma(m_d)}\sum_{l=0}^{j(m_d-1)}\omega_l^j\sum_{i=0}^{l}\mathcal{C}_i^l\left(\frac{m_d}{\Omega_d\eta_r}\right)^{m_d+i}\frac{\Gamma(q+m_I)}{\Gamma(m_I)}\xi_{i,j,l}\sum_{k=0}^{m_d+i-1}\frac{\Gamma(m_d+i)}{k!}$$
$$\times\Gamma\left(k+p+\frac{1}{2}\right)\chi_j^{(m_d+i-k)}\left(\frac{m_I}{\Omega_I}\right)^{-(q+m_I)}\left(\frac{m_I}{\Omega_I\beta_\delta}\right)^{k+p+\frac{1}{2}}$$
$$\times\ \Psi\left[k+p+\frac{1}{2}, k+p+\frac{1}{2}-(q+m_I-1), \frac{m_I}{\Omega_I\beta_\delta}\left(b+\beta_\delta+\frac{1}{\chi_j}\right)\right]. \tag{3.33}$$

Proof. See Appendix 3.E. ■

Achievable Diversity Order

To reveal more insights, we perform asymptotic analysis of the average SEP expression at high SNR regime and obtain the asymptotic expression under two cases, viz., $\rho_{rd}<1$ (i.e., outdated CSI) and $\rho_{rd}=1$ (i.e., perfect CSI), as

$$\mathcal{P}_e^{\infty} \simeq \frac{a}{2}\sqrt{\frac{b}{\pi}}\frac{\alpha^{N_s}}{N_s!(\eta_s)^{N_s}}\sum_{q=0}^{N_s}\mathcal{C}_q^{N_s}\frac{\Gamma(q+m_I)}{\Gamma(m_I)}\left(\frac{m_I}{\Omega_I}\right)^{-q}$$
$$\times\Gamma\left(N_s+\frac{1}{2}\right)b^{-\left(N_s+\frac{1}{2}\right)} + \begin{cases}\psi_1, & \text{if } \rho_{rd}<1\\ \psi_2, & \text{if } \rho_{rd}=1\end{cases}, \tag{3.34}$$

where ψ_1 and ψ_2 are given, respectively, as

$$\psi_1 = N\frac{a}{2}\sqrt{\frac{b}{\pi}}\sum_{j=0}^{N-1}\mathcal{C}_j^{N-1}\frac{(-1)^j}{\Gamma(m_d)}\Gamma\left(m_d+\frac{1}{2}\right)\frac{b^{-(m_d+\frac{1}{2})}}{[j(1-\rho_{rd})+1]^{m_d}}\left(\frac{m_d}{\Omega_d\eta_r}\right)^{m_d} \tag{3.35}$$

and

$$\psi_2 = \frac{a}{2}\sqrt{\frac{b}{\pi}}\frac{\Gamma\left(m_dN+\frac{1}{2}\right)b^{-\left(m_dN+\frac{1}{2}\right)}}{[\Gamma(m_d+1)]^N}\left(\frac{m_d}{\Omega_d\eta_r}\right)^{m_dN}. \tag{3.36}$$

Remarks: As can be observed from (3.34), under low level of CCI, system attains a diversity order of $\min(N_s, m_d)$ for outdated CSI and $\min(N_s, m_dN)$ for perfect CSI. In addition, it is shown, through numerical and simulation results in Section 3.3, that for a high CCI level i.e., when η_c increases in the same proportion as η_s and keeping the ratio $\frac{\eta_c}{\eta_s}$ a finite constant, the diversity order reduces to zero. Interestingly, it is realized that the achievable diversity order remains unaffected by the fading parameter m_s of the satellite link and the number of co-channel interferers M.

Next, we analyze the EC of the considered system with variable-gain and fixed-gain AF relay. As such the fixed-gain relays, that benefits from the knowledge of the first hop's average channel gain in contrast to the instantaneous channel information, shown to have comparable performance with variable gain relays which make them attractive from a practical standpoint [89].

3.2.3 EC Analysis

In this section, we determine analytical expressions of EC for the considered HSTRN under variable-gain AF relaying and fixed-gain AF relaying protocols. The EC (in bits/s/Hz) is defined as the statistical expectation of the instantaneous mutual information between the source and destination. For end-to-end SINR γ_{sd}, it is mathematically expressed as

$$\overline{C} = \frac{1}{2} E\left[\log_2(1+\gamma_{sd})\right], \tag{3.37}$$

where the factor 1/2 accounts for two-phase transmissions from S to D_n. We now proceed to derive closed-form expressions of EC for variable-gain AF relaying and fixed-gain AF relaying protocols under both uncorrelated and correlated shadowed-Rician fading cases.

Under Variable-Gain AF Relaying

On inserting the SINR γ_{sd} from (3.7) into (3.37), one can readily represent

$$\overline{C} = \frac{1}{2} E\left[\log_2\left(\frac{(1+\gamma_{sc})(1+\widetilde{\gamma}_{rd})}{1+\gamma_{sc}+\widetilde{\gamma}_{rd}}\right)\right], \tag{3.38}$$

where $\gamma_{sc} = \frac{\gamma_{sr}}{\gamma_c}$ is defined under the dominance of interference over noise. The direct computation of EC in (3.38) is cumbersome. Alternatively, we adopt the moment generating function (MGF)-based approach, as in [90], to evaluate EC as

$$\overline{C} = \frac{1}{2\ln 2}\int_0^\infty \mathrm{e}^{-s}\widehat{\mathcal{M}}_{\gamma_{sc}}(s)ds - \frac{1}{2\ln 2}\int_0^\infty \mathrm{e}^{-s}\widehat{\mathcal{M}}_{\gamma_{sc}}(s)\mathcal{M}_{\widetilde{\gamma}_{rd}}(s)ds, \tag{3.39}$$

where

$$\widehat{\mathcal{M}}_{\gamma_{sc}}(s) = \int_0^\infty \mathrm{e}^{-sx}\left[1-F_{\gamma_{sc}}(x)\right]dx \tag{3.40a}$$

and

$$\mathcal{M}_{\widetilde{\gamma}_{rd}}(s) = \int_0^\infty \mathrm{e}^{-sx} f_{\widetilde{\gamma}_{rd}}(x)dx. \tag{3.40b}$$

Herein, $\widehat{\mathcal{M}}_{\gamma_{sc}}(s)$ and $\mathcal{M}_{\widetilde{\gamma}_{rd}}(s)$ respectively denote the complementary MGF transform and the MGF of γ_{sc} and $\widetilde{\gamma}_{rd}$. Based on (3.39), we now derive closed-form expressions of EC for variable-gain AF relaying under uncorrelated and correlated shadowed-Rician fading cases.

Theorem 4. *The EC in (3.39) for variable-gain AF relaying under uncorrelated shadowed-Rician fading can be given as*

$$\overline{C} = \overline{C}_1 - \overline{C}_2, \tag{3.41}$$

where $\overline{C}_1$ *and* $\overline{C}_2$ *are respectively given as*

$$\begin{aligned}\overline{C}_1 = &\frac{1}{2\ln 2}\sum_{i_1=0}^{m_s-1}\cdots\sum_{i_{N_s}=0}^{m_s-1}\frac{\Xi(N_s)}{\eta_s^{\Lambda}}\sum_{p=0}^{\Lambda-1}\frac{\Gamma(\Lambda)}{p!}\beta_\delta^{-(\Lambda-p)}\left(\frac{\Omega_I}{m_I}\right)^p\\ &\times\frac{1}{\Gamma(m_I)}G_{2,2}^{2,2}\left[\frac{m_I}{\Omega_I\beta_\delta}\middle|\begin{matrix}1+p,1\\1+p,p+m_I\end{matrix}\right]\end{aligned} \tag{3.42}$$

and

$$\begin{aligned}\overline{C}_2 = &\frac{N}{2\ln 2}\sum_{i_1=0}^{m_s-1}\cdots\sum_{i_{N_s}=0}^{m_s-1}\frac{\Xi(N_s)}{\eta_s^{\Lambda}}\sum_{p=0}^{\Lambda-1}\frac{\Gamma(\Lambda)}{p!}\beta_\delta^{-(\Lambda-p)}\frac{1}{\Gamma(m_I)}\left(\frac{\Omega_I}{m_I}\right)^p\\ &\times\sum_{j=0}^{N-1}\mathcal{C}_j^{N-1}\frac{(-1)^j}{\Gamma(m_dN_d)}\sum_{l=0}^{j(m_dN_d-1)}\omega_l^j\sum_{i=0}^{l}\mathcal{C}_i^l\left(\frac{m_d}{\Omega_d\eta_r}\right)^{m_dN_d+i}\xi_{i,j,l}\\ &\times\chi_j^{m_dN_d+i}G_{1,[1:1],0,[2:1]}^{1,1,1,2,1}\left[\begin{matrix}\frac{m_I}{\Omega_I\beta_\delta}\\ \chi_j\end{matrix}\middle|\begin{matrix}-p;1;1-m_dN_d-i\\ --;m_I+p,1+p;0\end{matrix}\right],\end{aligned} \tag{3.43}$$

where $G_{2,2}^{2,2}[\cdot]$ *is the Meijer's G-function [59, eq. 8.2.1.1] and* $G_{1,[1:1],0,[2:1]}^{1,1,1,2,1}[\cdot]$ *is the generalized Meijer's G-function of two-variables [91].*

Proof. See Appendix 3.F. ■

Note that the Meijer's G-function can be readily evaluated using built-in function in Mathematica, while the generalized Meijer's G-function can be proficiently evaluated using approach as presented in [92, Table II]. As such, the derived expression in Theorem 4 is quite useful for precise EC performance evaluation of the considered HSTRN in the generic scenario with arbitrary number of antennas, users, and co-channel interferers.

The EC under correlated shadowed-Rician fading is presented in the following theorem.

Theorem 5. *The EC in (3.39) for variable-gain AF relaying under correlated shadowed-Rician fading can be given as*

$$\overline{C} = \overline{C}_{o1} - \overline{C}_{o2}, \tag{3.44}$$

where $\overline{C}_{o1}$ and $\overline{C}_{o2}$ are respectively given by

$$\overline{C}_{o1} = \frac{\zeta}{2\ln 2}\sum_{k=0}^{\infty}\varrho_k \sum_{\ell=0}^{m_sN_s+k-N_s}\varpi_{k,\ell}\sum_{p=0}^{N_s+\ell-1}\frac{\Gamma(N_s+\ell)}{p!}\left(\frac{\varphi}{\eta_s}\right)^{-(N_s+\ell-p)}$$
$$\times\frac{1}{\Gamma(m_I)}\left(\frac{\Omega_I}{m_I}\right)^p G_{2,2}^{2,2}\left[\frac{\frac{m_I}{\Omega_I}}{\frac{\varphi}{\eta_s}}\middle|\begin{matrix}1+p,1\\1+p,p+m_I\end{matrix}\right] \tag{3.45}$$

and

$$\overline{C}_{o2} = \frac{\zeta N}{2\ln 2}\sum_{k=0}^{\infty}\varrho_k \sum_{\ell=0}^{m_sN_s+k-N_s}\varpi_{k,\ell}\sum_{p=0}^{N_s+\ell-1}\frac{\Gamma(N_s+\ell)}{p!}\left(\frac{\varphi}{\eta_s}\right)^{-(N_s+\ell-p)}$$
$$\times\frac{1}{\Gamma(m_I)}\left(\frac{\Omega_I}{m_I}\right)^p\sum_{j=0}^{N-1}\mathcal{C}_j^{N-1}\frac{(-1)^j}{\Gamma(m_dN_d)}\sum_{l=0}^{j(m_dN_d-1)}\omega_l^j\sum_{i=0}^{l}\mathcal{C}_i^l\left(\frac{m_d}{\Omega_d\eta_r}\right)^{m_dN_d+i}$$
$$\times\,\xi_{i,j,l}\;\chi_j^{m_dN_d+i}G_{1,[1:1],0,[2:1]}^{1,1,1,2,1}\left[\begin{matrix}\frac{m_I\eta_s}{\Omega_I\varphi}\\ \chi_j\end{matrix}\middle|\begin{matrix}-p;1;1-m_dN_d-i\\ --;m_I+p,1+p;0\end{matrix}\right]. \tag{3.46}$$

Proof. See Appendix 3.G. ■

It is worth mentioning that although the derived expression in Theorem 5 contains infinite series and Meijer's G-function, it can be evaluated efficiently through Mathematica by taking the finite number of terms to achieve the required accuracy, as illustrated numerically in Section 3.3.

Under Fixed-Gain AF Relaying

For fixed-gain AF relaying, the gain factor is calculated as

$$\mathcal{G}^{\mathrm{FG}} = \sqrt{\frac{1}{E[P_s|\mathbf{h}_{sr}^{\dagger}\mathbf{w}_{sr}|^2]+E[\sum_{i=1}^{N_s}P_{ci}|h_{ir}|^2]+\sigma^2}}, \tag{3.47}$$

thereby, the SINR, for fixed-gain AF relaying, can be obtained as

$$\gamma_{sd_n}^{\mathrm{FG}} = \frac{\gamma_{sr}\gamma_{rd_n}}{\gamma_{rd_n}(\gamma_c+1)+\mathcal{U}}, \tag{3.48}$$

where $\mathcal{U}\triangleq\frac{1}{(\mathcal{G}^{\mathrm{FG}}\sigma)^2}=E[\gamma_{sr}]+E[\gamma_c]+1$. Consequently, the actual end-to-end SINR associated with the scheduled user is given by

$$\gamma_{sd} = \frac{\gamma_{sr}\widetilde{\gamma}_{rd}}{\widetilde{\gamma}_{rd}(\gamma_c+1)+\mathcal{U}}. \tag{3.49}$$

On using the SINR from (3.49) into (3.37), we have

$$\overline{C} = \frac{1}{2\ln 2}E\left[\ln\left(1+\frac{\gamma_{sr}\widetilde{\gamma}_{rd}}{\widetilde{\gamma}_{rd}(\gamma_c+1)+\mathcal{U}}\right)\right]. \tag{3.50}$$

Under interference-limited scenario [27], we can simplify (3.50) by assuming the dominance of CCI over noise (i.e., $\gamma_c + 1 \simeq \gamma_c$) to express

$$\overline{C} = \frac{1}{2\ln 2} E\left[\ln\left(\frac{1+\frac{\widetilde{\gamma}_{rd}}{\mathcal{U}}(\gamma_{sr}+\gamma_c)}{1+\frac{\widetilde{\gamma}_{rd}}{\mathcal{U}}\gamma_c}\right)\right]$$
$$= \overline{C}_{\gamma_1} - \overline{C}_{\gamma_2}, \tag{3.51}$$

where $\overline{C}_{\gamma_l} = \frac{1}{2\ln 2} E[\ln(1+\gamma_l)]_{l\in\{1,2\}}$, $\gamma_1 = Z(\gamma_{sr}+\gamma_c)$, $\gamma_2 = Z\gamma_c$ with $Z \triangleq \frac{\widetilde{\gamma}_{rd}}{\mathcal{U}}$. Since γ_1 and γ_2 are statistically dependent, the evaluation of (3.51) is not very straightforward. To proceed, we first condition on $Z = z$ to compute the conditional expectation in (3.51) and then uncondition it by averaging over PDF of Z. Thus, we can write

$$\overline{C} = \int_0^\infty \left[\overline{C}_{\gamma_1|Z} - \overline{C}_{\gamma_2|Z}\right] f_Z(z)dz, \tag{3.52}$$

where $\overline{C}_{\gamma_l|Z} = \frac{1}{2\ln 2} E[\ln(1+\gamma_l|Z)]_{l\in\{1,2\}}$. Further, as in [93], $\overline{C}_{\gamma_l|Z}$ can be given by means of MGF transform as

$$\overline{C}_{\gamma_l|Z} = \frac{1}{2\ln 2}\int_0^\infty \frac{\mathrm{e}^{-s}}{s}\left(1-\mathcal{M}_{\gamma_l}(s|Z)\right)ds. \tag{3.53}$$

The conditional MGF transform of γ_1 involving the sum of RVs can be determined as $\mathcal{M}_{\gamma_1}(s|Z) = \mathcal{M}_{\gamma_{sr}}(zs|Z)\mathcal{M}_{\gamma_c}(zs|Z)$, where the fact $\mathcal{M}_{aX}(s) = \mathcal{M}_X(as)$ has also been applied. Similarly, we have $\mathcal{M}_{\gamma_2}(s|Z) = \mathcal{M}_{\gamma_c}(zs|Z)$. Making use of these MGFs in (3.53) along with the key transformation

$$\mathcal{M}_{\gamma_{sr}}(zs|Z) = 1 - zs\int_0^\infty \mathrm{e}^{-zsx}\left(1-F_{\gamma_{sr}}(x)\right)dx, \tag{3.54}$$

we can rewrite (3.52) as

$$\overline{C} = \frac{1}{2\ln 2}\int_0^\infty\int_0^\infty \frac{\mathrm{e}^{-s}}{s}\mathcal{M}_{\gamma_c}(zs|Z)(1-\mathcal{M}_{\gamma_{sr}}(zs|Z))f_Z(z)dsdz, \tag{3.55}$$

which, after some manipulation, can be expressed as

$$\overline{C} = \frac{1}{2\ln 2}\int_0^\infty\int_0^\infty z\mathrm{e}^{-s}\widehat{\mathcal{M}}_{\gamma_{sr}}(zs|Z)\mathcal{M}_{\gamma_c}(zs|Z)f_Z(z)dsdz, \tag{3.56}$$

where $\widehat{\mathcal{M}}_{\gamma_{sr}}(zs|Z) \triangleq \int_0^\infty \mathrm{e}^{-zsx}\left(1-F_{\gamma_{sr}}(x)\right)dx$ is the conditional complementary MGF transform.

Now, we proceed to determine various quantities in (3.56) to evaluate EC for fixed-gain AF relaying under uncorrelated and correlated shadowed-Rician fading scenarios in the sequel.

Theorem 6. *The expression of EC for fixed-gain AF relaying under uncorrelated* *shadowed-Rician fading can be given as*

$$\begin{aligned}\overline{C} = &\frac{N}{2\ln 2}\sum_{i_1=0}^{m_s-1}\cdots\sum_{i_{N_s}=0}^{m_s-1}\frac{\Xi(N_s)}{(\eta_s)^{\Lambda}}\sum_{p=0}^{\Lambda-1}\frac{\Gamma(\Lambda)\left(\beta_\delta\right)^{-\Lambda-1}}{p!\Gamma(m_I)}\sum_{j=0}^{N-1}\mathcal{C}_j^{N-1}\frac{(-1)^j}{\Gamma(m_dN_d)}\\ &\times\sum_{l=0}^{j(m_dN_d-1)}\omega_l^j\sum_{i=0}^{l}\mathcal{C}_i^l\left(\frac{m_d}{\Omega_d\eta_r}\right)^{m_dN_d+i}\xi_{i,j,l}\frac{\mathcal{U}^{2(m_dN_d+i)+1}}{{\chi_j}^{m_dN_d+i+1}}\\ &\times G^{2,1,1,1,1}_{2,[1:1],0,[1:1]}\left[\begin{matrix}\frac{\mathcal{U}}{\chi_j\beta_\delta}\\ \frac{\mathcal{U}}{\chi_j}\left(\frac{\Omega_I}{m_c}\right)\end{matrix}\middle|\begin{matrix}-m_dN_d-i,0;1+p;m_I\\ -;0;0\end{matrix}\right].\end{aligned}\tag{3.57}$$

Proof. See Appendix 3.H. ■

Further, we follow the similar steps as in previous case by replacing the CDF in (3.11) with (3.13) to obtain the desired EC expression for fixed-gain AF relaying under correlated shadowed-Rician fading case as

$$\begin{aligned}\overline{C} = &\frac{N\xi}{2\ln 2}\sum_{k=0}^{\infty}\varrho_k\sum_{\ell=0}^{m_sN_s+k-N_s}\varpi_{k,\ell}\sum_{p=0}^{N_s+\ell-1}\frac{\Gamma(N_s+\ell)}{p!\Gamma(m_I)}\left(\frac{\varphi}{\eta_s}\right)^{-(N_s+\ell+1)}\sum_{j=0}^{N-1}\mathcal{C}_j^{N-1}\\ &\times\frac{(-1)^j}{\Gamma(m_dN_d)}\sum_{l=0}^{j(m_dN_d-1)}\omega_l^j\sum_{i=0}^{l}\mathcal{C}_i^l\left(\frac{m_d}{\Omega_d\eta_r}\right)^{m_dN_d+i}\xi_{i,j,l}\frac{\mathcal{U}^{2(m_dN_d+i)+1}}{{\chi_j}^{m_dN_d+i+1}}\\ &\times G^{2,1,1,1,1}_{2,[1:1],0,[1:1]}\left[\begin{matrix}\frac{\mathcal{U}}{\chi_j}\left(\frac{\eta_s}{\varphi}\right)\\ \frac{\mathcal{U}}{\chi_j}\left(\frac{\Omega_I}{m_I}\right)\end{matrix}\middle|\begin{matrix}-m_dN_d-i,0;1+p;m_I\\ -;0;0\end{matrix}\right].\end{aligned}\tag{3.58}$$

Remarks: It can be observed from (3.58) that EC relies on the parameters ξ, ϱ_k, and $\varpi_{k,\ell}$, reflecting that the system's EC is directly governed by the number N_s of source antennas.

3.3 Numerical and Simulation Results

To evaluate the performance of the considered HSTRN and to assess the usefulness of our derived analytical and asymptotic expressions, we perform numerical investigations and validate the theoretical results through Monte-Carlo simulations in this section. We set $\Omega_d = 1$, $\gamma_{\text{th}} = 0$ dB, $\eta_c = 1$ dB (unless stated otherwise), and $\eta_s = \eta_r$ as transmit SNR. The shadowed-Rician fading parameters for satellite $(S - R)$ link are considered as $(m_s, b, \Omega_s = 1, 0.063, 0.0007)$ under heavy shadowing and $(m_s, b, \Omega_s = 5, 0.251, 0.279)$ in average shadowing scenario [58]. In addition, the parameters of interference channels have been set as $\{m_{ci}\}_{i=1}^{6} = \{1, 2, 2.5, 3, 3.5, 3.5\}$ and $\{\Omega_{ci}\}_{i=1}^{6} = \{1, 2.5, 2.5, 3.2, 3.5, 4\}$. For each set of interfering signals, the parameters calculated for respective analytical curves are depicted in Table 3.1.

Table 3.1: Estimated Parameters for Interfering Signals involved in (3.21)

M	2	3	4	5	6
m_I	2.9697	5.4340	8.4317	11.9136	15.4
Ω_I	3.5	6	9.2	12.7	16.7

3.3.1 Investigation with Uncorrelated Shadowed-Rician Fading

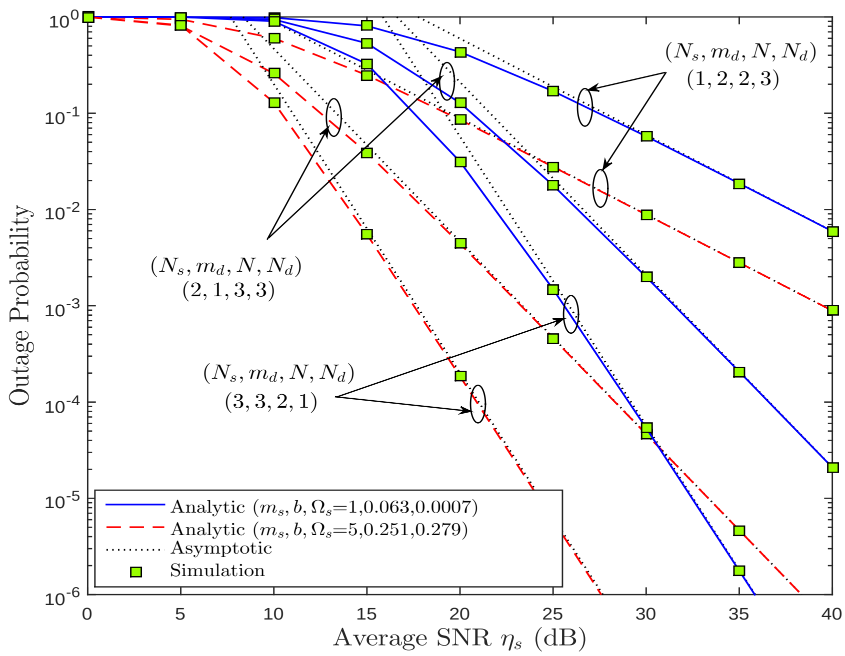

Figure 3.2: OP curves under various diversity parameters.

Fig. 3.2 plots the OP curves versus SNR for the considered HSTRN over uncorrelated shadowed-Rician faded satellite links and Nakagami-m faded terrestrial links. In particular, we obtain the OP curves with various parameters (N_s, m_d, N, N_d) under both average and heavy shadowing scenarios by setting $\rho_{rd} = 0.8$ and number of interferes $M = 3$. The analytical and asymptotic OP curves are plotted using the derived expressions in (3.25) and (3.26), respectively, which are clearly found to be aligned and corroborated with the simulation results. From Fig. 3.2, one can also observe that system's OP curves justify the diversity order of $\min(N_s, m_d N_d)$ as long as the interference power level remains low as compared to transmit power (i.e., $\eta_c \ll \eta_s$). For instance, the diversity order of 3 can be realized through the slopes of the OP curves when (N_s, m_d, N, N_d) being $(3, 3, 2, 1)$ as compared with $(2, 1, 3, 3)$ for diversity order of 2. Accordingly, system's OP performance improves when these diversity parameters increase. Moreover, we can see that the system outage performance becomes better in average fading condition as compared to heavy shadowing scenario, as expected. Indeed, a relative shift in the OP curves can be seen which is due to the system coding gain influenced by system/channel parameters.

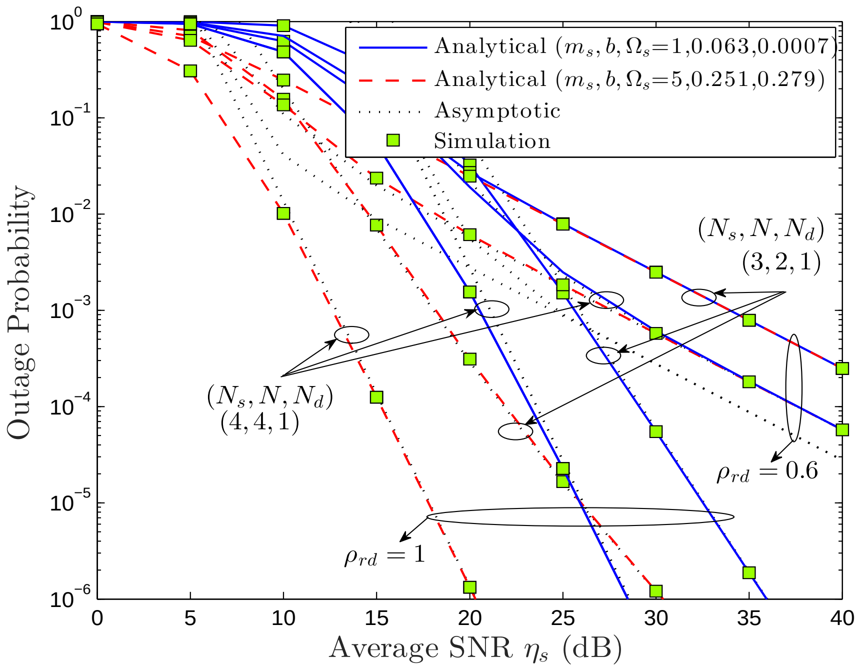

Figure 3.3: Impact of multiple users on OP performance.

Fig. 3.3 illustrates the impact of multi-user diversity on the system outage performance under both perfect and outdated CSI condition. Herein, we set the fading severity parameter $m_d = 1$ and number of interferers $M = 2$. We can clearly see from this figure that, for a given set of parameters $(N_s, N, N_d) = (3, 2, 1)$, the system exploits multi-user diversity of order 2 in case of perfect CSI ($\rho_{rd} = 1$) while system attains a diversity order of 1 for outdated CSI ($\rho_{rd} = 0.6$) case. The various curves confirm the achievable diversity order of $\min(N_s, m_d N_d N)$ in perfect CSI case and $\min(N_s, m_d N_d)$ in outdated CSI case wherein the multi-user diversity cannot be realized. As such, when $N_s \leq m_d N_d N$, the system performance is dominated by satellite links and hence a notable performance difference appears under heavy and average fading scenarios. Otherwise, if $N_s > m_d N_d N$, the system performance is limited by terrestrial links, and hence the curves for both heavy and average fading scenarios are merging at high SNR e.g., see the respective curves for $(N_s, N, N_d) = (3, 2, 1)$.

Fig. 3.4 depicts the effect of different interferers and interference power on the outage performance of considered HSTRN. Herein, we plot the OP curves for $M = 1$ and $M = 6$ with a set of interference power $\eta_c = (1, 10)$ dB under both average and

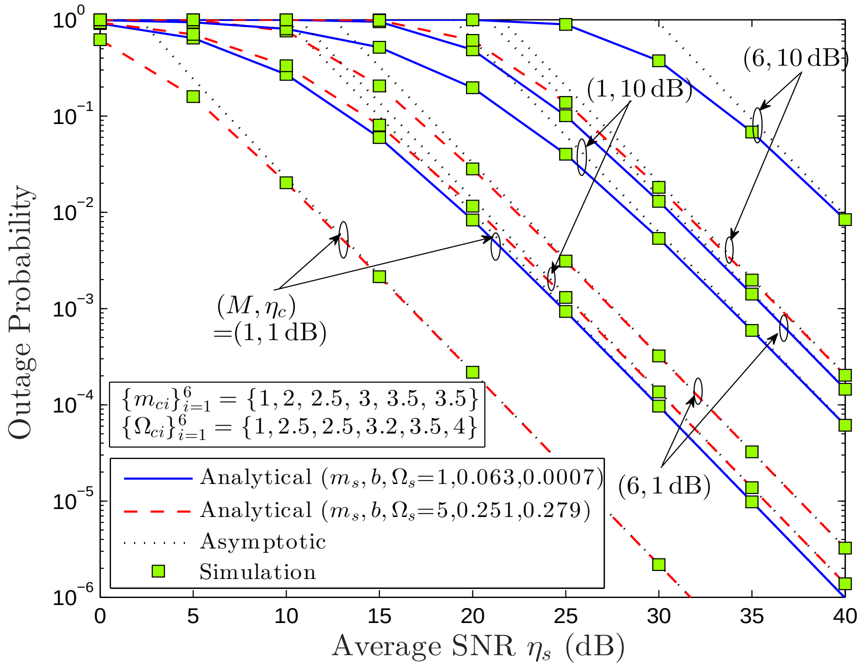

Figure 3.4: Impact of interferers on OP performance.

heavy shadowed-Rician fading cases. For this, we set $N_s = 2$, $N = 2$, $m_d = 1$, $N_d = 3$, and $\rho_{rd} = 0.4$. It can be observed from Fig. 3.4 that, as the number of interferes or interference power increases, the OP performance of the system degrades as revealed clearly by set of curves $(M, \eta_c) = (1, 1\,\text{dB})$, $(1, 10\,\text{dB})$, $(6, 1\,\text{dB})$, $(6, 10\,\text{dB})$. Moreover, the analytical and asymptotic curves corresponding to the OP evaluation for finite number of interferers are found to be very accurate to exact simulation results and they are closely aligned in the high SNR regime.

Fig. 3.5 shows the OP curves for the considered HSTRN under high interference power levels, where we set $M = 1$, $N = 3$, $m_d = 2$, and $N_d = 1$. Herein, we consider high interference power η_c such that η_c varies proportionally with η_s, while maintaining $\frac{\eta_s}{\eta_c}$ as a constant ratio of 25 dB. It is observed that the high interference power level brings zero diversity floor to the system performance. Note that for both $\rho_{rd} = 1$ (perfect CSI) and $\rho_{rd} < 1$ (outdated CSI) cases, the system holds zero diversity gain under high interference power level. Further, one can see that the outdated CSI ($\rho_{rd} = 0.8$) degrades the system OP performance. It is worth noting that when CSI is outdated ($\rho_{rd} < 1$) for a fixed number of interferes M, the system OP performance deteriorates owing to the affect on coding gain. Nevertheless, increase in the number of source antennas from $N_s = 1$ to $N_s = 2$ brings improvement in the system outage performance. The agreement between the analytical and asymptotic behaviour is noticeable which is confirmed by simulation, and graphically no visible difference can be found at high SNR.

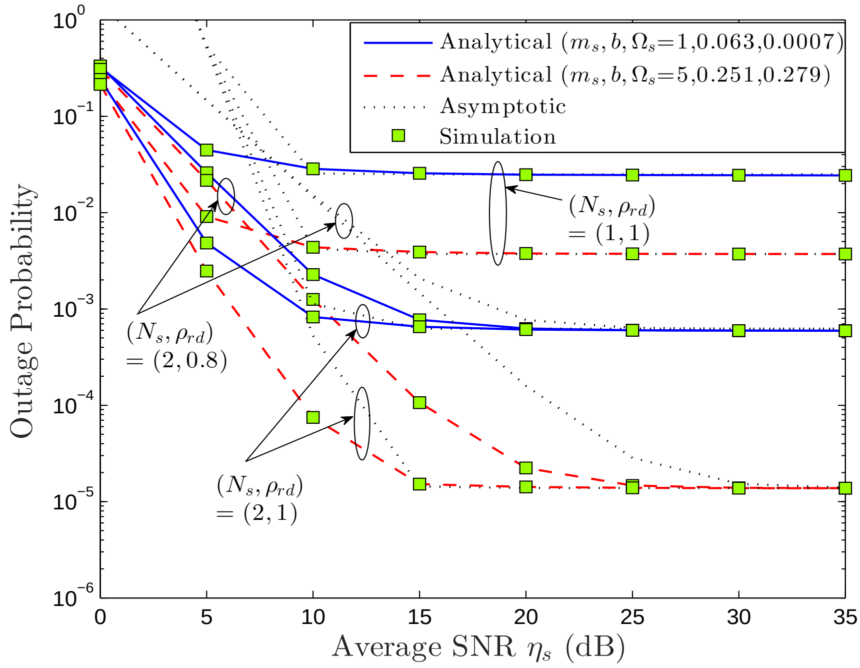

Figure 3.5: Effect of high interference power levels.

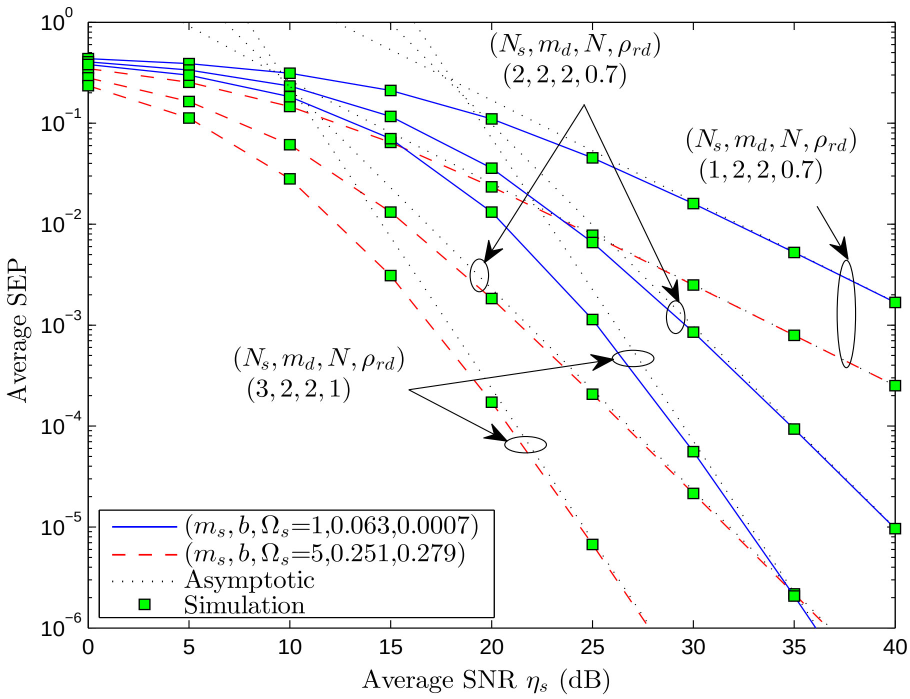

Figure 3.6: Average SEP curves for the considered HSTRN under various system/channel parameters.

Fig. 3.6 illustrates the average SEP performance of the considered HSTRN against transmit SNR for various diversity parameters (i.,e., N_s, m_d, N, ρ_{rd}). It is evident from the figure that the slope of the curves justify the system achievable diversity order of $\min(N_s, m_d)$ for outdated CSI and $\min(N_s, m_d N)$ for perfect CSI cases. For instance, one can realize the achievable diversity orders of 1 and 2 for the curves being $(1, 2, 2, 0.7)$ and $(2, 2, 2, 0.7)$ for outdated CSI. Besides, a diversity order of 3 can be clearly observed from the curves with the parameters $(3, 2, 2, 1)$. Moreover, note that, with an increase in the satellite antennas, the average SEP performance significantly improves which illuminates the importance of a multi-antenna satellite in the proposed network. In addition, we found that the system SEP performance becomes superior in average shadowing scenario as compared to heavy shadowing scenario, however, achievable diversity order remains same in both the scenarios.

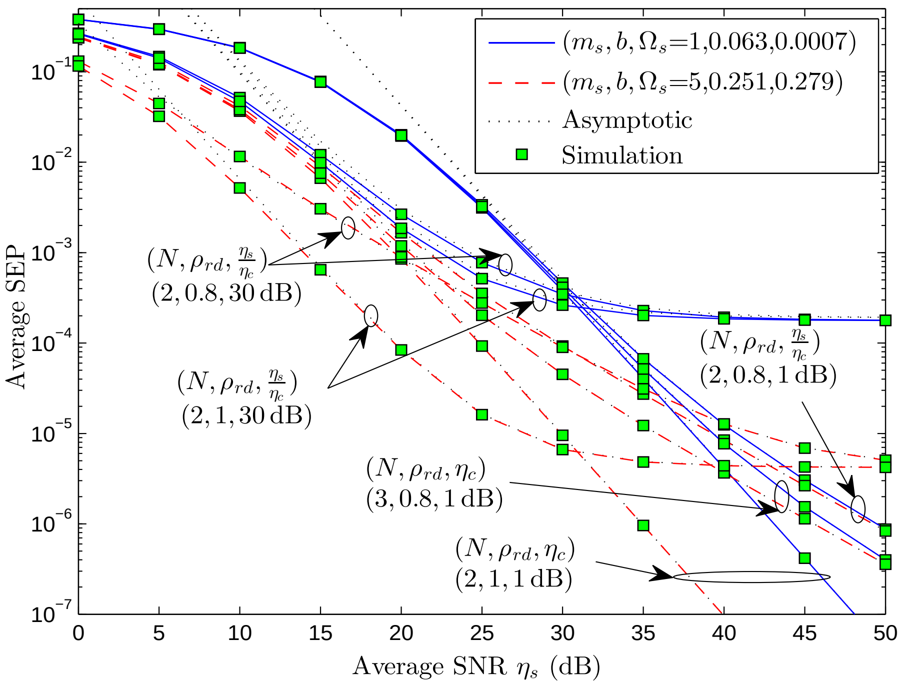

Figure 3.7: Impact of multiple users and high interference power levels on average SEP performance.

Fig. 3.7 shows the impact of the number of users and high interference power level on the average SEP performance with $N_s = 2$, $m_d = 1$. It is apparently seen, from the curves being $(2, 0.8, 1$ dB) and $(3, 0.8, 1$ dB), that the system average SEP performance improves with an increasing number of users. However, system experiences better performance under perfect CSI against outdated CSI condition with the same number of terrestrial users which can be realized by comparing the respective curves with the parameters $(2, 1, 1$ dB) and $(2, 0.8, 1$ dB). In addition, we plot the average SEP curves under high interference power level by varying η_c proportionally with η_s while maintaining $\frac{\eta_s}{\eta_c}$ as a constant with 30 dB, and noticed that the system achievable diversity order reduces to zero under high interference power level, regardless of the outdated or perfect CSI condition of terrestrial users.

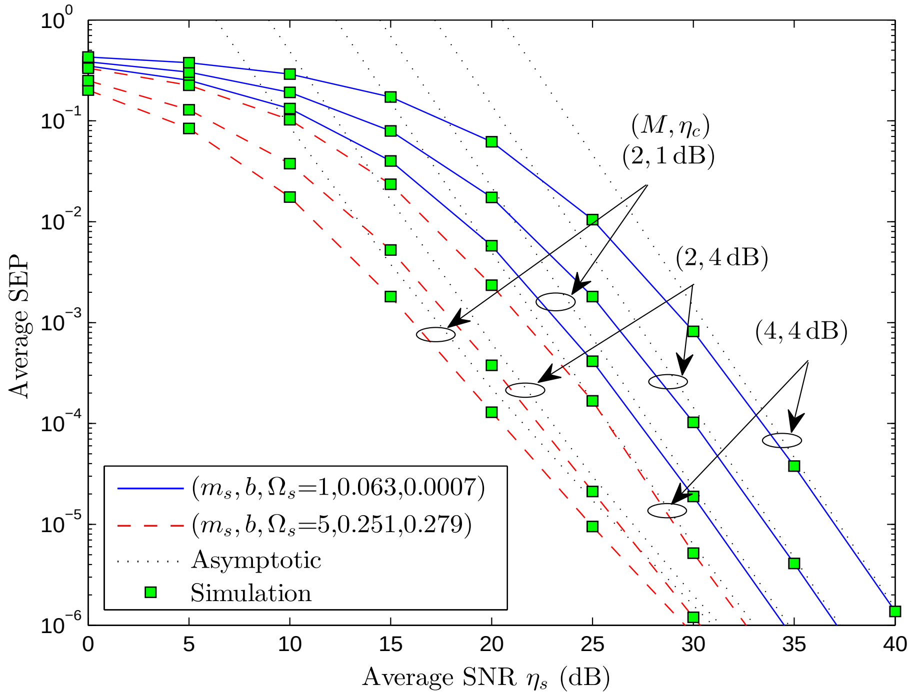

Figure 3.8: Impact of interferers on average SEP performance.

In Fig. 3.8, we have demonstrated the impact of the number of interferers and interference power on the average SEP performance by setting $N_s = 3$, $m_d = 2$, $N = 2$, and $\rho_{rd} = 0.5$. It can be manifestly observed that the system average SEP performance deteriorates as the number of interferes or interference power increases. It is worth noting that the number of interferers does not affect the system achievable diversity order.

In Fig. 3.9, curves highlight the impact of number of users/destinations with multiple antennas on the EC performance for variable-gain AF relaying. Specifically, the EC curves are drawn for the four different sets of parameters (N, N_d, ρ_{rd}) under the setting $N_s = 2$, $m_d = 1$, and $M = 1$. As can be readily observed, the expected result that the EC of the considered system improves when an increase in number of destinations and/or number of antennas at destinations, vindicating the advantages of using multiple destinations with multiple antennas. For example, system configuration with parameters (N, N_d, ρ_{rd})=$(1, 4, 1)$ and $(4, 1, 1)$ can obtain a capacity enhancement compared with $(1, 1, 1)$. However, it is worth pointing that increasing

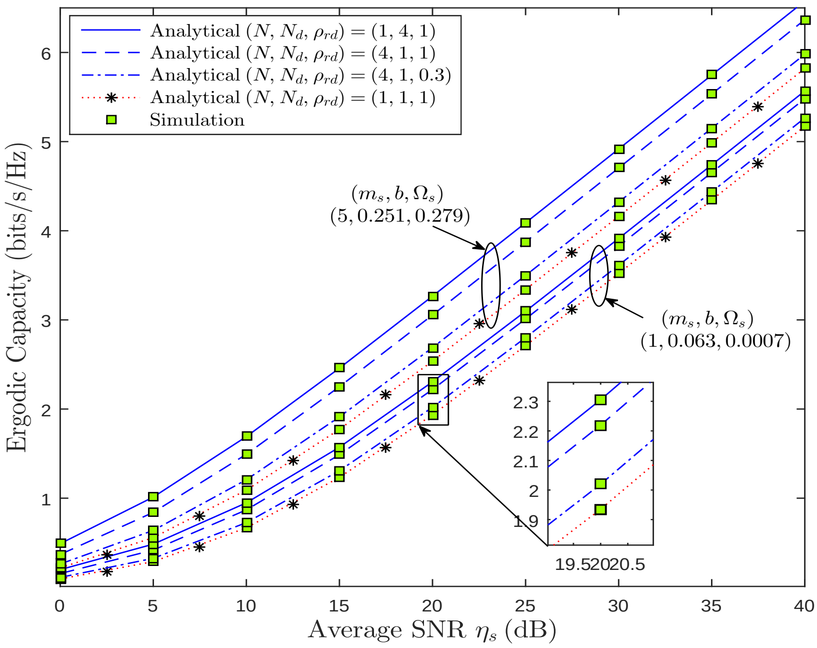

Figure 3.9: Impact of users/destinations with multiple antennas on the system EC performance under variable-gain AF relaying protocol.

number of destinations N shows marginal improvement in the system EC under the outdated CSI case (i.e., $\rho_{rd} = 0.3$), whereas significant enhancement can be realized in EC performance by increasing the number of destinations N and/or destination antennas N_d in case of perfect CSI (i.e., $\rho_{rd} = 1$). Hence, as expected system EC performance improves when CSI becomes perfect. Moreover, it is important to observe that system achieves high EC in average fading as compared to heavy fading scenario for the satellite channels. As we can see, for all the cases in this figure, the analytical and corresponding simulation results show perfect agreement.

In Fig. 3.10, we plot the EC curves for different source antenna configurations under the influence of interferers M and different levels of $\frac{\eta_s}{\eta_c}$ for heavy fading scenarios of satellite links. EC curves are drawn for under variable-gain AF relaying protocol. For this, we have considered $N = 1$, $N_d = 2$, and $m_d = 2$. It can be clearly observed that EC performance of the considered HSTRN improves with an increase in the number N_s of source antennas. However, diminution in EC is obvious when the number M of interferers or/and interference power level increases. As apparent from the curves, for small number of interferers and low interference power level η_c i.e., $(M, \eta_s/\eta_c)$=$(1, 20\text{dB})$, the system attains high EC as compared to large number of interferers and high interference power level i.e., $(M, \eta_s/\eta_c)$=$(2, 10\text{dB})$. Also, one

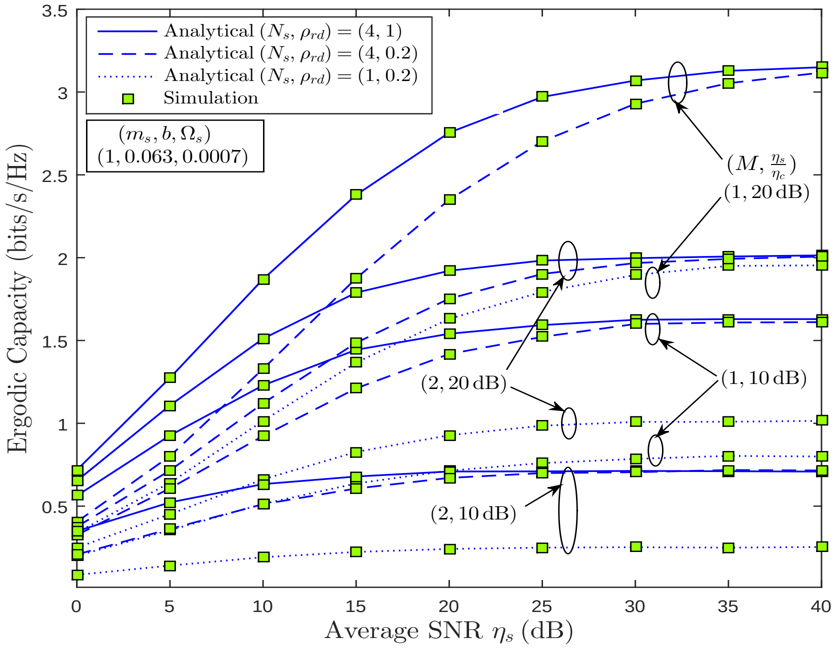

Figure 3.10: Impact of satellite antennas on EC under different interferers and interference levels under variable-gain AF relaying protocol.

can observe that the system's EC saturates at high SNR owing to the dominating effect of CCI on the system performance. Moreover, it is apparent from the curves that system achieves enhanced EC for perfect CSI ($\rho_{rd} = 1$) over outdated CSI ($\rho_{rd} = 0.2$) case. As seen can be seen from the figure that analytical results perfectly match with the simulation results.

Fig. 3.11 depicts the EC curves of considered HSTRN with different sets of parameters N_s and (N, ρ_{rd}) under i.i.d. shadowed-Rician fading links for fixed-gain AF relaying protocol. The analytical curves are drawn using (3.57) for both average and heavy shadowing scenarios of satellite links. Herein, we set $m_d = 1$, $N_d = 1$, $\eta_c = 1$ dB, and $M = 1$. We can observe that increasing number of users N has marginal impact on the EC performance in the case of outdated CSI ($\rho_{rd} = 0.6, 0.2$), while the EC is notably improved by increasing N under the perfect CSI ($\rho_{rd} = 1$) case. However, this performance improvement becomes limited when N increases to a certain extent, as evident by comparing the curves for $(N, \rho_{rd}) = (5, 1)$ and $(10, 1)$. This is due to bottleneck effect of the satellite link. Thereby, we can see a significant EC performance improvement with the increase of number of antennas N_s at satellite. Moreover, one can readily observe that the proposed HSTRN attains higher EC under average shadowing as compared to heavy shadowing condition of the satellite channels.

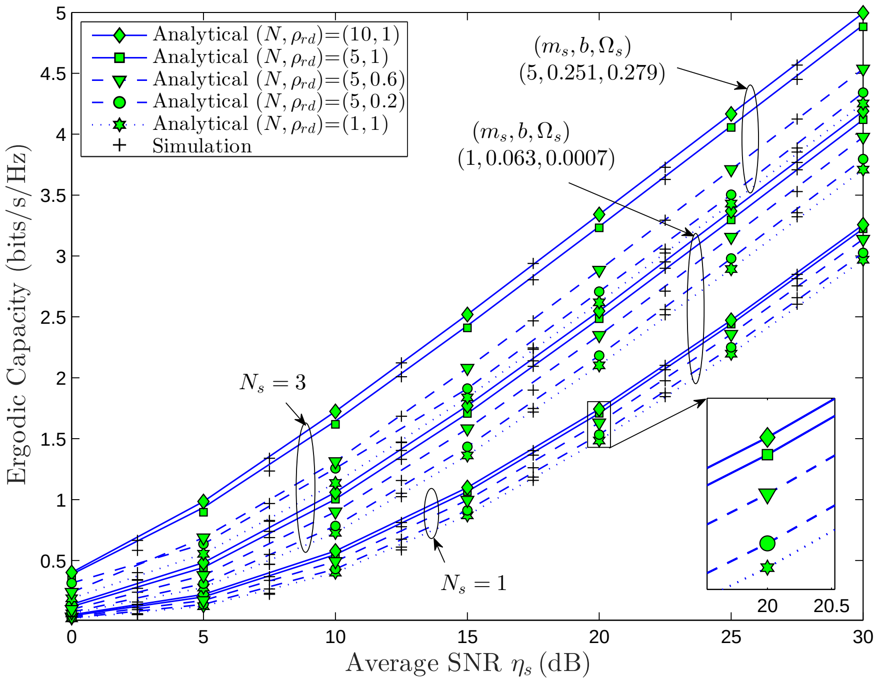

Figure 3.11: EC curves for different sets of N_s and (N, ρ_{rd}) under shadowed-Rician fading for fixed-gain AF relaying protocol.

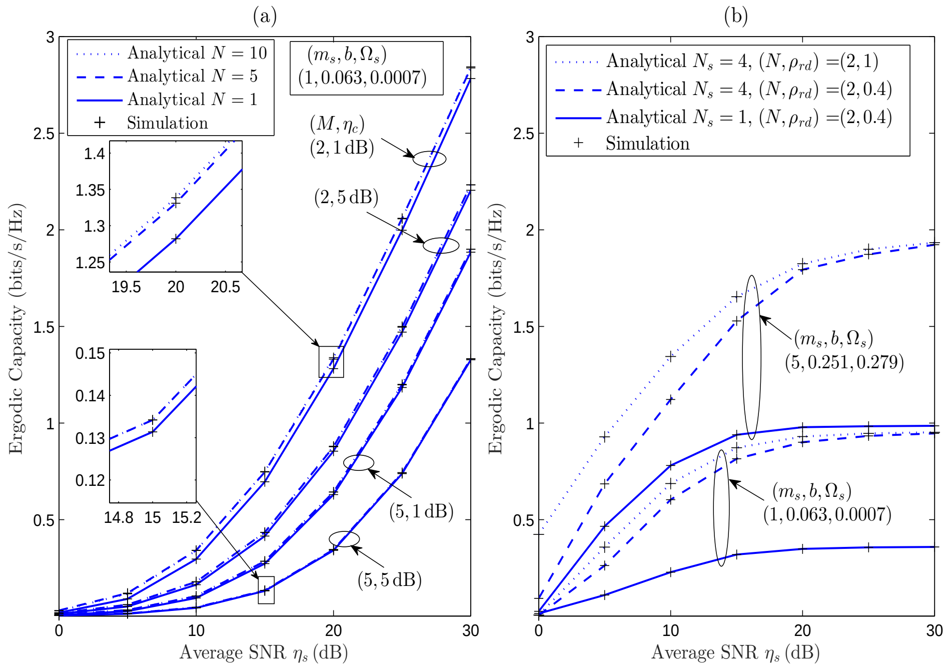

Figure 3.12: Impact of interferers and interference power on EC performance under fixed-gain AF relaying protocol.

In Fig. 3.12, we study the impact of interferers and interference power levels on EC performance of HSTRN with i.i.d. shadowed-Rician fading satellite links for fixed-gain AF relaying protocol. With setting $\rho_{rd} = 1$, $m_d = 2$, $N_d = 1$, and $N_s = 2$ in Fig. 3.12(a), we can readily observe that system attains higher EC for lower interference power level and/or lesser number of interferers. For instance, the EC value computed for $(M, \eta_c) = (2, 1 \text{ dB})$ is 2.78 bits/s/Hz as compared to 1.37 bits/s/Hz for $(5, 5 \text{ dB})$ with $N = 1$ at 30 dB SNR. Moreover, when $M = 2$ (or 5), we see that increasing the number of users N has a marginal impact on the EC performance. Further, in Fig. 3.12(b), we plot the EC curves by considering the case when η_c varies proportionally with η_s such that the ratio $\frac{\eta_s}{\eta_c}$ remains fixed at 15 dB. Herein, we set $m_d = 1$, $M = 3$, and $N = 2$. As such, we see that the EC curves become saturated in high SNR regime. This is due to the dominating effect of CCI on the EC performance. However, increasing the number of antennas at the satellite provides further EC performance enhancement.

3.3.2 Investigation with Correlated Shadowed-Rician Fading

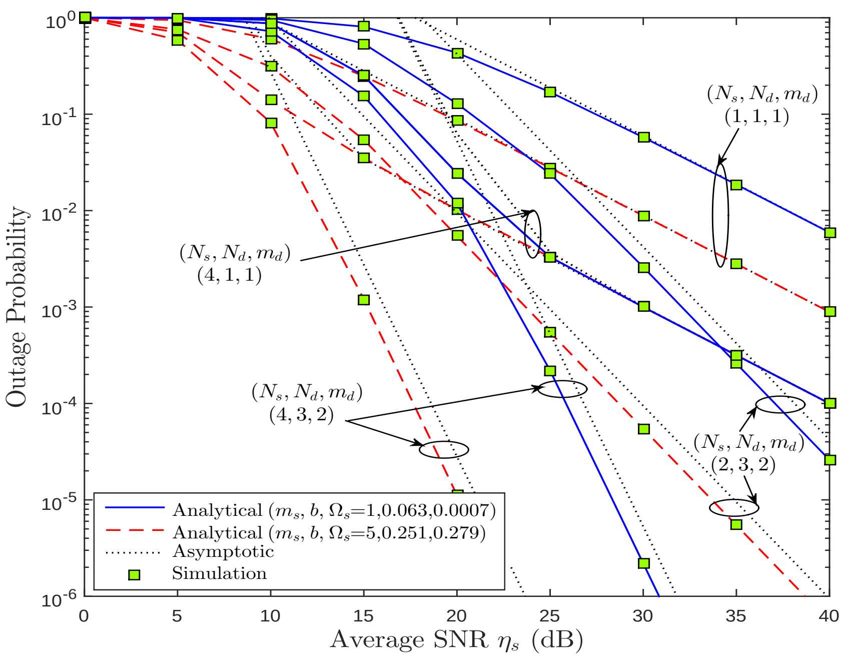

Figure 3.13: OP over correlated shadowed-Rician fading.

In Fig. 3.13, we study and verify the simulated and analytical OP of HSTRN for the exponentially correlated shadowed-Rician fading channels of satellite links. Curves are plotted for both average and heavy shadowed-Rician fading scenarios. Elements of pertaining correlation matrix are generated as $\mathbf{A}_s = [\rho_{i_{p,q}}]$, $p, q = 1, 2, ..., N_s$, where correlation coefficient $\rho_{i_{p,q}}$ between the pth and qth antennas of source is given as $\rho_{i_{p,q}} = \rho_i^{|p-q|}$. Herein, the plots are obtained for OP by setting $N = 2$, $M = 3$, $\rho_{rd} = 0.6$, and $\rho_i = 0.8$. In this figure, all the analytical curves

Table 3.2: Number of Terms for Infinite Series Calculation

No. of terms	5	15	25	35	38	40
Eq. (3.29)	0.5018	0.1671	0.0638	0.0320	0.0257	0.0257
Eq. (3.30)	0.0215	0.0358	0.0402	0.0415	0.0419	0.0419
Eq. (3.44)‡	0.83	1.70	2.42	2.63	2.64	2.64

are obtained by truncating the infinite series at 40th term in (3.29) and (3.30). We provide Table 3.2 to reflect the number of terms required for attaining sufficient accuracy[6]. The simulated results corroborate the analytical results. It can be observed further that system attains the same diversity order as obtained in uncorrelated shadowed-Rician fading case. Thereby, one can clearly see that correlation doesn't affect the system diversity order. Moreover, the performance improvement can be observed when the number of antennas at either source or at destinations increases.

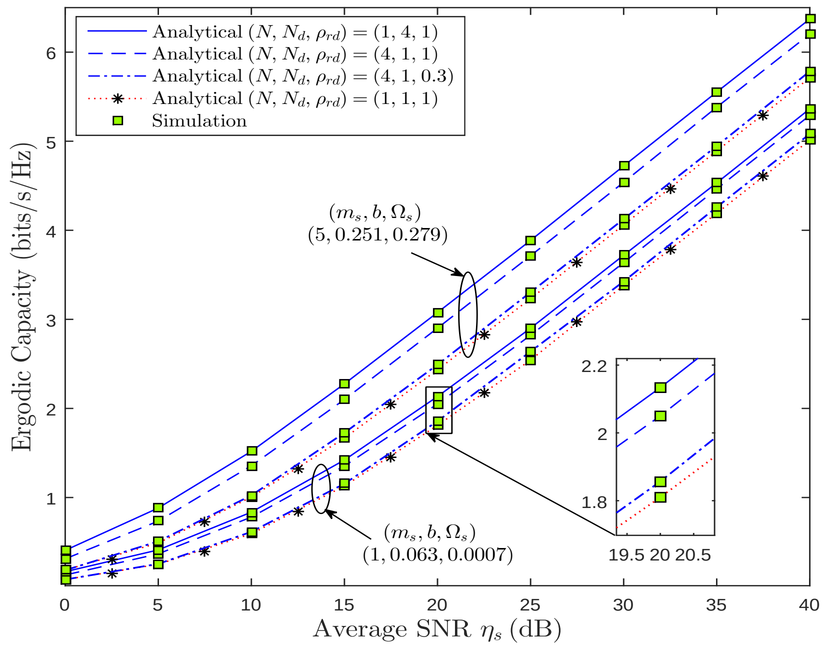

Figure 3.14: EC over correlated shadowed-Rician fading under variable-gain AF relaying protocol.

The EC performance is depicted in Fig. 3.14 over correlated satellite channels for both average and heavy shadowed-Rician fading scenarios under variable-gain AF relaying protocol. To obtain the analytical EC curves, we use first 40 terms

[6]In Table 3.2, we have performed computation of (3.29) and (3.30) by setting $(N_s, N, M, m_d, N_d, \eta_c, \rho_{rd}, \rho_i) = (2, 2, 3, 2, 3, 1\text{dB}, 0.6, 0.8)$ and of (3.44) by setting $(N_s, N, M, m_d, N_d, \eta_c, \rho_{rd}, \rho_i) = (2, 4, 1, 1, 1, 1\text{dB}, 0.3, 0.5)$ with the aid of Table 3.1 at 25 dB SNR under heavy shadowed-Rician fading.

Table 3.3: Number of Terms for Infinite Series Calculation

Number of Terms	5	10	15	20	23	25
Eq.(3.58) (in bits/s/Hz)	0.987	1.769	2.618	3.538	3.554	3.554

for infinite series calculation at each SNR value in (3.44). Herein, the EC curves are drawn for different sets of parameters as adopted for Fig. 3.9 and by fixing correlation coefficient $\rho_i = 0.5$. Good agreement between simulated and analytical curves is evident. On comparing the curves in Fig. 3.9 and Fig. 3.14, one can infer that owing to correlated fading, the EC of the proposed HSTRN deteriorates. For instance, with a given set of parameters $(N, N_d, \rho_{rd}) = (1, 4, 1)$ under heavy shadowing at 40 dB SNR, one can see that the EC of the system over correlated fading channels is 5.36 bits/s/Hz as illustrated in Fig. 3.14, whereas EC achieved by system for uncorrelated fading case is 5.56 bits/s/Hz as clear from Fig. 3.9.

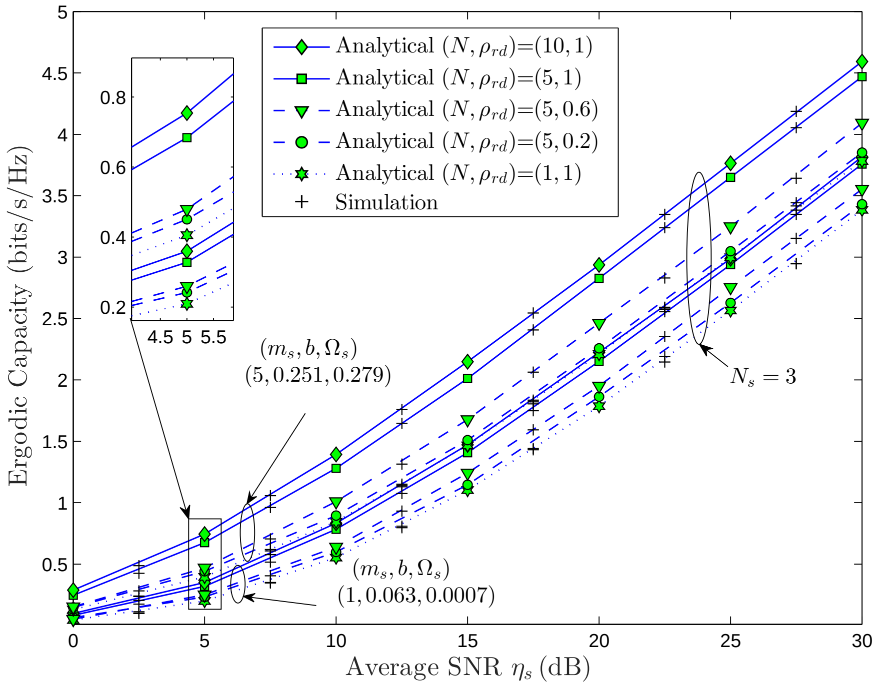

Figure 3.15: EC performance of HSTRN under correlated shadowed-Rician fading scenarios for fixed-gain AF relaying protocol.

In Fig. 3.15, EC performance of HSTRN is examined under exponentially correlated shadowed-Rician fading channels of satellite links for fixed-gain AF relaying protocol. For comparison purposes, we analyze the achievable EC under the same sets of system/channel parameters as adopted in Fig. 3.11 along with $\rho_i = 0.8$. We obtain the EC curves by using first 25 terms of infinite series[7] as involved in analyt-

[7] Table-3.3 shows the convergence of infinite series. Herein, we have computed EC using (3.58)

ical expression (3.58). It can be observed clearly that the EC performance degrades under the influence of correlated shadowed-Rician fading channels. However, even under correlated satellite channels, a significant improvement in EC performance can be realized when the number of antennas N_s at satellite increases from 1 to 3. Note that the curves drawn using truncated analytical expression in (3.58) show excellent agreement with simulation results.

3.4 Summary

In this chapter, we conducted a comprehensive performance analysis of a multi-user AF-based HSTRN by deploying multiple antennas at satellite under shadowed-Rician fading for satellite links and Nakagami-m fading for terrestrial links. Herein, for complexity-aware HSTRN design in real operating conditions, we considered opportunistic scheduling of users with outdated CSI and CCI signals at relay. We derived accurate and generalized expressions for OP and EC measures of the considered HSTRN by taking both uncorrelated and correlated shadowed-Rician fading channels into account. We also derived the closed-form yet accurate average SEP expression under uncorrelated shadowed-Rician fading channels. By further deriving the asymptotic OP and average SEP expressions, we deduced the achievable diversity orders of the considered system. We substantiated that the system diversity order is greatly influenced by number of antennas, users and level of CSI and CCI, but independent of the correlation and fading parameter of the LOS in multi-antenna satellite links. Our results identified various key system/channel parameters and provided useful insights for deployment of HSTRN in futuristic wireless systems.

Appendix 3.A: Proof of Theorem 1

The CDF $F_{\gamma_{sd}}(x)$ can be written using (3.7) as

$$\begin{aligned} F_{\gamma_{sd}}(x) &= \Pr[\gamma_{sd} < x] \\ &= \Pr\left[\frac{\gamma_{sr}\widetilde{\gamma}_{rd}}{\gamma_{sr} + (\widetilde{\gamma}_{rd}+1)(\gamma_c+1)} < x\right]. \end{aligned} \tag{3.59}$$

for a set of parameters as $N_s = 3$, $N = 5$, $N_d = 1$ $M = 1$, $m_d = 1$, $\Omega_d = 1$, $\eta_c = 1$ dB, $\rho_{rd} = 0.6$, and $\rho_i = 0.8$ at 30 dB SNR under heavy shadowing scenario. It is clear from the table that the first 25 terms are substantial in order to achieve good settlement of infinite series.

Under the interference limited scenario [84], the CDF $F_{\gamma_{sd}}(x)$ in (3.59) can be simplified and expressed in terms of expectation over γ_c as

$$F_{\gamma_{sd}}(x) = E_{\gamma_c}\Bigg[\int_0^x f_{\widetilde{\gamma}_{rd}}(z)dz + \int_x^\infty F_{\gamma_{sr}}\left(\frac{x(z+1)\gamma_c}{z-x}\right) f_{\widetilde{\gamma}_{rd}}(z)dz\Bigg], \tag{3.60}$$

which can be simplified further and given as

$$F_{\gamma_{sd}}(x) = 1 - E_{\gamma_c}[\Phi(x,\gamma_c)], \tag{3.61}$$

where $\Phi(x,\gamma_c)$ is defined by an integral as

$$\Phi(x,\gamma_c) = \int_x^\infty \left[1 - F_{\gamma_{sr}}\left(\frac{x(z+1)\gamma_c}{z-x}\right)\right] f_{\widetilde{\gamma}_{rd}}(z)dz. \tag{3.62}$$

On invoking the CDF of γ_{sr} from (3.11) and the PDF of $\widetilde{\gamma}_{rd}$ from (3.16) into (3.62), and simplifying subsequently with the help of [59, eqs. 1.111, 3.471.9], we obtain the result as given as

$$\begin{aligned}\Phi(x,\gamma_c) = 2N &\sum_{i_1=0}^{m_s-1}\cdots\sum_{i_{N_s}=0}^{m_s-1}\frac{\Xi(N_s)}{\eta_s^\Lambda}\sum_{p=0}^{\Lambda-1}\frac{\Gamma(\Lambda)}{p!}\sum_{j=0}^{N-1}\mathcal{C}_j^{N-1}\frac{(-1)^j}{\Gamma(m_dN_d)}\sum_{l=0}^{j(m_dN_d-1)}\omega_l^j\\ &\times\sum_{i=0}^{l}\mathcal{C}_i^l\left(\frac{m_d}{\Omega_d\eta_r}\right)^{m_dN_d+i}\xi_{i,j,l}\,\mathrm{e}^{-\frac{x}{\chi_j}}\sum_{q=0}^{p}\mathcal{C}_q^p\sum_{\nu=0}^{m_dN_d+i-1}\mathcal{C}_\nu^{m_dN_d+i-1}\\ &\times\beta_\delta^{-\Lambda+p+\frac{\nu-q+1}{2}}\chi_j^{\frac{\nu-q+1}{2}}(1+x)^{\frac{\nu+q+1}{2}}x^{m_dN_d+i+p-\left(\frac{\nu+q+1}{2}\right)}\\ &\times\gamma_c^{p+\frac{\nu-q+1}{2}}\mathrm{e}^{-\beta_\delta x\gamma_c}\,\mathcal{K}_{\nu-q+1}\left(2\sqrt{\frac{\beta_\delta x(1+x)\gamma_c}{\chi_j}}\right),\end{aligned} \tag{3.63}$$

where $\mathcal{K}_v(\cdot)$ is the modified Bessel function of the second kind and order v [59, eq. 8.432.6]. Now, by performing the expectation of (3.63) over γ_c using the PDF from (3.21) as

$$E_{\gamma_c}[\Phi(x,\gamma_c)] = \int_0^\infty \Phi(x,\gamma_c)|_{\gamma_c=y} f_{\gamma_c}(y)dy, \tag{3.64}$$

with the aid of [59, eq. 6.641.3], and finally, by substituting the obtained result in (3.61), one can reach (3.25).

Appendix 3.B: Derivation of (3.26)

In the high SNR regime, the end-to-end SINR in (3.7) can be represented as $\gamma_{sd} \simeq$

$\min\left(\frac{\gamma_{sr}}{\gamma_c}, \widetilde{\gamma}_{rd}\right)$, and hence the CDF $F_{\gamma_{sd}}(x)$ is written as

$$F_{\gamma_{sd}}(x) \simeq \Pr\left[\min\left(\frac{\gamma_{sr}}{\gamma_c}, \widetilde{\gamma}_{rd}\right) < x\right]. \tag{3.65}$$

By defining the ratio $\gamma_{sc} = \frac{\gamma_{sr}}{\gamma_c}$ and exploiting the independence among the involved RVs in (3.65), we can express $F_{\gamma_{sd}}(x)$ as

$$F_{\gamma_{sd}}(x) \simeq 1 - \left[1 - F_{\gamma_{sc}}(x)\right]\left[1 - F_{\widetilde{\gamma}_{rd}}(x)\right]. \tag{3.66}$$

To proceed further, we need to evaluate the asymptotic behavior for the CDFs $F_{\gamma_{sc}}(x)$ and $F_{\widetilde{\gamma}_{rd}}(x)$.

First, for $\eta_s \to \infty$, we can apply the Maclaurin series expansion of the exponential function in (3.10) to approximate the PDF of γ_{sr} as

$$f_{\gamma_{sr}}(x) \simeq \frac{\alpha^{N_s}}{(N_s - 1)!\eta_s^{N_s}} x^{N_s - 1}, \tag{3.67}$$

and the corresponding CDF follows asymptotic behavior as

$$F_{\gamma_{sr}}(x) \simeq \frac{\alpha^{N_s}}{(N_s)!\eta_s^{N_s}} x^{N_s}. \tag{3.68}$$

Then, using (3.68) and PDF from (3.21), one can calculate the asymptotic behavior of $F_{\gamma_{sc}}(x)$ as

$$F_{\gamma_{sc}}(x) = \int_0^\infty F_{\gamma_{sr}}(x\,y) f_{\gamma_c}(y) dy \tag{3.69}$$

$$\simeq \frac{\alpha^{N_s} x^{N_s}}{N_s!(\eta_s)^{N_s}} \left(\frac{\Omega_I}{m_I}\right)^{N_s} \frac{\Gamma(N_s + m_I)}{\Gamma(m_I)}. \tag{3.70}$$

And, to obtain asymptotic behavior of $F_{\widetilde{\gamma}_{rd}}(\gamma_{\text{th}})$, we first simplify the PDF in (3.16) for $\eta_r \to \infty$ and then integrate the result. Thereby, the asymptotic behavior of the corresponding CDF can be deduced for $\rho_{rd} < 1$ as

$$F_{\widetilde{\gamma}_{rd}}(x) \simeq N \sum_{j=0}^{N-1} \mathcal{C}_j^{N-1} \frac{(-1)^j}{\Gamma(m_d N_d)} \frac{\left(\frac{m_d}{\Omega_d}\right)^{m_d N_d} x^{m_d N_d}}{[j(1 - \rho_{rd}) + 1]^{m_d N_d} (\eta_r)^{m_d N_d}}. \tag{3.71}$$

For $\rho_{rd} = 1$, the asymptotic behavior of $F_{\widetilde{\gamma}_{rd}}(\gamma_{\text{th}})$ can be obtained straightforwardly as

$$F_{\widetilde{\gamma}_{rd}}(x) \simeq \frac{1}{[\Gamma(m_d N_d + 1)]^N} \left(\frac{m_d x}{\Omega_d \eta_r}\right)^{m_d N_d N}. \tag{3.72}$$

Now, after inserting (3.70)-(3.72) in (3.66), one can obtain (3.26).

Appendix 3.C: Proof of Theorem 2

To evaluate the CDF $F_{\gamma_{sd}}(x)$ under correlated shadowed-Rician fading case, we follow the same procedure as in Appendix 3.A. On invoking the CDF from (3.13) in (3.62) along with PDF $f_{\tilde{\gamma}_{rd}}(x)$ from (3.16), we get $\Phi(x,\gamma_c)$ for correlated shadowed-Rician fading case as

$$\begin{aligned}\Phi(x,\gamma_c) &= 2N\zeta\sum_{k=0}^{\infty}\varrho_k\sum_{\ell=0}^{m_sN_s+k-N_s}\varpi_{k,\ell}\sum_{p=0}^{N_s+\ell-1}\frac{\Gamma(N_s+\ell)}{p!}\left(\frac{\varphi}{\eta_s}\right)^{-(N_s+\ell-p)}\\ &\times\sum_{j=0}^{N-1}\mathcal{C}_j^{N-1}\frac{(-1)^j}{\Gamma(m_dN_d)}\sum_{l=0}^{j(m_dN_d-1)}\omega_l^j\sum_{i=0}^{l}\mathcal{C}_i^l\left(\frac{m_d}{\Omega_d\eta_r}\right)^{m_dN_d+i}\xi_{i,j,l}\;x^p\gamma_c^p\\ &\times\sum_{q=0}^{p}\mathcal{C}_q^p(1+x)^q\mathrm{e}^{-\left(\frac{\varphi}{\eta_s}\right)x\gamma_c}\sum_{\nu=0}^{m_dN_d+i-1}\mathcal{C}_\nu^{m_dN_d+i-1}x^{m_dN_d-1+i-\nu}\mathrm{e}^{-\frac{x}{\chi_j}}\\ &\times\left(\frac{\varphi}{\eta_s}(1+x)x\gamma_c\chi_j\right)^{\frac{\nu-q+1}{2}}\mathcal{K}_{\nu-q+1}\left(2\sqrt{\frac{\varphi}{\eta_s\chi_j}(1+x)x\gamma_c}\right).\end{aligned} \tag{3.73}$$

In the sequence, we calculate $E_{\gamma_c}[\Phi(x,\gamma_c)]$ by performing the expectation of (3.73) using the PDF from (3.21) along with the fact [59, eq. 6.641.3]. On substituting the so obtained result in (3.61), the closed-form CDF $F_{\gamma_{sd}}(x)$ in (3.29) is achieved.

Appendix 3.D: Derivation of (3.30)

The asymptotic expression of $F_{\gamma_{sd}}(x)$ can be evaluated similarly as in Appendix 3.B. To proceed, we need to evaluate the asymptotic behavior for the CDF $F_{\gamma_{sc}}(x)$ over correlated shadowed-Rician fading channels. For this, we simplify the PDF in (3.12) for $\eta_s\to\infty$ as

$$f_{\gamma_{sr}}(x)\simeq\zeta\sum_{k=0}^{\infty}\varrho_k\frac{x^{N_s-1}}{(N_s-1)!\eta_s^{N_s}}\mathrm{e}^{-\left(\frac{\varphi}{\eta_s}\right)x}, \tag{3.74}$$

and the corresponding CDF follows asymptotic behavior as

$$F_{\gamma_{sr}}(x)\simeq\zeta\sum_{k=0}^{\infty}\varrho_k\frac{x^{N_s}}{(N_s-1)!\eta_s^{N_s}}. \tag{3.75}$$

Then, using (3.75) and PDF from (3.21), one can calculate the asymptotic behavior of $F_{\gamma_{sc}}(x)$ in (3.69) for correlated fading case as

$$F_{\gamma_{sc}}(x) \simeq \zeta \sum_{k=0}^{\infty} \frac{\epsilon_k x^{N_s}}{(2b)^{N_s}(N_s-1)!\eta_s^{N_s}} \left(\frac{2b}{2b+\lambda}\right)^{m_s N_s + k} \frac{\Gamma(N_s+m_I)}{\Gamma(m_I)} \left(\frac{\Omega_I}{m_I}\right)^{N_s}. \tag{3.76}$$

And, for $\eta_r \to \infty$, we use asymptotic behavior of $F_{\widetilde{\gamma}_{rd}}(\gamma_{\text{th}})$ as provided in (3.71) and (3.72). Finally, after plugging (3.76), (3.71), and (3.72) into (3.66), we obtain the result in (3.30).

Appendix 3.E: Derivation of (3.33)

To solve (3.32), we first require the expression of $F_{\gamma_{sd}}(x)$. However, one can realize that the exact calculation for CDF of γ_{sd}, using (3.7), is very complicated. Therefore, for analytical tractability, end-to-end SINR in (3.7) can be approximated and upper bounded as [95]

$$\gamma_{sd} \simeq \frac{\gamma_{src}\widetilde{\gamma}_{rd}}{\gamma_{src}+\widetilde{\gamma}_{rd}} < \min\left(\gamma_{src}, \widetilde{\gamma}_{rd}\right), \tag{3.77}$$

where $\gamma_{src} = \frac{\gamma_{sr}}{\gamma_c+1}$. Now, using (3.77), the closed-form expression for the CDF $F_{\gamma_{sd}}(x)$ can be written as

$$F_{\gamma_{sd}}(x) = \Pr[\min\left(\gamma_{src}, \widetilde{\gamma}_{rd}\right) < x], \tag{3.78}$$

which can be statistically expressed as

$$F_{\gamma_{sd}}(x) = F_{\gamma_{src}}(x) + F_{\widetilde{\gamma}_{rd}}(x) - F_{\gamma_{src}}(x)F_{\widetilde{\gamma}_{rd}}(x). \tag{3.79}$$

To further proceed, we first evaluate $F_{\gamma_{src}}(x)$ as

$$F_{\gamma_{src}}(x) = \int_0^{\infty} F_{\gamma_{sr}}(x(y+1)) f_{\gamma_c}(y) dy. \tag{3.80}$$

On invoking (3.11) and (3.21) into (3.80), and solving the integral using the fact [59, eq. 3.351.3], we obtain $F_{\gamma_{src}}(x)$ as

$$F_{\gamma_{src}}(x) = 1 - \sum_{i_1=0}^{m_s-1} \cdots \sum_{i_{N_s}=0}^{m_s-1} \frac{\Xi(N_s)}{\eta_s^{\Lambda}} \sum_{p=0}^{\Lambda-1} \frac{\Gamma(\Lambda)}{\Gamma(p+1)} \beta_\delta^{-(\Lambda-p)} \sum_{q=0}^{p} \mathcal{C}_q^p \left(\frac{m_I}{\Omega_I}\right)^{m_I}$$
$$\times \frac{\Gamma(q+m_I)}{\Gamma(m_I)} x^p \mathrm{e}^{-\beta_\delta x} \left(\beta_\delta x + \frac{m_I}{\Omega_I}\right)^{-(q+m_I)}. \tag{3.81}$$

And, after integrating (3.16) using [59, eqs. 3.351.2], we can obtain $F_{\widetilde{\gamma}_{rd}}(x)$ as

$$F_{\widetilde{\gamma}_{rd}}(x) = 1 - N \sum_{j=0}^{N-1} \mathcal{C}_j^{N-1} \frac{(-1)^j}{\Gamma(m_d)} \sum_{l=0}^{j(m_d-1)} \omega_l^j \sum_{i=0}^{l} \mathcal{C}_i^l \sum_{k=0}^{m_d+i-1} \left(\frac{m_d}{\Omega_d \eta_r}\right)^{m_d+i} \times \frac{\Gamma(m_d+i)}{k!} \chi_j^{(m_d+i-k)} \; \xi_{i,j,l} \; x^k \mathrm{e}^{-\frac{x}{\chi_j}}. \tag{3.82}$$

Finally, by substituting (3.81) and (3.82) into (3.79), the closed-form expression of CDF $F_{\gamma_{sd}}(x)$ can be obtained as

$$F_{\gamma_{sd}}(x) = 1 - N \sum_{i_1=0}^{m_s-1} \cdots \sum_{i_{N_s}=0}^{m_s-1} \frac{\Xi(N_s)}{\eta_s^{\Lambda}} \sum_{p=0}^{\Lambda-1} \frac{\Gamma(\Lambda)}{p!} {\beta_\delta}^{-(\Lambda-p)} \sum_{q=0}^{p} \mathcal{C}_q^p \left(\frac{m_I}{\Omega_I}\right)^{m_I} \times \frac{\Gamma(q+m_I)}{\Gamma(m_I)} \sum_{j=0}^{N-1} \mathcal{C}_j^{N-1} \frac{\omega_l^j (-1)^j}{\Gamma(m_d)} \sum_{l=0}^{j(m_d-1)} \sum_{i=0}^{l} \mathcal{C}_i^l \left(\frac{m_d}{\Omega_d \eta_r}\right)^{m_d+i} \times \sum_{k=0}^{m_d+i-1} \xi_{i,j,l} \frac{\Gamma(m_d+i)}{\chi_j^{-(m_d+i-k)} k!} \left(\beta_\delta x + \frac{m_I}{\Omega_I}\right)^{-(q+m_I)}. \tag{3.83}$$

Now, after inserting (3.83) into (3.32), and performing the solution with the use of [59, eq. 9.211.4], the closed-form expression of average SEP can be obtained as given in (3.33).

Appendix 3.F: Proof of Theorem 4

Under the hypotheses of Theorem 4, $\overline{C}_1$ can be written as

$$\overline{C}_1 = \frac{1}{2\ln 2} \int_0^{\infty} \mathrm{e}^{-s} \widehat{\mathcal{M}}_{\gamma_{sc}}(s) ds. \tag{3.84}$$

To evaluate complementary MGF transform of γ_{sc} in (3.84), first we require the CDF of γ_{sc}. On invoking the CDF from (3.11) and the PDF from (3.21) into (3.69), and after performing the required integration, the CDF $F_{\gamma_{sc}}(x)$ can be derived as

$$F_{\gamma_{sc}}(x) = 1 - \sum_{i_1=0}^{m_s-1} \cdots \sum_{i_{N_s}=0}^{m_s-1} \frac{\Xi(N_s)}{\eta_s^{\Lambda}} \sum_{p=0}^{\Lambda-1} \frac{\Gamma(\Lambda)}{p!} {\beta_\delta}^{-(\Lambda-p)} \times \frac{\Gamma(p+m_I)}{\Gamma(m_I)} \left(\frac{m_I}{\Omega_I}\right)^{m_I} x^p \left(\beta_\delta x + \frac{m_I}{\Omega_I}\right)^{-(p+m_I)}. \tag{3.85}$$

Then, on inserting the expression from (3.85) into (3.40a), we have

$$\widehat{\mathcal{M}}_{\gamma_{sc}}(s) = \int_0^{\infty} \mathrm{e}^{-sx} \left[\sum_{i_1=0}^{m_s-1} \cdots \sum_{i_{N_s}=0}^{m_s-1} \frac{\Xi(N_s)}{\eta_s^{\Lambda}} \sum_{p=0}^{\Lambda-1} \frac{\Gamma(\Lambda)}{p!} {\beta_\delta}^{-(\Lambda-p)} \times \frac{\Gamma(p+m_I)}{\Gamma(m_I)} \left(\frac{m_I}{\Omega_I}\right)^{m_I} x^p \left(\beta_\delta x + \frac{m_I}{\Omega_I}\right)^{-(p+m_I)} \right] dx. \tag{3.86}$$

To compute the integral in (3.86), we make use of the identities of Meijer's G-function as [96, eqs. (10) and (11)]

$$(1+ax)^{-\ell} = \frac{1}{\Gamma(\ell)} G_{1,1}^{1,1}\left[ax \middle| \begin{matrix} 1-\ell \\ 0 \end{matrix} \right]$$
$$\text{and } \mathrm{e}^{-bx} = G_{0,1}^{1,0}\left[bx \middle| \begin{matrix} - \\ 0 \end{matrix} \right]. \tag{3.87}$$

Thereby, solving the integral in (3.86) using (3.87) and [96, eq. (21)], and after simplifying with [59, eq. 9.31.2], we get

$$\widehat{\mathcal{M}}_{\gamma_{sc}}(s) = \sum_{i_1=0}^{m_s-1} \cdots \sum_{i_{N_s}=0}^{m_s-1} \frac{\Xi(N_s)}{\eta_s^{\Lambda}} \sum_{p=0}^{\Lambda-1} \frac{\Gamma(\Lambda)}{p!} {\beta_\delta}^{-(\Lambda-p)} \frac{1}{\Gamma(m_I)}$$
$$\times \left(\frac{m_I}{\Omega_I}\right)^{-p} s^{-(p+1)} G_{1,2}^{2,1}\left[\frac{\frac{m_I}{\Omega_I} s}{\beta_\delta} \middle| \begin{matrix} 1 \\ 1+p, p+m_I \end{matrix} \right]. \tag{3.88}$$

On inserting the above result in (3.84), and then solving the involved integral using [59, eq. 7.813.1], we get the expression of $\overline{C}_1$ as given in (3.42).

Further, to evaluate $\overline{C}$ in (3.39), we need to solve the component $\overline{C}_2$ which can be written as

$$\overline{C}_2 = \frac{1}{2\ln 2} \int_0^\infty \mathrm{e}^{-s} \widehat{\mathcal{M}}_{\gamma_{sc}}(s) \mathcal{M}_{\widetilde{\gamma}_{rd}}(s) ds. \tag{3.89}$$

We proceed by first evaluating the MGF transform of $\widetilde{\gamma}_{rd}$ from (3.40b) using the PDF from (3.16) as

$$\mathcal{M}_{\widetilde{\gamma}_{rd}}(s) = N \sum_{j=0}^{N-1} \mathcal{C}_j^{N-1} \frac{(-1)^j}{\Gamma(m_d N_d)} \sum_{l=0}^{j(m_d N_d-1)} \omega_l^j \sum_{i=0}^{l} \mathcal{C}_i^l$$
$$\times \frac{\xi_{i,j,l}\, \chi_j^{m_d N_d + i}}{\left(\frac{m_d}{\Omega_d \eta_r}\right)^{-(m_d N_d+i)}} G_{1,1}^{1,1}\left[\chi_j\, s \middle| \begin{matrix} 1-m_d N_d - i \\ 0 \end{matrix} \right]. \tag{3.90}$$

Finally, by substituting the results from (3.88) and (3.90) in (3.89), and performing the integration with the aid of [97, eq. 2.6.2], the expression as given in (3.43) can be obtained.

Appendix 3.G: Proof of Theorem 5

EC for the correlated shadowed-Rician fading case can be evaluated by using the similar steps as in Appendix 3.F. Under the hypotheses of Theorem 5, $\overline{C}_{o1}$ and $\overline{C}_{o2}$

represent the first and second integral terms in (3.39), which are equivalent to $\overline{C}_1$ in (3.84) and $\overline{C}_2$ in (3.89), respectively. Thereby, to evaluate $\overline{C}_{o1}$, we require the complementary MGF transform of γ_{sc}, which can be calculated by invoking CDF $F_{\gamma_{sc}}(x)$ in (3.40a) for correlated fading case. For this, we first obtain the CDF of γ_{sc}, by using (3.13) and (3.21) in (3.69), as

$$F_{\gamma_{sc}}(x) = 1 - \zeta \sum_{k=0}^{\infty} \varrho_k \sum_{\ell=0}^{m_s N_s + k - N_s} \varpi_{k,\ell} \sum_{p}^{N_s+\ell-1} \frac{\Gamma(N_s+\ell)}{p!} \left(\frac{\varphi}{\eta_s}\right)^{-(N_s+\ell-p)} \frac{\Gamma(p+m_I)}{\Gamma(m_I)} \times \left(\frac{m_I}{\Omega_I}\right)^{m_I} x^p \left(\frac{\varphi}{\eta_s}x + \frac{m_I}{\Omega_I}\right)^{-(p+m_I)}. \tag{3.91}$$

Now, substituting (3.91) in (3.40a) and solving involved integral with the aid of (3.87), [96, eq. (21)], and [59, eq.9.31.2], $\widehat{\mathcal{M}}_{\gamma_{sc}}(s)$ can be obtained as

$$\widehat{\mathcal{M}}_{\gamma_{sc}}(s) = \zeta \sum_{k=0}^{\infty} \varrho_k \sum_{\ell=0}^{m_s N_s + k - N_s} \varpi_{k,\ell} \sum_{p}^{N_s+\ell-1} \frac{\Gamma(N_s+\ell)}{p!} \left(\frac{\varphi}{\eta_s}\right)^{-(N_s+\ell-p)} \times \frac{1}{\Gamma(m_I)} \left(\frac{\Omega_I}{m_I}\right)^{p} s^{-(p+1)} G_{1,2}^{2,1}\left[\frac{\frac{m_I}{\Omega_I}s}{\frac{\varphi}{\eta_s}} \middle| \begin{matrix} 1 \\ 1+p, p+m_I \end{matrix}\right]. \tag{3.92}$$

Then, invoking (3.92) in (3.84), $\overline{C}_{o1}$ can be solved and thus given as in (3.45). And, in the similar way, plugging (3.92) and (3.90) in (3.89), one can get $\overline{C}_{o2}$ as given in (3.46).

Appendix 3.H: Proof of Theorem 6

Using the above CDF, we can readily obtain the conditional complementary MGF transform $\widehat{\mathcal{M}}_{\gamma_{sr}}(zs|Z)$ as

$$\widehat{\mathcal{M}}_{\gamma_{sr}}(zs|Z) = \sum_{i_1=0}^{m_s-1} \cdots \sum_{i_{N_s}=0}^{m_s-1} \frac{\Xi(N_s)}{(\eta_s)^{\Lambda}} \sum_{p=0}^{\Lambda-1} \frac{\Gamma(\Lambda)\Gamma(p+1)}{p!\,(\beta_\delta)^{\Lambda+1}} \left(1+\frac{zs}{\beta_\delta}\right)^{-p-1}. \tag{3.93}$$

We can represent (3.93) in a more general form, using the fact (3.87), as

$$\widehat{\mathcal{M}}_{\gamma_{sr}}(zs|Z) = \sum_{i_1=0}^{m_s-1} \cdots \sum_{i_{N_s}=0}^{m_s-1} \frac{\Xi(N_s)}{(\eta_s)^{\Lambda}} \sum_{p=0}^{\Lambda-1} \frac{\Gamma(\Lambda)}{p!} (\beta_\delta)^{-\Lambda-1} G_{1,1}^{1,1}\left[\frac{zs}{\beta_\delta} \middle| \begin{matrix} -p \\ 0 \end{matrix}\right]. \tag{3.94}$$

Next, we determine the MGF $\mathcal{M}_{\gamma_c}(zs|Z)$ as

$$\mathcal{M}_{\gamma_c}(zs|Z) = \int_0^{\infty} \mathrm{e}^{-zsx} f_{\gamma_c}(x)dx. \tag{3.95}$$

On solving (3.95) using the PDF of γ_c from (3.21) and subsequently applying the identity in (3.87), we attain

$$\mathcal{M}_{\gamma_c}(zs|Z) = \frac{1}{\Gamma(m_I)} G_{1,1}^{1,1}\left[zs\left(\frac{\Omega_I}{m_I}\right) \middle| \begin{matrix} 1-m_I \\ 0 \end{matrix} \right]. \tag{3.96}$$

Plugging (3.96) and (3.94) into (3.56), we get

$$\begin{aligned} \overline{C} = & \frac{1}{2\ln 2} \sum_{i_1=0}^{m_s-1} \cdots \sum_{i_{N_s}=0}^{m_s-1} \frac{\Xi(N_s)}{(\eta_s)^{\Lambda}} \sum_{p=0}^{\Lambda-1} \frac{\Gamma(\Lambda)}{p!} (\beta_\delta)^{-\Lambda-1} \frac{1}{\Gamma(m_I)} \\ & \times \int_0^\infty z \left(\int_0^\infty \mathrm{e}^{-s} G_{1,1}^{1,1}\left[\frac{zs}{\beta_\delta} \middle| \begin{matrix} -p \\ 0 \end{matrix} \right] G_{1,1}^{1,1}\left[zs\left(\frac{\Omega_I}{m_I}\right) \middle| \begin{matrix} 1-m_I \\ 0 \end{matrix} \right] ds \right) f_Z(z)dz. \end{aligned} \tag{3.97}$$

In (3.97), the inner integral can be solved as [97, eq. 2.6.2]

$$\begin{aligned} & \int_0^\infty \mathrm{e}^{-s} G_{1,1}^{1,1}\left[\frac{zs}{\beta_\delta} \middle| \begin{matrix} -p \\ 0 \end{matrix} \right] G_{1,1}^{1,1}\left[zs\left(\frac{\Omega_I}{m_I}\right) \middle| \begin{matrix} 1-m_I \\ 0 \end{matrix} \right] ds \\ & \quad = G_{1,[1:1],0,[1:1]}^{1,1,1,1,1}\left[\begin{matrix} \frac{z}{\beta_\delta} \\ z\left(\frac{\Omega_I}{m_I}\right) \end{matrix} \middle| \begin{matrix} 0;1+p;m_I \\ -;0;0 \end{matrix} \right]. \end{aligned} \tag{3.98}$$

Next, the PDF $f_Z(z)$ can be derived, using simple transformation $f_Z(z) = \mathcal{U} f_{\widetilde{\gamma}_{rd}}(\mathcal{U}z)$ and the fact [96, eq. 11], as

$$\begin{aligned} f_Z(z) = & \mathcal{U}N \sum_{j=0}^{N-1} \mathcal{C}_j^{N-1} \frac{(-1)^j}{\Gamma(m_d N_d)} \sum_{l=0}^{j(m_d N_d-1)} \omega_l^j \sum_{i=0}^{l} \mathcal{C}_i^l \left(\frac{m_d}{\Omega_d \eta_r}\right)^{m_d N_d+i} \\ & \times \xi_{i,j,l} (\mathcal{U}z)^{m_d N_d+i-1} G_{0,1}^{1,0}\left[\frac{\mathcal{U}z}{\chi_j} \middle| \begin{matrix} - \\ 0 \end{matrix} \right]. \end{aligned} \tag{3.99}$$

Now, pulling together (3.98) and (3.99) into (3.97), and after solving the required integral with the aid of [94, eq. 4.1], we obtain the desired EC expression as given in (3.57).

To calculate $\mathcal{U}$ in (3.57), one can find $E[\gamma_c] = \sum_{i=1}^{I} \eta_{ci}\Omega_{ci}$ and $E[\gamma_{sr}]$ using [59, eq. 3.351.3] as

$$\begin{aligned} E[\gamma_{sr}] = & \int_0^\infty x f_{\gamma_{sr}}(x)dx \\ = & \sum_{i_1=0}^{m_s-1} \cdots \sum_{i_{N_s}=0}^{m_s-1} \frac{\Xi(N_s)\Lambda!}{(\eta_s)^{\Lambda}} (\beta_\delta)^{-(\Lambda+1)}. \end{aligned} \tag{3.100}$$

CHAPTER 4

MULTI-USER HYBRID SATELLITE-TERRESTRIAL RELAY NETWORKS WITH A SINGLE EAVESDROPPER

In recent years, HSTRNs have been extensively studied by employing AF- or DF-based relay cooperation in order to improve system performance (e.g., see [18]-[26], [29], [30], [80]-[83] and references therein). However, the transmission security aspects are hardly examined for the HSTRNs. The information security is one of the major problem in the HSTRNs. In fact, due to the broadcasting nature of wireless channels, HSTRNs are more prone to security assaults. Hence, security and privacy concerns in such communication networks are challenging issues. Therefore, investigation of secrecy performance of HSTRNs is also important.

In this chapter, we investigate the secrecy performance of an AF-based multi-user HSTRN in the presence of a single eavesdropper. We resort to the PLS technique for analyzing secrecy performance of the considered HSTRN. With the PLS technique, very limited works have investigated the secrecy performance of the HSTRN [98]-[101]. The authors in [98] and [99] have proposed a secure design with the deployment of a multi-antenna relay, where MRC and transmit zero-forcing beamforming based schemes were utilized to exhort the security issues in HSTRNs. Moreover, authors in [100] and [101] have examined the PLS of a cognitive satellite-terrestrial network by considering underlay spectrum sharing technique. However, these aforementioned works are limited to a single-user scenario. To our best knowledge, the secrecy performance analysis of an HSTRN with a single-eavesdropper configuration has not been addressed so far. In fact, the deployment of multiple users makes the proposed configuration more favorable for practical applications.

In light of the above discussion, we conduct secrecy performance analysis of an AF-based multi-user HSTRN in the presence of a single eavesdropper. By employing opportunistic scheduling of terrestrial users, we derive accurate and asymptotic SOP expressions under pertinent fading channels for satellite and terrestrial links. The asymptotic SOP expression helps us in examining the achievable diversity order of the considered HSTRN. We also consider the round-robin scheduling for comparison purpose. The SOP expression under round-robin scheduling scheme are derived over the pertinent fading channels. The main focus of this chapter is to analyze a multi-user HSTRN and to highlight the impact of key parameters on the secrecy performance and achievable diversity order of such system.

The remainder of this chapter is organized as follows. In Section 4.1, we describe the system and channel models. Further, we perform secrecy performance analysis in Section 4.2. Section 4.3 presents the numerical and simulation results, and finally, the summary of this chapter is given in Section 4.4.

4.1 System and Channel Model Descriptions

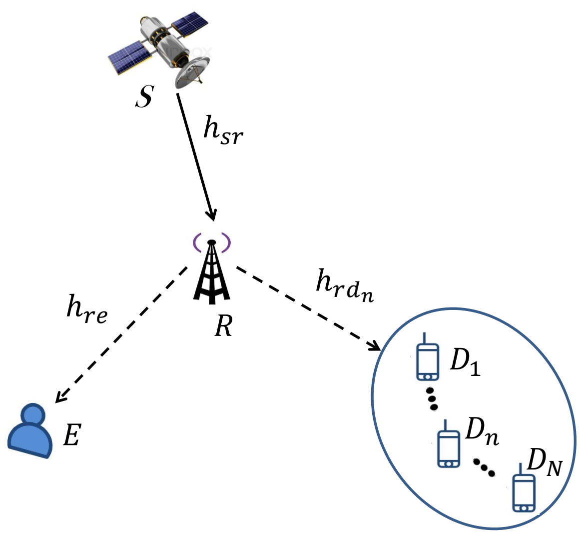

Figure 4.1: System model for a multi-user HSTRN with a single eavesdropper.

As shown in Fig. 4.1, we consider a downlink HSTRN consisting of a satellite source S, an AF relay R, N destinations $\{D_n\}_{n=1}^{N}$, and an eavesdropper E. All nodes are equipped with a single-antenna. The LOS links between S and $\{D_n\}_{n=1}^{N}$ as well as between S and E are not available owing to the masking effect. Therefore, S communicates with $\{D_n\}_{n=1}^{N}$ via a terrestrial AF relay R in the presence of eavesdropper E. The satellite link (i.e., $S \rightarrow R$ link) is assumed to undergo shadowed-Rician fading while terrestrial links (i.e., $R \rightarrow D_n$ and $R \rightarrow E$ links) experience Nakagami-m fading. All the receiving nodes are inflicted by AWGN with zero mean and variance σ^2. Herein, the $S \rightarrow R \rightarrow D_n$ and $S \rightarrow R \rightarrow E$ links are referred to as the main and the wiretap links, respectively.

The overall communication takes place in two time phases by employing an opportunistic user scheduling scheme. In the first phase, satellite source S transmits its signal x_s (with unit energy) to the relay R. Thus, the received signal at R can be given by

$$y_{sr} = \sqrt{P_s} h_{sr} x_s + n_r, \tag{4.1}$$

where P_s is the transmit power at S, h_{sr} is the channel coefficient between S and R, and n_r is the AWGN at R.

In the second phase, the relay R first amplifies the received signal y_{sr} using a gain factor G and then forwards it to the selected destination D_n. Meanwhile, the eavesdropper tries to overhear the signal transmitted from relay. Therefore, the signals received at destination D_n and eavesdropper E can be given, respectively, as

$$y_{rd_n} = \sqrt{P}_r h_{rd_n} G\, y_{sr} + n_{d_n} \tag{4.2a}$$

$$\text{and} \qquad y_{re} = \sqrt{P}_r h_{re} G\, y_{sr} + n_e, \tag{4.2b}$$

where P_r is the transmit power at relay R, h_{rd_n} and h_{re} denote the respective channel coefficients for $R \to D_n$ and $R \to E$ links, while n_{d_n} and n_e represent the AWGN variables at the respective nodes.

Based on (4.2a) and (4.2b), the instantaneous received SNRs at D_n and E can be obtained, respectively, as

$$\gamma_{D_n} = \frac{\gamma_{sr}\gamma_{rd_n}}{\gamma_{rd_n} + \frac{1}{G^2\sigma^2}} \tag{4.3a}$$

$$\text{and} \qquad \gamma_E = \frac{\gamma_{sr}\gamma_{re}}{\gamma_{re} + \frac{1}{G^2\sigma^2}}, \tag{4.3b}$$

where $\gamma_{sr} = \eta_s |h_{sr}|^2$, $\gamma_{rd_n} = \eta_r |h_{rd_n}|^2$, and $\gamma_{re} = \eta_r |h_{re}|^2$ with $\eta_s = \frac{P_s}{\sigma^2}$ and $\eta_r = \frac{P_r}{\sigma^2}$. For variable gain relaying, the gain factor G in (4.3a) and (4.3b) can be determined as

$$G = \sqrt{\frac{1}{P_s|h_{sr}|^2 + \sigma^2}}, \tag{4.4}$$

and thus, (4.3a) and (4.3b) can be simplified, respectively, as

$$\gamma_{D_n} = \frac{\gamma_{sr}\gamma_{rd_n}}{\gamma_{sr} + \gamma_{rd_n} + 1} \tag{4.5a}$$

$$\text{and} \qquad \gamma_E = \frac{\gamma_{sr}\gamma_{re}}{\gamma_{sr} + \gamma_{re} + 1}. \tag{4.5b}$$

Now, we illustrate the statistical characterization for fading channels of each hop. As the satellite link (i.e., $S \rightarrow R$) follows independent shadowed-Rician fading distribution, the PDF of γ_{sr} can be derived, using (2.3) and making a transformation of variates, as

$$f_{\gamma_{sr}}(x) = \alpha \sum_{\kappa=0}^{m_s-1} \frac{\zeta(\kappa)}{(\eta_s)^{\kappa+1}} x^{\kappa} \mathrm{e}^{-\beta_\delta x}, \tag{4.6}$$

and by integrating (4.6), the CDF of γ_{sr} can be obtained as

$$F_{\gamma_{sr}}(x) = 1 - \alpha \sum_{\kappa=0}^{m_s-1} \frac{\zeta(\kappa)}{(\eta_s)^{\kappa+1}} \sum_{p=0}^{\kappa} \frac{\kappa!}{p!} \beta_\delta^{-(\kappa+1-p)} x^p \mathrm{e}^{-\beta_\delta x}. \tag{4.7}$$

For terrestrial links, the channel coefficients h_{rd_n} and h_{re} undergo Nakagami-m distribution with fading severity m_{d_n} and m_e, and average power Ω_{d_n} and Ω_e, respectively. As such, the PDF and CDF of channel gain γ_{rd_n} are given, respectively, by

$$f_{\gamma_{rd_n}}(x) = \left(\frac{m_{d_n}}{\varrho_{d_n}}\right)^{m_{d_n}} \frac{x^{m_{d_n}-1}}{\Gamma(m_{d_n})} \mathrm{e}^{-\frac{m_{d_n}}{\varrho_{d_n}} x} \tag{4.8a}$$

$$\text{and} \qquad F_{\gamma_{rd_n}}(x) = \frac{1}{\Gamma(m_{d_n})} \Upsilon\left(m_{d_n}, \frac{m_{d_n}}{\varrho_{d_n}} x\right), \tag{4.8b}$$

where $\varrho_{d_n} = \eta_r \Omega_{d_n}$. Similarly, the PDF and CDF of channel gain γ_{re} are given, respectively, as

$$f_{\gamma_{re}}(x) = \left(\frac{m_e}{\varrho_e}\right)^{m_e} \frac{x^{m_e-1}}{\Gamma(m_e)} \mathrm{e}^{-\frac{m_e}{\varrho_e} x} \tag{4.9a}$$

$$\text{and} \qquad F_{\gamma_{re}}(x) = \frac{1}{\Gamma(m_e)} \Upsilon\left(m_e, \frac{m_e}{\varrho_e} x\right), \tag{4.9b}$$

where $\varrho_e = \eta_r \Omega_e$.

4.2 Multi-User Scheduling and SOP Analysis

In this section, by employing opportunistic user scheduling, we first derive the SOP expression of the considered HSTRN and then analyze the asymptotic behavior of the SOP expression at high SNR regime. Further, we obtain the analytical and asymptotic SOP expressions under round-robin scheduling scheme as a benchmark.

4.2.1 Opportunistic Scheduling

To harness the multi-user diversity in the considered network, we utilize the opportunistic scheduling scheme, where the relay select the best user based on the highest instantaneous SNR of $R \rightarrow D_n$ links as

$$\gamma_{rd} = \max_{1 \le n \le N} \gamma_{rd_n}. \tag{4.10}$$

Hence, the actual SNR with the scheduled user can be written as

$$\gamma_D = \frac{\gamma_{sr}\gamma_{rd}}{\gamma_{sr} + \gamma_{rd} + 1}. \tag{4.11}$$

As such, we can define instantaneous capacity of the main link and of the wiretap link by $C_D = \frac{1}{2}\log_2(1+\gamma_D)$ and $C_E = \frac{1}{2}\log_2(1+\gamma_E)$, respectively. Thereby, the achievable secrecy capacity of the considered HSTRN is given as

$$\begin{aligned} C_{\text{sec}} &= [C_D - C_E]^+ \\ &= \left[\frac{1}{2}\log_2(1+\gamma_D) - \frac{1}{2}\log_2(1+\gamma_E)\right]^+. \end{aligned} \tag{4.12}$$

Now, we proceed to obtain the SOP expression. The secrecy outage event is said to occur when the transmitter sends data at a rate $\mathcal{R}_{\text{s}}$ higher than the secrecy capacity C_{sec}. Hence, the SOP for considered HSTRN is formulated as

$$\mathcal{P}_{\text{sec}} = \Pr\left[C_{\text{sec}} < \mathcal{R}_{\text{s}}\right], \tag{4.13}$$

which can be expressed using (4.12) as

$$\mathcal{P}_{\text{sec}} = \Pr\left[\frac{1+\gamma_D}{1+\gamma_E} < \gamma_{\text{s}}\right], \tag{4.14}$$

where $\gamma_{\text{s}} = 2^{2\mathcal{R}_{\text{s}}}$. On performing some appropriate approximation, (4.14) can be given as

$$\mathcal{P}_{\text{sec}} \approx \Pr\left[\frac{\gamma_D}{\gamma_E} < \gamma_{\text{s}}\right], \tag{4.15}$$

where we have used the approximation $\frac{1+x}{1+y} \approx \frac{x}{y}$, which is widely adopted in literature [102], [103] and shown to have negligible effect in broad SNR region. Further, on invoking the SNR expressions from (4.5b) and (4.11) into (4.15) and doing some manipulations for large transmit power, we obtain

$$\begin{aligned} \mathcal{P}_{\text{sec}} &\approx \Pr\left[\frac{\gamma_{sr}\gamma_{rd}}{\gamma_{\text{s}}\gamma_{sr} + (\gamma_{\text{s}} - 1)\gamma_{rd}} < \gamma_{re}\right] \\ &= \int_0^\infty F_Z(z) f_{\gamma_{re}}(z) dz, \end{aligned} \tag{4.16}$$

where the last expression results after defining $Z \triangleq \frac{\gamma_{sr}\gamma_{rd}}{\gamma_{\rm s}\gamma_{sr}+(\gamma_{\rm s}-1)\gamma_{rd}}$. To proceed further, we require the CDF $F_Z(z)$ which can be derived as

$$F_Z(z) = 1 - \int_0^\infty \left(1 - F_{\gamma_{sr}}\left(\frac{z(\gamma_{\rm s}-1)(x+z\gamma_{\rm s})}{x}\right)\right) f_{\gamma_{rd}}(x+z\gamma_{\rm s})dx. \tag{4.17}$$

To solve (4.17), we require the PDF of γ_{rd}. After applying order statistics, $f_{\gamma_{rd}}(x)$ can be given as

$$f_{\gamma_{rd}}(x) = N\left(F_{\gamma_{rd_n}}(x)\right)^{N-1} f_{\gamma_{rd_n}}(x). \tag{4.18}$$

On invoking (4.8b) with series exploration of $\Upsilon(\cdot,\cdot)$ [59, eq. 8.352.1], the corresponding PDF from (4.8a) into (4.18), and then applying binomial [59, eq. 1.111] and multinomial [59, eq. 0.314] expansions, we obtain $f_{\gamma_{rd}}(x)$ as

$$f_{\gamma_{rd}}(x) = N\sum_{\jmath=0}^{N-1}\mathcal{C}_\jmath^{N-1}\sum_{l=0}^{\jmath(m_{d_n}-1)}\frac{\omega_l^\jmath}{\Gamma(m_{d_n})}(-1)^\jmath\left(\frac{m_{d_n}}{\varrho_{d_n}}\right)^{m_{d_n}+l} x^{m_{d_n}+l-1}e^{-\left(\frac{m_{d_n}}{\varrho_{d_n}}\right)(\jmath+1)x}, \tag{4.19}$$

where the coefficients $\omega_l^\jmath$, for $0 \le l \le \jmath(m_{d_n}-1)$, can be calculated recursively (with $\varepsilon_l = \frac{1}{l!}$) as $\omega_0^\jmath = (\varepsilon_0)^\jmath$, $\omega_1^\jmath = \jmath(\varepsilon_1)$, $\omega^\jmath_{\jmath(m_{d_n}-1)} = (\varepsilon_{m_{d_n}-1})^\jmath$, $\omega_l^\jmath = \frac{1}{l\varepsilon_0}\sum_{q=1}^{l}[q\jmath - l+q]\varepsilon_q\omega_{l-q}^\jmath$ for $2 \le l \le m_{d_n}-1$, and $\omega_l^\jmath = \frac{1}{l\varepsilon_0}\sum_{q=1}^{m_{d_n}-1}[q\jmath-l+q]\varepsilon_q\omega_{l-q}^\jmath$ for $m_{d_n} \le l < \jmath(m_{d_n}-1)$.

Now, using (4.7) and (4.19) into (4.17), we can obtain $F_Z(z)$ with the help of [59, eq. 3.471.9], and then substituting the resultant of (4.17) along with (4.9a) into (4.16), and then solving the integration with the use of [59, eq. 7.813.1], we obtain SOP which is given as

$$\begin{aligned}\mathcal{P}_{\rm sec} = 1 - \alpha N &\sum_{\kappa=0}^{m_s-1}\sum_{p=0}^{\kappa}\sum_{\jmath=0}^{N-1}\sum_{l=0}^{\jmath(m_{d_n}-1)}\sum_{q=0}^{t+l}\mathcal{C}_\jmath^{N-1}\mathcal{C}_q^{t+l}\frac{(\gamma_{\rm s}-1)^p\kappa!\zeta(\kappa)}{p!(\eta_s)^{\kappa+1}}\beta_\delta^{-(\kappa+1-p)}\omega_l^\jmath\frac{(-1)^\jmath}{\Gamma(m_{d_n})}\\ &\times\left(\frac{m_{d_n}}{\varrho_{d_n}}\right)^{m_{d_n}+l}\frac{2\sqrt{\pi}}{\Gamma(m_e)}\left(\frac{m_e}{\varrho_e}\right)^{m_e}\left(\Phi + 2\sqrt{\beta_\delta\gamma_{\rm s}(\gamma_{\rm s}-1)\frac{m_{d_n}}{\varrho_{d_n}}(\jmath+1)}\right)^{-(\mu+l+v)}\\ &\times(\gamma_{\rm s})^{t+l-q}\left(4\beta_\delta\gamma_{\rm s}(\gamma_{\rm s}-1)\right)^v\frac{\Gamma(\mu+l+v)\Gamma(\mu+l-v)}{\Gamma(\mu+l+\frac{1}{2})}\\ &\times{}_2F_1\left(\mu+l+v; v+\frac{1}{2}; \mu+l+\frac{1}{2}; \frac{\Phi - 2\sqrt{\beta_\delta\gamma_{\rm s}(\gamma_{\rm s}-1)\frac{m_{d_n}}{\varrho_{d_n}}(\jmath+1)}}{\Phi + 2\sqrt{\beta_\delta\gamma_{\rm s}(\gamma_{\rm s}-1)\frac{m_{d_n}}{\varrho_{d_n}}(\jmath+1)}}\right),\end{aligned} \tag{4.20}$$

where $t = p+m_{d_n}-1$, $v = q-p+1$, $\mu = t+m_e+1$, $\Phi = \beta_\delta(\gamma_{\rm s}-1)+\frac{m_{d_n}}{\varrho_{d_n}}(\jmath+1)\gamma_{\rm s}+\frac{m_e}{\varrho_e}$, and ${}_2F_1(\cdot,\cdot;\cdot;\cdot)$ is the hypergeometric function of second kind [59, eq. 9.111].

To shed more light onto the considered HSTRN secrecy performance, we analyze the asymptotic behaviour of the SOP expression in the high SNR regime. For this,

Z can be simplified as $Z \simeq \min(\gamma_{\rm s}\gamma_{sr}, (\gamma_{\rm s}-1)\gamma_{rd})$ and the CDF $F_Z(x)$ can be approximated by neglecting the higher order term as

$$F_Z(x) \simeq F_{\gamma_{sr}}((\gamma_{\rm s}-1)x) + F_{\gamma_{rd}}(\gamma_{\rm s}x). \tag{4.21}$$

To proceed, we require asymptotic expressions for $F_{\gamma_{sr}}(x)$ and $F_{\gamma_{rd}}(x)$. At high SNR regime, we assume $\eta_s \to \infty$ and apply the Maclaurin series expansion of the exponential function in (4.6) to approximate the PDF $f_{\gamma_{sr}}(x)$ as

$$f_{\gamma_{sr}}(x) \simeq \frac{\alpha}{\eta_s}, \tag{4.22}$$

and hence, by integrating (4.22), the asymptotic behaviour of $F_{\gamma_{sr}}(x)$ can be given as

$$F_{\gamma_{sr}}(x) \simeq \frac{\alpha}{\eta_s}x. \tag{4.23}$$

Likewise, one can derive

$$F_{\gamma_{rd}}(x) \simeq \frac{x^{m_{d_n}N}}{[\Gamma(m_{d_n}+1)]^N}\left(\frac{m_{d_n}}{\varrho_{d_n}}\right)^{m_{d_n}N}. \tag{4.24}$$

Now, invoking (4.23) and (4.24) into (4.21), and substituting the obtained result into (4.16) along with (4.9a), and then solving the involved integral using [59, eq. 3.351.3], we can obtain the asymptotic SOP expression as

$$\mathcal{P}_{\rm sec}^{\infty} \simeq \frac{\alpha(\gamma_{\rm s}-1)\varrho_e}{\eta_s} + \frac{(m_{d_n}N+m_e-1)!}{[\Gamma(m_{d_n}+1)]^N\,\Gamma(m_e)}\left(\frac{m_{d_n}}{\varrho_{d_n}}\right)^{m_{d_n}N}\gamma_{\rm s}^{m_{d_n}N}\left(\frac{m_e}{\varrho_e}\right)^{-m_{d_n}N}, \tag{4.25}$$

which clearly reflects the achievable diversity order of $\min(1, m_{d_n}N)$.

Remarks: Our asymptotic analysis of SOP reveals that the considered HSTRN attains a diversity order of $\min(1, m_{d_n}N)$. Importantly, the diversity order is mainly bottlenecked by the satellite link, whereby it remains unaffected by the fading severity parameter of satellite link.

4.2.2 Round-Robin Scheduling

In order to prove the superiority of the opportunistic scheduling, we herein present the SOP performance of considered multi-user HSTRN under round-robin scheduling scheme for comparison. Round-robin scheduling scheme guarantees fair scheduling to all users. The closed-form SOP expression under round-robin scheduling scheme are derived over the pertinent fading channels. Given that user D_n is selected, the

SOP for n-th user can be expressed as

$$\mathcal{P}_{\mathrm{sec},n} = \Pr\left[C_{\mathrm{sec},n} < \mathcal{R}_{\mathrm{s}}\right], \tag{4.26}$$

where $C_{\mathrm{sec},n} = \left[\frac{1}{2}\log_2(1+\gamma_{D_n}) - \frac{1}{2}\log_2(1+\gamma_E)\right]^+$. Substituting $C_{\mathrm{sec},n}$ into (4.26) yields

$$\mathcal{P}_{\mathrm{sec},n} = \Pr\left[\frac{1+\gamma_{D_n}}{1+\gamma_E} < \gamma_{\mathrm{s}}\right], \tag{4.27}$$

which is further approximated and simplified as

$$\begin{aligned}\mathcal{P}_{\mathrm{sec},n} &\approx \Pr\left[Z_n < \gamma_{re}\right] \\ &= \int_0^\infty F_{Z_n}(z) f_{\gamma_{re}}(z) dz,\end{aligned} \tag{4.28}$$

where $Z_n \triangleq \frac{\gamma_{sr}\gamma_{rd_n}}{\gamma_{\mathrm{s}}\gamma_{sr}+(\gamma_{\mathrm{s}}-1)\gamma_{rd_n}}$. To solve further, $F_{Z_n}(z)$ can be obtained as

$$F_{Z_n}(z) = 1 - \int_0^\infty \left(1 - F_{\gamma_{sr}}\left(\frac{z(\gamma_{\mathrm{s}}-1)(x+z\gamma_{\mathrm{s}})}{x}\right)\right) f_{\gamma_{rd_n}}(x+z\gamma_{\mathrm{s}}) dx. \tag{4.29}$$

By invoking (4.7) and (4.8a) into (4.29), and applying [59, eq. 3.471.9], we can obtain $F_{Z_n}(z)$, and then substituting the resultant of (4.29) along with (4.9a) into (4.28), and then performing solution with the fact [59, eq. 7.813.1], we obtain $\mathcal{P}_{\mathrm{sec},n}$ as

$$\begin{aligned}\mathcal{P}_{\mathrm{sec},n} = 1 - \alpha \sum_{\kappa=0}^{m_s-1}\sum_{p=0}^{\kappa}\sum_{q=0}^{t} \mathcal{C}_q^t \frac{(\gamma_{\mathrm{s}}-1)^p \kappa! \zeta(\kappa)}{p!(\eta_s)^{\kappa+1}} \beta_\delta^{-(\kappa+1-p)} \frac{1}{\Gamma(m_{d_n})}\left(\frac{m_{d_n}}{\varrho_{d_n}}\right)^{m_{d_n}} \\ \times \frac{2\sqrt{\pi}}{\Gamma(m_e)}\left(\frac{m_e}{\varrho_e}\right)^{m_e} (\gamma_{\mathrm{s}})^{t-q}\left(4\beta_\delta\gamma_{\mathrm{s}}(\gamma_{\mathrm{s}}-1)\right)^v \frac{\Gamma(\mu+v)\Gamma(\mu-v)}{\Gamma(\mu+\frac{1}{2})} \\ \times \left(\beta_\delta(\gamma_{\mathrm{s}}-1) + \frac{m_{d_n}}{\varrho_{d_n}}\gamma_{\mathrm{s}} + \frac{m_e}{\varrho_e} + 2\sqrt{\beta_\delta\gamma_{\mathrm{s}}(\gamma_{\mathrm{s}}-1)\frac{m_{d_n}}{\varrho_{d_n}}}\right)^{-(\mu+v)} \\ \times {}_2F_1\left(\mu+v; v+\frac{1}{2}; \mu+\frac{1}{2}; \frac{\beta_\delta(\gamma_{\mathrm{s}}-1) + \frac{m_{d_n}}{\varrho_{d_n}}\gamma_{\mathrm{s}} + \frac{m_e}{\varrho_e} - 2\sqrt{\beta_\delta\gamma_{\mathrm{s}}(\gamma_{\mathrm{s}}-1)\frac{m_{d_n}}{\varrho_{d_n}}}}{\beta_\delta(\gamma_{\mathrm{s}}-1) + \frac{m_{d_n}}{\varrho_{d_n}}\gamma_{\mathrm{s}} + \frac{m_e}{\varrho_e} + 2\sqrt{\beta_\delta\gamma_{\mathrm{s}}(\gamma_{\mathrm{s}}-1)\frac{m_{d_n}}{\varrho_{d_n}}}}\right).\end{aligned} \tag{4.30}$$

The SOP for the round-robin scheduling scheme is given, by the mean of N users' secrecy outage probabilities, as

$$\mathcal{P}_{\mathrm{sec}}^{\text{Round-Robin}} = \frac{1}{N}\sum_{n=1}^{N}\mathcal{P}_{\mathrm{sec},n}, \tag{4.31}$$

where $\mathcal{P}_{\mathrm{sec},n}$ is given by (4.30).

Moreover, the asymptotic SOP under round-robin scheduling scheme can be derived as

$$\mathcal{P}_{\text{sec},n}^{\infty,\text{Round-Robin}} \simeq \frac{\alpha(\gamma_{\text{s}}-1)\varrho_e}{\eta_s} + \frac{(m_{d_n}+m_e-1)!}{\Gamma(m_{d_n}+1)\Gamma(m_e)}\left(\frac{m_{d_n}}{\varrho_{d_n}}\right)^{m_{d_n}} \gamma_{\text{s}}^{m_{d_n}} \left(\frac{m_e}{\varrho_e}\right)^{-m_{d_n}}. \tag{4.32}$$

From (4.32), one can clearly observe that system achieves a diversity order of $\min(1, m_{d_n})$ under round-robin scheduling scheme.

4.3 Numerical and Simulation Results

In this section, we present numerical and simulation results to confirm the validity of the proposed theoretical studies and examine the impact of various system/channel parameters on the secrecy performance of the considered system. For this, we set $\eta_s = \eta_r$ as transmit SNR. The shadowed-Rician fading parameters for $S \rightarrow R$ link are adopted as $(m_s, b, \Omega_s = 1, 0.063, 0.0007)$ under heavy shadowing and $(m_s, b, \Omega_s = 5, 0.251, 0.279)$ under average shadowing scenarios [58]. For validation of theoretical analysis we carried out Monte-Carlo simulations.

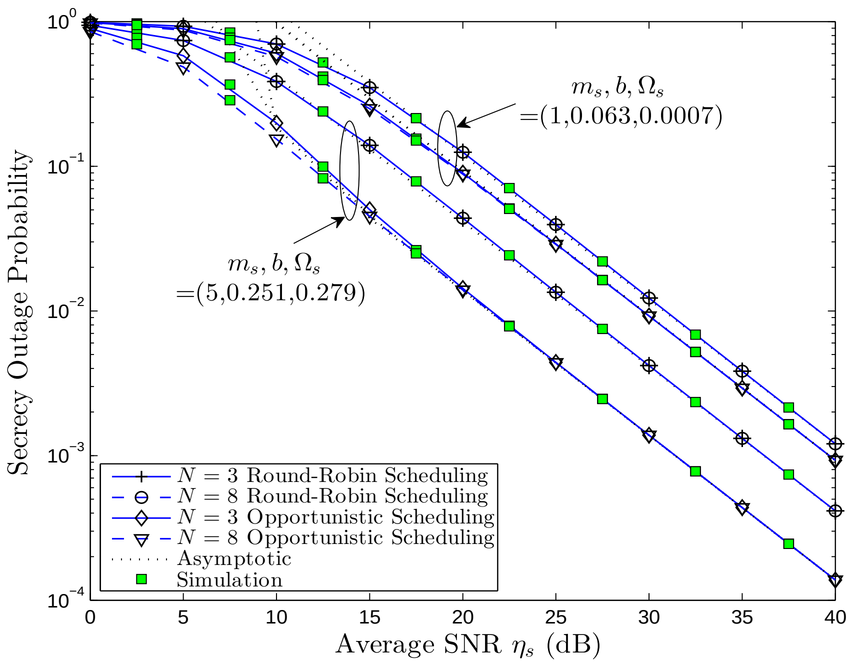

Figure 4.2: SOP versus η_s under round-robin scheduling and opportunistic scheduling schemes with different number of users N.

In Fig. 4.2, we draw the SOP curves under round-robin scheduling and opportunistic scheduling schemes for different number of terrestrial users under average and heavy shadowing scenarios of shadowed-Rician fading. Herein, we set $\mathcal{R}_{\text{s}} = 0.4$,

$m_{d_n} = 1$, $m_e = 2$, and $\varrho_e = 2$ dB. It can be observed in the Fig. 4.2 that when the number of users increases from $N = 3$ to $N = 8$, the SOP of the conventional round-robin scheduling remains unchanged. By contrast, the secrecy performance under opportunistic scheduling scheme corresponding to $N = 8$ is notably better than that corresponding to $N = 3$. This further confirms the security performance advantage of the opportunistic scheduling over the round-robin scheduling scheme.

Observing the superiority of opportunistic scheduling scheme over round-robin scheduling scheme, we now discuss the numerical and simulation results based on opportunistic scheduling scheme in subsequent figures.

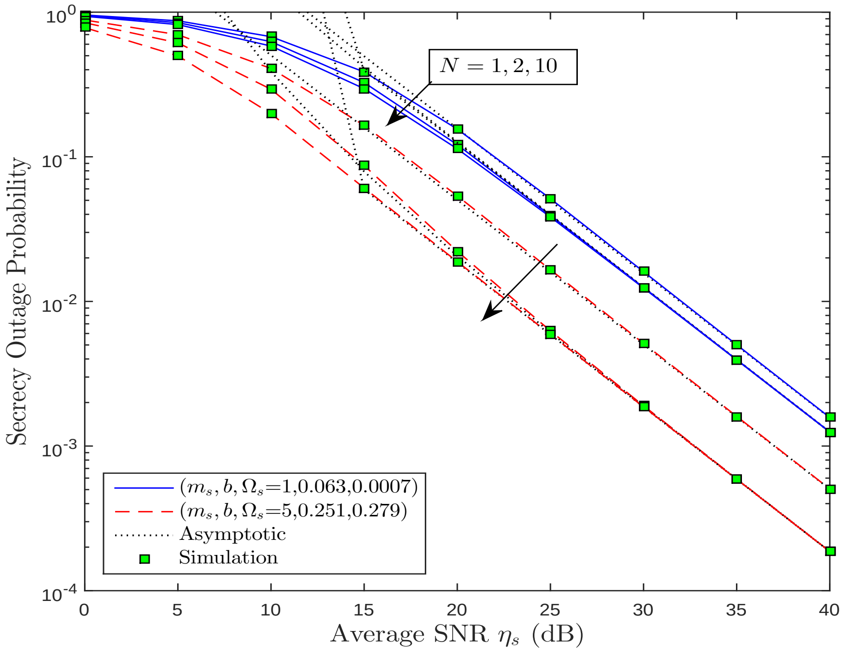

Figure 4.3: SOP versus η_s for different number of terrestrial users under opportunistic scheduling scheme.

Fig. 4.3 depicts the SOP performance of the considered HSTRN versus η_s for various number of terrestrial users under average and heavy shadowing scenarios of shadowed-Rician fading channel. By fixing $\mathcal{R}_{\rm s} = 0.5$, $m_{d_n} = 1$, $m_e = 1$, and $\varrho_e = 2$ dB, SOP curves are drawn using (4.20). In addition, we also drawn the asymptotic SOP curves using (4.25) (for the same configuration), which agree very well with the exact ones in the high SNR region. We can see from this figure that secrecy performance of the system improves with an increase in the number of terrestrial users. However, owing to the bottleneck effect of the satellite link, this performance improvement becomes limited when N increases to a certain extent, as reflected by comparing the curves for $N = 2$ and $N = 10$. It is important to note that the

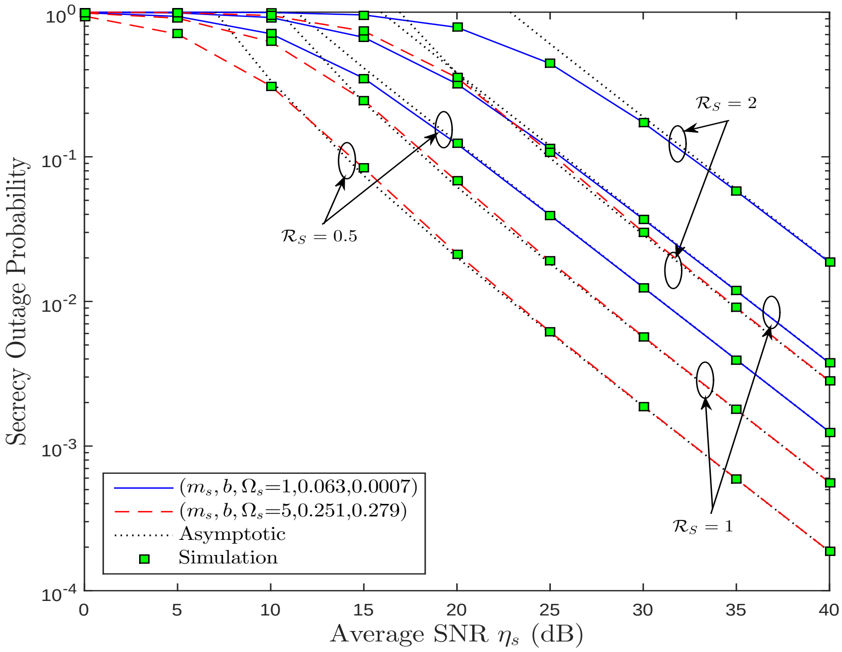

Figure 4.4: SOP versus η_s with different $\mathcal{R}_\mathrm{s}$ under opportunistic scheduling scheme.

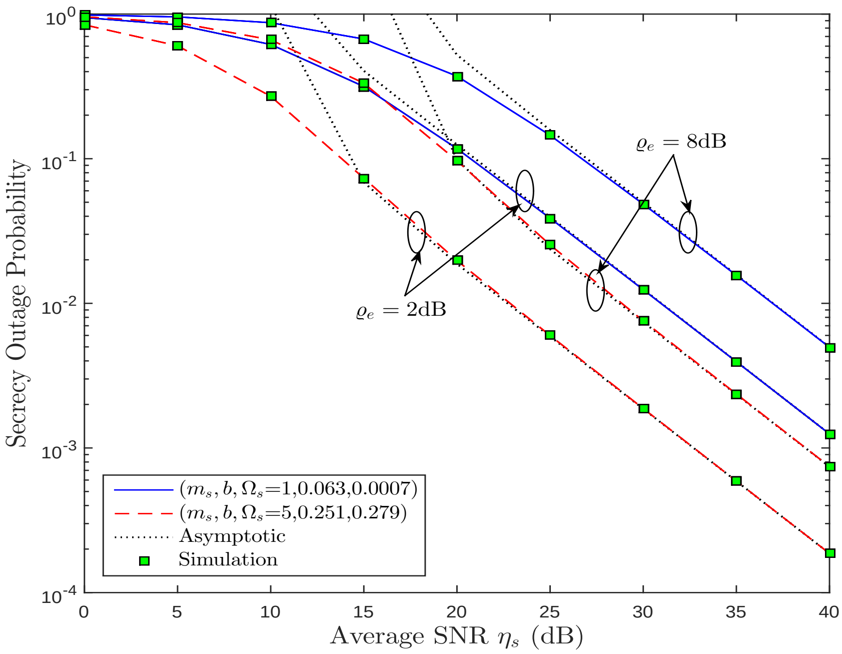

Figure 4.5: SOP versus η_s with different ϱ_e under opportunistic scheduling scheme.

system attains the diversity order of $\min(1, m_{d_n}N)$ i.e., unity, which can be seen by the slope of the curves. Moreover, it can be realized that the system performs better under average shadowed-Rician fading as compared to heavy shadowed-Rician fading scenario.

In Fig. 4.4, we illustrate the SOP performance versus η_s with different values of secrecy rate $\mathcal{R}_\mathrm{s}$ by assuming $m_{d_n} = 1$, $m_e = 2$, $\varrho_e = 2$ dB, and $N = 1$. The curves are plotted under average and heavy shadowed scenarios of $S \to R$ link. As can be expected, the SOP of the considered HSTRN degrades with an increase in the secrecy rate $\mathcal{R}_{\mathrm{s}}$. Importantly, this increase in the $\mathcal{R}_{\mathrm{s}}$ does not affect the achievable diversity order of the system.

Fig. 4.5 illustrates the SOP of the system for different values of ϱ_e. As shown in the figure, curves are drawn for two different values of ϱ_e (i.e., 2 dB and 8 dB) under average and heavy shadowing scenarios of shadowed-Rician fading channels by keeping $N = 2$, $m_{d_n} = 2$, $m_e = 1$, and $\mathcal{R}_{\mathrm{s}} = 0.5$. One can clearly observe that the SOP of the considered HSTRN increases as the ϱ_e increases which indicates the detrimental impact of a more powerful eavesdropper.

4.4 Summary

In this chapter, we have investigated the secrecy performance of a downlink multi-user HSTRN using AF relaying and opportunistic user scheduling. We also considered the conventional round-robin scheduling scheme for comparison. By following shadowed-Rician fading for satellite link and Nakagami-m fading for terrestrial links, we derived accurate and asymptotic SOP expressions for the considered system under both the scheduling schemes. Numerical results showed that the opportunistic user scheduling outperforms the round-robin scheduling in terms of SOP performance. For opportunistic scheduling scheme, we obtained the system achievable diversity order and revealed that it depends on the fading severity parameter of the relay-destinations links and number of terrestrial users while remains unaffected by the fading severity parameter of satellite link. We highlighted the impact of various key system/channel parameters on the secrecy performance of the considered system. Our results revealed that the increase of the number of terrestrial users plays an important role in improving the secrecy performance of the considered HSTRN.

CHAPTER 5

MULTI-RELAY HYBRID SATELLITE-TERRESTRIAL RELAY NETWORKS WITH A SINGLE EAVESDROPPER

In the previous chapter, a single-relay assisted HSTRNs have been studied in the context of PLS. Recently, the multi-relay systems have been widely explored (e.g. [51], [105] and references cited therein) to improve the performance of secure communications, where the best relay is selected to forward information toward the destination. The fundamental idea behind the multi-relay cooperation is to introduce additional channels between the source and destination using intermediate nodes. In fact, these relay cooperation can enhance spatial diversity without increasing the number of antennas and can provide extended coverage [104]. Although, several studies have been carried out towards the performance analysis of HSTRNs, however, the secrecy performance of an HSTRN with multiple relays has overlooked in the literature. Since the relay selection schemes have been proved as an efficient technique to improve system performance and reliability [51], it is important to investigate the relay selection schemes and their performance for HSTRNs in view of PLS towards 5G and future networks.

In this chapter, we consider an AF-based multi-relay HSTRN, where a satellite communicates with a terrestrial destination via multiple relays in the presence of a single eavesdropper. Herein, we present optimal and partial relay selection schemes that opportunistically select a single-relay based on the CSI requirements of the main and eavesdropper links. The optimal scheme depends on both main and wiretapper links, while the partial scheme relies only on the legitimate terrestrial links. Adopting shadowed-Rician fading for satellite links and Nakagami-m fading for terrestrial links, we derive the closed-form SOP expressions for both selection schemes. The underlying selection strategies are designed to minimize the SOP of the considered HSTRN. We further simplify these expressions at asymptotic high

SNR regime to reveal useful insights on achievable diversity gains.

5.1 System and Channel Model Descriptions

As depicted in Fig. 5.1, we consider an HSTRN consisting of one satellite source S, multiple terrestrial relays R_k ($k = 1, ..., K$), a destination D, and an eavesdropper E. Herein, the LOS links between S and D as well as between S and E are considered to be unavailable owing to the masking effect. Therefore, the data transmission from the satellite S to the destination D can take place via R_k relays only, with the possible wiretap from an eavesdropper E at the ground. Each node is assumed to be equipped with a single-antenna. The S-R_k links follow the shadowed-Rician fading while the R_k−D and R_k−E links are assumed to undergo Nakagami-m fading. We also assume that all the links are inflicted by AWGN with zero mean and variance N_0. The overall communication takes place in two time phases by employing an

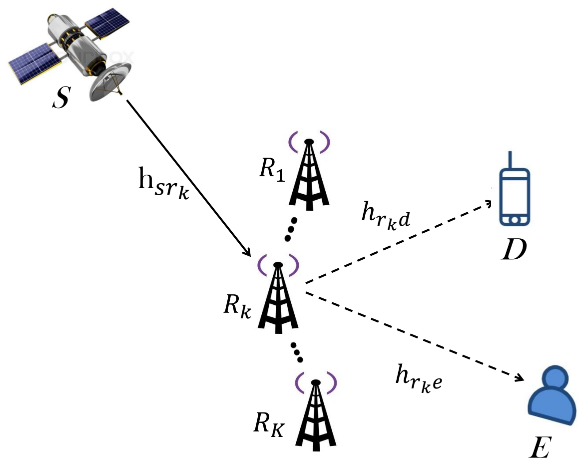

Figure 5.1: System model of a multi-relay HSTRN with a single eavesdropper.

AF-based opportunistic relay selection scheme. We will discuss the appropriate selection strategies in subsequent section. In the first phase, satellite source S sends its signal x_s, having unit energy, to the relay R_k. The received signal at R_k can be thus given by

$$y_{sr_k} = \sqrt{P_s} h_{sr_k} x_s + n_{sr_k}, \tag{5.1}$$

where P_s is the transmit power at S, h_{sr_k} is the channel coefficient between S and R_k, and n_{sr_k} is the AWGN at R_k. During the second phase, the relay R_k forwards an amplified version of y_{sr_k} using a gain factor $\mathcal{G} = \sqrt{\frac{P_r}{P_s|h_{sr_k}|^2+N_0}}$, where P_r is the transmit power at relay R_k. Therefore, the signals received at destination D and eavesdropper E can be given, respectively, as

$$y_{r_k d} = h_{r_k d}\mathcal{G}y_{sr_k} + n_{r_k d} \tag{5.2}$$

and

$$y_{r_k e} = h_{r_k e}\mathcal{G}y_{sr_k} + n_{r_k e}, \tag{5.3}$$

where $h_{r_k d}$ and $h_{r_k e}$ represent the respective channel coefficients for $R_k{-}D$ and $R_k{-}E$ links, while $n_{r_k d}$ and $n_{r_k e}$ denote the AWGN variables at the respective nodes. From the above equations, we can deduce the instantaneous received SNRs at D and E, respectively, as

$$\Lambda_{D,k} = \frac{\gamma_{sr_k}\gamma_{r_k d}}{\gamma_{sr_k} + \gamma_{r_k d} + 1}, \tag{5.4}$$

and

$$\Lambda_{E,k} = \frac{\gamma_{sr_k}\gamma_{r_k e}}{\gamma_{sr_k} + \gamma_{r_k e} + 1}, \tag{5.5}$$

where $\gamma_{sr_k} = \eta_s|h_{sr_k}|^2$, $\gamma_{r_k d} = \eta_r|h_{r_k d}|^2$, and $\gamma_{r_k e} = \eta_r|h_{r_k e}|^2$ with $\eta_s = \frac{P_s}{N_0}$ and $\eta_r = \frac{P_r}{N_0}$. Thus, with AF relaying transmission using R_k, the instantaneous capacity of the main channel (for destination) and of the wiretap channel (for eavesdropper) are given, respectively, by $C_{D,k} = \frac{1}{2}\log_2(1 + \Lambda_{D,k})$ and $C_{E,k} = \frac{1}{2}\log_2(1 + \Lambda_{E,k})$. Consequently, the secrecy capacity is given by the difference between the capacity of the main channel and the wiretap channel i.e.,

$$C_{\mathrm{sec},k} = [C_{D,k} - C_{E,k}]^+. \tag{5.6}$$

Considering shadowed-Rician fading model for the satellite links, the PDF of $\gamma_{sr_k} = \eta_s|h_{sr_k}|^2$ can be given, using (2.3) and making a transformation of variates, as

$$f_{\gamma_{sr_k}}(x) = \alpha \sum_{\kappa=0}^{m_s-1} \frac{\zeta(\kappa)}{(\eta_s)^{\kappa+1}} x^{\kappa} \mathrm{e}^{-\beta_\delta x}. \tag{5.7}$$

The CDF $F_{\gamma_{sr_k}}(x)$ can be obtained, by integrating the PDF in (5.7) with the use of [59, eq. 3.351.2], as

$$F_{\gamma_{sr_k}}(x) = 1 - \alpha \sum_{\kappa=0}^{m_s-1} \frac{\zeta(\kappa)}{(\eta_s)^{\kappa+1}} \sum_{p=0}^{\kappa} \frac{\kappa!}{p!} \beta_\delta^{-(\kappa+1-p)} x^p \mathrm{e}^{-\beta_\delta x}. \tag{5.8}$$

For terrestrial links, the channel coefficient $h_{r_k j}$, for $j \in \{d, e\}$, follows Nakagami-m distribution with fading severity m_j and average power Ω_j. As such, the PDF and CDF of channel gain γ_{r_kj} are given, respectively, by

$$f_{\gamma_{r_kj}}(x) = \left(\frac{m_j}{\varrho_j}\right)^{m_j} \frac{x^{m_j-1}}{\Gamma(m_j)} \mathrm{e}^{-\frac{m_j}{\varrho_j}x} \tag{5.9}$$

$$\text{and} \qquad F_{\gamma_{r_kj}}(x) = \frac{1}{\Gamma(m_j)} \Upsilon\left(m_j, \frac{m_j}{\varrho_j}x\right), \tag{5.10}$$

where $\varrho_j = \eta_r \Omega_j$.

5.2 Opportunistic Relay Selection and Secrecy Outage Analysis

For the HSTRN as described previously, the secrecy outage event is said to occur when the secrecy capacity falls below a predefined secrecy rate $\mathcal{R}_\mathrm{s}$. Hence, the SOP for considered HSTRN with k-th relay is formulated as

$$\mathcal{P}_{\mathrm{sec},k} = \Pr\left[C_{\mathrm{sec},k} < \mathcal{R}_\mathrm{s}\right], \tag{5.11}$$

which can be expressed using (5.6) as

$$\mathcal{P}_{\mathrm{sec},k} = \Pr\left[\frac{1+\Lambda_{D,k}}{1+\Lambda_{E,k}} < \gamma_\mathrm{s}\right], \tag{5.12}$$

where $\gamma_\mathrm{s} = 2^{2\mathcal{R}_\mathrm{s}}$. Now, we study the opportunistic relay selection schemes to minimize the SOP of the considered HSTRN. Hereby, we first discuss the optimal selection scheme under the assumption that the CSI of all the main and eavesdropper links are available. Then, we consider a partial selection scheme that relies only on the knowledge of the CSI of relay-destination links and not on relay-eavesdropper links. In the sequel, we derive the closed-form SOP expressions for both optimal and partial selection schemes over heterogeneous channels.

5.2.1 Optimal Relay Selection

The optimal relay selection strategy to minimize the SOP in (5.12) can be formulated as

$$k^* = \arg \max_{k=1,\ldots,K} \left(\frac{1+\Lambda_{D,k}}{1+\Lambda_{E,k}}\right). \tag{5.13}$$

Based on (5.13), we apply order statistics over K relays to represent the SOP of the considered HSTRN with selected relay R_{k^*} as

$$\mathcal{P}_{\mathrm{sec},k^*}^{\mathrm{opt}} = \prod_{k=1}^{K} \left[\mathcal{P}_{\mathrm{sec},k}\right]. \tag{5.14}$$

However, on inserting (5.4) and (5.5) into (5.12), one can realize that the exact evaluation of $\mathcal{P}_{\mathrm{sec},k}$ in (5.14) is very tedious. Therefore, we first approximate (5.12) as

$$\mathcal{P}_{\mathrm{sec},k} \approx \Pr\left[\frac{\Lambda_{D,k}}{\Lambda_{E,k}} < \gamma_{\mathrm{s}}\right], \tag{5.15}$$

where we have used the approximation $\frac{1+u}{1+v} \approx \frac{u}{v}$, which is widely adopted in literature [102], [103] and shown to have negligible effect in high SNR region. Further, on invoking the SNR expressions from (5.4) and (5.5) into (5.15) and doing some manipulations for large transmit power, we obtain

$$\begin{aligned}\mathcal{P}_{\mathrm{sec},k} &\approx \Pr\left[\frac{\gamma_{sr_k}\gamma_{r_kd}}{\gamma_{\mathrm{s}}\gamma_{sr_k} + (\gamma_{\mathrm{s}}-1)\gamma_{r_kd}} < \gamma_{r_ke}\right] \\ &= \int_0^\infty F_{Z_k}(z) f_{\gamma_{r_ke}}(z) dz, \end{aligned} \tag{5.16}$$

where the last expression results after defining $Z_k = \frac{\gamma_{sr_k}\gamma_{r_kd}}{\gamma_{\mathrm{s}}\gamma_{sr_k}+(\gamma_{\mathrm{s}}-1)\gamma_{r_kd}}$. To proceed further, we require the CDF $F_{Z_k}(z)$ which can be derived as

$$F_{Z_k}(z) = 1 - \int_0^\infty \left(1 - F_{\gamma_{sr_k}}\left(\frac{z(\gamma_{\mathrm{s}}-1)(x+z\gamma_{\mathrm{s}})}{x}\right)\right) f_{\gamma_{r_kd}}(x+z\gamma_{\mathrm{s}}) dx. \tag{5.17}$$

Now, using the CDF $F_{\gamma_{sr_k}}(\cdot)$ from (5.8) and the PDF $f_{\gamma_{r_kd}}(\cdot)$ from (5.9) into (5.17), performing simplifications with [59, eqs. 1.111, 3.471.9], and then using the result to further solve (5.16) to obtain the closed-form expression for $\mathcal{P}^{\mathrm{opt}}_{\mathrm{sec},k^*}$ as

$$\begin{aligned}\mathcal{P}^{\mathrm{opt}}_{\mathrm{sec},k^*} = \Bigg[1 - \widetilde{\sum_{\{\kappa,p\}}^{m_s}} \frac{1}{\Gamma(m_d)}\left(\frac{m_d}{\varrho_d}\right)^{m_d} \sum_{q=0}^{t} \mathcal{C}_q^t (\gamma_{\mathrm{s}})^{t-q} \frac{2\sqrt{\pi}}{\Gamma(m_e)}\left(\frac{m_e}{\varrho_e}\right)^{m_e} \\ \times \left(\frac{4\xi\varrho_d}{m_d}\right)^{v}\left(\psi_{(\gamma_{\mathrm{s}},0)} + 2\sqrt{\xi}\right)^{-(\mu+v)} \frac{\Gamma(\mu+v)\Gamma(\mu-v)}{\Gamma(\mu+\frac{1}{2})} \\ \times {}_2F_1\left(\mu+v; v+\frac{1}{2}; \mu+\frac{1}{2}; \frac{\psi_{(\gamma_{\mathrm{s}},0)} - 2\sqrt{\xi}}{\psi_{(\gamma_{\mathrm{s}},0)} + 2\sqrt{\xi}}\right)\Bigg]^K, \end{aligned} \tag{5.18}$$

where $\widetilde{\sum_{\{\kappa,p\}}^{m_s}} = \sum_{\kappa=0}^{m_s-1} \frac{\alpha\zeta(\kappa)}{(\eta_s)^{\kappa+1}} \sum_{p=0}^{\kappa} \frac{\kappa!(\gamma_{\mathrm{s}}-1)^p}{p!} (\beta_\delta)^{-(\kappa+1-p)}$, $t = p+m_d-1$, $v = q-p+1$, $\mu = t+m_e+1$, $\xi = \frac{\beta-\delta}{\eta_s}\gamma_{\mathrm{s}}(\gamma_{\mathrm{s}}-1)\frac{m_d}{\varrho_d}$, $\psi_{(\gamma_{\mathrm{s}},\tau)} = \frac{\beta-\delta}{\eta_s}(\gamma_{\mathrm{s}}-1) + \frac{m_d}{\varrho_d}(\tau+1)\gamma_{\mathrm{s}} + \frac{m_e}{\varrho_e}$, and ${}_2F_1(\cdot,\cdot;\cdot;\cdot)$ is the hypergeometric function of second kind [59, eq. 9.111].

To attain more insights, we pursue an asymptotic analysis of SOP at high SNR ($\eta_s \to \infty$) and high main-to-eavesdropper ratio (MER) with $\varrho_d \gg \varrho_e$. Herein, we apply $\mathrm{e}^{-z} \underset{z\to 0}{\simeq} 1-z$ in (5.8) and $\Upsilon(a,z) \underset{z\to 0}{\simeq} \frac{z^a}{a}$ in (5.10) and use the simplified results to solve (5.16) subsequently to obtain an asymptotic SOP expression as

$$\mathcal{P}^{\mathrm{opt}}_{\mathrm{sec},k^*} \simeq \left[\frac{\alpha(\gamma_{\mathrm{s}}-1)\varrho_e}{\eta_s} + \frac{\Gamma(m_d+m_e)}{\Gamma(m_d+1)\Gamma(m_e)}\left(\frac{m_d}{\varrho_d}\right)^{m_d} \gamma_{\mathrm{s}}^{m_d}\left(\frac{m_e}{\varrho_e}\right)^{-m_d}\right]^K, \tag{5.19}$$

which clearly reflects the diversity order of $K\min(1, m_d)$.

5.2.2 Partial Relay Selection

As stated before, the optimal relay selection scheme in (5.13) requires the CSI knowledge of the relay-eavesdropper links and therefore its practical implementation is jeopardized. The proposed partial relay selection technique incorporates the best instantaneous SNR towards the destination. So, to devise a partial selection scheme that can depend only on the CSI of relay-destination links, we can write the selected relay R_{k^*} as

$$k^* = \arg \max_{k=1,\ldots,K} \gamma_{r_k d}. \tag{5.20}$$

Then, the SOP of the considered HSTRN with selected relay R_{k^*} for partial selection scheme can be evaluated as

$$\mathcal{P}^{\text{par}}_{\text{sec},k^*} = \Pr\left[\frac{1+\Lambda_{D,k^*}}{1+\Lambda_{E,k^*}} < \gamma_{\text{s}}\right], \tag{5.21}$$

which can be further simplified as in (5.16) to

$$\begin{aligned}\mathcal{P}^{\text{par}}_{\text{sec},k^*} &\approx \Pr\left[Z_{k^*} < \gamma_{r_{k^*}e}\right] \\ &= \int_0^\infty F_{Z_{k^*}}(z) f_{\gamma_{r_{k^*}e}}(z) dz,\end{aligned} \tag{5.22}$$

where $Z_{k^*} = \frac{\gamma_{sr_{k^*}}\gamma_{r_{k^*}d}}{\gamma_{\text{s}}\gamma_{sr_{k^*}}+(\gamma_{\text{s}}-1)\gamma_{r_{k^*}d}}$. Since the satellite and eavesdropper links are not involved in the relay selection, we can derive the CDF of Z_{k^*} as in (5.17) by using the CDF $F_{\gamma_{sr_{k^*}}}(\cdot)$ from (5.8) and the PDF $f_{\gamma_{r_{k^*}d}}(\cdot)$ as

$$f_{\gamma_{r_{k^*}d}}(x) = \widetilde{\sum_{\{\jmath,l\}}^{m_d}} \omega_l^\jmath \frac{(-1)^\jmath}{\Gamma(m_d)} \left(\frac{m_d}{\varrho_d}\right)^{m_d+l} x^{m_d+l-1} e^{-\frac{m_d}{\varrho_d}(\jmath+1)x}, \tag{5.23}$$

where $\widetilde{\sum_{\{\jmath,l\}}^{m_d}} = K\sum_{\jmath=0}^{K-1}\mathcal{C}_\jmath^{K-1}\sum_{l=0}^{\jmath(m_d-1)}$ and the coefficients $\omega_l^\jmath$ is defined similarly as in (4.19). Then, on inserting the result along with PDF of $\gamma_{r_{k^*}e}$ from (5.9) into (5.22), and after performing the integration, we obtain a closed-form expression of $\mathcal{P}^{\text{par}}_{\text{sec},k^*}$ as

$$\begin{aligned}\mathcal{P}^{\text{par}}_{\text{sec},k^*} &= 1 - \widetilde{\sum_{\{\kappa,p\}}^{m_s}} \widetilde{\sum_{\{\jmath,l\}}^{m_d}} \omega_l^\jmath \frac{(-1)^\jmath}{\Gamma(m_d)}\left(\frac{m_d}{\varrho_d}\right)^{m_d+l} \sum_{q=0}^{t+l} \mathcal{C}_q^{t+l}(\gamma_{\text{s}})^{t+l-q} \frac{2\sqrt{\pi}}{\Gamma(m_e)}\left(\frac{m_e}{\varrho_e}\right)^{m_e} \\ &\times \left(\psi_{(\gamma_{\text{s}},\jmath)} + 2\sqrt{\xi(\jmath+1)}\right)^{-(\mu+l+v)} \left(\frac{4\xi\varrho_d}{m_d}\right)^v \frac{\Gamma(\mu+l+v)\Gamma(\mu+l-v)}{\Gamma(\mu+l+\frac{1}{2})} \\ &\times {}_2F_1\left(\mu+l+v; v+\frac{1}{2}; \mu+l+\frac{1}{2}; \frac{\psi_{(\gamma_{\text{s}},\jmath)} - 2\sqrt{\xi(\jmath+1)}}{\psi_{(\gamma_{\text{s}},\jmath)} + 2\sqrt{\xi(\jmath+1)}}\right).\end{aligned} \tag{5.24}$$

Moreover, the asymptotic SOP for partial selection scheme can be derived as

$$\mathcal{P}_{\text{sec},k^*}^{\text{par}} \simeq \frac{\alpha(\gamma_{\text{s}}-1)\varrho_e}{\eta_s} + \frac{\Gamma(m_d K + m_e)}{[\Gamma(m_d+1)]^K \Gamma(m_e)} \left(\frac{m_d}{\varrho_d}\right)^{m_d K} \gamma_{\text{s}}^{m_d K} \left(\frac{m_e}{\varrho_e}\right)^{-m_d K}. \quad (5.25)$$

From the above expression, one can readily observe that the system experiences a diversity order of $\min(1, m_d K)$ only for partial selection scheme.

5.3 Numerical and Simulation Results

In this section, we perform numerical investigations for the aforementioned secrecy analysis and validate our derived results through Monte-Carlo simulations. The simulation results are obtained with 10^6 channel realizations. Herein, we compare the SOP performance as a function of $\varrho_d = \eta_s$ between the optimal relay selection scheme and partial relay selection scheme. For numerical investigation, we set $m_d = 1$, $m_e = 3$, and adopt the shadowed-Rician fading parameters for the satellite-relay links under the heavy shadowing scenario $(m_s, b, \Omega_s = 1, 0.063, 0.0007)$.

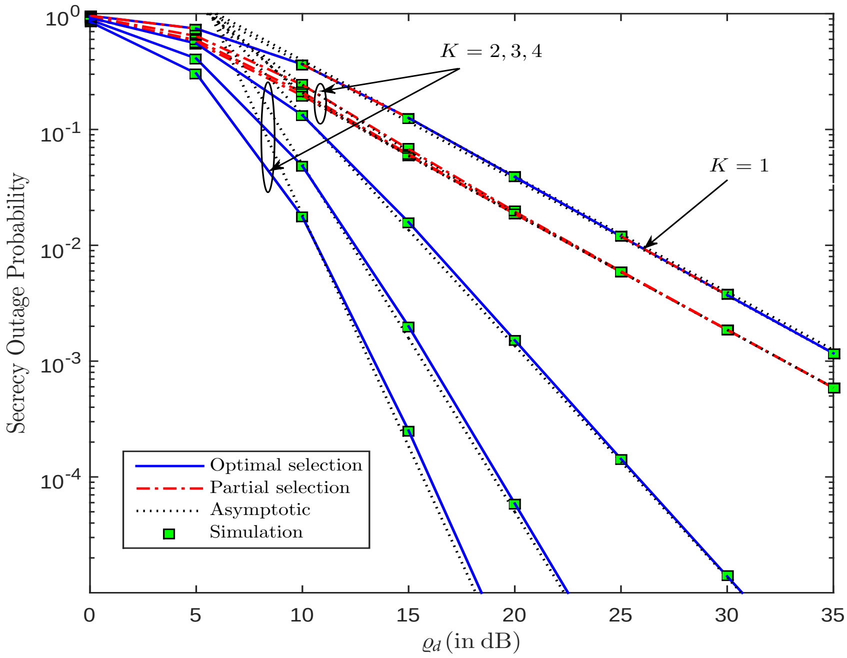

Figure 5.2: SOP versus ϱ_d for different number of relays.

In Fig. 5.2, we plot the SOP curves for the considered HSTRN with various number of relays, where the average SNR is set to $\varrho_e = 2$ dB and the target secrecy rate $\mathcal{R}_{\text{s}} = 0.1$ bps/Hz. The analytical and asymptotic curves are drawn using (5.18) and (5.19) for optimal scheme, and (5.24) and (5.25) for partial scheme, respectively, which are clearly found to be aligned and corroborated with the simulation results.

One can readily observe that the optimal selection scheme outperforms the partial selection scheme. It is apparent that for partial selection scheme, the secrecy outage diversity order is not affected by number of relays, as indicated by the parallel slopes of the asymptotes. However, the secrecy outage diversity order for optimal selection scheme depends on the number of relays K.

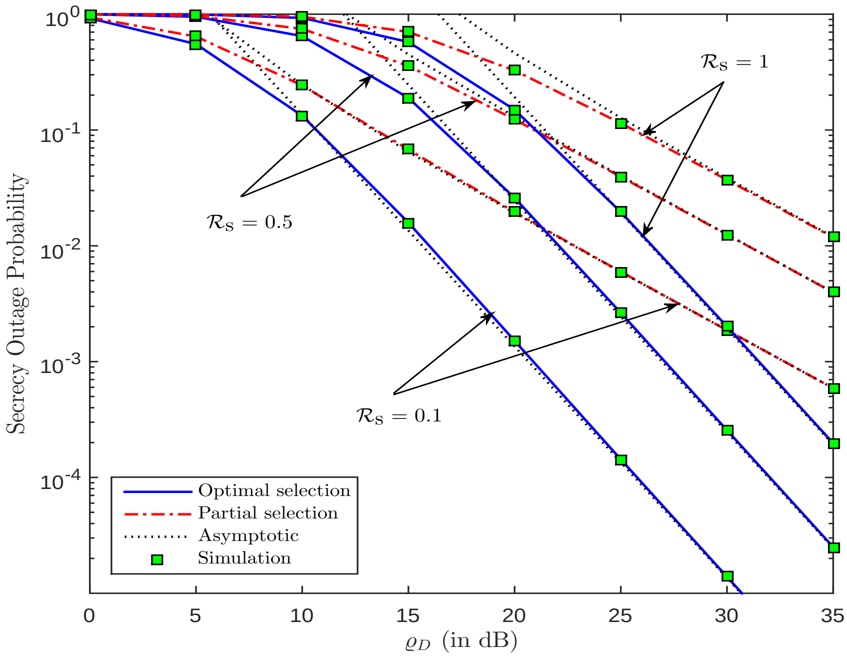

Figure 5.3: SOP versus ϱ_d for different $\mathcal{R}_s$.

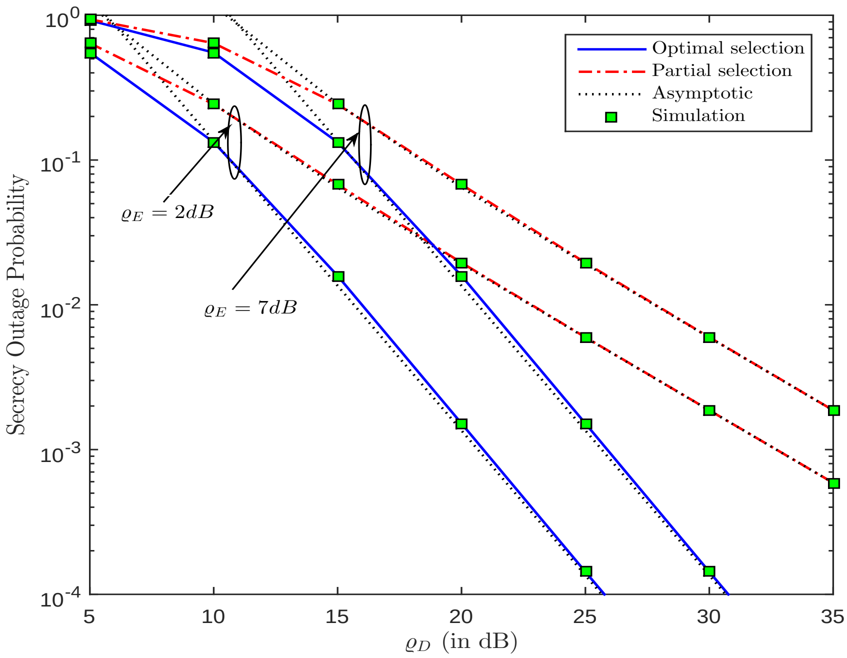

Figure 5.4: SOP versus ϱ_d for different ϱ_e.

Both relay selection schemes are compared in terms of SOP by fixing $\varrho_e = 2$ dB, $K = 2$, and varying ϱ_d in steps of 5 dB for different target secrecy rates in Fig. 5.3. Specifically, we can observe that system gives better performance at small value of $\mathcal{R}_{\mathrm{s}}$. As can be expected, the secrecy outage performance of the system degrades with an increase of target secrecy rate.

Fig. 5.4 depicts the probability of secrecy outage versus ϱ_d of multi-relay HSTRN for different eavesdropper's average SNR ϱ_e. As shown in the figure, with the increase of the ϱ_e, the SOP decreases, which reflects the detrimental effects of a more egregious eavesdropper.

5.4 Summary

In this chapter, we evaluated the secrecy outage performance of a multi-relay HSTRN employing optimal and partial relay selection schemes in the presence of an eavesdropper. Specifically, we designed optimal and partial relay selection schemes based on the CSI requirements of the main and wiretapper links. Then, we derived the closed-form and asymptotic SOP expressions for the considered HSTRN. Our results illustrated that the optimal selection scheme outperforms the partial selection scheme. Moreover, our results revealed that an increase in the number of terrestrial relays plays an important role in improving the secrecy performance of the considered HSTRN.

CHAPTER 6

SINGLE-USER SINGLE-RELAY HYBRID SATELLITE-TERRESTRIAL RELAY NETWORKS WITH MULTIPLE EAVESDROPPERS

In the previous chapters, secrecy analysis was limited to a single-eavesdropper scenario. However, in practice, it is highly probable that a large number of malicious nodes try to attack the legitimate transmission. These eavesdroppers may be collude together and work collaboratively or scattered randomly to increase the chance of wiretapping. As discussed previously, considerable attention has been paid towards the secrecy performance investigation of HSTRNs, but, most of them were mainly concentrated on a single-eavesdropper scenario. Recently, PLS performance in HSTRNs with multiple eavesdroppers has been investigated in [99] and [108], where authors have considered independent and identically distributed (i.i.d.) Rayleigh fading for terrestrial nodes. To the extent of the our knowledge, investigation of PLS performance of an HSTRN with multiple independent and non-identically distributed (i.ni.d.) eavesdroppers has not been done so far. Indeed, the eavesdroppers are unintended users which may be randomly scattered in the vicinity of the intended terrestrial user. And, due to rapidly growing wireless communication technologies, accessing and exchanging the information has become an easily accomplished task. Thereby, it is essential to analyze the effect of the multiple i.ni.d. eavesdroppers on the secrecy performance of the HSTRNs. To fill this research gap, we take i.ni.d. multiple colluding eavesdroppers into account and analyze PLS performance of HSTRN.

Motivated by the above, in this chapter, we consider an AF-based HSTRN with a terrestrial user and a multi-antenna satellite in the presence of multiple i.ni.d. colluding eavesdroppers. Such a communication set-up can be feasible in various practical scenarios (e.g., under military and defence services), where a multi-antenna satellite source communicates to an intended user with the cooperation of a relay node in the presence of multiple non-intended users (e.g., high-speed smart devices such as, handheld, vehicle mounted, and nomadic devices) at the ground. Albeit, securing downlink satellite transmissions poses different mathematical challenges, we conduct a comprehensive secrecy performance analysis of the proposed HSTRN in terms of SOP and ESC. The main contributions of this chapter are summarized as follows:

- We characterize the framework for PLS in an HSTRN with multiple antennas at the satellite and with multiple eavesdroppers at the ground. We concentrate on the effect of i.ni.d. Nakagami-m fading channels for multiple eavesdroppers and investigate the key measures of secrecy performance for the proposed HSTRN. Comparing to existing works such as [99], [108] where i.i.d. Rayleigh fading channel coefficients are considered for multiple eavesdroppers and satellite is restricted to a single-antenna source, this chapter focuses on the impact of i.ni.d. Nakagami-m fading channels with a multi-antenna satellite, and emphasizes the importance of a multi-antenna satellite in enhancement of the secrecy performance.

- By assuming shadowed-Rician fading for satellite channel and i.ni.d. Nakagami-m fading for terrestrial channels, we derive novel expression for SOP of the proposed HSTRN. Also, we obtain the SOP expression at high SNR regime and reveal the secrecy diversity order of the system. Based on the asymptotic analysis, we highlight the dependency of system/channel parameters on the achievable secrecy diversity of the proposed HSTRN.

- We further evaluate the expressions of ESC for the considered HSTRN. To justify our analysis, we present numerical and simulation results and explore the effect of the key parameters on PLS performance.

The remainder of this chapter is organized as follows. We illustrate system and channel model for an HSTRN with multiple colluding eavesdroppers in Section 6.1. We obtain the expressions of SOP, asymptotic SOP and ESC of the considered system in Section 6.2. Further, we present the numerical and simulation results in Section 6.3. The summary of this chapter is presented in Section 6.4.

6.1 System and Channel Model Descriptions

We consider an HSTRN consisting of a satellite source S equipped with N_s antennas, one terrestrial relay R, and one terrestrial destination D in the presence of L colluding eavesdroppers $\{E_l\}_{l=1}^L$. The schematic diagram of the considered network is depicted in Fig. 6.1. In this network, the direct links between S and D as well as between S and $\{E_l\}$ are considered to be unavailable due to severe shadowing and masking effect [18], [80]. Thereby, the communication between S and D takes place with the assistance of R, albeit in the presence of illegal hearing from L eavesdroppers at the ground. The satellite channel (i.e., $S \rightarrow R$ channel) is assumed to follow shadowed-Rician fading whereas terrestrial channels (i.e., $R \rightarrow D$ and $R \rightarrow E_l$ channels) undergo Nakagami-m fading. Note that the channel gains between R and $\{E_l\}$ are modelled as i.ni.d. Nakagami-m fading RVs. We consider that both satellite and terrestrial channels are inflicted by AWGN with variance $\mathcal{N}_0$ and zero mean. Further, we denote $S \rightarrow R \rightarrow D$ channel as the main channel and $S \rightarrow R \rightarrow E_l$ channels as the wiretap channels, respectively.

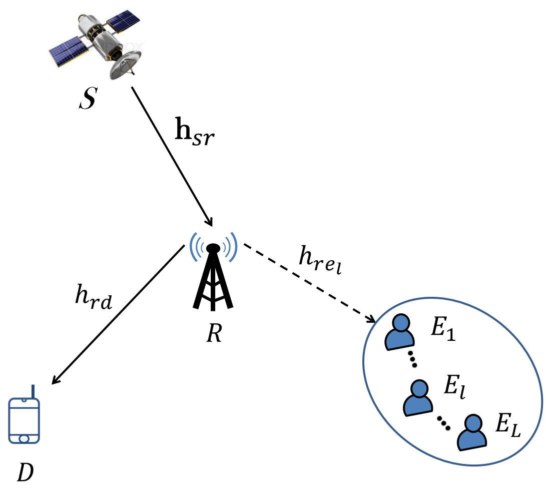

Figure 6.1: System model of a single-user single-relay HSTRN with multiple eavesdroppers.

The end-to-end signal transmission takes place in two time phases. Let x_s be the unit energy signal transmitted by the satellite to relay. In the first time phase, satellite S beamforms x_s to R. Hence, the signal received at relay R can be written as

$$y_r = \sqrt{P_s}\mathbf{h}_{sr}^{\dagger}\mathbf{w}_s x_s + u_r, \tag{6.1}$$

where P_s is the transmit power at S, $\mathbf{h}_{sr} = \left[h_{sr}^{(1)}, h_{sr}^{(2)}, \cdots, h_{sr}^{(N_s)}\right]^T$ be the $N_s \times 1$ channel vector for $S\rightarrow R$ channel, $u_r \sim \mathcal{CN}(0, \mathcal{N}_0)$ is AWGN at R, and $\mathbf{w}_s$ is the $N_s \times 1$ transmit weight vector which is chosen, according to the principle of MRT [85], as $\mathbf{w}_s = \frac{\mathbf{h}_{sr}}{||\mathbf{h}_{sr}||_F}$.

During the second time phase, the relay R first amplifies the received signal y_r by a variable gain factor $\mathcal{G}$ as

$$\mathcal{G} = \sqrt{\frac{1}{P_s|\mathbf{h}_{sr}^{\dagger}\mathbf{w}_s|^2 + \mathcal{N}_0}}, \tag{6.2}$$

and then forwards it to the destination D. Thus, the received signal at the destination D can be given as

$$y_d = \sqrt{P_r}h_{rd}\mathcal{G}y_r + u_d, \tag{6.3}$$

where P_r is the transmit power at R, h_{rd} is channel coefficient of $R\rightarrow D$ link, and $u_d \sim \mathcal{CN}(0, \mathcal{N}_0)$ is AWGN variable at D. At the same time, the eavesdroppers keep an eye on the signal transmitted by relay R and try to intercept the information. Since the direct links from S to $\{E_l\}$ are assumed to be unavailable, it is nearly impossible for the eavesdroppers to overhear the information transmitted from S in first time phase. Thereby, it is considered that eavesdroppers can track only the signal forwarded by the relay and hence, the received signal at the l-th eavesdropper can be given as

$$y_{e_l} = \sqrt{P_r}h_{re_l}\mathcal{G}y_r + u_{e_l}, \tag{6.4}$$

where h_{re_l} represents the fading coefficient of $R\rightarrow E_l$ link and $u_{e_l} \sim \mathcal{CN}(0, \mathcal{N}_0)$ is AWGN variable at eavesdropper E_l.

Thus, based on (6.3) and (6.4), the received instantaneous end-to-end SNRs at the destination D and l-th eavesdropper can be obtained, respectively, as

$$\gamma_D = \frac{\gamma_{sr}\gamma_{rd}}{\gamma_{sr} + \gamma_{rd} + 1} \tag{6.5}$$

and

$$\gamma_{E_l} = \frac{\gamma_{sr}\gamma_{re_l}}{\gamma_{sr} + \gamma_{re_l} + 1}, \tag{6.6}$$

where $\gamma_{sr} = \eta_s||\mathbf{h}_{sr}||_F^2$, $\gamma_{rd} = \eta_r|h_{rd}|^2$, and $\gamma_{re_l} = \eta_r|h_{re_l}|^2$, with $\eta_s = \frac{P_s}{\mathcal{N}_0}$ and $\eta_r = \frac{P_r}{\mathcal{N}_0}$.

Since we have assumed the colluding scenario of eavesdroppers, they can exchange the information with each other and work collectively to strengthen the wiretapping ability. In this case, we consider the MRC at eavesdroppers, thereby, instantaneous end-to-end SNR at colluding eavesdroppers can be represented as [109]

$$\gamma_E = \frac{\gamma_{sr}\gamma_{rE}}{\gamma_{sr} + \gamma_{rE} + 1}. \tag{6.7}$$

where $\gamma_{rE} = \sum_{l=1}^{L} \gamma_{re_l}$.

The instantaneous end-to-end SNRs in (6.5) and (6.7) will be used in secrecy performance analysis in Section 6.2.

Following the shadowed-Rician channel model for satellite links, the PDF and CDF of $\gamma_{sr} = \eta_s ||\mathbf{h}_{sr}||_F^2$ can be respectively given, similar to (3.10) and (3.11), as

$$f_{\gamma_{sr}}(x) = \sum_{i_1=0}^{m_s-1} \cdots \sum_{i_{N_s}=0}^{m_s-1} \frac{\Xi(N_s)}{\eta_s^{\Lambda}} x^{\Lambda-1} \mathrm{e}^{-(\beta_\delta)x} \tag{6.8}$$

and

$$F_{\gamma_{sr}}(x) = 1 - \sum_{i_1=0}^{m_s-1} \cdots \sum_{i_{N_s}=0}^{m_s-1} \frac{\Xi(N_s)}{\eta_s^{\Lambda}} \sum_{p=0}^{\Lambda-1} \frac{(\Lambda-1)!}{p!} \beta_\delta^{-(\Lambda-p)} x^p \mathrm{e}^{-\beta_\delta x}, \tag{6.9}$$

where the involved parameters are defined after (3.10).

For the terrestrial network, we consider that the terrestrial links go through the Nakagami-m fading with fading severity m_j and average power Ω_j for $j \in \{d, e\}$. Therefore, the PDF of channel gain γ_{rd} and γ_{re_l} are given, respectively, by

$$f_{\gamma_{rd}}(x) = \left(\frac{m_d}{\varrho_d}\right)^{m_d} \frac{x^{m_d-1}}{\Gamma(m_d)} \mathrm{e}^{-\frac{m_d x}{\varrho_d}} \tag{6.10a}$$

$$\text{and} \qquad f_{\gamma_{re_l}}(x) = \left(\frac{m_{e_l}}{\varrho_{e_l}}\right)^{m_{e_l}} \frac{x^{m_{e_l}-1}}{\Gamma(m_{e_l})} \mathrm{e}^{-\frac{m_{e_l} x}{\varrho_{e_l}}}, \tag{6.10b}$$

where $\varrho_d = \eta_r \Omega_d$ and $\varrho_{e_l} = \eta_r \Omega_{e_l}$.

Now, differing from $f_{\gamma_{rd}}(x)$, the estimation of accurate PDF of γ_{rE} is rather complicated due to involvement of the sum of i.ni.d. gamma RVs. Even for a small number of eavesdroppers, it requires to perform a multifold convolution. Therefore, we adopt a very precise approximation approach [67] by which the PDF of γ_{rE} may be expressed effectively in terms of a single gamma RV as [66], [88]

$$f_{\gamma_{rE}}(y) \approx \left(\frac{m_E}{\Omega_E}\right)^{m_E} \frac{y^{m_E-1}}{\Gamma(m_E)} \mathrm{e}^{-\frac{m_E}{\Omega_E} y}, \tag{6.11}$$

where the parameters m_E and Ω_E are calculated from moment-based estimators. For this, we define $\Phi = \sum_{l=1}^{L} |h_{re_l}|^2$. Then, we have $\Omega_E = \mathbb{E}[\Phi] = \sum_{l=1}^{L} \Omega_{e_l}$ and $m_E = \frac{\Omega_E^2}{\mathbb{E}[\Phi^2] - \Omega_E^2}$. Herein, the exact moments of Φ can be acquired in the form of individual moments of the summands as

$$\mathbb{E}[\Phi^t] = \sum_{t_1=0}^{t}\sum_{t_2=0}^{t_1}\cdots\sum_{t_{L-1}=0}^{t_{L-2}} \mathcal{C}_{t_1}^{t}\mathcal{C}_{t_2}^{t_1}\cdots\mathcal{C}_{t_{L-1}}^{t_{L-2}}$$

$$\times\,\mathbb{E}\left[|h_{re_1}|^{2(t-t_1)}\right]\mathbb{E}\left[|h_{re_2}|^{2(t_1-t_2)}\right]\cdots\mathbb{E}\left[|h_{re_L}|^{2(t_{L-1})}\right], \tag{6.12}$$

$$\text{where}\qquad \mathbb{E}\left[|h_{re_l}|^t\right] = \frac{\Gamma\left(m_{e_l}+\frac{t}{2}\right)}{\Gamma(m_{e_l})}\left(\frac{\Omega_{e_l}}{m_{e_l}}\right)^{\frac{t}{2}}. \tag{6.13}$$

6.2 Performance Analysis

In this section, we characterize the secrecy performance of considered HSTRN in terms of SOP and ESC. In particular, we first derive the SOP expression and then analyze the asymptotic behavior of the SOP expression. Subsequently, we present the ESC expression. Thus, the achievable secrecy capacity of considered system can be given by

$$C_{\text{sec}} = [C_D - C_E]^+. \tag{6.14}$$

Herein, C_D is the channel capacity of main channel and C_E is the channel capacity of wiretap channel, which can be expressed, respectively, as

$$C_D = \frac{1}{2}\log_2(1+\gamma_D) \tag{6.15a}$$

$$\text{and}\qquad C_E = \frac{1}{2}\log_2(1+\gamma_E), \tag{6.15b}$$

where the term $1/2$ arises due to the two-stage communication process. Substituting (6.15a) and (6.15b) into (6.14), we can represent C_{sec} as

$$C_{\text{sec}} = \left[\frac{1}{2}\log_2(1+\gamma_D) - \frac{1}{2}\log_2(1+\gamma_E)\right]^+. \tag{6.16}$$

The above formulations help in the subsequent secrecy performance analysis.

6.2.1 SOP Analysis

The SOP is defined as the probability that the achievable secrecy capacity C_{sec} falls below a target secrecy rate $\mathcal{R}_{\text{s}}$. Therefore, the SOP of the proposed HSTRN can be mathematically represented as

$$\mathcal{P}_{\text{sec}} = \Pr\left[C_{\text{sec}} < \mathcal{R}_{\text{s}}\right]. \tag{6.17}$$

We acquire the solution of (6.17) in the theorem as given below.

Theorem 7. *The expression of $\mathcal{P}_{sec}$ can be given as*

$$\mathcal{P}_{sec} = 1 - 2\sum_{i_1=0}^{m_s-1} \dots \sum_{i_{N_s}=0}^{m_s-1} \frac{\Xi(N_s)}{(\eta_s)^{\Lambda}} \sum_{p=0}^{\Lambda-1} \frac{\Gamma\Lambda}{p!} \left(\frac{m_d}{\varrho_d}\right)^{m_d} \frac{1}{\Gamma(m_d)} \sum_{r=0}^{m_d-1} \mathcal{C}_r^{m_d-1} \sum_{q=0}^{p} \mathcal{C}_q^{p}$$
$$\times (\gamma_s)^{m_d}(\gamma_s-1)^{p+\tau}\left(\frac{m_E}{\Omega_E}\right)^{m_E} \frac{1}{\Gamma(m_E)} (\beta_\delta)^{-(\Lambda-p)} \frac{\sqrt{\pi}\,(4\,(\beta_\delta))^{\tau}}{(\varsigma+\xi)^{\mu+\tau}}$$
$$\times \frac{(\mu+\tau-1)!(\mu-\tau-1)!}{(\mu-\frac{1}{2})!}\, {}_2F_1\left(\mu+\tau;\tau+\frac{1}{2};\mu+\frac{1}{2};\frac{\varsigma-\xi}{\varsigma+\xi}\right), \tag{6.18}$$

where $\mu = m_d + m_E + p$, $\tau = r - q + 1$, $\varsigma = \beta_\delta(\gamma_s - 1) + \frac{m_d}{\varrho_d}\gamma_s + \frac{m_E}{\Omega_E}$, *and* $\xi = \left(2\sqrt{\beta_\delta\gamma_s(\gamma_s-1)\frac{m_d}{\varrho_d}}\right)$ *with* $\gamma_s = 2^{2\mathcal{R}_s}$.

Proof. See Appendix 6.A. ■

The obtained expression of the SOP for the considered HSTRN in Theorem 7 upholds for the complex heterogeneous channels with a number of satellite antennas and number of eavesdroppers over whole range of SNR regime.

6.2.2 Asymptotic SOP

We now perform asymptotic analysis of SOP expression to obtain the secrecy diversity order of the considered HSTRN. For this, at the high SNR regime, we consider $\eta_s, \eta_r \to \infty$ (with $\frac{\eta_s}{\eta_r}$ as a finite constant) and derive the asymptotic expression of $\mathcal{P}_{\text{sec}}$ in the following corollary.

Theorem 8. *At high SNR, $\mathcal{P}_{sec}$ can be calculated as*

$$\mathcal{P}_{sec}^{\infty} \simeq (\gamma_s-1)^{N_s} \frac{\alpha^{N_s}\Gamma(N_s+m_E)}{(N_s)!\eta_s^{N_s}\Gamma m_E}\left(\frac{\Omega_E}{m_E}\right)^{N_s}$$
$$+ \gamma_s^{N_s}\frac{\Gamma(m_d+m_E)}{\Gamma(m_d+1)\Gamma m_E}\left(\frac{m_d\,\Omega_E}{\varrho_d\,m_E}\right)^{m_d}. \tag{6.19}$$

Proof. See Appendix 6.B. ■

Remarks: It can be concluded from (6.19) that achievable secrecy diversity order of the considered HSTRN is $\min(N_s, m_d)$. It is worth mentioning that the achievable secrecy diversity order of the considered HSTRN jointly depends on the number of satellite antennas and the fading severity parameter of relay to destination channel (i.e. $R{\to}D$ channel), and remains independent from the fading severity parameter of satellite channel and number of eavesdroppers.

6.2.3 ESC Analysis

In this subsection, we obtain the ESC of the considered HSTRN which is defined as the average of the maximum achievable secrecy capacity. To evaluate the ESC expression, we define the EC of the main channel and of wiretap channel from (6.15a) and (6.15b), respectively, as

$$\overline{C}_D = \frac{1}{2}\mathbb{E}\left[\log_2\left(1+\Lambda_D\right)\right] \tag{6.20a}$$

$$\text{and} \qquad \overline{C}_E = \frac{1}{2}\mathbb{E}\left[\log_2\left(1+\Lambda_E\right)\right]. \tag{6.20b}$$

As such, the ESC for the proposed HSTRN can now be obtained as [110]

$$C_{\text{ESC}} = \left[\,\overline{C}_D - \overline{C}_E\right]^+. \tag{6.21}$$

To further proceed, we require the expressions for the EC of the main and wiretap channels (i.e, $\overline{C}_D$ and $\overline{C}_E$). Thus, we first simplify $\overline{C}_D$ using SNR from (6.5) into (6.20a) as

$$\overline{C}_D = \frac{1}{2\ln 2}\mathbb{E}\left[\ln\left(1+\frac{\gamma_{sr}\gamma_{rd}}{1+\gamma_{sr}+\gamma_{rd}}\right)\right], \tag{6.22}$$

Further, as in [111, eq.8], $\overline{C}_D$ in (6.22) can be expressed by means of MGF as

$$\overline{C}_D = I_1 - I_2, \tag{6.23}$$

where

$$I_1 = \frac{1}{2\ln 2}\int_0^\infty \mathrm{e}^{-s}\widehat{\mathcal{M}}_{\gamma_{sr}}(s)ds \tag{6.24a}$$

$$\text{and} \qquad I_2 = \frac{1}{2\ln 2}\int_0^\infty \mathrm{e}^{-s}\widehat{\mathcal{M}}_{\gamma_{sr}}(s)\mathcal{M}_{\gamma_{rd}}(s)ds. \tag{6.24b}$$

Herein, $\mathcal{M}_X(\cdot)$ and $\widehat{\mathcal{M}}_X(\cdot)$ are the MGF and complementary MGF transforms, which can be defined, respectively, as

$$\mathcal{M}_X(s) \triangleq \int_0^\infty \mathrm{e}^{-sx}f_X(x)dx \tag{6.25a}$$

$$\text{and} \qquad \widehat{\mathcal{M}}_X(s) \triangleq \int_0^\infty \mathrm{e}^{-sx}(1-F_X(x))dx. \tag{6.25b}$$

Similar to (6.23), $\overline{C}_E$ can be written using SNR from (6.7) as

$$\overline{C}_E = I_1 - I_3, \tag{6.26}$$

$$\text{where} \qquad I_3 = \frac{1}{2\ln 2}\int_0^\infty \mathrm{e}^{-s}\widehat{\mathcal{M}}_{\gamma_{sr}}(s)\mathcal{M}_{\gamma_{rE}}(s)ds. \tag{6.27}$$

Now, to calculate $\overline{C}_D$ and $\overline{C}_E$, we require the expressions of I_1, I_2, and I_3 in (6.24a), (6.24b) and in (6.27) which can be obtained by the lemma as given below, respectively.

Lemma 2. *The expressions of I_1, I_2 and I_3 can be given, respectively, as*

$$I_1 = \frac{1}{2\ln 2}\sum_{i_1=0}^{m_s-1}\cdots\sum_{i_{N_s}=0}^{m_s-1}\frac{\Xi(N_s)}{(\eta_s)^{\Lambda}}\sum_{p=0}^{\Lambda-1}\frac{\Gamma\Lambda}{p!}(\beta_\delta)^{-(\Lambda+1)}G_{2,1}^{1,2}\left[\frac{s}{\beta_\delta}\middle|\begin{matrix}0,-p\\0\end{matrix}\right], \tag{6.28}$$

$$I_2 = \frac{1}{2\ln 2}\sum_{i_1=0}^{m_s-1}\cdots\sum_{i_{N_s}=0}^{m_s-1}\frac{\Xi(N_s)}{(\eta_s)^{\Lambda}}\sum_{p=0}^{\Lambda-1}\frac{\Gamma\Lambda}{p!}\frac{\beta_\delta^{-(\Lambda+1)}}{\Gamma m_d}G_{1,[1:1],0,[1:1]}^{1,1,1,1,1}\left[\begin{matrix}\frac{1}{\beta_\delta}\\\frac{\varrho_d}{m_d}\end{matrix}\middle|\begin{matrix}1;-p;1-m_d\\-;0;0\end{matrix}\right], \tag{6.29}$$

and

$$I_3 = \frac{1}{2\ln 2}\sum_{i_1=0}^{m_s-1}\cdots\sum_{i_{N_s}=0}^{m_s-1}\frac{\Xi(N_s)}{(\eta_s)^{\Lambda}}\sum_{p=0}^{\Lambda-1}\frac{\Gamma\Lambda}{p!}\frac{(\beta_\delta)^{-(\Lambda+1)}}{\Gamma(m_E)}G_{1,[1:1],0,[1:1]}^{1,1,1,1,1}\left[\begin{matrix}\frac{1}{\beta_\delta}\\\frac{\Omega_E}{m_E}\end{matrix}\middle|\begin{matrix}1;-p;1-m_E\\-;0;0\end{matrix}\right], \tag{6.30}$$

where $G_{2,1}^{1,2}[\cdot]$ and $G_{1,[1:1],0,[1:1]}^{1,1,1,1,1}[\cdot]$ represent the Meijer's G-function of one and two variables [91], respectively.

Proof. See Appendix 6.C. ■

Now, after invoking (6.28) and (6.29) into (6.23), and (6.28) and (6.30) into (6.26), we get $\overline{C}_D$ and $\overline{C}_E$, respectively, as

$$\begin{aligned}\overline{C}_D = &\frac{1}{2\ln 2}\sum_{i_1=0}^{m_s-1}\cdots\sum_{i_{N_s}=0}^{m_s-1}\frac{\Xi(N_s)}{(\eta_s)^{\Lambda}}\sum_{p=0}^{\Lambda-1}\frac{\Gamma\Lambda}{p!}(\beta_\delta)^{-(\Lambda+1)}\\&\times\left\{G_{2,1}^{1,2}\left[\frac{s}{\beta_\delta}\middle|\begin{matrix}0,-p\\0\end{matrix}\right]-\frac{1}{\Gamma m_d}G_{1,[1:1],0,[1:1]}^{1,1,1,1,1}\left[\begin{matrix}\frac{1}{\beta_\delta}\\\frac{\varrho_d}{m_d}\end{matrix}\middle|\begin{matrix}1;-p;1-m_d\\-;0;0\end{matrix}\right]\right\}.\end{aligned} \tag{6.31}$$

$$\begin{aligned}\overline{C}_E = &\frac{1}{2\ln 2}\sum_{i_1=0}^{m_s-1}\cdots\sum_{i_{N_s}=0}^{m_s-1}\frac{\Xi(N_s)}{(\eta_s)^{\Lambda}}\sum_{p=0}^{\Lambda-1}\frac{\Gamma\Lambda}{p!}(\beta_\delta)^{-(\Lambda+1)}\\&\times\left\{G_{2,1}^{1,2}\left[\frac{s}{\beta_\delta}\middle|\begin{matrix}0,-p\\0\end{matrix}\right]-\frac{1}{\Gamma(m_E)}G_{1,[1:1],0,[1:1]}^{1,1,1,1,1}\left[\begin{matrix}\frac{1}{\beta_\delta}\\\frac{\Omega_E}{m_E}\end{matrix}\middle|\begin{matrix}1;-p;1-m_E\\-;0;0\end{matrix}\right]\right\}.\end{aligned} \tag{6.32}$$

Finally, after using (6.31) and (6.32) into (6.21), the expression for ESC can be obtained.

6.3 Numerical and Simulation Results

In this section, we present the numerical results to facilitate the secrecy performance analysis of the considered HSTRN and justify them through Monte-Carlo simulations. The i.i.d. shadowed-Rician fading parameters for $S \rightarrow R$ link is considered as illustrated in Table 6.1 for heavy and average shadowing scenarios. Moreover, we consider $\{E_l\}_{l=1}^{5}$ i.ni.d. Nakagami-m fading channels for $R \rightarrow E_l$ links where parameters have been fixed as $\{m_{e_l}\}_{l=1}^{5} = \{1, 2, 2.5, 3, 3.5\}$ and $\{\Omega_{e_l}\}_{l=1}^{5} = \{1, 2.5, 2.5, 3.2, 3.5\}$. For each set of i.ni.d. Nakagami-m fading channel parameters, the required parameters in (6.11) are estimated as provided in Table 6.2.

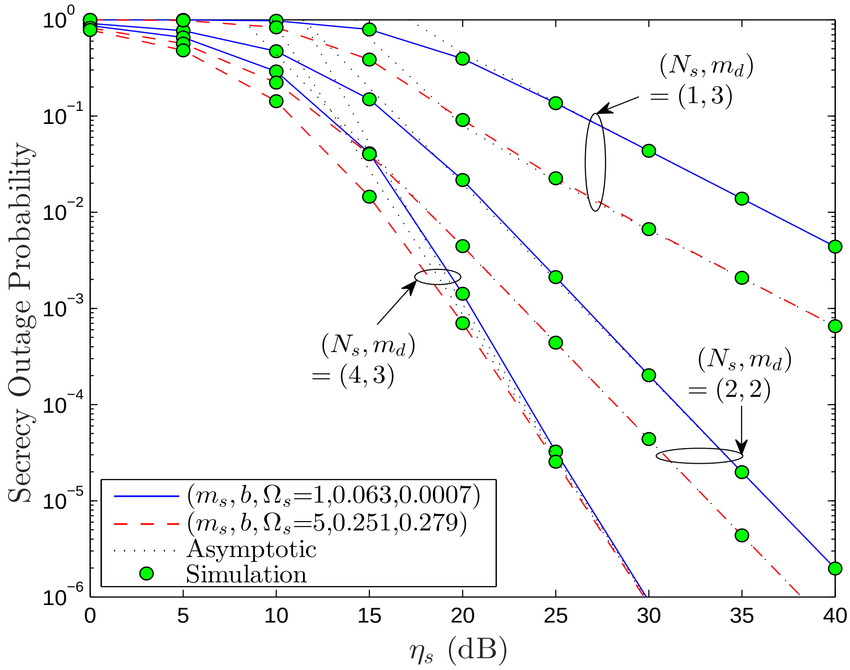

Figure 6.2: SOP performance of the considered HSTRN versus η_s.

In Fig. 6.2, we have drawn the SOP curves of considered system for different sets of satellite antennas and fading severity parameter of $R \rightarrow D$ link (i.e., for N_s and m_d) by keeping $\mathcal{R}_s = 0.5$ and $L = 2$. In addition, we have plotted the asymptotic behaviour of the SOP expression which coincide nicely with the SOP curves at high SNR. We can observe from Fig. 6.2 that the SOP diminishes with the increasing number of satellite antennas, which reflect that one can obtain better secrecy performance with large number of satellite antennas. Moreover, it is noteworthy that the system achieves the secrecy diversity order of $\min(N_s, m_d)$, which can be clearly observed by the slope of the various SOP curves. For example, the secrecy diversity

Table 6.1: Parameters for Satellite Channel [58]

Shadowing	m_s	b	Ω_s
Heavy shadowing	1	0.063	7×10^{-4}
Average shadowing	5	0.251	0.279

Table 6.2: Calculated Parameters involved in (6.11)

L	2	3	4	5
m_E	2.9697	5.4340	8.4317	11.9136
Ω_E	3.5	6	9.2	12.7

order of 2 can be obtained by the inclines of the SOP curves when (N_s, m_d) is $(2, 2)$ as compared with $(1, 3)$ for secrecy diversity order of 1. In addition, one can observe that when $N_s \geq m_d$, the SOP performance is bottlenecked by the satellite channel, and thus, a significant gap appears between heavy and average shadowing curves. However, when $N_s < m_d$, the SOP performance regularized by the terrestrial channels, hence, SOP curves under both the shadowing scenarios merged at high SNR.

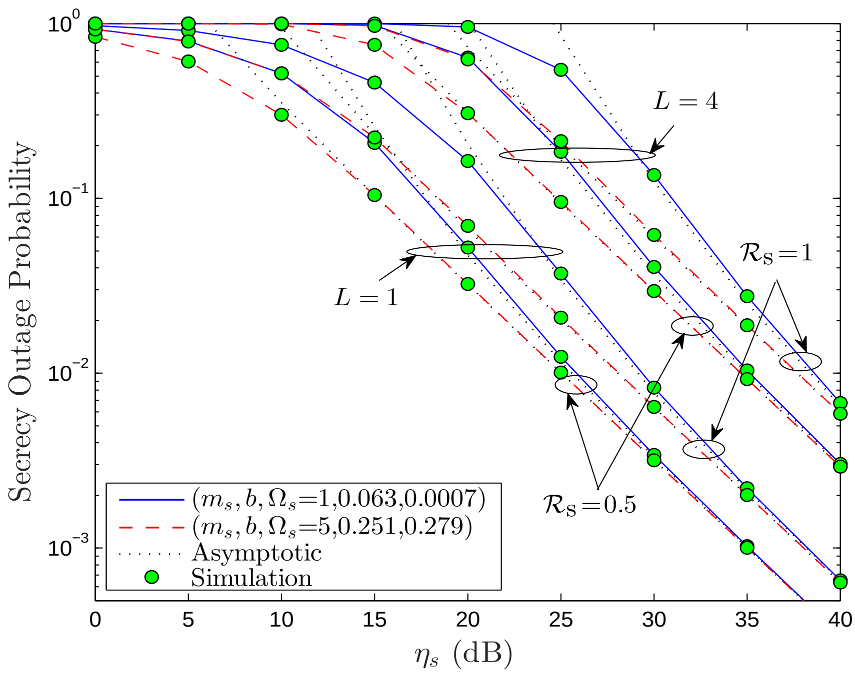

Figure 6.3: Impact of number of eavesdroppers and $\mathcal{R}_s$ on SOP.

Fig. 6.3 shows the impact of number of eavesdroppers L and targeted secrecy rate $\mathcal{R}_s$ on the secrecy performance of the considered HSTRN. For this, we have fixed $N_s = 2$, $m_d = 1$ and drawn the SOP curves for different sets of $(L, \mathcal{R}_s)$. As expected, the secrecy performance of the considered network degrades with an

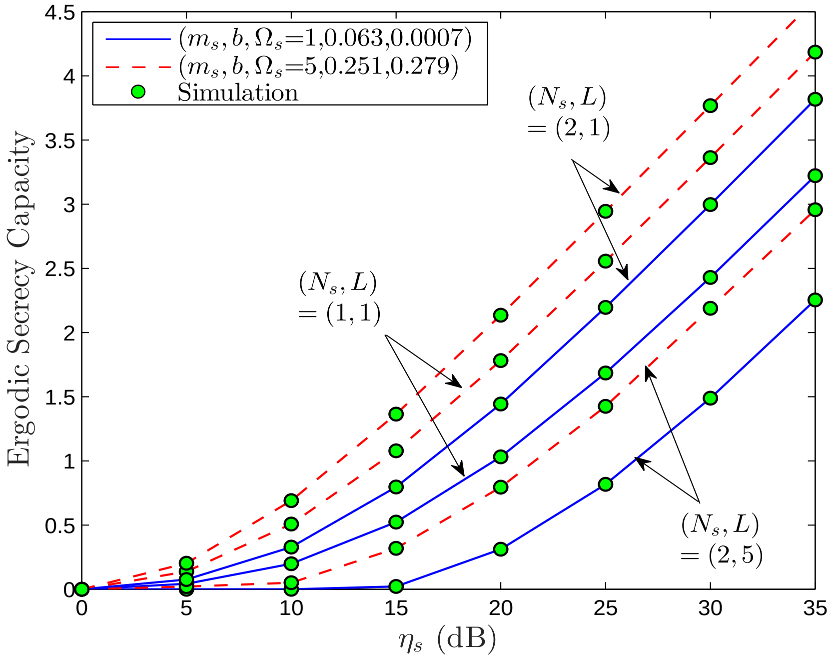

Figure 6.4: ESC performance versus η_s with different sets of (N_s, L).

increase in the number of eavesdroppers. Further, it can be observed from the figure that the system becomes more secure for small values of $\mathcal{R}_{\mathrm{s}}$.

From the various SOP curves in Fig. 6.2 and Fig. 6.3, one can visualize that the system performs better under average shadowing in contrast to heavy shadowing condition of the satellite channel.

In Fig. 6.4, we illustrate the joint impact of number of satellite antennas and eavesdroppers on the performance of ESC. The analytical curves for ESC are plotted for different sets of (N_s, L) by setting $m_d = 2$. From this figure, it is found that the ESC performance improves with an increase in number of satellite antennas, while, it degrades with an increasing number of eavesdroppers. Thus, the system can attain a higher ESC for small number of eavesdroppers and a large number of satellite antennas. In addition, we can readily found that the proposed system achieves higher ESC under average shadowed-Rician fading as compared to heavy shadowed-Rician fading.

6.4 Summary

In this chapter, we investigated the secrecy performance of an HSTRN in the existence of multiple non-identically distributed eavesdroppers. By adopting shadowed-Rician fading for satellite channel and Nakagami-m fading for terrestrial channels, we derived novel expressions of the SOP and ESC for the considered system. Moreover, we obtained the asymptotic SOP expression and revealed the achievable secrecy diversity order of the proposed HSTRN. Importantly, it is found that the system achievable secrecy diversity order jointly depends on the number of satellite antennas and fading severity parameter of the relay to destination channel, and remain unaffected by the fading severity parameter of the satellite channel. In addition, it was illustrated that the secrecy performance of the considered network can be significantly improved by exploiting the multiple antennas at the satellite. It is worth mentioning that the proposed analysis ensures the secure communication of the information to the intended user and our obtained results can play a critical role in the design of HSTRNs in near future.

Appendix 6.A: Proof of Theorem 7

With consideration of Theorem 7, we can rewrite $\mathcal{P}_{\text{sec}}$ after substituting (6.16) into (6.17) as

$$\mathcal{P}_{\text{sec}} = \Pr\left[\frac{1+\gamma_D}{1+\gamma_E} < \gamma_{\text{s}}\right]. \tag{6.33}$$

However, after invoking (6.5) and (6.7) in (6.33), the solution of (6.33) becomes very intricate, therefore, we have applied the well used approximation $\frac{1+u}{1+v} \approx \frac{u}{v}$ [102], [103] to simplify (6.33), and appeared to have negligible impact in entire SNR regime, as

$$\mathcal{P}_{\text{sec}} \approx \Pr\left[\frac{\gamma_D}{\gamma_E} < \gamma_{\text{s}}\right]. \tag{6.34}$$

Further, on invoking (6.5) and (6.7) into (6.34) and performing some manipulations, we can represent simplify (6.34), for large transmit power, as

$$\begin{aligned}\mathcal{P}_{\text{sec}} &\approx \Pr\left[\frac{\gamma_{sr}\gamma_{rd}}{\gamma_{\text{s}}\gamma_{sr} + (\gamma_{\text{s}}-1)\gamma_{rd}} < \gamma_{rE}\right] \\ &= \int_0^\infty F_Z(z) f_{\gamma_{rE}}(z)dz,\end{aligned} \tag{6.35}$$

herein, we have used $Z \triangleq \frac{\gamma_{sr}\gamma_{rd}}{\gamma_{\text{s}}\gamma_{sr}+(\gamma_{\text{s}}-1)\gamma_{rd}}$ for notational convenience. Further, we need $F_Z(z)$ which can be derived as

$$\begin{aligned}F_Z(z) = 1 - \int_0^\infty &\left(1 - F_{\gamma_{sr}}\left(\frac{z(\gamma_{\text{s}}-1)(x+z\gamma_{\text{s}})}{x}\right)\right) \\ &\times f_{\gamma_{rd}}(x+z\gamma_{\text{s}})dx.\end{aligned} \tag{6.36}$$

Then, on inserting (6.9) and (6.10a) into (6.36), and by utilizing [59, eq. 3.471.9], we can get $F_Z(z)$ as

$$\begin{aligned}F_Z(z) =& 1 - 2\sum_{i_1=0}^{m_s-1}\dots\sum_{i_{N_s}=0}^{m_s-1}\frac{\Xi(N_s)}{(\eta_s)^{\Lambda}}\sum_{p=0}^{\Lambda-1}\frac{\Gamma\Lambda\left(\beta_\delta\right)^{-(\Lambda-p)}}{p!}\sum_{q=0}^{p}\mathcal{C}_q^p\left(\frac{m_d}{\varrho_d}\right)^{m_d}\sum_{r=0}^{m_d-1}\mathcal{C}_r^{m_d-1}\\ &\times\frac{(\gamma_{\rm s}-1)^p z^{m_d+p}(\gamma_{\rm s})^{m_d-\tau}}{\Gamma(m_d)}\mathrm{e}^{-\left((\beta_\delta)(\gamma_{\rm s}-1)+\left(\frac{m_d}{\varrho_d}\right)\gamma_{\rm s}\right)z}\left(\frac{(\beta_\delta)\,\gamma_{\rm s}(\gamma_{\rm s}-1)\varrho_d}{m_d}\right)^{\frac{\tau}{2}}\\ &\times K_{r-q+1}\left(2\sqrt{(\beta_\delta)\,z^2\gamma_{\rm s}(\gamma_{\rm s}-1)\frac{m_d}{\varrho_d}}\right).\end{aligned}\tag{6.37}$$

Finally, using (6.37) and (6.10a) into (6.35), and fetching the solution of involved integration with the guide of [59, eq. 7.813.1], one can arrive at (6.18).

Appendix 6.B: Proof of Theorem 8

In the high SNR regime (i.e, $\eta_s, \eta_r \to \infty$), $Z \triangleq \frac{\gamma_{sr}\gamma_{rd}}{\gamma_{\rm s}\gamma_{sr}+(\gamma_{\rm s}-1)\gamma_{rd}}$ can be expressed in terms of well known approximation of harmonic mean [95] as

$$Z \simeq \min\left(\frac{\gamma_{sr}}{\gamma_{\rm s}-1}, \frac{\gamma_{rd}}{\gamma_{\rm s}}\right),\tag{6.38}$$

thereby, the CDF $F_Z(z)$ is written as

$$F_Z(z) \simeq \Pr\left[\min\left(\frac{\gamma_{sr}}{\gamma_{\rm s}-1}, \frac{\gamma_{rd}}{\gamma_{\rm s}}\right) < z\right].\tag{6.39}$$

Utilizing the fact of independency among the involved RVs in (6.39), we can represent $F_Z(z)$ as

$$F_Z(z) \simeq F_{\gamma_{sr}}\left((\gamma_{\rm s}-1)z\right) + F_{\gamma_{rd}}(\gamma_{\rm s}z) - F_{\gamma_{sr}}\left((\gamma_{\rm s}-1)z\right)F_{\gamma_{rd}}(\gamma_{\rm s}z).\tag{6.40}$$

Further, we require the asymptotic expressions for the CDFs $F_{\gamma_{sr}}(x)$ and $F_{\gamma_{rd}}(x)$. First, we obtain the asymptotic behaviour of $F_{\gamma_{sr}}(x)$. In this way, we approximate $f_{\gamma_{sr}}(x)$ at high SNR regime by applying the Maclaurin series expansion in terms of non-negative integer powers of the exponential term in (6.8) as

$$f_{\gamma_{sr}}(x) \simeq \frac{\alpha^{N_s}}{(N_s-1)!\eta_s^{N_s}}x^{N_s-1},\tag{6.41}$$

and thus, the corresponding CDF behaves asymptotically as

$$F_{\gamma_{sr}}(x) \simeq \frac{\alpha^{N_s}}{(N_s)!\eta_s^{N_s}}x^{N_s}.\tag{6.42}$$

Next, the asymptotic expression of the $F_{\gamma_{rd}}(x)$ can be given, at high SNR (i.e., for $\eta_r \to \infty$), as

$$F_{\gamma_{rd}}(x) \simeq \frac{1}{(m_d)!}\left(\frac{m_d\ x}{\varrho_d}\right)^{m_d}. \tag{6.43}$$

Now, by invoking (6.42) and (6.43) in (6.40), we can get $F_Z(z)$ as

$$F_Z(z) \simeq \frac{\alpha^{N_s} z^{N_s}(\gamma_{\rm s}-1)^{N_s}}{(N_s)!\eta_s^{N_s}} + \frac{z^{m_d}}{(m_d)!}\left(\frac{m_d\gamma_{\rm s}}{\varrho_d}\right)^{m_d}, \tag{6.44}$$

where the higher order term is omitted. After plugging (6.44) and (6.10a) into (6.35) and solving the involved integrals with the use of [59, eq. 3.351.3], we can get (6.19) as given in Theorem 8.

Appendix 6.C: Proof of the Lemma 2

Here, we evaluate the expressions for I_1, I_2, and I_3. First, to solve the integral in (6.24a) for calculating the expression of I_1, we proceed by evaluating $\widehat{\mathcal{M}}_{\gamma_{sr}}(s)$, which can be written as

$$\widehat{\mathcal{M}}_{\gamma_{sr}}(s) \triangleq \int_0^\infty \mathrm{e}^{-sx}(1-F_{\gamma_{sr}}(x))dx. \tag{6.45}$$

Now, using (6.9) in (6.45) and further solving the integration with the aid of [59, eq.3.351.3], we can attain $\widehat{\mathcal{M}}_{\gamma_{sr}}(s)$ as

$$\widehat{\mathcal{M}}_{\gamma_{sr}}(s) = \sum_{i_1=0}^{m_s-1}\cdots\sum_{i_{N_s}=0}^{m_s-1}\frac{\Xi(N_s)}{(\eta_s)^{\Lambda}}\sum_{p=0}^{\Lambda-1}\Gamma(\Lambda)\ \beta_\delta^{-(\Lambda+1)}\left(1+\frac{s}{\beta_\delta}\right)^{-(p+1)}, \tag{6.46}$$

which is further simplified using (3.87) as

$$\widehat{\mathcal{M}}_{\gamma_{sr}}(s) = \sum_{i_1=0}^{m_s-1}\cdots\sum_{i_{N_s}=0}^{m_s-1}\frac{\Xi(N_s)}{\eta_s^{\Lambda}}\sum_{p=0}^{\Lambda-1}\frac{\Gamma(\Lambda)}{p!}\beta_\delta^{-(\Lambda+1)}G_{1,1}^{1,1}\left[\frac{s}{\beta_\delta}\middle|\begin{matrix}-p\\0\end{matrix}\right]. \tag{6.47}$$

Then, using (6.47) in (6.24a) and solving the integral with the help of [59, eq. 7.813.1], we can obtain I_1 as given in (6.28).

Next, to calculated the expression of I_2 in (6.24b), we require $\mathcal{M}_{\gamma_{rd}}(s)$, which can be readily obtain using (6.10a) and [59, eq. 3.351.3] as

$$\mathcal{M}_{\gamma_{rd}}(s) = \frac{1}{\Gamma(m_d)}G_{1,1}^{1,1}\left[s\frac{\varrho_d}{m_d}\middle|\begin{matrix}1-m_d\\0\end{matrix}\right]. \tag{6.48}$$

Using (6.47) and (6.48) into (6.24b), and further performing the solution of integral with the use of [97, eq. 2.6.2], I_2 can be obtained finally as given in (6.29).

To solve the integral in (6.27) for I_3, we first obtain $\mathcal{M}_{\gamma_{rE}}(s) \triangleq \int_0^\infty \mathrm{e}^{-sx} f_{\gamma_{rE}}(x)dx$, using (6.11) as

$$\mathcal{M}_{\gamma_{rE}}(s) = \frac{1}{\Gamma(m_E)} G_{1,1}^{1,1}\left[s\frac{\Omega_E}{m_E} \middle| \begin{matrix} 1-m_E \\ 0 \end{matrix} \right]. \tag{6.49}$$

Herein, we have utilized (3.87) and the fact [59, eq. 3.351.3]. Now, after inserting (6.47) and (6.49) into (6.27) and solving the integral using [97, eq. 2.6.2], we can obtain I_3 as in (6.30).

CHAPTER 7

MULTI-USER MULTI-RELAY HYBRID SATELLITE-TERRESTRIAL RELAY NETWORKS WITH MULTIPLE EAVESDROPPERS

So far, we have analyzed different configurations of AF-based HSTRNs in the past chapters, for instance, a multi-user HSTRN with a single eavesdropper, a multi-relay HSTRN with a single eavesdropper, a single-user single-relay HSTRN with multiple eavesdroppers. In this chapter, we consider an extensive configuration of HSTRN which comprises multi-user, multi-relay, and multiple-eavesdropper with multi-antenna satellite. For this system, we investigate the secrecy performance by employing two classic cooperative protocols, namely, AF and DF at relays. Moreover, we consider two specific scenarios of eavesdropping based to eavesdroppers' colluding capability, i.e., colluding (COL) and non-colluding (N-COL) eavesdroppers. Note that in the previous chapter, we have considered multiple i.ni.d. COL eavesdroppers in a single-user single-relay HSTRN. However, herein, we explore a generalized HSTRN configuration with AF and DF relays under both COL and N-COL eavesdroppers scenarios. Therefore, to retain the mathematical tractability, we consider that these multiple eavesdroppers are i.i.d. over Nakagami-m fading. With this consideration, we conduct a comprehensive secrecy performance analysis of the proposed HSTRN by adopting shadowed-Rician fading for satellite links and Nakagami-m fading for terrestrial links. The major contributions of this chapter are summarized as follows:

- We define an analytical framework for PLS in a downlink multi-user multi-relay HSTRN using AF and DF relaying protocols in the presence of multiple eavesdroppers by considering practical channel characteristics.

- To comprehensively analyze the secrecy performance of the proposed HSTRN, we assume two practical intercepting scenarios. That is, Scenario I: the N-COL eavesdroppers and Scenario II: the COL eavesdroppers. Then, we present user-relay selection criteria and derive novel and accurate expressions for the SOP for Scenario I and Scenario II under both AF and DF relaying protocols.

- We further obtain asymptotic SOP expressions to determine the main channel/system parameters that regulate the secrecy performance at high SNR regime. Based on the asymptotic analysis, we reveal that the system attains same diversity order under both AF and DF relaying protocols and the achievable diversity order remains unaffected from the number of eavesdroppers, methods of intercepting at eavesdroppers, and fading severity parameter of satellite links.

- We next derive ESC expressions based on MGF transform for AF relaying protocol under both N-COL and COL eavesdropping scenarios for the considered network. The derived expressions allow us to proficiently evaluate the impact of various system/channel parameters in enhancing the secrecy performance of the HSTRNs.

The remainder of the chapter is structured as follows. In Section 7.1, detailed descriptions of the considered HSTRN are presented along with discussions of the adopted relaying protocols and intercepting scenarios. In Section 7.2, the user-relay selection criteria are presented, and based on that SOP performance is examined. While, in Section 7.3, the ESC expressions are derived for AF relaying under both intercepting scenarios. Numerical and simulation results are provided in Section 7.4 and, finally, summary of the chapter is presented in Section 7.5.

7.1 System and Channel Model Descriptions

As illustrated in Fig. 7.1, we consider an HSTRN consisting of a satellite source S, K relays $\{R_k\}_{k=1}^{K}$, N legitimate users/destinations $\{D_n\}_{n=1}^{N}$, and L eavesdroppers $\{E_l\}_{l=1}^{L}$. In this network, we assume S is equipped with N_s antennas while all other nodes are single-antenna devices. Owing to severe shadowing and masking effect, it is hard to establish the direct links between satellite and terrestrial users or eavesdroppers, therefore, similar to related literature [18], [80], the LOS links between S and D_n as well as between S and E_l are considered to be unavailable. Thereby, the communication from the satellite S to the destination D_n can take place via $\{R_k\}$ relays, albeit in the presence of possible overhearing from eavesdroppers at the earth. We have considered shadowed-Rician fading for satellite to relay ($S \rightarrow R_k$) links, while relay to destination ($R_k \rightarrow D_n$) and relay to eavesdropper ($R_k \rightarrow E_l$) links are assumed to undergo Nakagami-m fading. We assume that all the aforementioned links are inflicted by AWGN with zero mean and variance σ^2.

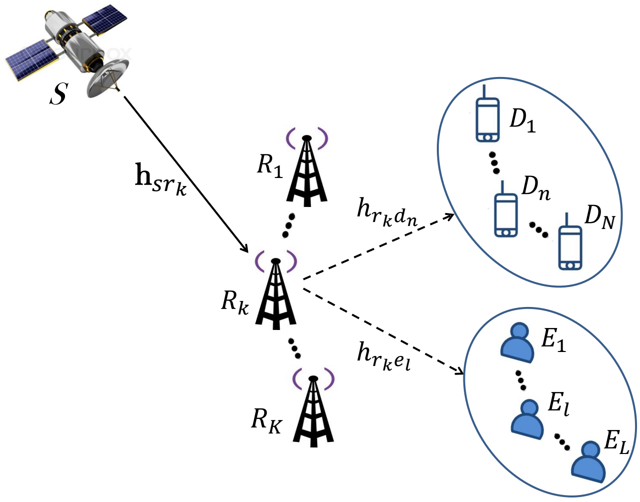

Figure 7.1: System model of a multi-user multi-relay HSTRN with multiple eavesdroppers.

The end-to-end communication takes place in two time phases by employing an opportunistic user-relay pair selection strategy. The criteria for selection of best user-relay pair will be discussed in Section 7.2. In the first phase, satellite S beamforms its signal to selected relay R_k, and in the second phase, relay R_k transmits the information to selected destination D_n through AF or DF relaying protocol, while eavesdroppers try to overhear the signal transmitted by the relay. Following this, both AF and DF relaying protocols and their end-to-end SNRs formulation will be discussed next.

7.1.1 AF Relaying

This subsection focuses on the AF relaying protocol in which the relay first amplifies the received signal by a scaling factor and then forwards this scaled outcome to destination. To be specific, the satellite broadcasts the signal to K relays and only the selected relay forwards the scaled version of satellite signal to the selected destination. Since all system nodes work in a half-duplex mode, the signal transmission from satellite to destination with the help of the selected relay requires two time phases. In the first phase, satellite S beamforms its unit energy signal x_s to the relay R_k using a weight vector $\mathbf{w}_{sr_k}$. The received signal at R_k can be thus given as

$$y_{sr_k} = \sqrt{P_s}\mathbf{h}_{sr_k}^{\dagger}\mathbf{w}_{sr_k}x_s + u_{r_k}, \tag{7.1}$$

where P_s is the transmit power at S, $\mathbf{h}_{sr_k} = \left[h_{sr_k}^{(1)}, h_{sr_k}^{(2)}, ..., h_{sr_k}^{(N_s)}\right]^T$ is the $N_s \times 1$ channel vector for $S \to R_k$ link, and $u_{r_k} \sim \mathcal{CN}(0, \sigma^2)$ is AWGN at the relay R_k. The transmit beamforming vector $\mathbf{w}_{sr_k} \in \mathbb{C}^{N_s \times 1}$ is chosen according to the principle of MRT [85] as $\mathbf{w}_{sr_k} = \frac{\mathbf{h}_{sr_k}}{||\mathbf{h}_{sr_k}||_F}$.

In the second phase, relay R_k first amplifies received signal y_{sr_k} using a gain factor $\mathcal{G}_k$ and then forwards it to the selected destination D_n. Meanwhile, the eavesdroppers track the signal transmitted from relay and try to overhear the information. Note that due to the masking effect, it is almost impossible for the eavesdroppers to intercept the signal from source directly. It is thereby assumed that eavesdroppers monitor only transmitted signal from relay for attack, as also followed commonly in literature [99]. Hence, the received signal at n-th user and l-th eavesdropper can be expressed, respectively, as

$$y_{r_k d_n}^{\mathrm{AF}} = \mathcal{G}_k\sqrt{P_r}h_{r_k d_n}y_{sr_k} + u_{d_n} \tag{7.2}$$

$$\text{and} \qquad y_{r_k e_l}^{\mathrm{AF}} = \mathcal{G}_k\sqrt{P_r}h_{r_k e_l}y_{sr_k} + u_{e_l}, \tag{7.3}$$

where P_r is the transmit power at R_k, $h_{r_k d_n}$ and $h_{r_k e_l}$ are channel coefficients of relay to destination ($R_k \to D_n$) and relay to eavesdropper ($R_k \to E_l$) links, respectively. $u_{d_n} \sim \mathcal{CN}(0, \sigma^2)$ and $u_{e_l} \sim \mathcal{CN}(0, \sigma^2)$ are AWGN variables at destination D_n and eavesdropper E_l, respectively. Based on (7.2) and (7.3), the end-to-end SNRs at user D_n and eavesdropper E_l can be obtained, respectively, as

$$\Lambda_{D_{n,k}}^{\mathrm{AF}} = \frac{\gamma_{sr_k}\gamma_{r_k d_n}}{\gamma_{r_k d_n} + \frac{1}{\mathcal{G}_k^2\sigma^2}} \tag{7.4}$$

$$\text{and} \qquad \Lambda_{E_{l,k}}^{\mathrm{AF}} = \frac{\gamma_{sr_k}\gamma_{r_k e_l}}{\gamma_{r_k e_l} + \frac{1}{\mathcal{G}_k^2\sigma^2}}, \tag{7.5}$$

where $\gamma_{sr_k} = \eta_s||\mathbf{h}_{sr_k}||_F^2$, $\gamma_{r_k d_n} = \eta_r|h_{r_k d_n}|^2$, and $\gamma_{r_k e_l} = \eta_r|h_{r_k e_l}|^2$, with $\eta_s = \frac{P_s}{\sigma^2}$ and $\eta_r = \frac{P_r}{\sigma^2}$. For variable gain relaying, the gain $\mathcal{G}_k$ in (7.4) and (7.5) can be determined as

$$\mathcal{G}_k = \sqrt{\frac{1}{P_s|\mathbf{h}_{sr_k}^{\dagger}\mathbf{w}_{sr_k}|^2 + \sigma^2}}, \tag{7.6}$$

and thus, for AF relaying technique, the instantaneous end-to-end SNRs at the n-th user and l-th eavesdropper can be given, respectively, as

$$\Lambda_{D_{n,k}}^{\mathrm{AF}} = \frac{\gamma_{sr_k}\gamma_{r_k d_n}}{\gamma_{sr_k} + \gamma_{r_k d_n} + 1} \tag{7.7}$$

$$\text{and} \qquad \Lambda_{E_{l,k}}^{\mathrm{AF}} = \frac{\gamma_{sr_k}\gamma_{r_k e_l}}{\gamma_{sr_k} + \gamma_{r_k e_l} + 1}. \tag{7.8}$$

7.1.2 DF Relaying

In this subsection, we rely on the DF relaying protocol in which basically the relay first decodes the received signal from source and then re-encodes and forwards the decoded output to the destination. More specifically, the satellite first broadcasts the signal to K relays that attempt to decode their received signals. For notational convenience, all those relays that successfully decode the satellite signal are symbolized by a set Δ, called decoding set. The sample space of this decoding set is given by $\Omega = \{\emptyset \bigcup \Delta_q, q = 1, 2, \cdots, 2^K - 1\}$, where $\emptyset$ is an empty set, $\bigcup$ represents the union operation, and Δ_q denotes the q-th non-empty subset of K relay nodes. If the decoding set is empty i.e., all the relays fail to decode the received satellite signal, then no signal is being forwarded from relay. Conversely, when decoding set is non-empty, all the relays in Δ_q are active to forward the encoded outcome and assist the signal transmission from satellite to destination. Herein, we consider that only the best relay is selected out of all the active relays for transmission.

For the considered HSTRN, the overall communication takes place in two time phases as stated previously. In the first phase, satellite S broadcasts its unit energy signal x_s to K relays, similar to AF relaying protocol. Thus, the signal received at relay R_k is same as given in (7.1). From (7.1), the instantaneous received SNR at relay R_k is expressed by

$$\gamma_{sr_k} = \eta_s ||\mathbf{h}_{sr_k}||_F^2, \tag{7.9}$$

and the mutual information between satellite S and relay R_k is thus given as

$$C_{sr_k} = \frac{1}{2}\log_2\left(1 + \gamma_{sr_k}\right). \tag{7.10}$$

According to the definition of adaptive DF relaying technique [112], for a particular relay R_k, if C_{sr_k} is greater than a predefined target data rate $\mathcal{R}_t$, then the relay R_k can decode the received satellite signal successfully and is activated to forward the decoded information in second phase.

During the second phase, one selected relay forwards the decoding signal x_s to selected destination which may be intercepted by eavesdroppers. Thus, received signal at n-th user and l-th eavesdropper can be given, respectively, as

$$y_{r_k d_n}^{\mathrm{DF}} = \sqrt{P_r} h_{r_k d_n} x_s + u_{d_n} \tag{7.11}$$

$$\text{and} \qquad y_{r_k e_l}^{\mathrm{DF}} = \sqrt{P_r} h_{r_k e_l} x_s + u_{e_l}. \tag{7.12}$$

From (7.11) and (7.12), we can obtain the received instantaneous SNRs at n-th user and l-th eavesdropper, respectively, as

$$\Lambda_{D_{n,k}}^{\mathrm{DF}} = \begin{cases} 0, & \text{if } |\Delta| = 0 \\ \gamma_{r_k d_n}, & \text{if } |\Delta| \neq 0 \end{cases} \tag{7.13}$$

$$\text{and} \qquad \Lambda_{E_{l,k}}^{\mathrm{DF}} = \begin{cases} 0, & \text{if } |\Delta| = 0 \\ \gamma_{r_k e_l}, & \text{if } |\Delta| \neq 0, \end{cases} \tag{7.14}$$

where $|\Delta|$ is the cardinality of decoding set Δ.

As such, each eavesdropper receives an independent copy of signal transmitted from relay, we assume two ways of wiretapping at eavesdroppers i.e., N-COL eavesdroppers scenario and COL eavesdroppers scenario, respectively.

N-COL Eavesdroppers Scenario

In this case, it is assumed that the eavesdroppers are incapable of exchanging the signal with each other, hence they cannot work collectively to strengthen the overhearing ability. It implies that the security of the system can be accomplished when the quality of the main channel is superior to that of any eavesdropper's channel [113]. Hence, for N-COL eavesdroppers scenario, the instantaneous end-to-end SNRs at eavesdroppers, for $\lambda \in \{\mathrm{AF}, \mathrm{DF}\}$, can be defined as [114], [115]

$$\Lambda_{E,k}^{\lambda,\text{N-COL}} = \max_{1 \le l \le L} \{\Lambda_{E_{l,k}}^{\lambda}\}. \tag{7.15}$$

Now, for AF relaying protocol, it can be realized from (7.8) that $\frac{\gamma_{sr_k}\gamma_{r_k e_l}}{\gamma_{sr_k}+\gamma_{r_k e_l}+1}$ is an increasing function with respect to $\gamma_{r_k e_l}$ for a given relay R_k. Thereby, with $\lambda = \mathrm{AF}$, (7.15) can be treated as [115], [116]

$$\Lambda_{E,k}^{\mathrm{AF},\text{N-COL}} = \frac{\gamma_{sr_k}\gamma_{r_k E}^{\text{N-COL}}}{\gamma_{sr_k} + \gamma_{r_k E}^{\text{N-COL}} + 1}, \tag{7.16}$$

where $\gamma_{r_k E}^{\text{N-COL}} = \max_{1 \le l \le L}\{\gamma_{r_k e_l}\}$.

Sequentially, under DF relaying protocol, (7.15) can be given for N-COL eavesdroppers scenario, using (7.14), as [117]

$$\Lambda_{E,k}^{\text{DF,N-COL}} = \begin{cases} 0, & \text{if } |\Delta| = 0 \\ \gamma_{r_k E}^{\text{N-COL}}, & \text{if } |\Delta| \neq 0. \end{cases} \tag{7.17}$$

COL Eavesdroppers Scenario

On the contrary, eavesdroppers can work collaboratively with each other for reinforcing the wiretapping ability in COL eavesdroppers scenario. Thus, for this case, we assume that maximal ratio combining is considered at eavesdroppers [118]. Thereby, under COL eavesdroppers scenario, the instantaneous end-to-end SNR at eavesdroppers can be represented for AF relaying protocol as [109]

$$\Lambda_{E,k}^{\text{AF,COL}} = \frac{\gamma_{sr_k}\gamma_{r_k E}^{\text{COL}}}{\gamma_{sr_k} + \gamma_{r_k E}^{\text{COL}} + 1}, \tag{7.18}$$

where $\gamma_{r_k E}^{\text{COL}} = \sum_{l=1}^{L} \gamma_{r_k e_l}$.

In this order, under DF relaying protocol, the end-to-end SNR can be expressed as [117]

$$\Lambda_{E,k}^{\text{DF,COL}} = \begin{cases} 0, & \text{if } |\Delta| = 0 \\ \gamma_{r_k E}^{\text{COL}}, & \text{if } |\Delta| \neq 0. \end{cases} \tag{7.19}$$

The instantaneous end-to-end SNRs from (7.16) to (7.19) will be used in subsequent secrecy performance analysis in Section 7.2.

Considering shadowed-Rician fading model for satellite links, the PDF of γ_{sr_k} under i.i.d.shadowed-Rician fading[1] can be derived by following the procedure given in [58, App. A] and making a transformation of variates using (3.9), and given as

$$f_{\gamma_{sr_k}}(x) = \sum_{i_1=0}^{m_s-1} \cdots \sum_{i_{N_s}=0}^{m_s-1} \frac{\Xi(N_s)}{\eta_s^{\Lambda}} x^{\Lambda-1} \mathrm{e}^{-\beta_\delta x}, \tag{7.20}$$

[1]We consider that the $\{R_k\}_{k=1}^{K}$ relays are situated relatively close together and lie in a cluster whose span is negligible as compared to the distances of relays from other terminals. This assumption also holds for the N users and L eavesdroppers. Under this consideration, channel coefficients over each hop are assumed to be independent and identically distributed (i.i.d.) [29]-[80]. Moreover, we consider the channel vector $\mathbf{h}_{sr_k}$ with i.i.d. shadowed-Rician fading model [80] for satellite links.

and CDF of γ_{sr_k} can be obtained by integrating (7.20) as

$$F_{\gamma_{sr_k}}(x) = 1 - \sum_{i_1=0}^{m_s-1} \cdots \sum_{i_{N_s}=0}^{m_s-1} \frac{\Xi(N_s)}{\eta_s^{\Lambda}} \sum_{p=0}^{\Lambda-1} \frac{\Gamma(\Lambda)}{p!} {\beta_\delta}^{-(\Lambda-p)} x^p \mathrm{e}^{-\beta_\delta x}. \tag{7.21}$$

For terrestrial links, we consider Nakagami-m fading channels for analyzing the secrecy performance of considered HSTRN. Herein, assuming the terrestrial links with a cluster of users/eavesdroppers, the pertinent channels follow i.i.d. Nakagami-m fading with integer-valued fading severity m_j and average power Ω_j for $j \in \{d, e\}$. As such, the PDF and CDF of channel gain $\gamma_{r_k j_\epsilon}$ are given, for $\epsilon = n$ when $j = d$ and $\epsilon = l$ when $j = e$, by

$$f_{\gamma_{r_k j_\epsilon}}(x) = \left(\frac{m_j}{\varrho_j}\right)^{m_j} \frac{x^{m_j-1}}{\Gamma(m_j)} \mathrm{e}^{-\frac{m_j}{\varrho_j}x} \tag{7.22}$$

$$\text{and} \qquad F_{\gamma_{r_k j_\epsilon}}(x) = \frac{1}{\Gamma(m_j)} \Upsilon\left(m_j, \frac{m_j x}{\varrho_j}\right), \tag{7.23}$$

respectively, where $\varrho_j = \eta_r \Omega_j$.

Lemma 3. *For N-COL eavesdroppers scenario, the PDF of $\gamma_{r_k E}^{N\text{-}COL}$ can be given as*

$$f_{\gamma_{r_k E}^{\text{N-COL}}}(x) = L \sum_{r=0}^{L-1} \mathcal{C}_r^{L-1} \sum_{s=0}^{r(m_e-1)} \omega_s^r \frac{(-1)^r}{\Gamma m_e} \left(\frac{m_e}{\varrho_e}\right)^{m_e+s} x^{m_e+s-1} e^{-\frac{x}{\chi_e}}, \tag{7.24}$$

where $\chi_e = \frac{\varrho_e}{m_e(r+1)}$ and the coefficients ω_s^r, for $0 \leq s \leq r(m_e-1)$, can be calculated recursively (with $\ell_s = \frac{1}{s!}$) as $\omega_0^r = (\ell_0)^r$, $\omega_1^r = r(\ell_1)$, $\omega_{r(m_e-1)}^r = (\ell_{m_e-1})^r$, $\omega_s^r = \frac{1}{s\ell_0}\sum_{g=1}^{s}[gr - s + g]\ell_g \omega_{s-g}^r$ for $2 \leq s \leq m_e - 1$, and $\omega_s^r = \frac{1}{s\ell_0}\sum_{g=1}^{m_e-1}[gr - s + g]\ell_g \omega_{s-g}^r$ for $m_e \leq s < r(m_e - 1)$.

Proof. Under the assumption of i.i.d. channels, the PDF of $\gamma_{r_k E}^{\text{N-COL}}$ can be obtained by getting the maximum value from L eavesdroppers' channel gains as

$$f_{\gamma_{r_k E}^{\text{N-COL}}}(x) = \frac{dF_{\gamma_{r_k E}^{\text{N-COL}}}(x)}{dx} = \frac{d}{dx}[F_{\gamma_{r_k e_l}}(x)]^L, \tag{7.25}$$

and it can be further simplified as

$$f_{\gamma_{r_k E}^{\text{N-COL}}}(x) = L[F_{\gamma_{r_k e_l}}(x)]^{L-1} f_{\gamma_{r_k e_l}}(x). \tag{7.26}$$

Now, plugging (7.22) and (7.23) for $j_\epsilon = e_l$ with series exploration of $\Upsilon(\cdot,\cdot)$ [59, eq. 8.352.1] into (7.26), and then using multinomial [59, eq. 0.314] and binomial [59, eq. 1.111] expansions, we obtain the expression of $f_{\gamma_{r_k E}^{\text{N-COL}}}(x)$ as shown in (7.24). ■

Moreover, for the COL scenario, the PDF of $\gamma_{r_kE}^{\mathrm{COL}}$ can be presented as [119]

$$f_{\gamma_{r_kE}^{\mathrm{COL}}}(x) = \left(\frac{m_e}{\varrho_e}\right)^{m_eL} \frac{x^{m_eL-1}}{\Gamma(m_eL)} \mathrm{e}^{-\frac{m_ex}{\varrho_e}}. \tag{7.27}$$

7.2 User-Relay Selection and SOP Analysis

In this section, we derive accurate and asymptotic expressions of SOP for N-COL and COL eavesdroppers scenarios, and present the user-relay selection criteria for minimizing the SOP under both AF and DF relaying protocols. The SOP of the considered HSTRN can be formulated for $\lambda \in \{\mathrm{AF}, \mathrm{DF}\}$ and $\flat \in \{\text{N-COL}, \mathrm{COL}\}$ as

$$\mathcal{P}_{\mathrm{sec},k,n}^{\lambda,\flat} = \Pr\left[C_{\mathrm{sec},k,n}^{\lambda,\flat} < \mathcal{R}_{\mathrm{s}}\right], \tag{7.28}$$

where $C_{\mathrm{sec},k,n}^{\lambda,\flat}$ is the secrecy capacity and $\mathcal{R}_{\mathrm{s}}$ is target secrecy rate. The secrecy capacity of considered system can be given by

$$C_{\mathrm{sec},k,n}^{\lambda,\flat} = [C_{D_{n,k}}^{\lambda} - C_{E,k}^{\lambda,\flat}]^{+}. \tag{7.29}$$

Herein, $C_{D_{n,k}}^{\lambda}$ is the channel capacity of main link and $C_{E,k}^{\lambda,\flat}$ is the channel capacity of wiretap link.

7.2.1 AF Relaying

In this subsection, we formulate the appropriate SOP followed by user-relay selection criterion under AF relaying protocol and then derive both accurate and asymptotic expressions for SOP of the considered system for N-COL and COL eavesdroppers scenarios.

SOP Analysis

In order to obtain SOP under AF relaying protocol, we proceed as follows:

Using (7.29) in (7.28) for $\lambda = \mathrm{AF}$, the SOP under AF relaying protocol can be written as

$$\mathcal{P}_{\mathrm{sec},k,n}^{\mathrm{AF},\flat} = \Pr\left[\left(C_{D_{n,k}}^{\mathrm{AF}} - C_{E,k}^{\mathrm{AF},\flat}\right) < \mathcal{R}_{\mathrm{s}}\right]. \tag{7.30}$$

Herein, $C_{D_{n,k}}^{\mathrm{AF}}$ and $C_{E,k}^{\mathrm{AF},\flat}$ are the instantaneous channel capacities of main and wiretap links under AF relaying protocol, which can be given, respectively, as

$$C_{D_{n,k}}^{\mathrm{AF}} = \frac{1}{2}\log_2\left(1+\Lambda_{D_{n,k}}^{\mathrm{AF}}\right) \tag{7.31}$$

and

$$C_{E,k}^{\mathrm{AF},\flat} = \frac{1}{2}\log_2\left(1+\Lambda_{E,k}^{\mathrm{AF},\flat}\right), \tag{7.32}$$

where factor 1/2 accounts for the two-hop communication. Now, using (7.31) and (7.32) into (7.30), $\mathcal{P}_{\mathrm{sec},k,n}^{\mathrm{AF},\flat}$ can be written as

$$\mathcal{P}_{\mathrm{sec},k,n}^{\mathrm{AF},\flat} = \Pr\left[\left(\frac{1}{2}\log_2\left(1+\Lambda_{D_{n,k}}^{\mathrm{AF}}\right) - \frac{1}{2}\log_2\left(1+\Lambda_{E,k}^{\mathrm{AF},\flat}\right)\right) < \mathcal{R}_{\mathrm{s}}\right], \tag{7.33}$$

which can be further simplified as

$$\mathcal{P}_{\mathrm{sec},k,n}^{\mathrm{AF},\flat} = \Pr\left[\frac{1+\Lambda_{D_{n,k}}^{\mathrm{AF}}}{1+\Lambda_{E,k}^{\mathrm{AF},\flat}} < \gamma_{\mathrm{s}}\right], \tag{7.34}$$

where $\gamma_{\mathrm{s}} = 2^{2\mathcal{R}_{\mathrm{s}}}$.

Then, based on (7.34), we can devise a user-relay pair selection criterion for minimizing SOP of the considered HSTRN as

$$(n^*, k^*) = \arg\max_{n=1,\ldots,N}\max_{k=1,\ldots,K}\left(\frac{1+\Lambda_{D_{n,k}}^{\mathrm{AF}}}{1+\Lambda_{E,k}^{\mathrm{AF},\flat}}\right). \tag{7.35}$$

Note that the user-relay pair selection criterion in (7.35) is based on maximizing the ratio of received SNRs of user and eavesdropper links. In accordance to (7.35), we find that the statistics involved in the user-relay pair (n^*, k^*) selection is maximum of $K \times N$ variables. However, these $K \times N$ variables are not independent of each other, since the satellite-relay link remains common for N users for a given relay. In fact, the dependence involved herein causes performance analysis intricate. To tackle this troublesome, we first select the best user with the maximum of $\gamma_{r_k d_n}$ conditioned on a given relay R_k i.e., $n_k^\star = \arg\max_{n=1,\ldots,N}\{\gamma_{r_k d_n}\}$. Therefore, we apply order statistics over K relays to express the SOP of the considered HSTRN with selected relay R_{k^*} as

$$\mathcal{P}_{\mathrm{sec},k^*,n^*}^{\mathrm{AF},\flat} = \prod_{k=1}^{K}\left[\mathcal{P}_{\mathrm{sec},k,n_k^\star}^{\mathrm{AF},\flat}\right]. \tag{7.36}$$

To proceed, we need to obtain the expression for $\mathcal{P}_{\mathrm{sec},k,n_k^\star}^{\mathrm{AF},\flat}$ in (7.36). However, after inserting (7.7) and (7.16) for $\flat$ = N-COL or (7.18) for $\flat$ = COL in (7.34), one can realize that the exact evaluation of SOP leads to very tedious analysis. Therefore, we approximate $\mathcal{P}^{\mathrm{AF},\flat}_{\mathrm{sec},k,n_k^\star}$ using (7.34) as

$$\mathcal{P}^{\mathrm{AF},\flat}_{\mathrm{sec},k,n_k^\star} \approx \Pr\left[\frac{\Lambda^{\mathrm{AF}}_{D_{n_k^\star},k}}{\Lambda^{\mathrm{AF},\flat}_{E,k}} < \gamma_{\mathrm{s}}\right], \tag{7.37}$$

where we have used the approximation $\frac{1+a}{1+b} \approx \frac{a}{b}$, which is widely adopted in literature [102], [103]. Further, on invoking the end-to-end SNRs from (7.7) and (7.16) for $\flat = $ N-COL or (7.18) for $\flat = $ COL into (7.37), and performing some straightforward manipulations, we obtain

$$\mathcal{P}^{\mathrm{AF},\flat}_{\mathrm{sec},k,n_k^\star} \approx \Pr\left[\frac{\gamma_{sr_k}\gamma_{r_k d_{n_k^\star}}}{\gamma_{\mathrm{s}}\gamma_{sr_k} + (\gamma_{\mathrm{s}}-1)\gamma_{r_k d_{n_k^\star}}} < \gamma^\flat_{r_k E}\right] \triangleq \Theta^\flat. \tag{7.38}$$

By defining $Z_{k,n_k^\star} = \frac{\gamma_{sr_k}\gamma_{r_k d_{n_k^\star}}}{\gamma_{\mathrm{s}}\gamma_{sr_k} + (\gamma_{\mathrm{s}}-1)\gamma_{r_k d_{n_k^\star}}}$, we can write $\Theta^\flat$ in (7.38) as

$$\begin{aligned}\Theta^\flat &= \Pr\left[Z_{k,n_k^\star} < \gamma^\flat_{r_k E}\right]\\ &= \int_0^\infty F_{Z_{k,n_k^\star}}(z) f_{\gamma^\flat_{r_k E}}(z)dz.\end{aligned} \tag{7.39}$$

The expression of $\Theta^\flat$ in (7.39), for $\flat \in \{\text{N-COL}, \text{COL}\}$ (i.e., for N-COL and COL eavesdroppers scenarios), can be evaluated, respectively, by theorems as given below.

Theorem 9. *The expression of* $\Theta^{\text{N-COL}}$ *can be given as*

$$\begin{aligned}\Theta^{\text{N-COL}} &= 1 - 2NL\sum_{i_1=0}^{m_s-1}\cdots\sum_{i_{N_s}=0}^{m_s-1}\sum_{\jmath=0}^{N-1}\mathcal{C}^{N-1}_{\jmath}\sum_{l=0}^{\jmath(m_d-1)}\omega^{\jmath}_{l}\frac{(-1)^{\jmath}}{\Gamma m_d}\left(\frac{m_d}{\varrho_d}\right)^{m_d+l}\sum_{r=0}^{L-1}\mathcal{C}^{L-1}_{r}\\ &\times\sum_{s=0}^{r(m_e-1)}\omega^{r}_{s}\frac{(-1)^r}{\Gamma m_e}\left(\frac{m_e}{\varrho_e}\right)^{m_e+s}\frac{\Xi(N_s)}{(\eta_s)^{\Lambda}}\sum_{p=0}^{\Lambda-1}\frac{(\Lambda-1)!}{p!}\sum_{q=0}^{p}\mathcal{C}^{p}_{q}\\ &\times\sum_{v=0}^{m_d+l-1}\mathcal{C}^{m_d+l-1}_{v}\gamma_s^{m_d+l-\frac{\tau}{2}}(\gamma_s-1)^{p+\frac{\tau}{2}}\chi_d^{\frac{\tau}{2}}\beta_\delta^{\frac{\tau}{2}-\Lambda+p}\frac{\sqrt{\pi}\,(4\rho)^{\tau}}{(\psi+2\rho)^{\mu+\tau}}\\ &\times\frac{\Gamma(\mu+\tau)\Gamma(\mu-\tau)}{\Gamma(\mu+\frac{1}{2})}{}_2F_1\left(\mu+\tau;\tau+\frac{1}{2};\mu+\frac{1}{2};\frac{\psi-2\rho}{\psi+2\rho}\right),\end{aligned} \tag{7.40}$$

where $\tau = v-q+1$, $\mu = p+m_d+m_e+l+s$, $\chi_d = \frac{\varrho_d}{m_d(\jmath+1)}$, $\rho = \sqrt{\beta_\delta(\gamma_s-1)\frac{\gamma_s}{\chi_d}}$, $\psi = \left(\beta_\delta(\gamma_s-1)+\frac{\gamma_s}{\chi_d}+\frac{1}{\chi_e}\right)$, *and the coefficients* $\omega^{\jmath}_{l}$, *for* $0 \le l \le \jmath(m_d-1)$, *can be calculated recursively (with* $\varepsilon_l = \frac{1}{l!}$*) as* $\omega^{\jmath}_0 = (\varepsilon_0)^{\jmath}$, $\omega^{\jmath}_1 = \jmath(\varepsilon_1)$, $\omega^{\jmath}_{\jmath(m_d-1)} = (\varepsilon_{m_d-1})^{\jmath}$, $\omega^{\jmath}_l = \frac{1}{l\varepsilon_0}\sum_{g=1}^{l}[g\jmath-l+g]\varepsilon_g\omega^{\jmath}_{l-g}$ *for* $2 \le l \le m_d-1$, *and* $\omega^{\jmath}_l = \frac{1}{l\varepsilon_0}\sum_{g=1}^{m_d-1}[g\jmath-l+g]\varepsilon_g\omega^{\jmath}_{l-g}$ *for* $m_d \le l < \jmath(m_d-1)$.

Proof. See Appendix 7.A. ■

Further, plugging (7.40) in (7.38), and the resultant in (7.36), SOP of the considered HSTRN can be obtained for N-COL eavesdroppers scenario under AF relaying protocol.

Sequentially, we now turn our attention to the COL eavesdroppers scenario of interception.

Theorem 10. *The expression of Θ^{COL} can be given as*

$$\Theta^{COL} = 1 - 2\,N \sum_{i_1=0}^{m_s-1} \dots \sum_{i_{N_s}=0}^{m_s-1} \sum_{\jmath=0}^{N-1} \mathcal{C}_{\jmath}^{N-1} \sum_{l=0}^{\jmath(m_d-1)} \omega_l^{\jmath} \frac{(-1)^{\jmath}}{\Gamma m_d} \left(\frac{m_d}{\varrho_d}\right)^{m_d+l} \frac{\Xi(N_s)}{(\eta_s)^{\Lambda}} \sum_{p=0}^{\Lambda-1} \frac{(\Lambda-1)!}{p!}$$
$$\times \sum_{q=0}^{p} \mathcal{C}_q^p \sum_{v=0}^{m_d+l-1} \mathcal{C}_v^{m_d+l-1} \gamma_s^{m_d+l-\frac{\tau}{2}} \beta_\delta^{\frac{\tau}{2}-\Lambda+p} \left(\frac{m_e}{\varrho_e}\right)^{m_e L} \frac{(\gamma_s-1)^{p+\frac{\tau}{2}} \chi_d^{\frac{\tau}{2}}}{\Gamma(m_e L)}$$
$$\times \frac{\sqrt{\pi}\,(4\rho)^{\tau}}{(\varsigma+2\rho)^{\vartheta+\tau}} \frac{\Gamma(\vartheta+\tau)\Gamma(\vartheta-\tau)}{\Gamma(\vartheta+\frac{1}{2})} \, {}_2F_1\left(\vartheta+\tau; \tau+\frac{1}{2}; \vartheta+\frac{1}{2}; \frac{\varsigma-2\rho}{\varsigma+2\rho}\right), \qquad (7.41)$$

where $\vartheta = p + l + m_d + m_e L$ and $\varsigma = \left(\beta_\delta\,(\gamma_s - 1) + \frac{\gamma_s}{\chi_d} + \frac{m_e}{\varrho_e}\right)$.

Proof. Following the similar steps as in Appendix 7.A with $f_{\gamma_{r_kE}^{\text{COL}}}(x)$ from (7.27) in place of $f_{\gamma_{r_kE}^{\text{N-COL}}}(x)$ in (7.39), one can reach at (7.41). ∎

Then, invoking (7.41) in (7.38), and the resultant in (7.36), SOP of the considered HSTRN for COL eavesdroppers scenario can be obtained under AF relaying protocol.

Thus, Theorem 9 and Theorem 10 provide the analytical expressions for the SOP of the considered HSTRN for both N-COL and COL eavesdroppers scenarios under AF relaying protocol, and it upholds for the complex hybrid channels with arbitrary number of satellite antennas, number of relays, number of users, and number of eavesdroppers over entire SNR regime.

Achievable Diversity Order

Although the obtained analytical SOP expressions using (7.40) and (7.41) are quite useful and provide several insights from numerical results, however, they are too complex to understand the diversity order of the proposed HSTRN. Thus, we perform asymptotic analysis of SOP expressions to obtain the diversity order of the considered HSTRN. For this, we assume $\eta_s, \eta_r \to \infty$ at the high SNR regime and derive the asymptotic expression of $\Theta^\flat$ for $\flat \in \{\text{N-COL}, \text{COL}\}$ under AF relaying protocol in the following corollaries.

Corollary 1. *$\Theta^{N\text{-}COL}$ at high SNR regime can be given as*

$$\begin{aligned}\Theta^{N\text{-}COL} \simeq\, & L\sum_{r=0}^{L-1}\mathcal{C}_r^{L-1}\sum_{s=0}^{r(m_e-1)}\omega_s^r\frac{(-1)^r}{\Gamma m_e}\left(\frac{m_e}{\varrho_e}\right)^{m_e+s}\\ &\times\left(\frac{\alpha^{N_s}(\gamma_s-1)^{N_s}}{(N_s)!\eta_s^{N_s}}\Gamma(N_s+m_e+s)\ \chi_e^{N_s+m_e+s}\right.\\ &\left.+\left(\frac{m_d\gamma_s}{\varrho_d}\right)^{m_dN}\frac{\Gamma(m_dN+m_e+s)}{[\Gamma(m_d+1)]^N}\ \chi_e^{m_dN+m_e+s}\right).\end{aligned} \tag{7.42}$$

Proof. See Appendix 7.B. ■

Further, the asymptotic SOP expression of HSTRN for N-COL eavesdroppers scenario can be obtained using (7.42) in (7.38) and the resultant in (7.36).

We now take our attention to the COL way of wiretapping.

Corollary 2. *Θ^{COL} at high SNR regime can be given as*

$$\begin{aligned}\Theta^{COL} \simeq\, & \frac{\alpha^{N_s}(\gamma_s-1)^{N_s}}{(N_s)!\eta_s^{N_s}}\frac{\Gamma(N_s+m_eL)}{\Gamma(m_eL)}\left(\frac{\varrho_e}{m_e}\right)^{N_s}\\ &+\left(\frac{m_d\gamma_s}{\varrho_d}\right)^{m_dN}\frac{\Gamma(m_dN+m_eL)}{[\Gamma(m_d+1)]^N\Gamma(m_eL)}\left(\frac{\varrho_e}{m_e}\right)^{m_dN}.\end{aligned} \tag{7.43}$$

Proof. The proof of (7.43) follows the similar steps as used in Appendix 7.B with the aid of the PDF of $\gamma_{r_kE}^{\text{COL}}$ from (7.27) in place of PDF of $\gamma_{r_kE}^{\text{N-COL}}$. ■

Now, using (7.43) in (7.38) and the resultant in (7.36), the asymptotic SOP expression of HSTRN for COL eavesdroppers scenario can be obtained.

As such, one can find the achievable diversity order of the proposed HSTRN system under AF relaying protocol for both N-COL and COL eavesdroppers scenarios is $K\min(N_s, m_dN)$.

Remarks: It is worth mentioning that the achievable diversity order of the considered HSTRN i.e., $K\min(N_s, m_dN)$ remains unaffected by the number of eavesdroppers, ways of intercepting at eavesdroppers, and fading severity parameter of satellite links. Moreover, the importance of a multi-antenna satellite is apparently emphasized by the achievable diversity order of the considered system.

7.2.2 DF Relaying

In this subsection, we propose the user-relay selection criterion and then derive accurate and asymptotic expressions for SOP based on the defined criteria for DF relaying protocol. We select the best user D_{n^*} and best relay R_{k^*} based on maximizing the received instantaneous SNR as

$$(n^*, k^*) = \arg \max_{1 \le n \le N,\, k \in \Delta} \{\Lambda_{D_{n,k}}^{\mathrm{DF}}\}. \tag{7.44}$$

SOP Analysis

We calculate the SOP of the proposed HSTRN for DF relaying case. In this regard, using (7.29) in (7.28) for $\lambda = \mathrm{DF}$, the SOP under DF relaying protocol can be written, with $\flat \in \{\text{N-COL}, \text{COL}\}$, as

$$\mathcal{P}_{\mathrm{sec},k,n}^{\mathrm{DF},\flat} = \Pr\left[\left(C_{D_{n,k}}^{\mathrm{DF}} - C_{E,k}^{\mathrm{DF},\flat}\right) < \mathcal{R}_{\mathrm{s}}\right], \tag{7.45}$$

where $C_{D_{n,k}}^{\mathrm{DF}}$ and $C_{E,k}^{\mathrm{DF},\flat}$ are the instantaneous channel capacities of main and wiretap links under DF relaying protocol, respectively. With D_{n^*} user and R_{k^*} relay, the channel capacity of main and wiretap links can be given using (7.13) and (7.17) for $\flat = \text{N-COL}$ or (7.19) for $\flat = \text{COL}$, respectively, as

$$C_{D_{n^*,k^*}}^{\mathrm{DF}} = \frac{1}{2}\log_2\left(1 + \Lambda_{D_{n^*,k^*}}^{\mathrm{DF}}\right) \tag{7.46}$$

and

$$C_{E_{l,k^*}}^{\mathrm{DF},\flat} = \frac{1}{2}\log_2\left(1 + \Lambda_{E,k}^{\mathrm{DF},\flat}\right). \tag{7.47}$$

On invoking (7.46) and (7.47) into (7.45) and applying the user-relay selection criterion from (7.44), we can write (7.45) as

$$\mathcal{P}_{\mathrm{sec},k^*,n^*}^{\mathrm{DF},\flat} = \Pr\left[\frac{1 + \gamma_{r_{k^*}d_{n^*}}}{1 + \gamma_{r_k E}^{\flat}} < \gamma_{\mathrm{s}}, |\Delta| = k^*\right], \tag{7.48}$$

where $\gamma_{r_{k^*}d_{n^*}} = \max_{1 \le n \le N,\, k \in \Delta}\{\gamma_{r_k d_n}\}$.

Now, to obtain $\mathcal{P}_{\mathrm{sec},k^*,n^*}^{\mathrm{DF},\flat}$ in (7.48), we assume that there may exist M elements ($M = 0, 1, 2, \cdots, K$) in the decoding set Δ. Thereby, we can express (7.48), by using the law of total probability, as

$$\mathcal{P}_{\mathrm{sec},k^*,n^*}^{\mathrm{DF},\flat} = \Pr\left[|\Delta| = k^*\right] \Pr\left[\frac{1 + \gamma_{r_{k^*}d_{n^*}}}{1 + \gamma_{r_k E}^{\flat}} < \gamma_{\mathrm{s}}\right], \tag{7.49}$$

where k^* denotes the best selected relay for transmission in second time phase. Further, we can simplify (7.49) as

$$\mathcal{P}_{\mathrm{sec},k^*,n^*}^{\mathrm{DF},\flat} = \sum_{M=0}^{K} \mathcal{C}_M^K \prod_{k \in \Delta} \Pr\left[\gamma_{sr_k} \ge \gamma_t\right] \prod_{k \in \overline{\Delta}} \Pr\left[\gamma_{sr_k} < \gamma_t\right] \Pr\left[\frac{1 + \gamma_{r_{k^*}d_{n^*}}}{1 + \gamma_{r_k E}^{\flat}} < \gamma_{\mathrm{s}}\right], \tag{7.50}$$

where $\gamma_t = 2^{2\mathcal{R}_t} - 1$ and $\overline{\Delta}$ denotes the complement of decoding set Δ. We can simply represent (7.50) as

$$\mathcal{P}^{\text{DF},\flat}_{\text{sec},k^*,n^*} = \sum_{M=0}^{K} \mathcal{C}_M^K \left[1 - F_{\gamma_{sr_k}}(\gamma_t)\right]^M \left[F_{\gamma_{sr_k}}(\gamma_t)\right]^{K-M} \underbrace{\Pr\left[\frac{1+\gamma_{r_{k^*}d_{n^*}}}{1+\gamma^{\flat}_{r_kE}} < \gamma_{\text{s}}\right]}_{\Phi^{\flat}}. \quad (7.51)$$

The expression of $\Phi^{\flat}$ in (7.51), for $\flat \in \{\text{N-COL}, \text{COL}\}$, can be respectively obtained in the theorems given below.

Theorem 11. *The expression for $\Phi^{N\text{-}COL}$ can be given as*

$$\Phi^{N\text{-}COL} = L \sum_{r=0}^{L-1} \mathcal{C}_r^{L-1} \sum_{s=0}^{r(m_e-1)} \omega_s^r \frac{(-1)^r}{\Gamma m_e} \left(\frac{m_e}{\varrho_e}\right)^{m_e+s} \sum_{\jmath=0}^{MN} \mathcal{C}_\jmath^{MN} (-1)^\jmath \sum_{l=0}^{\jmath(m_d-1)} \omega_l^\jmath \left(\frac{m_d}{\varrho_d}\right)^l \times \sum_{q=0}^{l} \mathcal{C}_q^l \gamma_s^q (\gamma_s - 1)^{l-q} \, \Gamma(q + m_e + s) e^{-\frac{m_d}{\varrho_d}\jmath(\gamma_s - 1)} \left(\frac{m_d}{\varrho_d}\jmath\gamma_s + \frac{1}{\chi_e}\right)^{-(q+m_e+s)}. \quad (7.52)$$

Proof. See Appendix 7.C. ■

Thus, after inserting (7.52) into (7.51) for $\flat = \text{N-COL}$, we obtain $\mathcal{P}^{\text{DF,N-COL}}_{\text{sec},k^*,n^*}$ as

$$\mathcal{P}^{\text{DF,N-COL}}_{\text{sec},k^*,n^*} = L \sum_{M=0}^{K} \mathcal{C}_M^K \left[1 - F_{\gamma_{sr_k}}(\gamma_t)\right]^M \left[F_{\gamma_{sr_k}}(\gamma_t)\right]^{K-M} \sum_{\jmath=0}^{MN} \mathcal{C}_\jmath^{MN} \sum_{r=0}^{L-1} \mathcal{C}_r^{L-1} \times \sum_{s=0}^{r(m_e-1)} \omega_s^r \frac{(-1)^r}{\Gamma m_e} \left(\frac{m_e}{\varrho_e}\right)^{m_e+s} \sum_{l=0}^{\jmath(m_d-1)} (-1)^\jmath \omega_l^\jmath \left(\frac{m_d}{\varrho_d}\right)^l \sum_{q=0}^{l} \mathcal{C}_q^l \times \frac{\gamma_{\text{s}}^q \Gamma(q + m_e + s)}{(\gamma_{\text{s}} - 1)^{q-l}} \text{e}^{-\frac{m_d}{\varrho_d}\jmath(\gamma_{\text{s}} - 1)} \left(\frac{m_d}{\varrho_d} \jmath \gamma_{\text{s}} + \frac{1}{\chi_e}\right)^{-(q+m_e+s)}. \quad (7.53)$$

Finally, we can evaluate the SOP expression for N-COL eavesdroppers scenario under DF relaying protocol after inserting CDF $F_{\gamma_{sr_k}}(\cdot)$ from (7.21) into (7.53).

Theorem 12. *The expression for Φ^{COL} can be given as*

$$\Phi^{COL} = \sum_{\jmath=0}^{MN} \mathcal{C}_\jmath^{MN} \sum_{l=0}^{\jmath(m_d-1)} \sum_{q=0}^{l} \mathcal{C}_q^l (-1)^\jmath \omega_l^\jmath \left(\frac{m_d}{\varrho_d}\right)^l \left(\frac{m_e}{\varrho_e}\right)^{m_e L} \frac{\Gamma(q + m_e L)}{\Gamma(m_e L)} \times \gamma_s^q (\gamma_s - 1)^{l-q} e^{-\frac{m_d}{\varrho_d}\jmath(\gamma_s - 1)} \left(\frac{m_d}{\varrho_d}\jmath\gamma_s + \frac{m_e}{\varrho_e}\right)^{-(q+m_e L)}. \quad (7.54)$$

Proof. The Φ^{COL} in (7.54) can be evaluated by following the similar steps as in Appendix 7.C with the use of PDF of $\gamma^{\text{COL}}_{r_kE}$ from (7.27) in place of PDF of $\gamma^{\text{N-COL}}_{r_kE}$. ■

Further, after plugging (7.54) into (7.51) for $\flat = \text{COL}$, we obtain $\mathcal{P}^{\text{DF,COL}}_{\text{sec},k^*,n^*}$ as

$$\begin{aligned}\mathcal{P}^{\text{DF,COL}}_{\text{sec},k^*,n^*} = &\sum_{M=0}^{K} \mathcal{C}^K_M \left[1 - F_{\gamma_{sr_k}}(\gamma_t)\right]^M \left[F_{\gamma_{sr_k}}(\gamma_t)\right]^{K-M} \sum_{\jmath=0}^{MN} \mathcal{C}^{MN}_{\jmath} \\ &\times \sum_{l=0}^{\jmath(m_d-1)} \sum_{q=0}^{l} \mathcal{C}^l_q (-1)^{\jmath} \omega^{\jmath}_l \left(\frac{m_d}{\varrho_d}\right)^l \left(\frac{m_e}{\varrho_e}\right)^{m_e L} \frac{\Gamma(q + m_e L)}{\Gamma(m_e L)} \\ &\times \gamma_{\text{s}}^q (\gamma_{\text{s}} - 1)^{l-q} \mathrm{e}^{-\frac{m_d}{\varrho_d}\jmath(\gamma_{\text{s}}-1)} \left(\frac{m_d}{\varrho_d}\jmath\gamma_{\text{s}} + \frac{m_e}{\varrho_e}\right)^{-(q+m_e L)}. \qquad (7.55)\end{aligned}$$

Finally, after inserting CDF $F_{\gamma_{sr_k}}(\cdot)$ from (7.21) into (7.55), one can evaluate the SOP expression for COL eavesdroppers scenario under DF relaying protocol.

Hence, Theorem 11 and Theorem 12 provide the analytical SOP expressions for N-COL and COL eavesdroppers scenarios under DF relaying protocol. Especially, to the best of the authors' knowledge, obtained SOP expressions are novel and are valid for the considered system with arbitrary number of satellite antennas, number of relays, number of users, and number of eavesdroppers with different integer-valued channel fading severities over entire SNR regime.

Achievable Diversity Order

In this subsection, we concentrate on analysing the asymptotic behaviour of SOP expressions at high SNR regime to assess the diversity order under DF relaying protocol. To be specific, we derive the asymptotic SOP expressions at high SNR regime (i.e., $\eta_s, \eta_r \to \infty$) for N-COL and COL eavesdroppers scenarios in the following corollaries.

Corollary 3. *Under DF relaying protocol, the asymptotic SOP expression for N-COL eavesdroppers scenario can be given as*

$$\begin{aligned}\mathcal{P}^{DF^{\infty},N\text{-}COL}_{sec,k^*,n^*} \simeq L &\sum_{M=0}^{K} \sum_{q=0}^{m_d MN} \sum_{r=0}^{L-1} \sum_{s=0}^{r(m_e-1)} \mathcal{C}^K_M \mathcal{C}^{m_d MN}_q \mathcal{C}^{L-1}_r \frac{(-1)^r \omega^r_s}{\Gamma m_e} \left(\frac{m_e}{\varrho_e}\right)^{m_e+s} \\ &\times \left(\frac{m_d}{\varrho_d}\right)^{m_d MN} \left(\frac{\alpha^{N_s}\gamma_t^{N_s}}{(N_s)!\eta_s^{N_s}}\right)^{K-M} \frac{\gamma_s^q (\gamma_s - 1)^{m_d MN - q}}{[\Gamma(m_d+1)]^{MN}} \Gamma(q+m_e+s)\chi_e^{q+m_e+s}.\end{aligned}$$

(7.56)

Proof. See Appendix 7.D. ■

Corollary 4. *The asymptotic SOP expression for COL eavesdroppers scenario can be given as*

$$\mathcal{P}_{sec,k^*,n^*}^{DF^\infty,COL} \simeq \sum_{M=0}^{K} \sum_{q=0}^{m_dMN} \mathcal{C}_M^K \mathcal{C}_q^{m_dMN} \left(\frac{m_d}{\varrho_d}\right)^{m_dMN} \left(\frac{\alpha^{N_s}\gamma_t^{N_s}}{(N_s)!\eta_s^{N_s}}\right)^{K-M} \times \left(\frac{\varrho_e}{m_e}\right)^q \frac{\Gamma(q+m_eL)}{\Gamma(m_eL)} \frac{\gamma_s^q(\gamma_s-1)^{m_dMN-q}}{[\Gamma(m_d+1)]^{MN}}. \tag{7.57}$$

Proof. The expression of $\mathcal{P}_{\mathrm{sec},k^*,n^*}^{\mathrm{DF}^\infty,\mathrm{COL}}$ in (7.57) can be obtained abiding by the similar steps as in Appendix 7.D for $\flat = \mathrm{COL}$. ■

From above corollaries, we can deduce that the achievable diversity order of the considered HSTRN under DF relaying protocol is $K\min(N_s, m_dN)$, irrespective of the collusion scenarios. This is same result as obtained previously in Section 7.2.1 for the case of AF relaying protocol.

Remarks: It is noteworthy that the achievable diversity order of the proposed HSTRN is not affected by the method of relaying as well as the way of intercepting. Importantly, it remains independent of the number of eavesdroppers and fading severity parameter of satellite links.

7.3 ESC Analysis Under AF Relaying

In this section, we derive the ESC expressions for both N-COL and COL scenarios under AF relaying protocol considering a single-relay (i.e., $K = 1$) in the proposed HSTRN. Thus, based on received signals at D_n and E_l, we can obtain the received instantaneous end-to-end SNRs at the n-th destination and l-th eavesdropper, respectively, as

$$\Lambda_{D_n} = \frac{\gamma_{sr}\gamma_{rd_n}}{\gamma_{sr}+\gamma_{rd_n}+1} \tag{7.58}$$

and

$$\Lambda_{E_l} = \frac{\gamma_{sr}\gamma_{re_l}}{\gamma_{sr}+\gamma_{re_l}+1}, \tag{7.59}$$

where $\gamma_{sr} = \eta_s||\mathbf{h}_{sr}||_F^2$, $\gamma_{rd_n} = \eta_r|h_{rd_n}|^2$, and $\gamma_{re_l} = \eta_r|h_{re_l}|^2$.

To exploit the multi-user diversity, we adopt the opportunistic user scheduling scheme, where the best user is selected based on the highest instantaneous SNR [120] of $R\to D_n$ links i.e., $\gamma_{rd} = \max_{1\le n\le N}\{\gamma_{rd_n}\}$. Thus, the exact SNR with the scheduled user can be given as

$$\Lambda_D = \frac{\gamma_{sr}\gamma_{rd}}{\gamma_{sr} + \gamma_{rd} + 1}. \tag{7.60}$$

Similar to (7.16) and (7.18), the end-to-end SNRs at eavesdroppers can be represented using (7.59), for $\flat \in \{\text{N-COL}, \text{COL}\}$, as

$$\Lambda_E^\flat = \frac{\gamma_{sr}\gamma_{rE}^\flat}{\gamma_{sr} + \gamma_{rE}^\flat + 1}. \tag{7.61}$$

Now, the secrecy capacity of considered system for $\flat \in \{\text{N-COL}, \text{COL}\}$ is given as

$$C_{\text{sec}}^\flat = [C_{\Lambda_D} - C_{\Lambda_E}^\flat]^+. \tag{7.62}$$

Herein, C_{Λ_D} and $C_{\Lambda_E}^\flat$ are the instantaneous channel capacity of main link and of wiretap link, which can be expressed, respectively, as

$$C_{\Lambda_D} = \frac{1}{2}\log_2(1 + \Lambda_D) \tag{7.63}$$

and

$$C_{\Lambda_E}^\flat = \frac{1}{2}\log_2\left(1 + \Lambda_E^\flat\right). \tag{7.64}$$

Note that the EC of the main and the wiretap links can be obtained, respectively, as follows:

$$\overline{C}_{\Lambda_D} = \frac{1}{2}\mathbb{E}\left[\log_2(1 + \Lambda_D)\right] \tag{7.65}$$

and

$$\overline{C}_{\Lambda_E^\flat} = \frac{1}{2}\mathbb{E}\left[\log_2\left(1 + \Lambda_E^\flat\right)\right], \tag{7.66}$$

where $\mathbb{E}[\cdot]$ denotes the expectation. As such, in PLS technique, ESC is considered to be positive, thereby, the ESC for the considered HSTRN can now be obtained as [110]

$$C_{\text{ESC}}^\flat = \left[\overline{C}_{\Lambda_D} - \overline{C}_{\Lambda_E^\flat}\right]^+. \tag{7.67}$$

Further, using SNR from (7.60) into (7.65), we can simplify $\overline{C}_{\Lambda_D}$ as

$$\overline{C}_{\Lambda_D} = \frac{1}{2\ln(2)}\mathbb{E}\left[\ln\left(\frac{(1 + \gamma_{sr})(1 + \gamma_{rd})}{1 + \gamma_{sr} + \gamma_{rd}}\right)\right], \tag{7.68}$$

which can be expressed, as in [111, eq.8], by means of MGF as

$$\overline{C}_{\Lambda_D} = \frac{1}{2\ln(2)}\int_0^\infty \mathrm{e}^{-\mathcal{S}}\widehat{\mathcal{M}}_{\gamma_{sr}}(\mathcal{S})\left(1 - \mathcal{M}_{\gamma_{rd}}(\mathcal{S})\right)d\mathcal{S}, \tag{7.69}$$

where $\mathcal{M}_{\gamma_{rd}}(\cdot)$ is the MGF transform and $\widehat{\mathcal{M}}_{\gamma_{sr}}(\cdot)$ is complementary MGF transform which are defined, respectively, as

$$\mathcal{M}_{\gamma_{rd}}(\mathcal{S}) \triangleq \int_0^\infty \mathrm{e}^{-\mathcal{S}x} f_{\gamma_{rd}}(x)dx \tag{7.70}$$

and

$$\widehat{\mathcal{M}}_{\gamma_{sr}}(\mathcal{S}) \triangleq \int_0^\infty \mathrm{e}^{-\mathcal{S}x}(1 - F_{\gamma_{sr}}(x))dx. \tag{7.71}$$

Similar to (7.69), the EC of wiretap link $\overline{C}_{\Lambda_E^\flat}$ can be given, using SNR from (7.61) into (7.66), as

$$\overline{C}_{\Lambda_E^\flat} = \frac{1}{2\ln(2)} \int_0^\infty \mathrm{e}^{-\mathcal{S}} \widehat{\mathcal{M}}_{\gamma_{sr}}(\mathcal{S}) \left(1 - \mathcal{M}_{\gamma_{rE}^\flat}(\mathcal{S})\right) d\mathcal{S}, \tag{7.72}$$

Now, on solving (7.69) and (7.72) for $\flat \in \{\text{N-COL}, \text{COL}\}$, and further using the obtained results in (7.67), we can get the expressions for ESC under N-COL and COL eavesdropping scenarios, which are presented in next subsections, respectively.

7.3.1 ESC Calculation with N-COL Scenario

The ESC can be mathematically represented from (7.67), under N-COL scenario (i.e., for $\flat = \text{N-COL}$), as

$$C_{\text{ESC}}^{\text{N-COL}} = \left[\overline{C}_{\Lambda_D} - \overline{C}_{\Lambda_E^{\text{N-COL}}}\right]^+. \tag{7.73}$$

In order to evaluate $C_{\text{ESC}}^{\text{N-COL}}$ in (7.73), we require the expressions of $\overline{C}_{\Lambda_D}$ and $\overline{C}_{\Lambda_E^{\text{N-COL}}}$ which can be given by the below lemmas, respectively.

Lemma 4. *The expression of $\overline{C}_{\Lambda_D}$ can be derived as*

$$\begin{aligned}\overline{C}_{\Lambda_D} = \frac{1}{2\ln(2)} \sum_{i_1=0}^{m_s-1} \cdots \sum_{i_{N_s}=0}^{m_s-1} \frac{\Xi(N_s)}{(\eta_s)^\Lambda} \sum_{p=0}^{\Lambda-1} \frac{\Gamma\Lambda}{p!} \beta_\delta^{-(\Lambda+1)} \Bigg(G_{2,1}^{1,2}\left[\frac{1}{\beta_\delta}\middle|\begin{matrix}0, -p\\ 0\end{matrix}\right] \\ - N \sum_{\jmath=0}^{N-1} \mathcal{C}_\jmath^{N-1} \sum_{l=0}^{\jmath(m_d-1)} \frac{1}{\Gamma m_d} \frac{\omega_l^\jmath\ (-1)^\jmath}{(\jmath+1)^{m_d+l}} G_{1,[1:1],0,[1:1]}^{1,1,1,1,1}\left[\begin{matrix}\frac{1}{\beta_\delta}\\ \chi_d\end{matrix}\middle|\begin{matrix}1; -p; 1-m_d-l\\ -; 0; 0\end{matrix}\right]\Bigg).\end{aligned} \tag{7.74}$$

Proof. See Appendix 7.E. ∎

Lemma 5. *The expression of* $\overline{C}_{\Lambda_E^{N\text{-}COL}}$ *can be obtained as*

$$\overline{C}_{\Lambda_E^{N\text{-}COL}} = \frac{1}{2\ln(2)}\Bigg(\sum_{i_1=0}^{m_s-1}\cdots\sum_{i_{N_s}=0}^{m_s-1}\frac{\Xi(N_s)}{(\eta_s)^\Lambda}\sum_{p=0}^{\Lambda-1}\frac{\Gamma\Lambda}{p!}\beta_\delta^{-(\Lambda+1)}G_{2,1}^{1,2}\left[\frac{1}{\beta_\delta}\middle|\begin{matrix}0,-p\\0\end{matrix}\right]$$
$$-L\sum_{i_1=0}^{m_s-1}\cdots\sum_{i_{N_s}=0}^{m_s-1}\frac{\Xi(N_s)}{(\eta_s)^\Lambda}\sum_{p=0}^{\Lambda-1}\frac{\Gamma\Lambda}{p!}\beta_\delta^{-(\Lambda+1)}\sum_{r=0}^{L-1}\mathcal{C}_r^{L-1}\frac{(-1)^r}{\Gamma m_e}$$
$$\times\sum_{s=0}^{r(m_e-1)}\frac{\omega_s^r}{(r+1)^{m_e+s}}G_{1,[1:1],0,[1:1]}^{1,1,1,1,1}\left[\begin{matrix}\frac{1}{\beta_\delta}\\\chi_e\end{matrix}\middle|\begin{matrix}1;-p;1-m_e-s\\-;0;0\end{matrix}\right]\Bigg). \qquad (7.75)$$

Proof. See Appendix 7.F. ■

Now, using (7.74) and (7.75) into (7.73), the ESC expression of the considered HSTRN for N-COL scenario can be obtained.

7.3.2 ESC Calculation with COL Scenario

For COL scenario, the ESC can be written from (7.67) as

$$C_{\text{ESC}}^{\text{COL}} = \left[\overline{C}_{\Lambda_D} - \overline{C}_{\Lambda_E^{\text{COL}}}\right]^+. \qquad (7.76)$$

To get $C_{\text{ESC}}^{\text{COL}}$ in (7.76), we require $\overline{C}_{\Lambda_E^{\text{COL}}}$ which can be obtained, by following the similar steps as used in Appendix 7.F with replacing $f_{\gamma_{rE}^{\text{N-COL}}}$ to $f_{\gamma_{rE}^{\text{COL}}}$ from (7.27), as

$$\overline{C}_{\Lambda_E^{\text{COL}}} = \frac{1}{2\ln(2)}\Bigg(\sum_{i_1=0}^{m_s-1}\cdots\sum_{i_{N_s}=0}^{m_s-1}\frac{\Xi(N_s)}{(\eta_s)^\Lambda}\sum_{p=0}^{\Lambda-1}\frac{\Gamma\Lambda}{p!}\beta_\delta^{-(\Lambda+1)}G_{2,1}^{1,2}\left[\frac{1}{\beta_\delta}\middle|\begin{matrix}0,-p\\0\end{matrix}\right]$$
$$-\sum_{i_1=0}^{m_s-1}\cdots\sum_{i_{N_s}=0}^{m_s-1}\frac{\Xi(N_s)}{(\eta_s)^\Lambda}\sum_{p=0}^{\Lambda-1}\frac{\Gamma\Lambda}{p!}\frac{\beta_\delta^{-(\Lambda+1)}}{\Gamma(m_eL)}G_{1,[1:1],0,[1:1]}^{1,1,1,1,1}\left[\begin{matrix}\frac{1}{\beta_\delta}\\\frac{\varrho_e}{m_e}\end{matrix}\middle|\begin{matrix}1;-p;1-m_eL\\-;0;0\end{matrix}\right]\Bigg). \qquad (7.77)$$

On invoking (7.74) and (7.77) into (7.76), the expression for ESC under COL scenario can be obtained.

7.4 Numerical and Simulation Results

To examine the effectiveness of the derived SOP expressions for both N-COL and COL way of intercepting under AF and DF relaying protocols, we present numerical and simulation results in this section. For this, we have fixed $\mathcal{R}_\text{s} = 0.5$, $\varrho_e = 2$ dB, $\mathcal{R}_t = 0.5$, and $\eta_s = \eta_r$ as transmit SNR. The shadowed-Rician fading parameters for $S \rightarrow R_k$ links are adopted as $(m_s, b, \Omega_s = 1, 0.063, 0.0007)$ for heavy shadowing and $(m_s, b, \Omega_s = 5, 0.251, 0.279)$ under average shadowing scenarios [58]. It is worth mentioning that the analytical results are plotted using the derived expressions and the simulation results are obtained through Monte-Carlo method by performing 10^7 iterations. It is found that the simulation results coincide nicely to validate the analytical results.

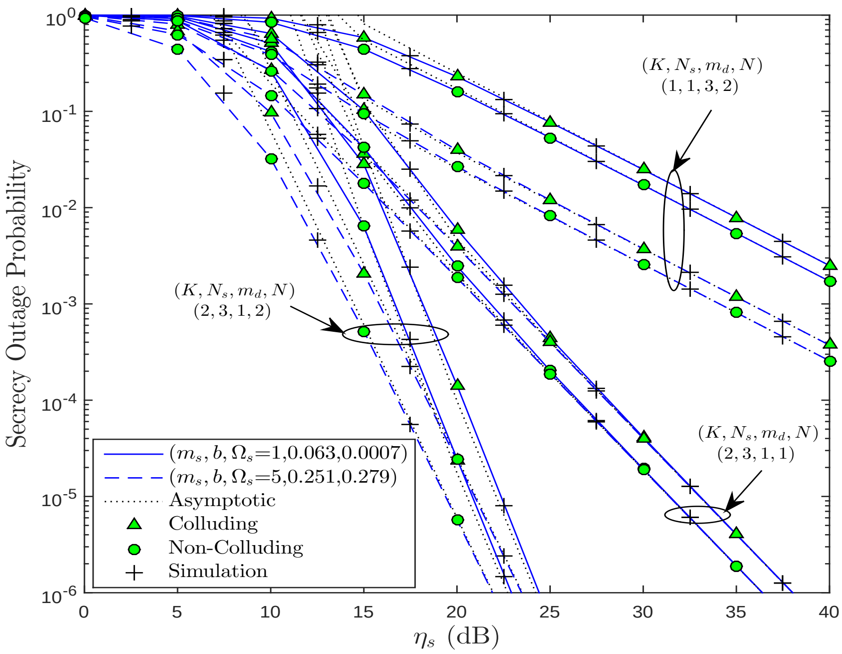

Figure 7.2: SOP performance of HSTRN for various system/channel parameters under AF relaying protocol.

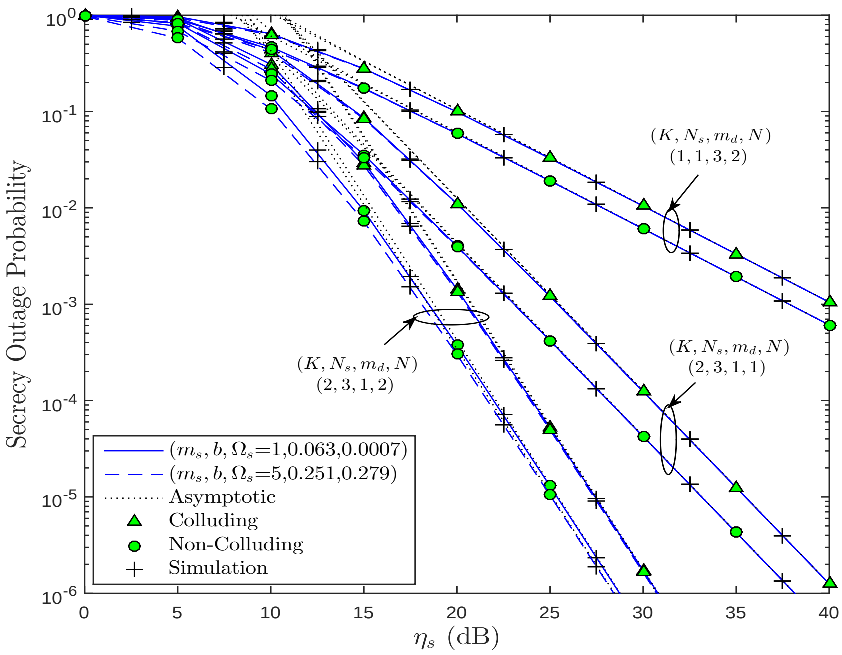

Figure 7.3: SOP performance of HSTRN for various system/channel parameters under DF relaying protocol.

In Figs. 7.2 and 7.3, we illustrate the impact of various system/channel parameters on secrecy performance of considered HSTRN for AF and DF relaying protocols, respectively. By fixing $m_e = 2$ and the number of eavesdroppers $L = 2$, we have drawn SOP curves versus transmit SNR (i.e., η_s) under both N-COL and COL eavesdroppers scenarios. In these figures, both average and heavy shadowing cases of shadowed-Rician fading are considered. It is apparent that the curves justify the system diversity order of $K \min(N_s, m_d N)$ for both N-COL and COL eavesdroppers scenarios. For example, one can realize the diversity order of 4 through the slopes of the SOP curves when $(K, N_s, m_d, N) = (2, 3, 1, 2)$ and diversity order of 1 with the curves caused by $(K, N_s, m_d, N) = (1, 1, 3, 2)$. More importantly, one can observe from these figures that the system achieves same diversity order under both AF and DF relaying protocols. We can also observe that the SOP performance with N-COL eavesdroppers scenario is better as compared to COL eavesdroppers scenario. This is due to the fact that collusion can enhance the intercepting gain for eavesdroppers. Furthermore, it is found that the system outperforms under average shadowed-Rician fading against heavy shadowed-Rician fading scenario. However, when $N_s > m_d N$, the system secrecy performance is dominated by the terrestrial links and hence the curves of average and heavy shadowed-Rician fading scenarios get merged at high SNR. This can be clearly observed via the curves for $(K, N_s, m_d, N) = (2, 3, 1, 1)$ and $(K, N_s, m_d, N) = (2, 3, 1, 2)$. On the contrary, when $N_s \leq m_d N$, the system secrecy performance is limited by satellite links and hence a significant performance difference appears under average and heavy shadowed-Rician fading scenarios e.g., see the particular curves for $(1, 1, 3, 2)$.

In Figs. 7.4 and 7.5, we have drawn the SOP curves for different number of relays K under AF and DF relaying protocols, respectively, by setting other system parameters as $m_e = 2$, $m_d = 1$, $L = 2$, $N = 1$, and $N_s = 2$. As depicted in these two figures, we can see that increasing the number of relays has improved the secrecy outage performance under both the relaying protocols.

Figs. 7.6 and 7.7 depict the impact of the different number of terrestrial users on secrecy performance of considered HSTRN under AF and DF relaying protocols, respectively. By adopting system parameters as $m_d = 1$, $K = 1$, $N_s = 3$, $m_e = 2$, and $L = 3$, we have drawn the SOP curves for different number of terrestrial users. From these figures, one can observe that the system achieves better secrecy

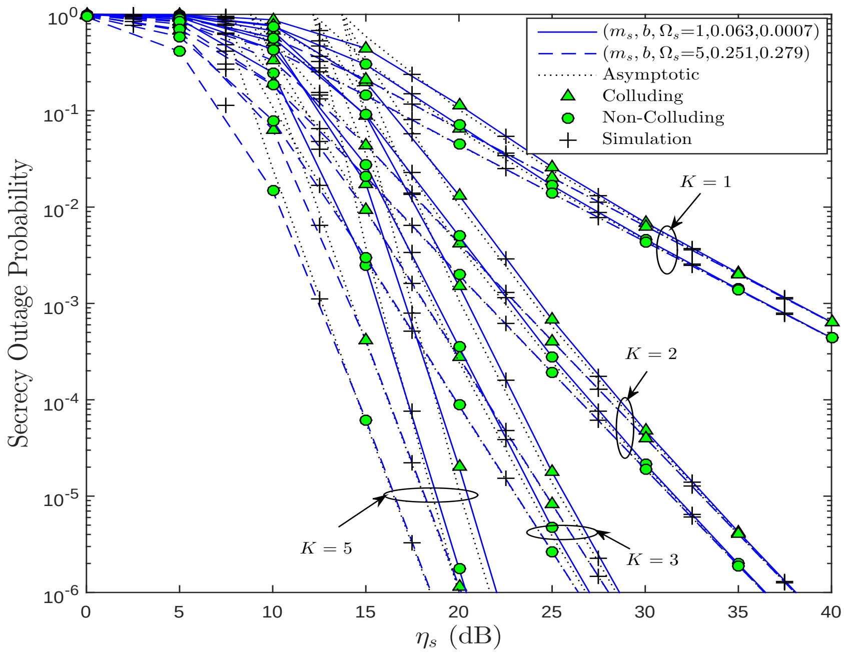

Figure 7.4: Impact of number of relay K on SOP performance of HSTRN under AF relaying protocol.

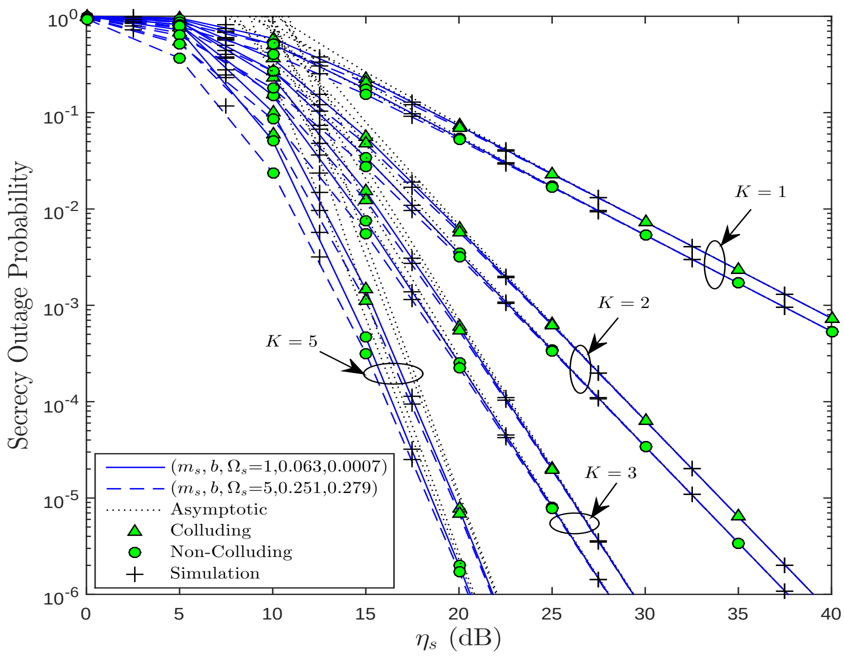

Figure 7.5: Impact of number of relay K on SOP performance of HSTRN under DF relaying protocol.

performance for large number of terrestrial users. In fact, having large number of users can enhance the diversity gain, which leads to an improved quality for main channel.

In Figs. 7.8 and 7.9, we illustrate the impact of the eavesdroppers on the secrecy

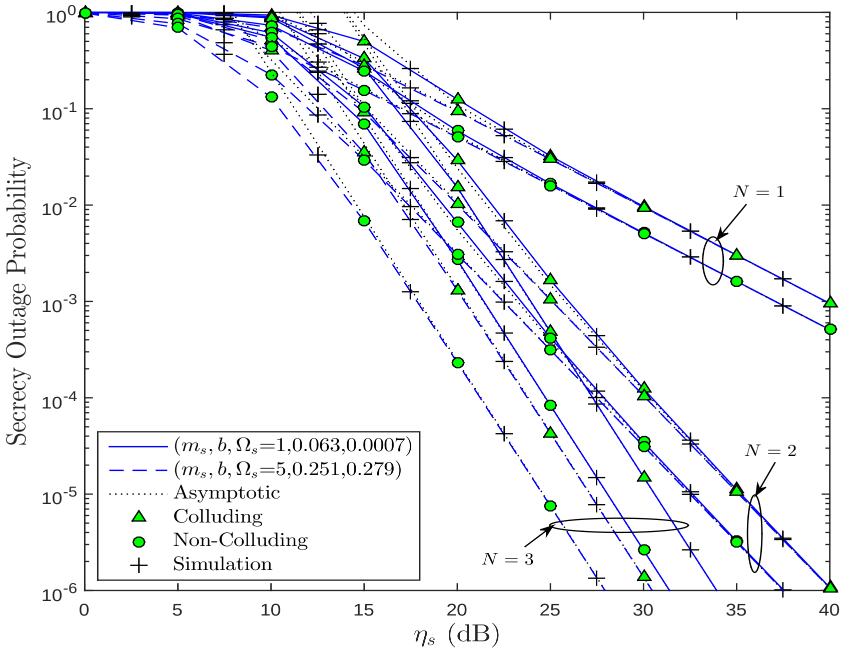

Figure 7.6: SOP versus η_s with different number of users N under AF relaying protocol.

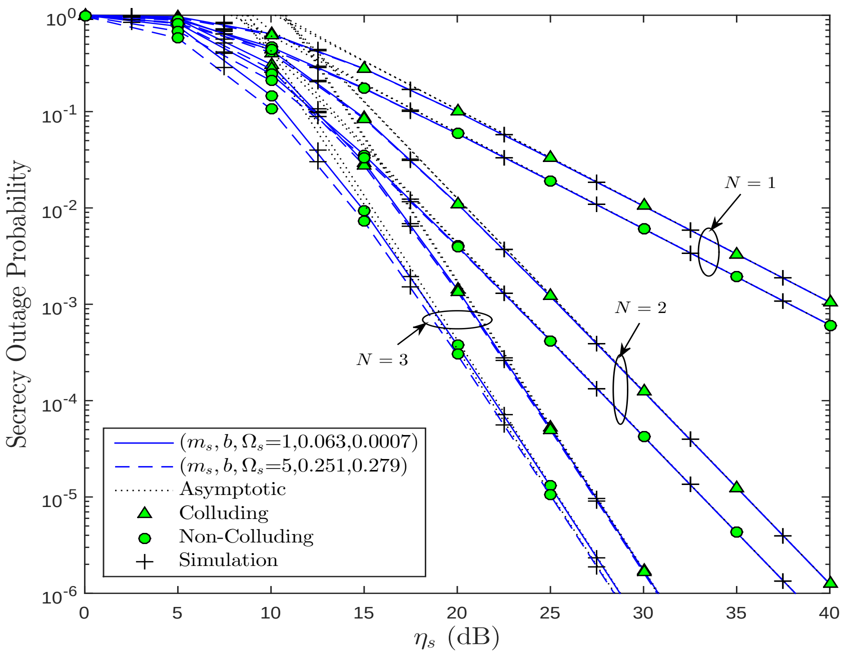

Figure 7.7: SOP versus η_s with different number of users N under DF relaying protocol.

performance of the considered HSTRN for both N-COL and COL eavesdroppers scenarios of intercepting under AF and DF relaying protocols, respectively. For this, we have set system parameters as $m_d = 1$, $m_e = 1$, $N_s = 2$, $K = 2$, $N = 2$, and $\eta_s = 20$ dB. As expected, secrecy performance of considered HSTRN degrades with

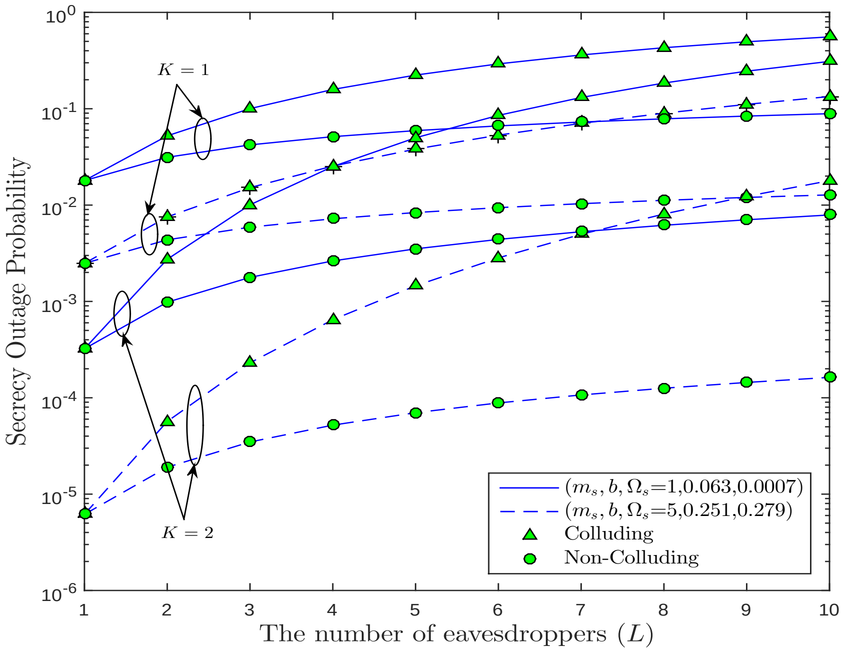

Figure 7.8: Impact of number of eavesdroppers L on SOP performance of HSTRN under AF relaying protocol.

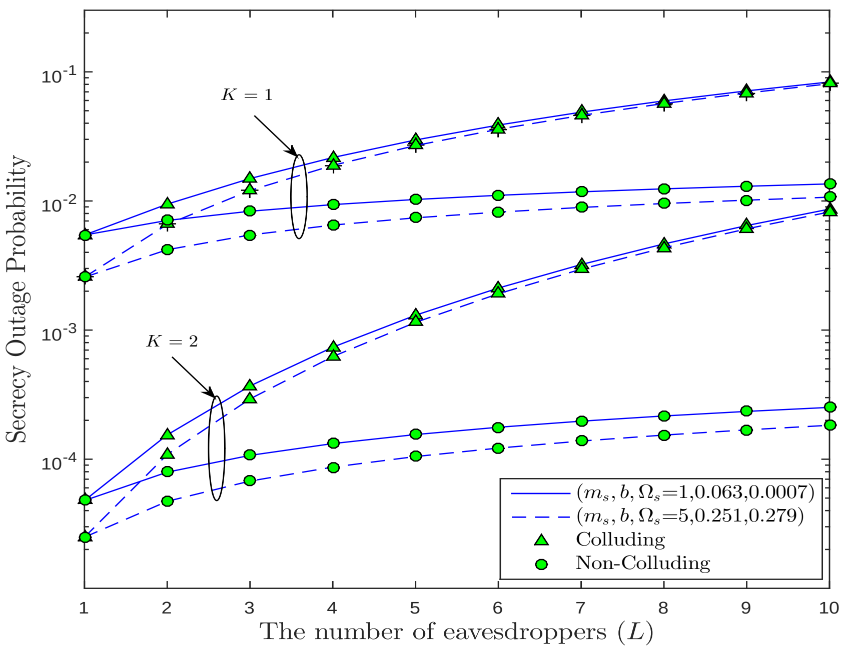

Figure 7.9: Impact of number of eavesdroppers L on SOP performance of HSTRN under DF relaying protocol.

an increase in the number of eavesdroppers. This is due to the fact that increasing the number of eavesdroppers positively affects the ability of eavesdropping, hence system becomes less secure when a large number of eavesdroppers succeed in attacking. Besides, it can be readily observed that the secrecy performance gap between

N-COL eavesdroppers scenario and COL eavesdroppers scenario expands with an increasing number of eavesdroppers. This is expected since COL way of intercepting can enhance the intercepting gain for eavesdroppers.

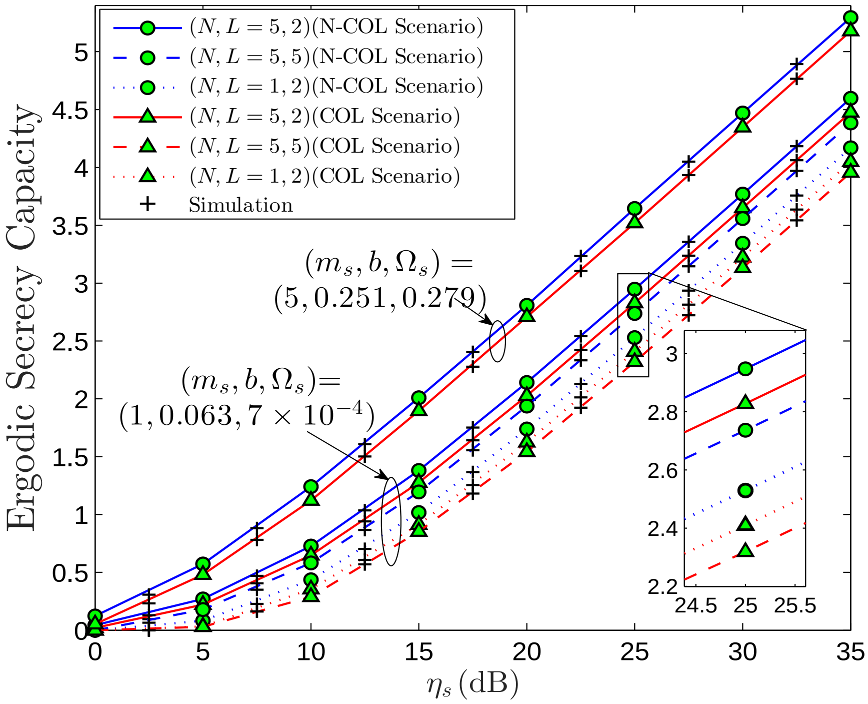

Figure 7.10: Impact of N and L on ESC of the considered HSTRN.

In Fig. 7.10, we draw the ESC curves of considered HSTRN for different number of terrestrial users and number of terrestrial eavesdroppers under both N-COL and COL intercepting scenarios. For this, we have fixed $m_d = 1$, $N_s = 5$, $m_e = 1$, $\varrho_e = 0$ dB, and considered both heavy and average shadowing scenarios of satellite link. As expected, the system ESC increases with an increasing number of N (e.g., see the respective curves for $(1, 2)$ and $(5, 2)$), whereas it degrades with the increasing of the number of L (e.g., as apparent by the curves being $(5, 2)$ and $(5, 5)$). This is due to the fact that a large number of terrestrial users can increase the probability of achieving higher quality of the main link while having more number of eavesdroppers positively affect the intercepting feasibility. Importantly, it can be readily observed that the gap between the ESC curves for N-COL and COL scenarios magnifies for a large L. For instance, gap between the curves being $(5, 5)$ is more as compared to curves for $(5, 2)$ for N-COL and COL scenarios.

Fig. 7.11 depicts the impact of different number of satellite antennas on the ESC performance of the considered HSTRN by setting other system parameters as $L = 3$, $N = 2$, $m_d = m_e = 2$, and $\varrho_e = 2$ dB. We can see that the ESC performance of

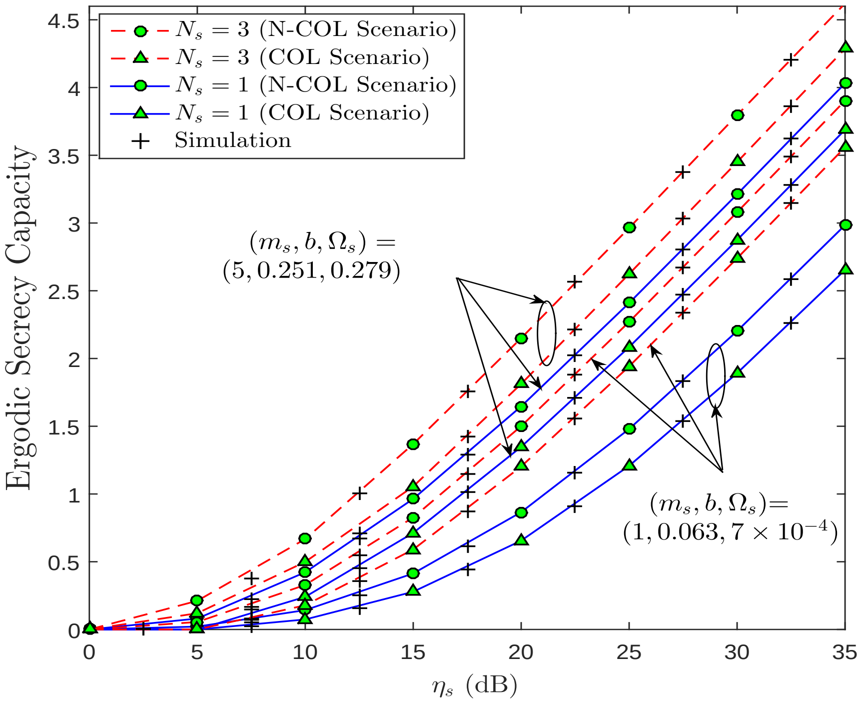

Figure 7.11: Impact of N_s on ESC of the considered HSTRN.

the proposed system improves with an increase in the number of N_s, vindicating the advantages of deployment of a multi-antenna satellite. Moreover, we have also compared average shadowing scenario with heavy shadowing scenario of satellite link and it is observed that system attains enhanced ESC under average shadowing.

7.5 Summary

In this chapter, we have analyzed the PLS of a multi-user multi-relay HSTRN with multiple eavesdroppers under AF and DF relaying protocols. Specifically, we have proposed best user-relay pair selection criteria for minimizing SOP of the considered system. We derived accurate SOP expressions for N-COL and COL eavesdroppers scenarios by adopting shadowed-Rician fading channels for satellite links and Nakagami-m fading channels for terrestrial links. Furthermore, we derived the asymptotic SOP expressions at high SNR regime and presented important insights in terms of the achievable diversity order of the considered HSTRN. Next, we derived novel and accurate expressions of ESC for AF relaying protocol under N-COL and COL scenarios of interception. Through our results, we have demonstrated that system diversity gain remains unaffected by the method of relaying protocol and type of eavesdropping. Also, we illustrated that the system performance can largely degraded by the COL eavesdroppers than its counterpart N-COL eavesdroppers. Since the secrecy performance analysis of HSTRN is a key research area in satellite communications, our technical contributions in this chapter will serve as a benchmark for the design of future HSTRN.

Appendix 7.A: Proof of Theorem 9

To solve the integral in (7.39), we require the CDF $F_{Z_{k,n_k^\star}}(\cdot)$ which can be evaluated as

$$F_{Z_{k,n_k^\star}}(z) = \Pr\left[\frac{\gamma_{sr_k}\gamma_{r_k d_{n_k^\star}}}{\gamma_{\mathrm{s}}\gamma_{sr_k} + (\gamma_{\mathrm{s}} - 1)\gamma_{r_k d_{n_k^\star}}} < z\right], \tag{7.78}$$

and can be rewritten as

$$F_{Z_{k,n_k^\star}}(z) = \Pr\left[\gamma_{sr_k} < \frac{z(\gamma_{\mathrm{s}} - 1)\gamma_{r_k d_{n_k^\star}}}{\gamma_{r_k d_{n_k^\star}} - z\gamma_{\mathrm{s}}}\right]. \tag{7.79}$$

Then, we acquire

$$F_{Z_{k,n_k^\star}}(z) = \int_0^{z\gamma_{\mathrm{s}}} f_{\gamma_{r_k d_{n_k^\star}}}(x)dx + \int_{z\gamma_{\mathrm{s}}}^{\infty} F_{\gamma_{sr_k}}\left(\frac{z(\gamma_{\mathrm{s}} - 1)x}{x - z\gamma_{\mathrm{s}}}\right) f_{\gamma_{r_k d_{n_k^\star}}}(x)dx, \tag{7.80}$$

which can be further simplified as

$$F_{Z_{k,n_k^\star}}(z) = 1 - \int_0^{\infty}\left(1 - F_{\gamma_{sr_k}}\left(\frac{z(\gamma_{\mathrm{s}} - 1)(x + z\gamma_{\mathrm{s}})}{x}\right)\right) f_{\gamma_{r_k d_{n_k^\star}}}(x + z\gamma_{\mathrm{s}})dx. \tag{7.81}$$

To further solve (7.81), we require PDF of $\gamma_{r_k d_{n_k^\star}} = \max_{1\le n\le N}\{\gamma_{r_k d_n}\}$. Thereby, on applying order statistics, the corresponding CDF can be expressed as

$$F_{\gamma_{r_k d_{n_k^\star}}}(x) = \prod_{n=1}^{N} F_{\gamma_{r_k d_n}}(x). \tag{7.82}$$

Now, the PDF $f_{\gamma_{r_k d_{n_k^\star}}}(x)$ can be calculated after performing differentiation of corresponding CDF as

$$f_{\gamma_{r_k d_{n_k^\star}}}(x) = \frac{dF_{\gamma_{r_k d_{n_k^\star}}}(x)}{dx} = \frac{d}{dx}[F_{\gamma_{r_k d_n}}(x)]^N, \tag{7.83}$$

which can be further simplified as

$$f_{\gamma_{r_k d_{n_k^\star}}}(x) = N\left(F_{\gamma_{r_k d_n}}(x)\right)^{N-1} f_{\gamma_{r_k d_n}}(x). \tag{7.84}$$

Further, by invoking $F_{\gamma_{r_k d_n}}(\cdot)$ from (7.23) with series exploration of $\Upsilon(\cdot,\cdot)$ [59, eq. 8.352.1], the corresponding PDF from (7.22) for $j_\epsilon = d_n$ into (7.84), and then applying binomial [59, eq. 1.111] and multinomial [59, eq. 0.314] expansions, we obtain

PDF $f_{\gamma_{r_k d_{n_k^\star}}}(x)$ as

$$f_{\gamma_{r_k d_{n_k^\star}}}(x) = N \sum_{\jmath=0}^{N-1} \mathcal{C}_{\jmath}^{N-1} \sum_{l=0}^{\jmath(m_d-1)} \omega_l^{\jmath} \frac{(-1)^{\jmath}}{\Gamma m_d} \left(\frac{m_d}{\varrho_d}\right)^{m_d+l} x^{m_d+l-1} \mathrm{e}^{-\frac{x}{\chi_d}}. \tag{7.85}$$

Now, using the CDF $F_{\gamma_{sr_k}}(\cdot)$ from (7.21) and the PDF $f_{\gamma_{r_k d_{n_k^\star}}}(\cdot)$ from (7.85) into (7.81), we can obtain $F_{Z_{k,n_k^\star}}(z)$ with the aid of [59, eq. 3.471.9], and then substituting the resultant of (7.81) along with (7.24) into (7.39), we solve the integration using [59, eq. 6.621.3] to obtain $\Theta^{\text{N-COL}}$ as given in (7.40) under Theorem 9.

Appendix 7.B: Proof of Corollary 1

Note that $Z_{k,n_k^\star} = \frac{\gamma_{sr_k}\gamma_{r_k d_{n_k^\star}}}{\gamma_{\mathrm{s}}\gamma_{sr_k}+(\gamma_{\mathrm{s}}-1)\gamma_{r_k d_{n_k^\star}}}$ can be simply written as

$$Z_{k,n_k^\star} = \frac{1}{\frac{\gamma_{\mathrm{s}}}{\gamma_{r_k d_{n_k^\star}}} + \frac{\gamma_{\mathrm{s}}-1}{\gamma_{sr_k}}}, \tag{7.86}$$

which, at the high SNR regime (i.e, $\eta_s, \eta_r \to \infty$), can be represented in terms of well known approximation of harmonic mean [95] as

$$Z_{k,n_k^\star} \simeq \min\left(\frac{\gamma_{sr_k}}{\gamma_{\mathrm{s}}-1}, \frac{\gamma_{r_k d_{n_k^\star}}}{\gamma_{\mathrm{s}}}\right). \tag{7.87}$$

Hence, the CDF $F_{Z_{k,n_k^\star}}(x)$ is given as

$$F_{Z_{k,n_k^\star}}(x) \simeq \Pr\left[\min\left(\frac{\gamma_{sr_k}}{\gamma_{\mathrm{s}}-1}, \frac{\gamma_{r_k d_{n_k^\star}}}{\gamma_{\mathrm{s}}}\right) < x\right]. \tag{7.88}$$

Exploiting the independence among the involved random variables in (7.88), we can express $F_{Z_{k,n_k^\star}}(x)$ as

$$F_{Z_{k,n_k^\star}}(x) \simeq F_{\gamma_{sr_k}}((\gamma_{\mathrm{s}}-1)x) + F_{\gamma_{r_k d_{n_k^\star}}}(\gamma_{\mathrm{s}}x) - F_{\gamma_{sr_k}}((\gamma_{\mathrm{s}}-1)x)\, F_{\gamma_{r_k d_{n_k^\star}}}(\gamma_{\mathrm{s}}x). \tag{7.89}$$

To proceed, we need to evaluate the asymptotic behavior for the CDFs $F_{\gamma_{sr_k}}(x)$ and $F_{\gamma_{r_k d_{n_k^\star}}}(x)$. Thus, we first obtain the asymptotic expression of $F_{\gamma_{sr_k}}(x)$. For this, we apply the Maclaurin series expansion of the exponential function in (7.20) to approximate the PDF of γ_{sr_k} at high SNR regime as

$$f_{\gamma_{sr_k}}(x) \simeq \frac{\alpha^{N_s}}{(N_s-1)!\eta_s^{N_s}} x^{N_s-1}, \tag{7.90}$$

and hence, the corresponding CDF follows asymptotic behavior as

$$F_{\gamma_{sr_k}}(x) \simeq \frac{\alpha^{N_s}}{(N_s)!\eta_s^{N_s}} x^{N_s}. \tag{7.91}$$

Further, to obtain asymptotic behavior of $F_{\gamma_{r_k d_{n_k^\star}}}(x)$, we first simplify the PDF in (7.85) for $\eta_r \to \infty$ (hence $\varrho_d \to \infty$) and then integrate the result. Thereby, the asymptotic behavior of the corresponding CDF can be deduced as

$$F_{\gamma_{r_k d_{n_k^\star}}}(x) \simeq \frac{1}{[\Gamma(m_d+1)]^N}\left(\frac{m_d\, x}{\varrho_d}\right)^{m_d N}. \tag{7.92}$$

Now, after inserting (7.91) and (7.92) into (7.89), one can obtain $F_{Z_{k,n_k^\star}}(x)$ as

$$F_{Z_{k,n_k^\star}}(x) \simeq \frac{\alpha^{N_s}(\gamma_{\rm s}-1)^{N_s}}{(N_s)!\eta_s^{N_s}} x^{N_s} + \frac{x^{m_d N}}{[\Gamma(m_d+1)]^N}\left(\frac{m_d \gamma_{\rm s}}{\varrho_d}\right)^{m_d N}, \tag{7.93}$$

where the higher order term is neglected. On invoking (7.93) along with PDF $f_{\gamma_{r_k E}^{\text{N-COL}}}(x)$ from (7.24) into (7.39) and solving the involved integrals with the aid of [59, eq. 3.351.3], $\Theta^{\text{N-COL}}$ at high SNR regime can be given as (7.42) in Corollary 1.

Appendix 7.C: Proof of Theorem 11

By definition, $\Phi^\flat$ in (7.51) for $\flat =$ N-COL can be statistically written in the form of integration as

$$\Phi^{\text{N-COL}} = \int_0^\infty F_X(\gamma_{\rm s} y + \gamma_{\rm s} - 1) f_{\gamma_{r_k E}^{\text{N-COL}}}(y) dy, \tag{7.94}$$

where $X = \gamma_{r_{k^*} d_{n^*}}$. Now, we require the CDF $F_X(\cdot)$ and PDF $f_{\gamma_{r_k E}^{\text{N-COL}}}(\cdot)$ to solve the integration in (7.94). It is worth noting that $X = \max_{1\le n\le N,\, k\in\Delta}\{\gamma_{r_k d_n}\}$ is the maximum of $N\times M$ random variables, where M is the number of relay which succeed in decoding. Since, these $N\times M$ variables are independent, we can write X as

$$X = \max_{1\le n\le N} \theta_n, \tag{7.95}$$

where $\theta_n = \max_{k\in\Delta}\{\gamma_{r_k d_n}\}$. Thus, by applying order statistics, $F_X(\cdot)$ can be given as

$$F_X(x) = \prod_{n=1}^N F_{\theta_n}(x). \tag{7.96}$$

Further, using (7.23) with series form of $\Upsilon(\cdot,\cdot)$ [59, eq. 8.352.1], CDF of θ_n can be given as

$$F_{\theta_n}(x) = \left(1 - {\rm e}^{-\frac{m_d}{\varrho_d}x}\sum_{l=0}^{m_d-1}\frac{(m_d\, x)^l}{l!(\varrho_d)^l}\right)^M. \tag{7.97}$$

Then, on invoking (7.97) into (7.96), one can obtain $F_X(x)$ as

$$F_X(x) = \sum_{\jmath=0}^{MN} \mathcal{C}_{\jmath}^{MN} (-1)^{\jmath} \mathrm{e}^{-\frac{m_d}{\varrho_d}\jmath x} \sum_{l=0}^{\jmath(m_d-1)} \omega_l^{\jmath} \left(\frac{m_d x}{\varrho_d}\right)^l. \tag{7.98}$$

Now, on inserting (7.98) and (7.24) into (7.94), performing simplification with the help of [59, eq. 1.111], and further solving the integration with the aid of [59, eq. 3.471.9], we get $\Phi^{\text{N-COL}}$ as given in (7.52).

Appendix 7.D: Proof of Corollary 3

Considering high SNR (i.e., $\eta_s, \eta_r \to \infty$), we can approximate (7.51) using (7.91) for $\flat = $ N-COL, as

$$\mathcal{P}_{\text{sec},k^*,n^*}^{\text{DF}^\infty,\text{N-COL}} \simeq \sum_{M=0}^{K} \mathcal{C}_M^K \left(\frac{\alpha^{N_s}\gamma_t^{N_s}}{(N_s)!\eta_s^{N_s}}\right)^{K-M} \int_0^\infty F_{\gamma_{r_{k^*}d_{n^*}}}(\gamma_{\mathrm{s}} y + \gamma_{\mathrm{s}} - 1) f_{\gamma_{r_k E}^{\text{N-COL}}}(y) dy. \tag{7.99}$$

To solve the integration in (7.99), we require the asymptotic expressions of $F_{\gamma_{r_{k^*}d_{n^*}}}(\cdot)$ which is given as

$$F_{\gamma_{r_{k^*}d_{n^*}}}(x) \simeq \frac{1}{[\Gamma(m_d+1)]^{MN}} \left(\frac{m_d\ x}{\varrho_d}\right)^{m_d MN}. \tag{7.100}$$

Finally, on inserting (7.100) and (7.24) into (7.99), and then solving the integral with the aid of [59, eq. 3.351.3], asymptotic expression of SOP for N-COL eavesdroppers scenario under DF relaying protocol can be obtained as given in (7.56).

Appendix 7.E: Proof of Lemma 4

To solve (7.69), we first require the $\widehat{\mathcal{M}}_{\gamma_{sr}}(\mathcal{S})$ which can be obtained, using (7.21) into (7.71) and performing solution with the aid of [59, eq. 3.351.3], as

$$\widehat{\mathcal{M}}_{\gamma_{sr}}(\mathcal{S}) = \sum_{i_1=0}^{m_s-1} \cdots \sum_{i_{N_s}=0}^{m_s-1} \frac{\Xi(N_s)}{\eta_s^{\Lambda}} \sum_{p=0}^{\Lambda-1} \frac{\Gamma(\Lambda)}{p!} \beta_\delta^{-(\Lambda-p)} \Gamma(p+1) \left(\mathcal{S}+\beta_\delta\right)^{-(p+1)}. \tag{7.101}$$

Further, by using (3.87), we can simplify (7.101) as

$$\widehat{\mathcal{M}}_{\gamma_{sr}}(\mathcal{S}) = \sum_{i_1=0}^{m_s-1} \cdots \sum_{i_{N_s}=0}^{m_s-1} \frac{\Xi(N_s)}{\eta_s^{\Lambda}} \sum_{p=0}^{\Lambda-1} \frac{\Gamma(\Lambda)}{p!} \beta_\delta^{-(\Lambda+1)} G_{1,1}^{1,1}\left[\frac{\mathcal{S}}{\beta_\delta}\middle|\begin{matrix}-p\\0\end{matrix}\right]. \tag{7.102}$$

Now, to compute $\mathcal{M}_{\gamma_{rd}}(\mathcal{S})$ in (7.70), we require PDF of $\gamma_{rd} = \max_{1\leq n\leq N}\{\gamma_{rd_n}\}$, which can be calculated after applying order statistics as

$$f_{\gamma_{rd}}(x) = N\left(F_{\gamma_{rd_n}}(x)\right)^{N-1} f_{\gamma_{rd_n}}(x). \tag{7.103}$$

On inserting (7.22) and the corresponding CDF for $j_\epsilon = d_n$ with series exploration of $\Upsilon(\cdot,\cdot)$ [59, eq. 8.352.1], into (7.103), and then applying binomial [59, eq. 1.111] and multinomial [59, eq. 0.314] expansions, we obtain PDF $f_{\gamma_{rd}}(x)$ as

$$f_{\gamma_{rd}}(x) = N\sum_{\jmath=0}^{N-1}\mathcal{C}_{\jmath}^{N-1}\sum_{l=0}^{\jmath(m_d-1)}\omega_l^{\jmath}\frac{(-1)^{\jmath}}{\Gamma m_d}\left(\frac{m_d}{\varrho_d}\right)^{m_d+l} x^{m_d+l-1}\mathrm{e}^{-\frac{x}{\chi_d}}. \tag{7.104}$$

Next, using PDF $f_{\gamma_{rd}}(x)$ from (7.104) into (7.70), we can readily obtain $\mathcal{M}_{\gamma_{rd}}(\mathcal{S})$, with the help of [59, eq. 3.351.3] and (3.87), as

$$\mathcal{M}_{\gamma_{rd}}(\mathcal{S}) = N\sum_{\jmath=0}^{N-1}\mathcal{C}_{\jmath}^{N-1}\sum_{l=0}^{\jmath(m_d-1)}\omega_l^{\jmath}\frac{(-1)^{\jmath}}{\Gamma m_d}(\jmath+1)^{-(m_d+l)}\, G_{1,1}^{1,1}\left[\mathcal{S}\chi_d\middle|\begin{matrix}1-m_d+l\\0\end{matrix}\right]. \tag{7.105}$$

Finally, after inseting (7.102) and (7.105) into (7.69), and solving the integral with the use of [97, eq. 2.6.2], we obtain $\overline{C}_{\Lambda_D}$ as shown in (7.74).

Appendix 7.F: Proof of Lemma 5

To obtain $\overline{C}_{\Lambda_E^{\text{N-COL}}}$, we require to solve (7.72) for $\flat$ = N-COL. Hence, we first determine $\mathcal{M}_{\gamma_{rE}^{\text{N-COL}}}(\mathcal{S})$ which can be written as

$$\mathcal{M}_{\gamma_{rE}^{\text{N-COL}}}(\mathcal{S}) \triangleq \int_0^{\infty}\mathrm{e}^{-\mathcal{S}x} f_{\gamma_{rE}^{\text{N-COL}}}(x)dx. \tag{7.106}$$

Further, on invoking (7.24) into (7.106), performing solution of the integral with the help of [59, eq. 3.351.3], and simplifying by making use of (3.87), we get $\mathcal{M}_{\gamma_{rE}^{\text{N-COL}}}(\mathcal{S})$ as

$$\mathcal{M}_{\gamma_{rE}^{\text{N-COL}}}(\mathcal{S}) = L\sum_{r=0}^{L-1}\mathcal{C}_r^{L-1}\sum_{s=0}^{r(m_e-1)}\omega_s^r\frac{(-1)^r}{\Gamma m_e}\left(\frac{m_e}{\varrho_e}\right)^{m_e+s}\chi_e^{m_e+s} G_{1,1}^{1,1}\left[\mathcal{S}\chi_e\middle|\begin{matrix}1-m_e+s\\0\end{matrix}\right]. \tag{7.107}$$

Then, after plugging (7.102) and (7.107) into (7.72) for $\flat$ = N-COL, and solving the integral using [97, eq. 2.6.2], one can reach to (7.75).

CHAPTER 8

CONCLUSIONS AND FUTURE WORKS

This chapter concludes the main contributions and insights of this thesis and provides some possible research directions for future works.

8.1 Conclusions

This thesis presented a comprehensive performance analysis of hybrid satellite-terrestrial architectures as well as discussed the practical design challenges for the deployment of future networks. Firstly, we investigated the performance of basic LMS systems in a shadowed-Rician fading channel environment. We examined PLS performance of a LMS system, where a satellite transmits signal to an interference-limited legitimate user in the presence of an eavesdropper. By considering multiple CCI signals under Nakagami-m fading at the user destination node, we derived analytical and asymptotic expressions of SOP for the considered system. We revealed the system diversity order and illustrated that it remains unaffected of the number of interferers. We further explored the secrecy performance of a LMS system with a legitimate user and an eavesdropper by employing a UAV-based friendly jammer. For this analytical framework, we derived exact and asymptotic expressions of the SOP under pertinent heterogeneous channels for the satellite links and the air-to-ground jammer. Our results depicted that while the satellite channel conditions have severe impact on the LMS system performance, the UAV jammer can notably improve the secrecy performance.

We further investigated the performance of a multi-user HSTRN employing opportunistic user scheduling. In this system design, we studied the joint impact of outdated CSI and CCI by taking uncorrelated and correlated shadowed-Rician fading channels into account. Specifically, we developed unified analytical frameworks for the assessment of OP, EC and average SEP performance by adopting Nakagami-m fading for the terrestrial links. We further perform the asymptotic analysis at high SNR regime to reveal the diversity order of the considered system. Moreover, we emphasized the advantages of a multi-antenna satellite and highlighted that the antenna correlation does not affect the achievable diversity order. Our study also showed that the considered system can achieve full diversity as long as the interference power level remains low. We moreover pointed out the detrimental effect of the channel imperfection and CCI on the system performance and eventually provided useful insights for designing the practical systems.

Then, we focused on the PLS performance analysis of the HSTRNs. Initially, we investigated the secrecy performance of HSTRNs with single-eavesdropper scenario. Here, we first analyzed the secrecy performance of a multi-user HSTRN in the presence of an eavesdropper and derived analytical SOP expression by employing opportunistic scheduling of terrestrial users. Further, we performed asymptotic SOP analysis to reveal the achievable diversity order of the considered system. Thereafter, we considered a multi-relay HSTRN with a single eavesdropper. We proposed the optimal and partial relay selection schemes and derived analytical and asymptotic expressions for SOP by considering shadowed-Rician fading for satellite links and Nakagami-m fading for terrestrial links. Specifically, we herein revealed that an increase in the number of either terrestrial users or relays plays an important role in improving the HSTRNs performance. Also, we demonstrated that how a single eavesdropper can severely degrade the system secrecy performance.

Next, we concentrated on the case of multiple eavesdroppers with a multi-antenna satellite in the context of HSTRNs. According to eavesdroppers' colluding capability, we have considered two specific scenarios of eavesdropping i.e., COL and N-COL eavesdroppers. We first investigated the secrecy performance of an HSTRN in the presence of multiple COL eavesdroppers. We derived analytical and asymptotic expressions for the system SOP and revealed the achievable diversity order of the considered system. We further derived the ESC expression for the proposed system. We depicted that the multiple eavesdroppers have no role in deciding the diversity of system, however, they severely hinder the performance gain of the system. Further, we investigated the secrecy performance of a multi-user multi-relay HSTRN in the presence of multiple eavesdroppers. Herein, by considering both COL and N-COL eavesdropping scenarios, we conducted a comprehensive secrecy performance analysis under AF and DF relaying protocols. We proposed opportunistic user-relay selection criteria and derived novel and accurate expressions of the SOP by adopting shadowed-Rician fading for satellite links and Nakagami-m fading for terrestrial links. We also examined the asymptotic outage behavior to highlight further insights into the achievable diversity gain of the considered system. We emphasized that the proposed scheme can attain performance gain by exploiting not only the cooperative diversity but also the multi-user diversity. In addition, we carried out the ESC performance analysis of an HSTRN considering a single AF relay, multiple users, and multiple eavesdroppers. Our results showed that system diversity gain remains unaffected by the method of relaying protocol and type of eavesdropping. More importantly, we illustrated that the COL eavesdroppers are more hazardous to the system performance than N-COL eavesdroppers.

In essence, we have comprehensively investigated the performance of HSTNs to offer various useful design insights which may facilitate the deployment of HSTNs in the future wireless systems.

8.2 Future Works

With emerging 5G communication, there are many open problems related to the topics of this thesis that could be treated in future research. The HSTN configurations and PLS technique can be further promoted with emerging concepts such as spectral-efficient cognitive communication, non-orthogonal multiple access (NOMA), and energy harvesting (EH) techniques. Some future directions for the research work are indicated below in the sequel.

In wireless communication, spectrum scarcity has become a major concern due to the ever increasing data traffic. Cognitive radio has emerged as a promising candidate to improve the radio spectrum utilization. It is of great interest to integrate spectrum sharing technique into hybrid satellite-terrestrial systems.

In addition, NOMA has also been recently regarded as one of the most promising technologies in 5G, which basically utilizes the power domain to serve multiple users simultaneously and hence provide high spectral efficiency. The incorporation of NOMA capabilities with the heterogeneous architecture of HSTNs for a high spectral-efficient system design would be a challenging research interest in near future.

On the other hand, energy consumption of the wireless networks is rapidly rising day-by-day. The energy efficient systems are one of the important aspects to be considered in future wireless networks. To this end, various EH technologies have been pointed out as an effective solution to improve the energy efficiency. In future, how the EH technologies can be utilized in HSTN will be a topic worthy of in-depth study.

Moreover, it would be challenging to analyze the impact of hardware impairments in hybrid satellite-terrestrial systems which arise due to employment of low cost radio frequency transceiver.

Besides, heterogeneous networks, PLS, millimeter wave (mmWave), and massive MIMO are recognized as the key 5G and B5G technologies. In this thesis, the first two are slightly discussed in the context of HSTNs. The combination of mmWave and massive MIMO with the HSTNs have potential to further enhance the QoS and reliability of wireless networks. This can also be taken as a future research interest.

Furthermore, in this thesis work, the impact of friendly jamming was analyzed for the LMS systems. Since various jamming techniques have been proved as an effective way to improve the system secrecy performance, one can also perform this investigation for the HSTRNs.

With aforementioned future research prospects, one can further expand the existing design acquaintance of HSTNs for next generation wireless standards.

REFERENCES

[1] ETSI EN 102 585 V1.1.2, "Digital Video Broadcasting (DVB): System specifications for Satellite services to Handheld devices (SH) below 3 GHz," Apr. 2008.

[2] `https://www.3gpp.org/news-events/1933-sat_ntn`

[3] P. Chini, G. Giambene, and S. Kota, "A survey on mobile satellite systems," *Int. J. Sat. Commun.*, vol. 28, no. 1, pp. 29-57, Aug. 2009.

[4] E. Lutz, D. Cygan, M. Dippold, F. Dolainsky, and W. Papke, "The land mobile satellite communication channel-Recording, statistics, and channel model," *IEEE Trans. Veh. Technol.*, vol. 40, pp. 375-386, May 1991.

[5] B. Paillassa, B. Escrig, R. Dhaou, M.-L. Boucheret, and C. Bes, "Improving satellite services with cooperative communications," *Int. J. Sat. Commun.*, vol. 29, no. 6, pp. 479-500, Oct. 2011.

[6] V. Sakarellos, C. Kourogiorgas, and A. Panagopoulos, "Cooperative hybrid land mobile satellite-terrestrial broadcasting systems: Outage probability evaluation and accurate simulation," *Wireless Personal Commun.*, vol. 79, no. 2, pp. 1471-1481, Nov. 2014.

[7] B. Evans, M. Werner, E. Lutz, M. Bousquet, G. Corazza, G. Maral, and R. Rumeau, "Integration of satellite and terrestrial systems in future media

communications," *IEEE Trans. Wireless Commun.*, vol. 12, no. 5, pp. 72-80, Oct. 2005.

[8] A. Sendonaris, E. Erkip, and B. Aazhang, "User cooperation diversity-part I: System description," *IEEE Trans. Commun.*, vol. 51, no. 11, pp. 1927-1938, Nov. 2003.

[9] T. Cover and A. E. Gamal, "Capacity theorems for the relay channel," *IEEE Trans. Inf. Theory*, vol. 25, no. 5, pp. 572-584, Sep. 1979.

[10] J. N. Laneman, D. N. C. Tse, and G. W.Wornell, "Cooperative diversity in wireless networks: Efficient protocols and outage behavior," *IEEE Trans. Inf. Theory*, vol. 50, no. 12, pp. 3062-3080, Dec. 2004.

[11] A. Nosratinia, T. E. Hunter, and A. Hedayat, "Cooperative communications in wireless networks," *IEEE Commun. Mag.*, vol. 42, no. 10, pp. 74-80, Oct. 2004.

[12] J. Hussein, S. Ikki, S. Boussakta, and C. Tsimenidis, "Performance analysis of opportunistic scheduling in dual-hop multi-user underlay cognitive network in the presence of co-channel interference," *IEEE Trans. Veh. Technol.*, vol. 65, no. 10, pp. 8163-8176, Oct. 2016.

[13] J. H. Winters, "Optimum combining in digital mobile radio with co-channel interference," *IEEE Trans. Veh. Technol.*, vol. 33, no. 3, pp. 144-155, Aug. 1984.

[14] A. Goldsmith, "Wireless Communications," 1st ed. New York, NY: Cambridge University Press, 2005.

[15] M. K. Simon and M. S. Alouini, "Digital Communication over Fading Channels: A Unified Approach to Performance Analysis," John Wiley & Sons, Inc., 2000.

[16] A. Abdi, W. Lau, M.-S. Alouini, and M. Kaveh, "A new simple model for land mobile satellite channels: First and second order statistics," *IEEE Trans. Wireless Commun.*, vol. 2, no. 3, pp. 519-528, May 2003.

[17] J. G. Andrews et al., "What will 5G be?," *IEEE J. Sel. Areas Commun.*, vol. 32, no. 6, pp. 1065-1082, Jun. 2014.

[18] M. R. Bhatnagar and Arti M. K., "Performance analysis of AF based hybrid satellite-terrestrial cooperative network over generalized fading channels," *IEEE Commun. Lett.*, vol. 17, no. 10, pp. 1912-1915, Oct. 2013.

[19] Arti M. K., "Imperfect CSI based AF relaying in hybrid satellite-terrestrial cooperative communication systems," in *Proc. IEEE Int. Conf. Commun. Workshop*, London, U.K., pp. 1681-1686, Jun. 2015.

[20] M. R. Bhatnagar and Arti M. K., "Performance analysis of hybrid satellite-terrestrial FSO cooperative system, " *IEEE Photon. Technol. Lett.*, vol. 25, no. 22, pp. 2197-2200, Nov. 2013.

[21] U. Javed, D. He, and P. Liu, "Performance characterization of a hybrid satellite-terrestrial system with co-channel interference over generalized fading channels," *Sensors*, 16(8):1236, 2016.

[22] M. Lin, J. Ouyang, and W.-P. Zhu, "On the performance of hybrid satellite-terrestrial cooperative networks with interferences," in *Proc. 48th Asilomar Conf. on Signals, Systems and Computers (ACSSC)*, Pacific Grove, California, Nov. 2014, pp. 1796-1800.

[23] L. Yang and M. O. Hasna, "Performance analysis of amplify-and-forward hybrid satellite-terrestrial networks with cochannel interference," *IEEE Trans. Commun.*, vol. 63, no. 12, pp. 5052-5061, Dec. 2015.

[24] S. Sreng, B. Escrig, and M.-L. Boucheret, "Exact symbol error probability of hybrid/integrated satellite-terrestrial cooperative network," *IEEE Trans. Wireless Commun.*, vol. 12, no. 3, pp. 1310-1319, Mar. 2013.

[25] K. An, J. Ouyang, M. Lin, and T. Liang, "Outage analysis of multi-antenna cognitive hybrid satellite-terrestrial relay networks with beamforming," *IEEE Commun. Lett.*, vol. 19, no. 7, pp. 1157-1160, Jul. 2015.

[26] K. An, M. Lin, J. Ouyang, Y. Huang, and G. Zheng, "Symbol error analysis of hybrid satellite-terrestrial cooperative networks with co-channel interference," *IEEE Commun. Lett.*, vol. 18, no. 11, pp. 1947-1950, Nov. 2014.

[27] K. T. Hemachandra and N. C. Beaulieu, "Outage analysis of opportunistic scheduling in dual-hop multiuser relay networks in the presence of interference," *IEEE Trans. Commun.*, vol. 61, no. 5, pp. 1786-1796, May 2013.

[28] L. Erwu, W. Dongyao, L. Jimin, S. Gang, and J. Shan, "Performance evaluation of bandwidth allocation in 802.16j mobile multi-hop relay networks," in *Proc. IEEE VTC-Spring*, Dublin, Ireland, Apr. 2007, pp. 939-943.

[29] K. An, M. Lin, and T. Liang, "On the performance of multiuser hybrid satellite-terrestrial relay networks with opportunistic scheduling," *IEEE Commun. Lett.*, vol. 19, no. 10, pp. 1722-1725, Oct. 2015.

[30] P. K. Upadhyay and P. K. Sharma, "Max-max user-relay selection scheme in multiuser and multirelay hybrid satellite-terrestrial relay systems," *IEEE Commun. Lett.*, vol. 20, no. 2, pp. 268-271, Feb. 2016.

[31] M. R. Bhatnagar, "Performance evaluation of decode-and-forward satellite relaying," *IEEE Trans. Veh. Technol.*, vol. 64, no. 10, pp. 4827-4833, Oct. 2015.

[32] N. Sklavos and X. Zhang, *Wireless Security and Cryptography: Specifications and Implementations*, 1st ed. Baco Raton, FL, USA: CRC Press, 2007.

[33] H. Cruickshank, M. Howarth, S. Iyengar, Z. Sun, and L. Claverotte, "Securing multicast in DVB-RCS satellite systems," *IEEE Wireless Commun.*, vol. 12, no. 5, pp. 38-45, Oct. 2005.

[34] V. K. Sakarellos and A. D. Panagopoulos, "Outage performance of cooperative land mobile satellite broadcasting systems," in Proc. *European Conf. on Antennas and Propagation (EuCAP)*, Gothenburg, Sweden, Apr. 2013.

[35] B. Awoyemi, T. Walingo, and F. Takawira, "Relay selection cooperative diversity in land mobile satellite systems," *2013 Africon*, Pointe-Aux-Piments, Mauritius, Sep. 2013.

[36] Arti M. K., "Performance evaluation of maximal ratio combining in shadowed-Rician fading land mobile satellite channels with estimated channel gains," *IET Commun.*, vol. 9, no. 16, pp. 2013-2022, Jul. 2015.

[37] G. Cocco, N. Alagha, and C. Ibars, "Cooperative coverage extension in vehicular land mobile satellite networks," *IEEE Trans. Veh. Technol.*, vol. 65, no. 8, pp. 5995-6009, Aug. 2016.

[38] Arti M. K. and S. K. Jindal, "OSTBC transmission in shadowed-Rician land mobile satellite links," *IEEE Trans. Veh. Technol.*, vol. 65, no. 7, pp. 5771-5777, July 2016.

[39] K. An , T. Liang , X. Yan , Y. Li, and X. Qiao, "Power allocation in land mobile satellite systems: An energy-efficient perspective," *IEEE Commun. Lett.*, vol. 22, no. 7, pp. 1374-1377, Jul. 2018.

[40] X. Yan H. Xiao, C.-X. Wang, K. An, A. T. Chronopoulos, and G. Zheng, "Performance analysis of NOMA-based land mobile satellite networks," *IEEE Access*, vol. 6, no. 1, pp. 31327-31339, Jun. 2018.

[41] M. Abo-zeed, J. B. Din, I. Shayea, and M. Ergen, "Survey on land mobile satellite system: Challenges and future research trends," *IEEE Access*, vol. 7, no. 1, pp. 137291-137304, Oct. 2019.

[42] A. D. Wyner, "The wire-tap channel," *Bell Syst. Technol. J.*, vol. 54, no. 8, pp. 1355-1387, Oct. 1975.

[43] J. Lei, Z. Han, M. A. V.-Castro, and A. Hjorungnes, "Secure satellite communication systems design with individual secrecy rate constraints," *IEEE Trans. Inf. Forens. Security*, vol. 6, no. 3, pp. 661-671, Sep. 2011.

[44] K. Guo, B. Zhang, Y. Huang, and D. Guo, "Secure performance analysis of satellite communication networks in shadowed-Rician channel," in *Proc. IEEE Int. Symp. Signal Processing and Inf. Tech. (ISSPIT)*, Limassol, Cyprus, Dec. 2016.

[45] D. K. Petraki, M. P. Anastasopoulos, and S. Papavassiliou, "Secrecy capacity for satellite networks under rain fading," *IEEE Trans. Depend. Secu. Comp.*, vol. 8, no. 5, pp. 777-782, Sep. 2011.

[46] G. Zheng, P. D. Arapoglou, and B. Ottersten, "Physical layer security in multibeam satellite systems," *IEEE Trans. Wireless Commun.*, vol. 11, no. 2, pp. 852-863, Feb. 2012.

[47] K. An, M. Lin, T. Liang, J. Ouyang, C. Yuan, and W. Lu, "Secrecy performance analysis of land mobile satellite communication systems over shadowed-Rician fading channels," in *Proc. 25th Wireless and Optical Commun. Conf. (WOCC)*, Chengdu, China, May 2016.

[48] K. An, M. Lin, T. Liang, J. Ouyang, and H. Chen, "Average secrecy capacity of land mobile satellite wiretap channels," in *Proc. Wireless Commun. and Signal Processing (WCSP)*, Yangzhou, China, Oct. 2016.

[49] K. An, T. Liang, X. Yan, and G. Zheng, "On the secrecy performance of land mobile satellite communication systems,", *IEEE Access*, vol. 6, no. 1, pp. 39606-39620, Jul. 2018.

[50] L. Yang and M. O. Hasna, "Performance analysis of amplify-and-forward hybrid satellite-terrestrial networks with cochannel interference," *IEEE Trans. Commun.*, vol. 63, no. 12, pp. 5052-5061, Dec. 2015.

[51] L. Dong, Z. Han, A. P. Petropulu, and H. V. Poor, "Improving wireless physical layer security via cooperating relays," *IEEE Trans. Signal Process.*, vol. 58, no. 3, pp. 1875-1888, Mar. 2010.

[52] B. Li, Y. Zou, J. Zhou, F. Wang, W. Cao, and Y. D. Yao, "Secrecy outage probability analysis of friendly jammer selection aided multiuser scheduling

for wireless networks," *IEEE Trans. Commun.*, vol. 65, no. 5, pp. 3482-3495, May 2019.

[53] S. Xu *et al.* "Improving secrecy for correlated main and wiretap channels using cooperative jamming," *IEEE Access*, vol. 7, no. 1, pp. 23788-23797 Feb. 2015.

[54] G. Zheng, I. Krikidis, J. Li, A. P. Petropulu, and B. Ottersten, "Improving physical layer secrecy using full-duplex jamming receivers," *IEEE Trans. Signal Process.*, vol. 61, no. 20, pp. 4962-4974 Oct. 2013.

[55] B. Vucetic, "Propagation," in *Satellite Communications-Mobile and Fixed Services,* M. J. Miller, B. Vucetic, and L. Berry, Eds. Boston, MA: Kluwer, pp. 57-101, 1993.

[56] C. Loo, "A statistical model for a land mobile satellite link," *IEEE Trans. Veh. Technol.*, vol. 34, no.3, pp. 122-127, Aug. 1985.

[57] A. Abdi, H. Allen Barger, and M. Kaveh, "A simple alternative to the log-normal model of shadow fading in terrestrial and satellite channels," in *Proc. IEEE Veh. Technol. Conf. (VTC)*, Atlantic City, NJ, pp. 2058-2062, 2001,

[58] N. I. Miridakis, D. D. Vergados, and A. Michalas, "Dual-hop communication over a satellite relay and shadowed-Rician channels," *IEEE Trans. Veh. Technol.*, vol. 64, no. 9, pp. 4031-4040, Sep. 2015.

[59] I. S. Gradshteyn and I. M. Ryzhik, *Tables of Integrals, Series and Products*, 6th ed. New York: Academic Press, 2000.

[60] G. Alfano and A. De Maio, "Sum of squared shadowed-Rice random variables and its application to communication systems performance prediction," *IEEE Trans. Wireless Commun.*, vol. 6, no. 10, pp. 3540-3545, Oct. 2007.

[61] M. Bloch, J. O. Barros, M. R. D. Rodrigues, and S. W. McLaughlin, "Wireless information-theoretic security," *IEEE Trans. Inf. Theory*, vol. 54, no. 6, pp. 2515-2534, Jun. 2008.

[62] C. E. Shannon, "Communication theory of secrecy systems," *Bell Syst. Technol. J.*, vol. 28, pp. 656-715, Oct. 1949.

[63] I. Csiszàr and J. Körner, "Broadcast channels with confidential messages," *IEEE Trans. Inf. Theory*, vol. 24, no. 3, pp. 339-348, May 1978.

[64] J. Barros and M. R. D. Rodrigues, "Secrecy capacity of wireless channels," in *Proc. 2006 IEEE International Symposium on Information Theory*, Seattle, WA, USA, Jul. 2006.

[65] P. Gopala, L. Lai, and H. El Gamal, "On the secrecy capacity of fading channels," *IEEE Trans. Inf. Theory*, vol. 54, no. 10, pp. 4687-4698, Oct. 2008.

[66] D. B. da Costa, H. Ding, and J. Ge, "Interference-limited relaying transmissions in dual-hop cooperative networks over Nakagami-m fading," *IEEE Commun. Lett.*, vol. 15, no. 5, pp. 503-505, May 2011.

[67] J. C. S. Santos Filho and M. D. Yacoub, "Nakagami-m approximation to the sum of M non-identical independent Nakagami-m variates," *Electron. Lett.*, vol. 40, no. 15, pp. 951-952, July 2004.

[68] Y. Zeng, R. Zhang, and T. J. Lim, "Wireless communications with unmanned aerial vehicles: Opportunities and challenges," *IEEE Commun. Mag.*, vol. 54, no. 5, pp. 36-42, May 2016.

[69] Y. Wang, Y. Xu, Y. Zhang, and P. Zhang, "Hybrid satellite-aerial-terrestrial networks in emergency scenarios: A survey," *China Commun.*, vol. 14, no. 7, pp. 1-13, July 2017.

[70] J. Zhao, F. Gao, Q. Wu, S. Jin, Y. Wu, and W. Jia, "Beam tracking for UAV mounted SatCom on-the-move with massive antenna array," *IEEE J. Sel. Areas Commun.*, vol. 36, no. 2, pp. 363-375, Feb. 2018.

[71] M. Erdelj, E. Natalizio, K. R. Chowdhury, and I. F. Akyildiz, "Help from the sky: Leveraging UAVs for disaster management," *IEEE Pervasive Comput.*, vol. 16, no. 1, pp. 24-32, Jan. 2017.

[72] X. Li, H. Yao, J. Wang, X. Xu, C. Jiang, and L. Hanzo, "A near-optimal UAV-aided radio coverage strategy for dense urban areas," *IEEE Trans. Veh. Technol.*, vol. 68, no. 9, pp. 9098-9109, Sep. 2019.

[73] A. Al-Hourani, S. Kandeepan, and S. Lardner, "Optimal LAP altitude for maximum coverage," *IEEE Wireless Commun. Letters*, vol. 3, no. 6, pp. 569-572, Dec. 2014.

[74] P. Arapoglou, K. Liolis, M. Bertinelli, A. Panagopoulos, P. Cottis, and R. De Gaudenzi, "MIMO over satellite: A review," *IEEE Commun. Surveys Tuts.*, vol. 13, no. 1, pp. 27-51, Feb. 2011.

[75] K. P. Liolis, A. D. Panagopoulos, and P. G. Cottis, "Multi-satellite MIMO communications at Ku-band and above: Investigations on spatial multiplexing for capacity improvement and selection diversity for interference mitigation," *EURASIP J. Wireless Commun. Netw.*, Jun. 2007.

[76] P. Petropoulou, E. T. Michailidis, A. D. Panagopoulos, and A. G. Kanatas, "Radio propagation channel measurements for multi-antenna satellite communication systems: A survey," *IEEE Antennas and Propagation Magazine*, vol. 56, no. 6, pp. 102-122, Dec. 2014.

[77] Y. Dhungana, N. Rajatheva, and C. Tellambura, "Performance analysis of antenna correlation on LMS-based dual-hop AF MIMO systems," *IEEE Trans. Veh. Technol.*, vol. 61, no. 8, pp. 3590-3602, Oct. 2012.

[78] Y. Dhungana and N. Rajatheva, "Analysis of LMS based dual hop MIMO systems with beamforming," in *Proc. IEEE Int. Conf. Commun. (ICC)*, Kyoto, Japan, June 2011, pp. 1-6.

[79] S. Gong, D. Wei, X. Xue, and M. Chen, "Study on the channel model and BER performance of single-polarization satellite-earth MIMO communication systems at Ka band," *IEEE Trans. Antennas and Propagation*, vol. 62, no. 10, pp. 5282-5297, Oct. 2014.

[80] K. An, M. Lin, T. Liang, J.-B. Wang, J. Wang, Y. Huang, and A. L. Swindlehurst, "Performance analysis of multi-antenna hybrid satellite-terrestrial relay networks in the presence of interference," *IEEE Trans. Commun.*, vol. 63, no. 11, pp. 4390-4404, Nov. 2015.

[81] X. Artiga, J. Núñez-Martínez, A. Pérez-Neira, G. J. L. Vela, J. M. F. Garcia, and G. Ziaragkas, "Terrestrial-satellite integration in dynamic 5G backhaul networks," in *Proc. 8th Advanced Satellite Multimedia Sys. Conf. and 14th Sig. Proc. Space Commun. Workshop (ASMS/SPSC)*, Palma de Mallorca, Spain, Sep. 2016.

[82] Y. Ruan, Y. Li, C.-X. Wang, R. Zhang, and H. Zhang, "Outage performance of integrated satellite-terrestrial networks with hybrid CCI," *IEEE Commun. Lett.*, vol. 21, no. 7, pp. 1545-1548, Jul. 2017.

[83] P. K. Sharma, P. K. Upadhyay, D. B. da Costa, P. S. Bithas, and A. G. Kanatas, "Overlay spectrum sharing in hybrid satellite-terrestrial systems with secondary network selection," *IEEE Trans. Wireless Commun.*, vol. 16, no. 10, pp. 6586-6601, Oct. 2017.

[84] H. A. Suraweera, H. K. Garg, and A. Nallanathan "Performance analysis of two hop amplify-and-forward systems with interference at the relay," *IEEE Commun. Lett.*, vol. 14, no. 8, pp. 692-694, Aug. 2010.

[85] M. K. Simon and M.-S. Alouini, *Digital Communications over Fading Channels: A Unified Approach to Performance Analysis.* Wiley, 2000.

[86] M. Li, M. Lin, W.-P. Zhu, Y. Huang, A. Nallanathan, and Q. Yu, "Performance analysis of MIMO MRC systems with feedback delay and channel estimation error," *IEEE Trans. Veh. Technol.*, vol. 65, no. 2, pp. 707-717, Feb. 2016.

[87] J. Tang and X. Zhang "Transmit selection diversity with maximal-ratio combining for multicarrier DS-CDMA wireless networks over Nakagami-m fading

channels," *IEEE J. Sel. Areas Commun.*, vol. 24, no. 1, pp. 104-112, Jan. 2006.

[88] D. B. da Costa and M. D. Yacoub, "Outage performance of two hop AF relaying systems with co-channel interferers over Nakagami-m fading," *IEEE Commun. Lett.*, vol. 15, no. 9, pp. 980-982, Sep 2011.

[89] M. O. Hasna and M-S. Alouini, "A performance study of dual-hop transmissions with fixed gain relays," *IEEE Trans. Wireless Commun.*, vol. 3, no. 6, pp. 1963-1968, Nov. 2014.

[90] I. Trigui, S. Affes, and A. Stephenne, "Ergodic capacity of two-hop multiple antenna AF systems with co-channel interference," *IEEE Wireless Commun. Lett.*, vol. 4, no. 1, pp. 26-29, Feb. 2015.

[91] R. P. Agrawal, "On certain transformation formulae and Meijer's G-function of two variables," *Indian J. Pure Appl. Math.*, vol. 1, no. 4, 1970.

[92] I. S. Ansari, S. Al-Ahmadi, F. Yilmaz, M.-S. Alouini, and H. Yanikomeroglu, "A new formula for the BER of binary modulations with dual-branch selection over generalized-K composite fading channels," *IEEE Trans. Commun.*, vol. 59, no. 10, pp. 2654-2658, Oct. 2011.

[93] K. A. Hamdi, "Capacity of MRC on correlated Rician fading channels," *IEEE Trans. Commun.*, vol. 56, no. 5, pp. 708-711, May 2008.

[94] R. U. Verma, "On some integrals involving Meijer's G-function of two variables," *Proc. Nat. Inst. Sci. India*, vol. 32, A, nos. 5 & 6, pp. 509-515, Jan. 1966.

[95] P. A. Anghel and M. Kaveh, "Exact symbol error probability of a cooperative network in a Rayleigh-fading environment," *IEEE Trans. Wireless Commun.*, vol. 3, no. 5, pp. 1416-1421, Sep. 2004.

[96] V. S. Adamchik and O. I. Marichev, "The algorithm for calculating integrals of hypergeometric type functions and its realization in reduce system," in *Proc.*

Int. Symp. Symbolic and Algebraic Computation (ISSAC), Tokyo, Japan, Aug. 1990, pp. 212-224.

[97] A. M. Mathai and R. K. Saxena, *The H-function with Applications in Statistics and Other Disciplines*. Wiley Eastern, 1978.

[98] K. An, M. Lin, T. Liang, J. Ouyang, C. Yuan, and Y. Li, "Secure transmission in multi-antenna hybrid satellite-terrestrial relay networks in the presence of eavesdropper," in *Proc. Int. Conf. Wireless Commun. and Signal Processing (WCSP)*, Nanjing, China, Oct. 2015.

[99] Q. Huang, M. Lin, K. An, J. Ouyang, and W.-P. Zhu, "Secrecy performance of hybrid satellite-terrestrial relay networks in the presence of multiple eavesdroppers," *IET Commun.*, vol. 12, no. 1, pp. 26-34, Jan. 2018.

[100] K. An, M. Lin, J. Ouyang, and W.-P. Zhu, "Secure transmission in cognitive satellite-terrestrial networks," *IEEE J. Sel. Areas Commun.*, vol. 34, no. 11, pp. 3025-3037, Nov. 2016.

[101] B. Li, Z. Fei, Z. Chu, F. Zhou, K.-K. Wong, and P. Xiao, "Robust chance-constrained secure transmission for cognitive satellite-terrestrial networks," *IEEE Trans. Veh. Technol.*, vol. 67, no. 5, pp. 4208-4219, May 2018.

[102] H. Jeon, N. Kim, J. Choi, H. Lee, and J. Ha, "Bounds on secrecy capacity over correlated ergodic fading channels at high SNR," *IEEE Trans. Inf. Theory*, vol. 57, no. 4, pp. 1975-1983, Apr. 2011.

[103] I. Krikidis, J. S. Thompson, and S. McLaughlin, "Relay selection for secure cooperative networks with jamming," *IEEE Trans. Wireless Commun.*, vol. 8, no. 10, pp. 5003-5011, Oct. 2009.

[104] A. Bletsas, A. Khisti, D. P. Reed, and A. Lippman, "A simple cooperative diversity method based on network path selection," *IEEE J. Sel. Areas Commun.*, vol. 24, no. 3, pp. 659–672, Mar. 2006.

[105] J. Li, A. Petropulu, and S. Weber, "On cooperative relaying schemes for wireless physical layer security," *IEEE Trans. Signal Process.*, vol. 59, no. 10, pp. 4985-4997, Oct. 2011.

[106] W. Cao, Y. Zou, Z. Yang, and J. Zhu, "Secrecy outage probability of hybrid satellite-terrestrial relay networks," in *Proc. IEEE Global Commun. Conf. (GLOBECOM 2017)*, Singapore, Dec. 2017.

[107] W. Cao, Y. Zou, Z. Yang, and J. Zhu, "Relay selection for improving physical-layer security in hybrid satellite-terrestrial relay networks," *IEEE Access*, vol. 6, no. 1, pp. 65275-65285, Oct. 2018.

[108] C. Chen and L. Song, "Secure communications in hybrid cooperative satellite-terrestrial networks," in *Proc. IEEE 87th Veh. Technol. Conf. (VTC)*, Porto, Portugal, Portugal, Jul. 2018.

[109] L. Fan, X. Lei, T. Q. Duong, M. Elkashlan, and G. K. Karagiannidis, "Secure multiuser communications in multiple amplify-and-forward relay networks," *IEEE Trans. Commun.*, vol. 62, no. 9, pp. 3299-3310, Jan. 2013.

[110] W. Liu, Z. Ding, T. Ratnarajah, and J. Xue, "On ergodic secrecy capacity of random wireless networks with protected zones," *IEEE Trans. Veh. Technol.*, vol. 65, no. 8, pp. 6146-6158, Aug. 2016.

[111] I. Trigui, S. Affes, and A. Stéphenne, "Ergodic capacity of two-hop multiple antenna AF systems with co-channel interference," *IEEE Wireless Commun. Lett.*, vol. 4, no. 1, pp. 26-29, Feb. 2015.

[112] A. Bletsas, H. Shin, and M. Z. Win, "Cooperative communications with outage-optimal opportunistic relaying," *IEEE Trans. Wireless Commun.*, vol. 6, no. 9, pp. 3450-3460, Sep. 2007.

[113] Y. Huang, F. S. Al-Qahtani, T. Q. Duong, and J. Wang, "Secure transmission in MIMO wiretap channels using general-order transmit antenna selection with outdated CSI," *IEEE Trans. Commun.*, vol. 63, no. 8, pp. 2959-2971, Aug. 2015.

[114] Y. Huang, P. Zhang, Q. Wu, and J. Wang, "Secrecy performance of wireless powered communication networks with multiple eavesdroppers and outdated CSI," *IEEE Access*, vol. 6, no. 1, pp. 33774-33788, Jul. 2018.

[115] L. Fan, X. Lei, T. Q. Duong, M. Elkashlan, and G. K. Karagiannidis, "Secure multiuser multiple amplify-and-forward relay networks in presence of multiple eavesdroppers," in *Proc. IEEE Global Commun. Conf. (GLOBECOM)* Austin, TX, USA, 2014.

[116] Y.-U. Jang and Y. H. Lee, "Performance analysis of user selection for multiuser two-way amplify-and-forward relay," *IEEE Commun. Lett.*, vol. 14, no. 11, pp. 1086-1088, Nov. 2010.

[117] M. Yang, D. Guo, Y. Huang, T. Q. Duong, and B. Zhang, "Secure multiuser scheduling in downlink dual-hop regenerative relay networks over Nakagami-m fading channels," *IEEE Trans. Wireless Commun.*, vol. 15, no. 12, pp. 8009-8024, Dec. 2016.

[118] Y. Yang, Q. Li, W.-K. Ma, J. Ge, and P. C. Ching, "Cooperative secure beamforming for AF relay networks with multiple eavesdroppers," *IEEE Signal Process. Lett.*, vol. 20, no. 1, pp. 35-38, Jan. 2013.

[119] M.-S. Alouini and M. K. Simon, "Performance of coherent receivers with hybrid SC/MRC over Nakagami-m fading channels," *IEEE Trans. Veh. Technol.*, vol. 48, no. 4, pp. 1155-1164, Jul. 1999.

[120] T. M. Hoang, T. Q. Duong, H. A. Suraweera, C. Tellambura, and H. V. Poor, "Cooperative beamforming and user selection for improving the security of relay-aided systems," *IEEE Trans. Commun.*, vol. 63, no. 12, pp. 5039-5050, Dec. 2015.

List of Publications

In Refereed Journals

1. **V. Bankey** and P. K. Upadhyay, "Physical layer security of hybrid satellite-terrestrial relay networks with multiple colluding eavesdroppers over non-identically distributed Nakagami-m fading channels," ***IET Communications***, vol. 13, no. 14, pp. 2115-2123, Aug. 2019.

2. **V. Bankey** and P. K. Upadhyay, "Physical layer security of multiuser multirelay hybrid satellite-terrestrial relay networks," ***IEEE Transactions on Vehicular Technology***, vol. 68, no. 3, pp. 2488-2501, Mar. 2019.

3. **V. Bankey** and P. K. Upadhyay, "Physical layer secrecy performance analysis of multi-user hybrid satellite-terrestrial relay networks," ***CSI Transactions on ICT***, vol. 6, no. 2, pp. 187-193, Jun. 2018.

4. **V. Bankey**, P. K. Upadhyay, D. B. da Costa, P. S. Bithas, A. G. Kanatas, and U. S. Dias, "Performance analysis of multi-antenna multiuser hybrid satellite-terrestrial relay systems for mobile services delivery," ***IEEE Access***, vol. 6, no. 1, pp. 24729-24745, Apr. 2018.

5. **V. Bankey** and P. K. Upadhyay, "Ergodic capacity of multiuser hybrid satellite-terrestrial fixed-gain AF relay networks with CCI and outdated CSI," ***IEEE Transactions on Vehicular Technology***, vol. 67, no. 5, pp. 4666-4671, May. 2018.

In Refereed Conferences

1. **V. Bankey** and P. K. Upadhyay, "Improving secrecy performance of land mobile satellite systems via a UAV friendly jammer," in Proc. ***IEEE Consumer Communications and Networking Workshop (CCNC Workshop): Unmanned Aerial Vehicle (UAV'20) Communications and Networks***, Las Vegas, United States, Jan. 2020.

2. **V. Bankey** and P. K. Upadhyay, "Average symbol error probability of interference-limited multiuser hybrid satellite-terrestrial relay networks with outdated channel state information," in Proc. ***IEEE Region 10 International Conference (TENCON)***, Kochi, Kerala, India, Oct. 2019.

3. **V. Bankey** and P. K. Upadhyay, "Ergodic secrecy capacity analysis of multiuser hybrid satellite-terrestrial relay networks with multiple eavesdroppers," in Proc. ***IEEE International Conference on Communications Workshops (ICC Workshops): Wireless Physical Layer Security***, Shanghai, China, May 2019. **(Received international travel grant from DST, Govt. of India for presenting this paper).**

4. **V. Bankey**, P. K. Upadhyay, and D. B. da Costa, "Physical layer security of interference-limited land mobile satellite communication systems," in Proc. ***International Conference on Advanced Communication Technologies and Networking (CommNet)***, Morocco, Apr. 2018.

5. **V. Bankey** and P. K. Upadhyay, "Secrecy outage analysis of hybrid satellite-terrestrial relay networks with opportunistic relaying schemes," in Proc. ***IEEE 85th Vehicular Technology Conference (VTC)***, Sydney, Australia, Jun. 2017.

In Book Chapter

1. **V. Bankey**, P. K. Upadhyay, and D. B. da Costa, "Physical Layer Security in Hybrid Satellite-Terrestrial Relay Networks," *Physical Layer Security-Theory and Practice, Khoa N. Le (Ed.),* ***Springer Nature***, 2020.